STRUCTURAL DYNAMICS OF ELONGATION FACTOR TU

Evan André Mercier
B.Sc. Brock University, 2009

A Thesis
Submitted to the School of Graduate Studies
of the University of Lethbridge
in Partial Fulfillment of the
Requirements for the Degree

DOCTOR OF PHILOSOPHY

IN

BIOMOLECULAR SCIENCE

Chemistry and Biochemistry
University of Lethbridge
LETHBRIDGE, ALBERTA, CANADA

© Evan André Mercier, 2013

This dissertation is dedicated to Mom and Sprio;
even through you never received your Ph.D.s please
know that you helped prepare me to attain mine.

Abstract

Elongation Factor (EF) Tu is universally conserved and delivers aminoacyl-tRNAs (aa-tRNAs) to the ribosome. To perform this essential task, EF-Tu binds aa-tRNA in an active GTP-bound state, and GTP hydrolysis is critical for deposition of aa-tRNA into the ribosome. Following each aa-tRNA delivery, nucleotide exchange is required for reactivation of EF-Tu•GDP to EF-Tu•GTP. EF-Tu undergoes a variety of conformational changes during each round of aa-tRNA delivery and reactivation. Here, molecular dynamics simulations *in silico* and kinetic measurements *in vitro* demonstrate that structural dynamics of EF-Tu on the sub-nanosecond timescale are correlated with EF-Tu functions on the timescale of seconds. Specifically, structural dynamics of the conserved P-loop and switch II regions are important for nucleotide binding in EF-Tu. Additionally, interactions between domain II of EF-Tu and the small ribosomal subunit, which stimulate GTP hydrolysis on EF-Tu, have the potential to regulate structural dynamics of switch I and switch II.

Acknowledgements

I would like to acknowledge the following students who assisted in collecting some of the data presented here: Benjamin Nilsson constructed the EF-Tu_{H22G} variant presented in Chapter 3; Dylan Girodat, Nils Niggerman, and Laura Keffer-Wilkes assisted in performing the *in vitro* experiments presented in Chapter 4; and Dylan also assisted in performing and analyzing MD simulations of the EF-Tu_{M112G}•EF-Ts complex presented in Chapter 4. I need to thank Fan Mo who performed all of the *in vitro* experiments presented in Chapter 5.

This work was funded by the National Science and Engineering Research Council of Canada, Alberta Innovates Technology Futures, and the University of Lethbridge; Computational resources were provided by WestGrid (Compute Canada). Special thanks to Quintin Steynen for technical assistance and consultation.

The journey that led to this summary of my past five and a half years has certainly had its ups and downs. Thanks to Evelina for making the bad days bearable and the good days even better.

Thank you to my family for all of their love and support: I am truly lucky to have a family with whom I can discuss both scientific and personal matters. Special thanks to Jen for keeping me well fed over the past few years.

Of course, thank you H-J. You certainly contributed many good ideas and keen insights into this work. More than that, I really appreciate the freedom I was given to explore science and answer my own questions.

Members of the Wieden and Kothe research groups, past and present, all made significant contributions to making my time at the University of Lethbridge both productive and fun.

I really appreciate all of the time the members of my Ph.D. committee dedicated to my education. Their comments were constructive and I truly feel as though we worked together as a team on this research project.

All of my friends played very important roles in helping me attain this degree: they never hesitated to help me out and they kept me well grounded. They are simply too many to name them all. I must especially thank Jeffy, Nitro, Adam, Toby, Brad, Susan, Darren, Laura, and Rodrigo: you guys were *always* there for me.

Table of Contents

List of Tables

List of Figures

List of Abbreviations

aa-tRNA	aminoacyl-tRNA
CHARMM	chemistry at Harvard molecular mechanics
GDPCP	5′-guanosyl-methylene-triphosphate
GDPNP	guanosine 5′-[β-γ-imido]triphosphate
EF	translation elongation factor
eEF	Eukaryotic translation elongation factor
eIF	Eukaryotic translation initiation factor
FRET	fluorescence resonance energy transfer
GAF	GTPase activating factor
GDI	guanine nucleotide dissociation inhibitor
GEF	guanine nucleotide exchange factor
IF	translation initiation factor
IPTG	isopropyl β-D-1-thiogalactopyranoside
mant	2′-/3′-methylanthrinioloyl
MD	molecular dynamics
NAMD	nanoscale molecular dynamics
OD_{600}	optical density at 600 nm
PEP	phosphoenolpyruvate
PK	pyruvate kinase
P-loop	phosphate-binding loop
SMD	steered molecular dynamics
SRL	sarcin/ricin loop
VMD	visual molecular dynamics

Chapter 1

Introduction

1.1. Introduction to G-proteins

G-proteins as Molecular Switches

G-proteins, or GTPases, are found in all organisms and possess the ability to bind and hydrolyze GTP. Many ATPases couple the energy released by hydrolysis of a phosphodiester bond to drive metabolic reactions or motor processes (Berger et al., 1945; Cohn et al., 1987; Voet and Voet, 2004) while G-proteins generally couple GTP hydrolysis to various molecular switch functions (Fung and Stryer, 1980; Milburn et al., 1990; Moore and Blobel, 1993; Trahey and McCormick, 1987). G-proteins are widely studied and a large number of reviews on their function and regulation are available (Bos et al., 2007; Bourne et al., 1991; Siderovski and Willard, 2005; Verstraeten et al., 2011; Wittinghofer and Vetter, 2011). As outlined in **Figure 1.1**, each G-protein cycles between a GTP-bound 'on' state and a GDP-bound 'off' state. In this manner, G-proteins regulate cellular processes including cell growth (Mulcahy et al., 1985; Trahey and McCormick, 1987), vision (Fung and Stryer, 1980), nuclear trafficking (Moore and Blobel, 1993), and protein synthesis (Cabrer et al., 1976). Examples of G-proteins involved in these processes are Ras (cell growth), heterotrimeric G-proteins (smell, vision), Ran (nuclear import/export), and Elongation Factor Tu (protein synthesis). In its 'on' state a G-protein interacts with downstream effectors to elicit a response that is specific to the G-protein/effector pair. Hydrolysis of GTP and subsequent dissociation of P_i terminates the 'on' signal and the G-protein cycles to its 'off' state. G-proteins, and consequently the signals they propagate, can be regulated in several ways (**Figure 1.1)**. Activation of G-protein requires exchange of GDP for GTP, a process that is often catalyzed by a Guanine nucleotide Exchange Factor (GEF). Deactivation of a G-protein, conversely, requires

GTP hydrolysis that is typically stimulated by GTPase Activating Factors (GAFs). In some cases, a G-protein may be sequestered in the inactive state by a Guanine nucleotide Dissociation Inhibitor (GDI), which prevents the exchange of GDP for GTP. Through use of one or more of these factors, a cell can fine-tune the timing, duration, and location of a signal through regulation of G-protein properties.

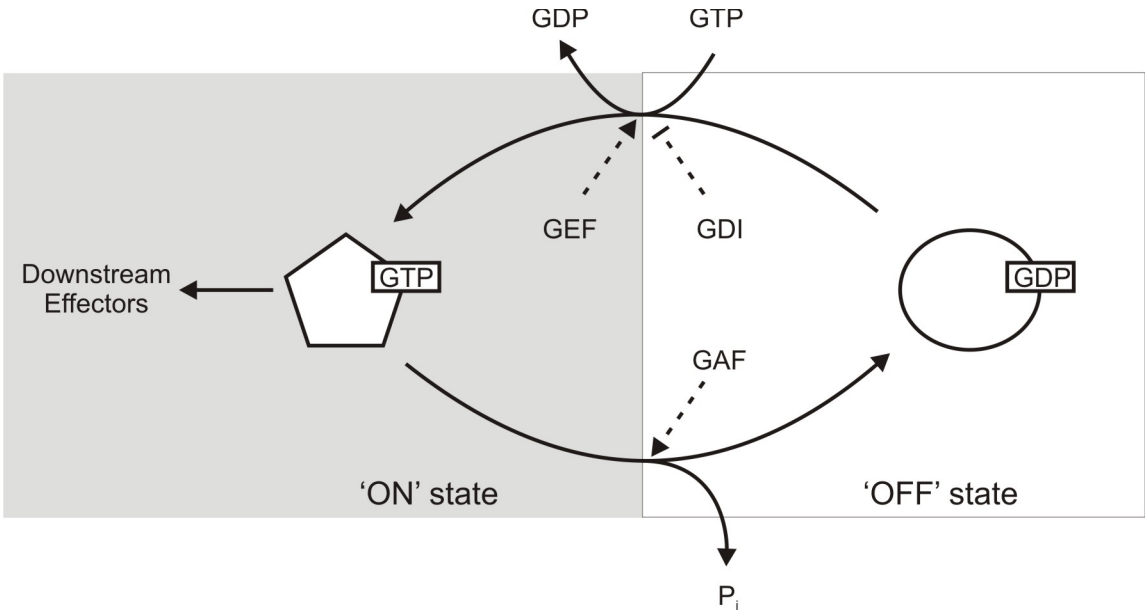

Figure 1.1. Generic cycle of the G-protein 'switch'. The GTP-bound 'on' state is deactivated by GTP hydrolysis (bottom), whereas the GDP-bound 'off' state is activated by GDP/GTP exchange (top). In the 'on' state, G-proteins interact with downstream effectors (left) to relay various signals. GTP hydrolysis is activated by GTPase Activating Factors (GAFs). Nucleotide exchange is stimulated by Guanine nucleotide Exchange Factors (GEFs) and inhibited by Guanine nucleotide Dissociation Inhibitors (GDIs).

In order to function, a G-protein must be able to effectively discriminate between GDP and GTP, and to respond by interacting with the appropriate partners. This basic function is performed by a conserved Rossmann fold G-domain. The canonical G-domain contains five conserved G-motifs (G-1 to G-5) (Bourne et al., 1991). The G-1 motif (also known as the Walker A motif or P-loop) is defined by the consensus sequence GxxxxGKS/T, although some variation is observed across the G-proteins (Bourne et al., 1991). It wraps around the phosphates of a bound nucleotide allowing the backbone amide nitrogens to

form hydrogen bonds with the β- and γ-phosphate oxygen atoms (Bourne et al., 1991). The sequence of the G-2 motif, also known as the switch I region, is well conserved within each G-protein family but poorly conserved between them (Bourne et al., 1991). Within the G-2 motif, a conserved threonine residue assists in coordinating Mg^{2+}, which is bound in the nucleotide-binding pocket and interacts with β- and γ-phosphates of the nucleotide. The G-3 motif, or switch II region, contains the conserved DxxG sequence (Bourne et al., 1991). The conserved aspartate residue contained in this sequence assists in coordinating the nucleotide-bound Mg^{2+}, while the glycine amino acid interacts, via the amide N-H bond with the γ-phosphate of GTP. The G-4 motif forms specific interactions with the guanine base through the sidechains of amino acids in the conserved sequence (N/T)(K/Q)xD. The asparagine (or threonine) and aspartate residues form hydrogen bonds with the Watson-Crick edge of the guanine base, while the lysine (or glutamine) forms electrostatic interactions with the endocyclic ribose oxygen (Bourne et al., 1991). The G-4 motif is responsible for the ability of G-proteins to bind guanine nucleotides with higher affinity than adenine nucleotides and mutations in this motif result in loss or change of this specificity (Weijland et al., 1994). The G-5 motif also assists in binding the guanine base of bound nucleotides, but this motif is poorly conserved across different G-protein families.

G-protein activation by Guanine Nucleotide Exchange Factors

Many G-proteins, including Ras and EF-Tu, have very high affinities for guanine nucleotides, with equilibrium dissociation constants (K_D's) on the order of nanomolar or picomolar (Gromadski et al., 2002; John et al., 1990). The high affinities likely reflect the importance of regulating G-proteins within the cell. The rate of intrinsic GDP

dissociation is very slow for many G-proteins (2 x 10^{-3} s^{-1} for EF-Tu (Gromadski et al., 2002) and 1 x 10^{-4} s^{-1} for Ras (Lenzen et al., 1998)) and, as a result, so too is the rate of 'spontaneous' activation. Activation of these G-proteins is regulated by GEFs that stimulate GDP dissociation and catalyze the exchange of GDP for GTP (Fung and Stryer, 1980; Gromadski et al., 2002; Jones et al., 1991; Klebe et al., 1995). The mechanism of GEF-induced G-protein activation starts with GEF binding to the GDP-bound form of the G-protein. Next, GDP rapidly dissociates from a G-protein•GDP•GEF complex resulting in the G-protein•GEF binary complex. GTP can then bind and cause GEF dissociation to yield the active, GTP-bound state, of the G-protein. Since each step in this mechanism is reversible, the ten-fold excess of GTP over GDP in the cell helps drive net G-protein activation (Bochner and Ames, 1982). Some G-proteins have evolved with fast intrinsic GDP dissociation rates and do not require the action of GEFs for their activation. For these proteins, rapid GDP dissociation (14 s^{-1} for Ffh (Jagath et al., 1998) or 300 s^{-1} for EF-G (Wilden et al., 2006)) and subsequent GTP binding driven by the 10:1 cellular GTP/GDP ratio (Bochner and Ames, 1982) are all that is required for G-protein activation.

Interestingly, different GEFs do not appear to be structurally related and bind to G-proteins at different positions and/or orientations (Bos et al., 2007). GEFs do, however, appear to share some common strategies for stimulating nucleotide dissociation from the G-domain. X-ray crystal structures, primarily of G-protein•GEF complexes, reveal that GEF binding is concomitant with conformational changes in the switch I, switch II, and (in some cases) P-loop regions (Boriack-Sjodin et al., 1998; Bos et al., 2007; Kawashima et al., 1996; Mossessova et al., 2003; Renault et al., 2001). Since switches I and II

contribute to binding the conserved Mg^{2+} in the nucleotide binding pocket, conformational changes in these elements likely destabilize Mg^{2+} and, subsequently, GDP binding. Some G-protein•GEF structures reveal conformational changes in the P-loop and suggest that disruption of the phosphate-binding site is an additional strategy contributing to nucleotide dissociation (Boriack-Sjodin et al., 1998; Chhatriwala et al., 2007; Kawashima et al., 1996). Our structural understanding of GEF function is limited by two main issues. First, the above hypotheses are primarily based on comparison of G-protein•nucleotide and G-protein•GEF binary complexes. As a result, it is difficult if not impossible to identify which structural rearrangements are the cause of, rather than the effect of, nucleotide dissociation. Second, the static structures provided by X-ray crystallography offer limited insight into how structural dynamics contribute to the nucleotide exchange process. As a consequence it is difficult to piece together a step-by-step mechanism of the structural rearrangements that lead to rapid nucleotide dissociation.

G-protein inactivation by GTP-hydrolysis

Inactivation of a GTP-bound G-protein requires GTP hydrolysis and subsequent P_i release, which will yield an inactive GDP-bound conformation of the enzyme. As reviewed in Bos *et al.* (2007), Siderovski and Willard (2005), and Wittinghofer and Vetter (2011), the intrinsic rates of GTP hydrolysis by many G-proteins is extremely slow, on the order of minutes to hours (Neal et al., 1988). If unaltered, this would translate into longstanding 'on' signals emanating from these G-proteins. This situation is exemplified by constitutively active Ras mutants, which are prevalent in many cancers (Karnoub and Weinberg, 2008). In order to facilitate termination of the 'on' state, many

G-proteins interact with GTPase Activating Factors (GAFs). Similar to GEFs, GAFs do not share a conserved structure despite employing a number of common mechanisms of action (Bos et al., 2007). The general mechanism of GTP hydrolysis is thought to be conserved among all G-proteins: a water molecule performs a nucleophilic attack on the γ-phosphate of GTP (Feuerstein et al., 1989; Grigorenko et al., 2008). This reaction is likely facilitated by the Mg^{2+} ion bound in the G-domain and backbone amide bonds of the P-loop, which help stabilize the increasing negative charges on β- and γ-phosphates during the course of the reaction. As reviewed by Bos *et al.* (2007), GAFs can accelerate this process by supplying a catalytic residue to activate the nucleophilic water; stabilizing the cis-acting catalytic residue; and/or contributing to charge stabilization of the transition state. In this manner, interaction between a G-protein and a GAF can result in rapid deactivation of the G-protein 'on' signal. As an example, the Ras GAP accelerates GTP hydrolysis by about 100,000 fold, from a rate of ~0.0001 s^{-1} to 10 s^{-1} (Gideon et al., 1992). Although, GAFs differ in their precise binding modes, each one must interact with regions close to the γ-phosphate of bound GTP.

The translation factor G-protein superfamily

Most of the work describing G-protein regulation has focused on small G-proteins and heterotrimeric G-proteins which are not found in bacteria (Alto, 2008; Simon et al., 1991). There are, however, eight universally conserved G-proteins as reviewed in Verstraeten *et al.* (2011). In prokaryotes, these G-proteins are named YihA, YchF, HflX, IF-2, EF-Tu, EF-G, Ffh, and FtsY. The protein YihA has been shown to co-purify with ribosomes, and deletion of this G-protein from genomic DNA causes reduction in the levels of mature ribosomes in the cell (Cooper et al., 2009). Thus, YihA is thought to

participate in ribosome assembly. The functions of IF-2, EF-Tu, EF-G, Ffh, and FtsY have each been well established and are central to protein synthesis. The proteins Ffh and FtsY are involved in the co-translational membrane insertion and translocation of proteins across the plasma membrane (Powers and Walter, 1997). Initiation factor (IF) 2 is involved in initiating protein synthesis on an mRNA transcript (Anderson et al., 1967). The initiation process includes the association of ribosomal subunits at the start codon and placement of the first aminoacyl-tRNA (aa-tRNA) in the ribosomal P-site. The elongation factors (EFs) Tu and G are both involved in the elongation phase of protein synthesis where amino acids are added sequentially to the growing polypeptide chain (Cabrer et al., 1976; Pape et al., 1998). However, the cellular functions of the universally conserved G-proteins YchF and HflX are currently unknown, although increasing evidence suggests a ribosome related function (Becker et al., 2012; Fischer et al., 2012; Shields et al., 2009).

Unlike the small G-proteins and G-protein coupled receptors that contribute to signal transduction in their GTP-bound 'on' states, some translational G-proteins appear to carry out their function concomitantly with GTP hydrolysis. For example, GTP hydrolysis by IF-2 signals the completed assembly of the initiation complex in bacteria (Marshall et al., 2009); in each round of elongation, delivery of aa-tRNA to the ribosomal A-site is dependent on GTP hydrolysis by EF-Tu (Ravel et al., 1968); and translocation of tRNAs and mRNA through the ribosome involves GTP hydrolysis by EF-G (Inoue-Yokosawa et al., 1974; Katunin et al., 2002). The G-proteins Ffh and FtsY, however, may have a more 'classic G-protein' function, as they deliver nascent peptides to the translocon in their GTP-bound 'on' states (Zhang et al., 2009). GTP hydrolysis by these proteins appears to

be involved in returning the factors to the cytosolic pool. The distinction between functioning in a GTP-bound 'on' state or concomitantly with GTP hydrolysis may be a matter of perspective. The translational G-proteins IF-2, EF-Tu, and EF-G could be thought of as searching the cytosol in their GTP-bound 'on' states for target ribosomes or ribosomal subunits.

In contrast to the numerous GEFs that have been identified to regulate small G-proteins (Bos et al., 2007), few GEFs have been identified that regulate the translational G-proteins. Nucleotide exchange on EF-Tu is catalyzed by EF-Ts in prokaryotes while eEF1Bα acts as a GEF on the eukaryotic homologue eEF1A (Iwasaki et al., 1976; Weissbach et al., 1970). Despite performing the same function on homologous targets, the GEFs EF-Ts and eEF1Bα are not homologues (Maessen et al., 1986). Based on its micromolar affinity for GDP, the prokaryotic IF2 has been suggested to function without the requirement of a GEF. The eukaryotic homologue of IF-2 (eIF2), however, requires the GEF eIF2B (Konieczny and Safer, 1983). The translational G-proteins EF-G (Wilden et al., 2006), YchF (Kirsten Rossler, personal communication), HflX (Fischer et al., 2012), Ffh, and FtsY (Jagath et al., 1998), however, all exchange nucleotides rapidly in the absence of other proteins. This suggests that GEFs may not be required to activate these G-proteins. Rapid kinetics studies of HflX demonstrate that the ribosome is able to modulate nucleotide-binding properties of this enzyme, and exchange of GDP for GTP may occur on the ribosome under physiological conditions (Fischer et al., 2012). A similar model for EF-G function was proposed based on steady-state kinetics experiments. In this model, EF-G binds to the ribosome in the GDP-bound 'off' state and the ribosome subsequently stimulates nucleotide exchange (Zavialov et al., 2005). This

model, however, is inconsistent with more recent rapid-kinetics data (Wilden et al., 2006). Thus, the majority of universally conserved translational G-proteins do not appear to require GEFs.

For many translational G-proteins, the ribosome or ribosomal subunits appear to act as GAFs. Stimulation of GTP hydrolysis by ribosomes has been shown *in vitro* for the translational G-proteins IF-2 (Marshall et al., 2009), EF-Tu (Haenni and Lucas-Lenard, 1968; Pape et al., 1998), EF-G (Inoue-Yokosawa et al., 1974), YchF (Becker et al., 2012), and HflX (Shields et al., 2009). For the G-proteins Ffh and FtsY, GTP hydrolysis is faster in the absence of target ribosomes leading to the hypothesis that hydrolysis of GTP occurs after Ffh/FtsY dissociation from the ribosome at the translocon (Zhang et al., 2009). Based on these findings, the ribosome does not appear to act as a GAF for Ffh and FtsY. The GTPase activity of YihA, on the other hand, is poorly understood. Thus, the ribosome appears to act as a GEF for the majority of universally conserved translational G-proteins.

1.2 Introduction to Elongation Factor Tu

Elongation Factor (EF) Tu is a universally conserved G-protein and plays an indispensable role in protein synthesis (Ravel et al., 1968; Schnell et al., 2003; Yokosawa et al., 1975). EF-Tu catalyzes the delivery of aminoacyl-tRNA (aa-tRNA) to ribosomes during the elongation phase of protein synthesis and is among the most abundant proteins in *E. coli* (Ishihama et al., 2008). In the cytosol of archaea and eukaryotes, the homologue of EF-Tu, EF-1A, performs this task. The mitochondria and chloroplasts of eukaryotes, however, rely on EF-Tu during protein synthesis as the protein synthesis machinery of

these organelles is distinct from that of the cytosol (Ciferri and Tiboni, 1973; Nagata et al., 1983). EF-Tu performs a variety of different functions: it binds all aa-tRNAs(Louie et al., 1984), it rapidly delivers aa-tRNAs to the ribosome (Pape et al., 1998; Rodnina et al., 1996), and it contributes to the accuracy of translation (Pape et al., 1999; Thompson and Stone, 1977). In this context, EF-Tu is required to be fast but accurate, bind *all* different tRNAs, and interact with the ribosome. Like all other G-proteins, EF-Tu acts as a molecular switch with a GTP-bound 'on' state, and a GDP-bound 'off' state. It is the 'on' state of EF-Tu that is responsible for binding aa-tRNAs and delivering them to the ribosome. EF-Tu is a three-domain protein (shown in **Figure 1.2**) in which domain I, the G-domain, is responsible for binding guanine nucleotides. Domains II and III are β-barrel domains that mediate interactions with other factors including aa-tRNA as shown in **Figure 1.3** (Nissen et al., 1995; Sanderson and Uhlenbeck, 2007). The 'on' and 'off' states of EF-Tu are structurally dissimilar as the EF-Tu•GTP complex is characterized by a compact arrangement of the three domains while in the EF-Tu•GDP complex, domain II does not contact domain I (Berchtold et al., 1993; Kjeldgaard et al., 1993; Song et al., 1999). This difference results in an obvious 'hole' among the domains of EF-Tu•GDP which is not present in EF-Tu•GTP.

The driving force for this dramatic conformational rearrangement has been suggested to originate in the switch I and switch II regions (Berchtold et al., 1993; Kjeldgaard et al., 1996). As their names suggest, the switch I and II regions have been implicated in 'switching' the G-protein conformation between 'on' and 'off' depending on which nucleotide is bound (Bourne et al., 1991; Kjeldgaard et al., 1996; Milburn et al., 1990). A comparison of the GDP- and GTP-bound conformations is shown in **Figure 1.2**. In this

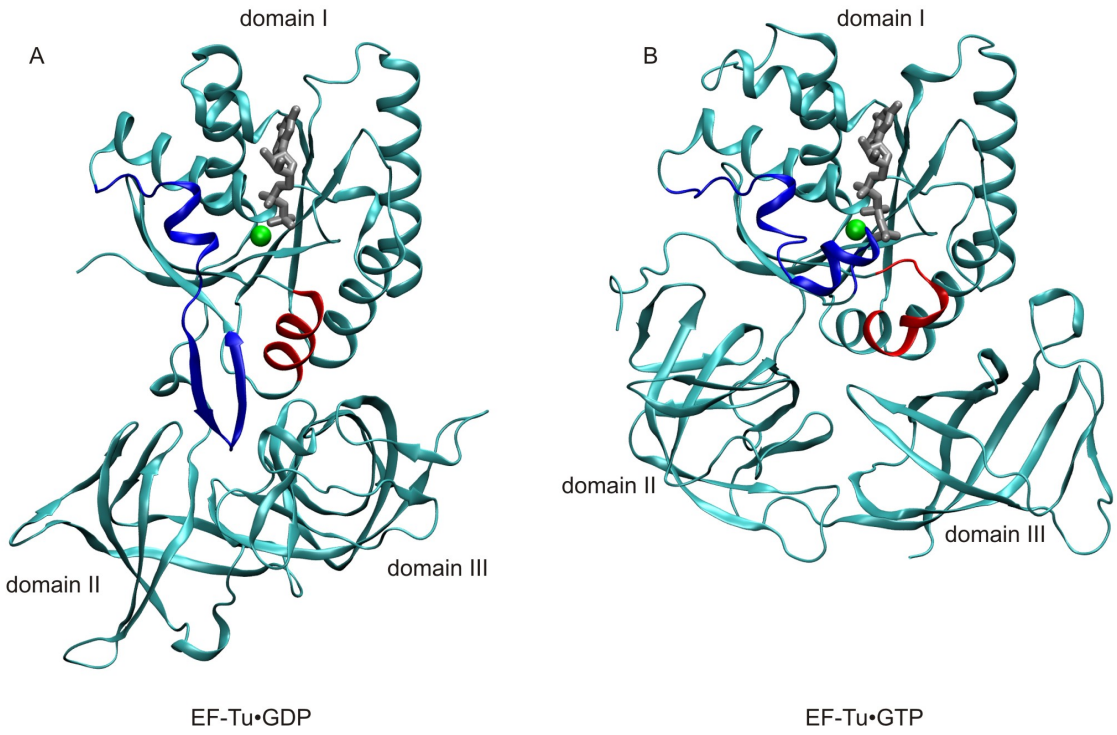

Figure 1.2. EF-Tu has distinct GDP-bound and GTP-bound conformations. Cartoon representations of EF-Tu•GDP (A PDBID: 1EFC) and EF-Tu•GDPNP (B; PDBID: 1EFT) are shown with the guanine nucleotide shown as silver sticks, Mg^{2+} as green spheres. The switch I region is coloured blue, and switch II is coloured red.

conversion, switch I appears to undergo the most dramatic change; in EF-Tu•GTP, switch I contains two short α-helices (A′ and A″), but in EF-Tu•GDP the helix A″ unwinds and reconfigures into two antiparallel β-sheets which extend towards domain III (Berchtold et al., 1993; Song et al., 1999). This rearrangement is likely triggered by movement of $Thr61_{Tu}$, which interacts with the γ-phosphate of bound GTP. The switch II region contains the conserved $Gly83_{Tu}$ that is just upstream of helix B. In EF-Tu•GTP $Gly83_{Tu}$ interacts with the γ-phosphate of bound GTP but has an alternate backbone conformation in EF-Tu•GDP. This presumably causes helix B to increase by four amino acids at the N-terminal end and decrease by 2 amino acids at the C-terminal end in transition from EF-Tu•GTP to EF-Tu•GDP. Helix B also reorients by 42° as it changes from packing closely with domain I in EF-Tu•GTP to extending towards domain III (in an N to C

direction) in EF-Tu•GDP. The reorientation of helix B has been proposed to trigger the large 90° rotation of domain I relative to domains II and III that is obvious upon comparison of EF-Tu•GTP and EF-Tu•GDP crystal structures shown in **Figure 1.2** (Berchtold et al., 1993). These conformational changes are well studied in EF-Tu and structural rearrangements observed in switch I and switch II in response to the presence or absence of a γ-phosphate are consistent with what is found in other G-proteins (Kjeldgaard et al., 1996). The order of events that underlie the conformational switch mechanism are still speculative since no one has yet 'seen' the time-resolved conformational change. Rapid kinetics studies have suggested that P_i release is rate limiting for and precedes the GTP to GDP conformational change in EF-Tu, but conformational changes in switch II may contribute to P_i release (Kothe and Rodnina, 2006). Understanding the structural mechanism of this rearrangement is of fundamental interest, as the GTP-bound to GDP-bound ('on' to 'off') transition in EF-Tu is linked to the release of aa-tRNA in the ribosomal A-site.

Conformational changes in switch I and switch II have been implicated in functions of EF-Tu including GTPase activation (Schmeing et al., 2009), GTP hydrolysis (Daviter et al., 2003; Vogeley et al., 2001), nucleotide exchange (Kawashima et al., 1996), and tRNA release (Nissen et al., 1995). It is likely that the switch regions of EF-Tu have evolved specific dynamic properties to enable different conformations involved in each of EF-Tu's functions. Structural studies have revealed that the interactions between switch I/switch II and the γ-phosphate of bound GTP may be a conserved trigger for conformational switching in all G-proteins (Kjeldgaard et al., 1996; Wittinghofer and Vetter, 2011). Switch I and II occupy the same region of each different G-protein

(relative to the core), but the sequences and lengths differ (Bourne et al., 1991). These differences are thought to account for the interaction of different G-proteins with different effectors (Bos et al., 2007; Bourne et al., 1991).

In the 'on' state, EF-Tu binds aa-tRNAs with nanomolar affinity (Louie et al., 1984) and recruits them to the A-site of the ribosome. A structure of EF-Tu bound to GDPNP and aa-tRNA obtained by X-ray crystallography is shown in **Figure 1.3**. Extensive

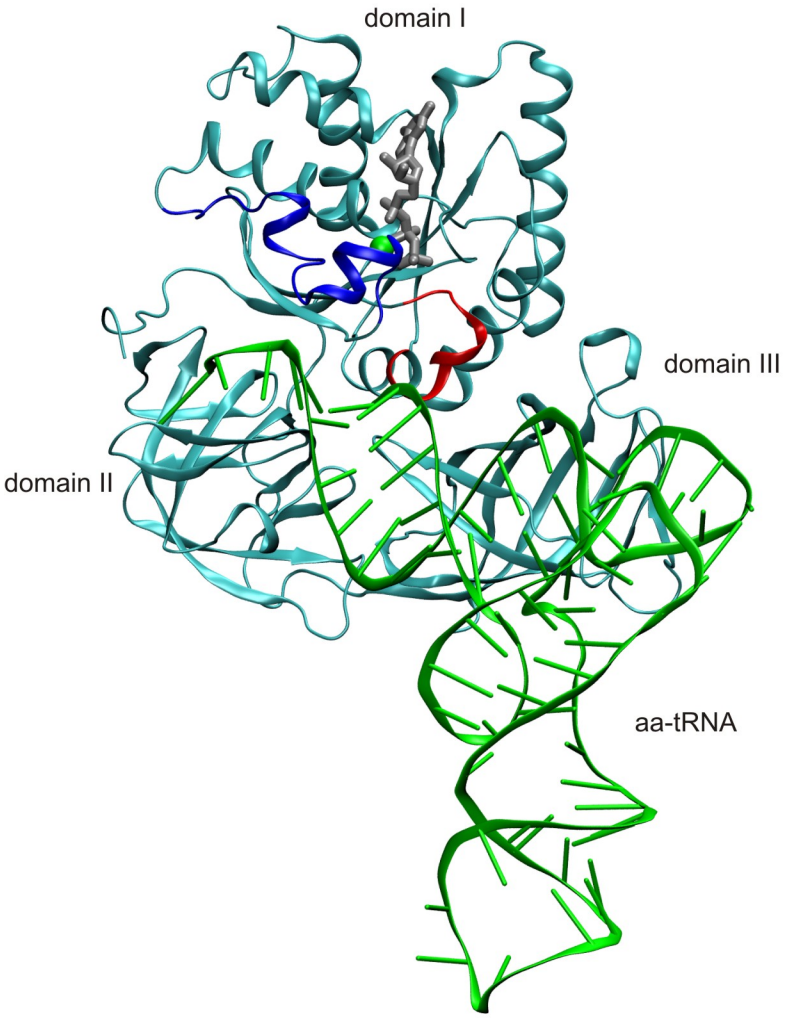

Figure 1.3. Structure of the EF-Tu•GDPNP•aa-tRNA ternary complex. Based on the structure 1TTT (Nissen et al., 1995). EF-Tu (cyan) and aa-tRNA (green) are shown in cartoon representations GDPNP as silver sticks, and Mg^{2+} as a green sphere. The switch I region is coloured blue and switch II red.

mutagenesis of both EF-Tu and the tRNA body have led to the hypothesis that strong interactions with the amino acid covalently linked to the 3′ end of tRNA are accompanied by weak interactions with the tRNA body and vice versa (LaRiviere et al., 2001; Sanderson and Uhlenbeck, 2007). This thermodynamic compensation ensures that all aminoacyl-tRNAs are bound to EF-Tu•GTP with comparable affinities (Louie et al., 1984). Work of Olke Uhlenbeck's group suggests that similar dissociation rates for each aa-tRNA from EF-Tu could be important when tRNAs are released from EF-Tu into the ribosome. This is supported by their observation that, for the aa-tRNAs tested, rates of peptide chain elongation correlate well with the rates of aa-tRNA dissociation from EF-Tu (Schrader et al., 2011). Thus, instead of evolving to optimally bind a single ligand, EF-Tu has evolved to bind all aa-tRNAs with similar nanomolar affinities.

The role of EF-Tu in delivering aa-tRNA to the ribosome has been mapped out through a number of kinetics experiments. The complete kinetic mechanism of EF-Tu-catalyzed delivery of aa-tRNA to the ribosome was published by Marina Rodnina's research group in 1998 and is summarized in **Figure 1.4** (Pape et al., 1998). The EF-Tu•GTP•aa-tRNA ternary complex initially binds to the ribosome to form a labile complex (**Figure 1.4.A**). This is followed by codon recognition in the decoding centre of the ribosomal A-site (**Figure 1.4.B**). These first two steps are rapid and reversible: two critical components to aa-tRNA selection. When the aa-tRNA bound to EF-Tu is non-cognate or near-cognate relative to the mRNA codon presented in the decoding centre, the reversibility of these steps leads to rapid dissociation of the EF-Tu•GTP•aa-tRNA ternary complex from the ribosome. This limits the amount of time that the ribosomal A-site is occupied by incorrect ternary complexes. When the correct ternary complex is present in the A-site,

however, correct codon/anticodon interactions in the decoding centre (**Figure 1.4.C**) trigger rapid, irreversible GTP-hydrolysis on EF-Tu (**Figure 1.4.D**) (Pape et al., 1999; Pape et al., 1998). In this way EF-Tu acts as the first step in aa-tRNA selection, separating A-site binding from aa-tRNA accommodation using the energy of GTP hydrolysis.

In order for a correct aa-tRNA to be accepted into the ribosome, it must dissociate from EF-Tu and undergo proper accommodation into the A-site. The dissociation process is promoted by the conformational change of EF-Tu from the GTP-bound 'on' state to the GDP-bound 'off' state (**Figure 1.4.E**). This conformational change is preceded by a

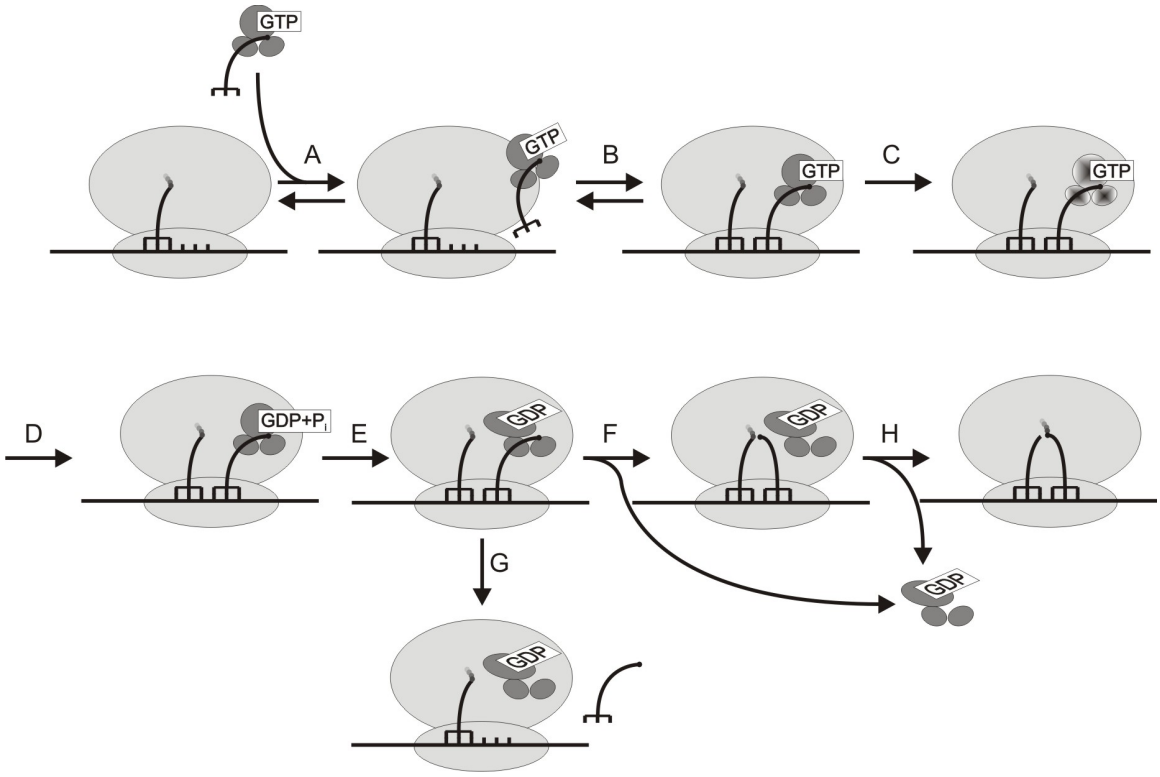

Figure 1.4. Kinetic mechanism of EF-Tu-dependent aa-tRNA delivery. Reversible initial binding of the EF-Tu•GTP•aa-tRNA ternary complex to the ribosome is followed by (B) codon recognition. If the correct codon/anticodon is detected in the decoding centre, the GTPase activity of EF-Tu is activated (C) and rapid, irreversible GTP hydrolysis takes place on EF-Tu (D). Following P_i release and conformational change of EF-Tu (E), accommodation of the aa-tRNA occurs (F). During the accommodation step, the aa-tRNA can be ejected from the ribosomal A-site (G), which is accelerated in the presence of a codon/anticodon mismatch. After accommodation of an aa-tRNA into the A-site, rapid peptide bond formation is catalyzed by the ribosome (H). Release of EF-Tu may occur at steps (F), (G), or (H).

kinetically distinct phosphate release step which is not explicitly shown in **Figure 1.4** (Kothe and Rodnina, 2006). Release of aa-tRNA from its binding site in EF-Tu is facilitated by the low affinity of aa-tRNA for the EF-Tu•GDP complex compared to the high affinity for EF-Tu•GTP (Dell et al., 1990; Ravel and Shorey, 1969). Once released from EF-Tu, the aa-tRNA must undergo accommodation into the ribosomal A-site (**Figure 1.4.F**). Accommodation involves movement of the acceptor stem of the tRNA from its initial position 'outside' the ribosome, to a position 'inside' the ribosome. The process of accommodation is the rate-limiting step during the delivery of aa-tRNA to the ribosome (Pape et al., 1998). The rate of accommodation is approximately 70-fold faster for cognate vs. near-cognate aa-tRNA, while near-cognate aa-tRNA is rejected from the ribosomal A-site about 20-fold more rapidly than cognate aa-tRNA (Pape et al., 1999). The result is a kinetic proofreading step, where near-cognate aa-tRNAs are rapidly ejected from the A-site (**Figure 1.4.G**), while cognate aa-tRNAs are rapidly accommodated (Thompson and Stone, 1977). In the accommodated state the aminoacyl ester bond at the CCA-end of the A-site aa-tRNA is positioned in the peptidyl-transferase centre (PTC) of the ribosome. In this conformation, the amino acid attached to the A-site tRNA is adjacent to the CCA end of the peptidyl-tRNA in the P-site. This positioning is essential for efficient peptide bond formation catalyzed by the ribosomal PTC (**Figure 1.4.H**). The rate of peptide bond formation is extremely rapid (>100 s^{-1}) and occurs essentially immediately following accommodation (Pape et al., 1998).

After the ribosome has catalyzed peptide bond formation between the peptide in the P-site and the aa-tRNA in the A-site, a peptidyl-tRNA will occupy the A-site. In order for the next aa-tRNA to be delivered to the ribosome, several steps must occur. First, EF-Tu

must dissociate from the ribosome as shown in **Figure 1.4.F or H**. The precise timing of EF-Tu•GDP dissociation from the ribosome is unclear as it may occur before, during or after aa-tRNA accommodation (Pape et al., 1998). Next, the translation factor EF-G (EF2 in eukaryotes) will bind to the ribosomal A-site and catalyze translocation of the mRNA•tRNA complex in a GTP-dependent manner (Inoue-Yokosawa et al., 1974). Translocation involves the concomitant movement of mRNA and tRNAs by one codon through the ribosome such that the deacyl-tRNA occupies the E-site, and the newly formed peptidyl-tRNA occupies the P-site. Following dissociation of EF-G, the A-site of the ribosome is left empty displaying the next mRNA codon in the decoding centre. The ribosome is then ready for the next round of the elongation cycle in which it can accept the next aa-tRNA into the A-site.

GTPase activation of EF-Tu is central to protein synthesis and the fidelity therein as it is the first step in aa-tRNA selection on the ribosome. X-ray crystal structures of EF-Tu bound to the ribosome, one of which is shown in **Figure 1.5**, highlight several factors that have been shown, through biochemical studies, to contribute to GTP hydrolysis (Schmeing et al., 2009; Schmeing et al., 2011; Voorhees et al., 2010). Firstly, the amino acid sidechain of $His84_{Tu}$ has been shown to contact the Sarcin/Ricin Loop (SRL) of the 23S rRNA in the large ribosomal subunit (Voorhees et al., 2010). Mutation of the invariant $His84_{Tu}$ to alanine results in more than one million-fold reduction in the rate of GTP hydrolysis on the ribosome in the presence of a cognate aa-tRNA (Daviter et al., 2003). The $His84_{Tu}$ sidechain has been proposed to activate a water molecule for nucleophilic attack of the γ-phosphate in GTP (Daviter et al., 2003; Grigorenko et al., 2008). Chemical modification of the SRL by the toxin α-sarcin has been shown to

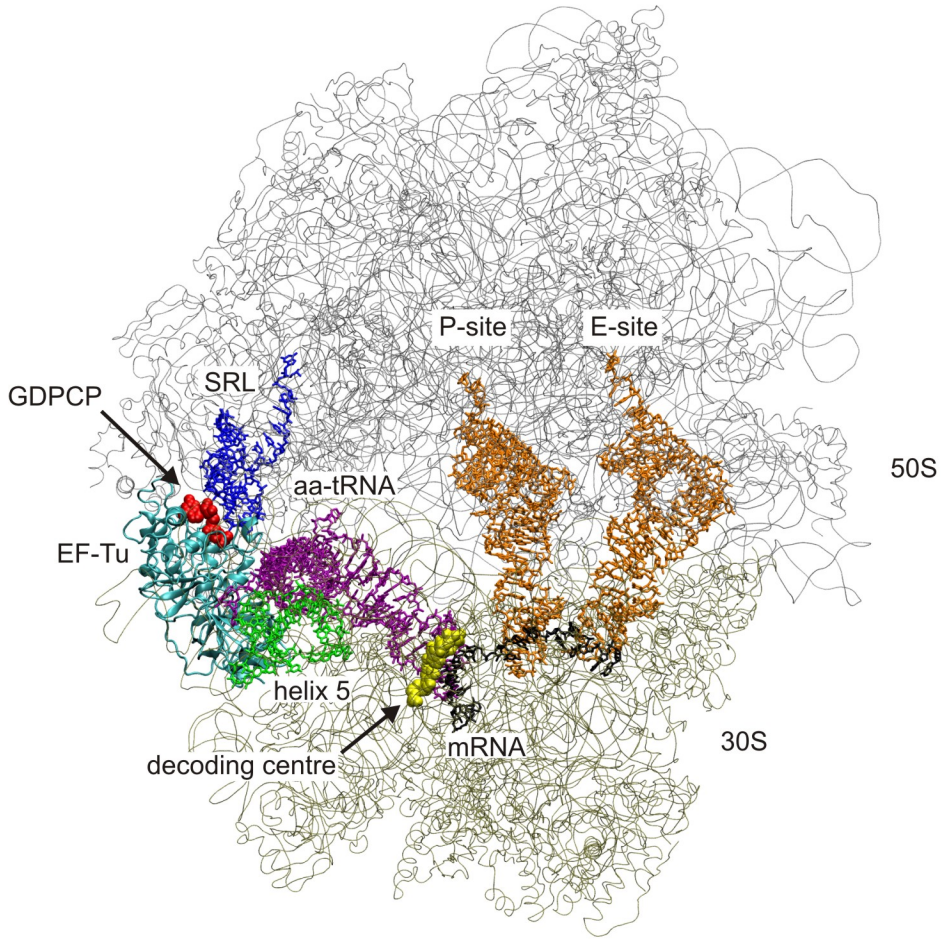

Figure 1.5. The structure of EF-Tu on the ribosome (PDBID: 2XQD & 2XQE, (Voorhees et al., 2010)). The 50S ribosomal subunit (grey) and 30S ribosomal subunit (tan) are shown bound to mRNA (black), E- and P- site tRNAs (orange), and an EF-Tu•GDPCP•aa-tRNA ternary complex in the A-site. EF-Tu is shown in cyan, the non-hydrolyzable GTP analogue GDPCP in red, and the aa-tRNA in purple. The decoding centre on the 30S ribosomal subunit is shown in yellow, the sarcin-ricin loop (SRL) in blue, and helix 5 of the 16S rRNA in green.

prevent EF-Tu-catalyzed delivery of aa-tRNAs to the ribosome (Hausner et al., 1987). It is unclear, however, if α-sarcin treatment affects the binding of EF-Tu•GTP•aa-tRNA to the ribosome or GTP hydrolysis (Shi et al., 2012), but the functional importance of this rRNA element is clear. Interestingly, contacts observed between helix 5 of 16S rRNA in the 30S ribosomal subunit and domain II of EF-Tu were also suggested to participate in GTPase activation (Schmeing et al., 2009). This hypothesis is in line with work of the

Rodnina group that demonstrated a G222D substitution in domain II of EF-Tu, located close to helix 5 when bound to the ribosome, inhibits GTPase activation (Vorstenbosch et al., 1996). Interestingly, this effect is overcome at high concentrations of Mg^{2+} (10 mM vs. 5 mM). Biochemical studies *in vivo* have revealed that ribosomes bearing mutations in helix 5 have less than 10% activity compared to wild type ribosomes (McClory et al., 2010). These findings however, cannot discriminate between effects on EF-Tu and EF-G, which interact with the ribosomal A-site in a similar manner, or between effects on initiation, elongation, and termination of protein synthesis (Gao et al., 2009; Moazed et al., 1988).

During GTPase activation of EF-Tu, a signal presumably travels from the decoding centre in the A-site on the 30S ribosomal subunit to EF-Tu. Structural studies have revealed that within the decoding centre, bases A1492 and A1493 of helix 44 and G530 of the 16S rRNA flip out to interact with the minor groove of the codon/anticodon interaction (Ogle et al., 2001). How this recognition is relayed to EF-Tu is not fully understood, but biochemical studies indicate the importance of aa-tRNA in this mechanism. When aa-tRNA is replaced by two discretely folded halves of the aa-tRNA, GTP-hydrolysis by EF-Tu on the ribosome is extremely slow (Piepenburg et al., 2000). It seems likely that the body of the tRNA therefore plays some role in communicating a GTPase activating signal from the decoding centre on the 30S ribosomal subunit to EF-Tu.

Following GTP hydrolysis by EF-Tu, P_i is released and the enzyme changes from the 'on' (GTP-bound) state to the 'off' (GDP-bound) state. The factor must be recycled back to EF-Tu•GTP in order to participate in another round of elongation. The challenge of

recycling EF-Tu•GTP in the cell lies in the fact that EF-Tu•GDP dissociation is extremely slow (k_{off} = 0.002 s^{-1}), (Gromadski et al., 2002). In order to accelerate the nucleotide exchange process, EF-Ts binds to the EF-Tu•GDP complex and stimulates GDP dissociation by about 60,000 fold (Gromadski et al., 2002). The kinetic mechanism of nucleotide exchange in EF-Tu is depicted in **Scheme 1.1**. Following the binding of EF-Ts to EF-Tu•GDP and rapid GDP dissociation, GTP binds to the EF-Tu•EF-Ts complex. EF-Ts can then dissociate from the EF-Tu•GTP•EF-Ts ternary complex to leave EF-Tu in the GTP-bound 'on' state. The high concentration of aa-tRNA in the cell ensures that EF-Tu•GTP•aa-tRNA forms rapidly and draws the equilibrium towards the formation of EF-Tu•GTP. The estimated overall rate of nucleotide exchange in EF-Tu (30 s^{-1}) is fast enough to keep up with protein synthesis on the order of 10 amino acids per second (Forchhammer and Lindahl, 1971; Proshkin et al., 2010).

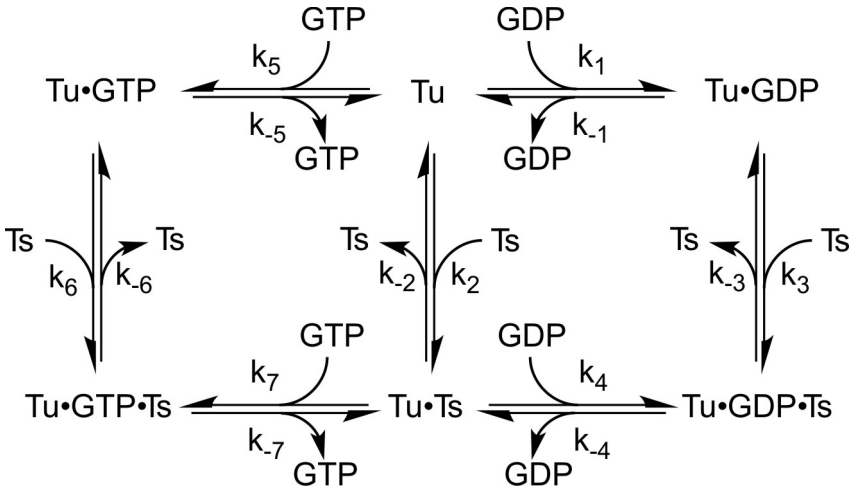

Scheme 1.1. The mechanism of EF-Ts catalyzed nucleotide exchange in EF-Tu.

Structural and mutational studies have revealed some of the interactions that are important for EF-Ts-stimulated nucleotide dissociation from EF-Tu (Dahl et al., 2006; Kawashima et al., 1996; Schümmer et al., 2007; Zhang et al., 1998). EF-Ts binds to the

'edge' of EF-Tu formed by domains I and III. The N-terminal domain of EF-Ts contacts domain I of EF-Tu, while the C-terminal domain contacts domain III of EF-Tu. In addition, the C-terminal motif, an α-helix at the C-terminus of EF-Ts, binds to domain I of EF-Tu near the nucleotide binding pocket (Kawashima et al., 1996). All of the conserved amino acids in EF-Ts that interact with EF-Tu in the EF-Tu•EF-Ts complex were subjected to substitution and subsequent biochemical analysis (Zhang et al., 1998). Each of these EF-Ts variants was impaired in its ability to bind EF-Tu, and most displayed reduced activity in stimulating nucleotide exchange in EF-Tu under equilibrium conditions. One interaction in the EF-Tu•EF-Ts complex that has received a lot of attention is $Phe81_{Ts}$, which penetrates between $His118_{Tu}$ and $His84_{Tu}$ of helix C and switch II. This interaction was proposed to cause a displacement of switch II, disrupt Mg^{2+} coordination in the nucleotide binding pocket of EF-Tu, and promote nucleotide dissociation (Kawashima et al., 1996). Consistent with this, substitution of $Phe81_{Ts}$ with alanine reduced the ability of EF-Ts to stimulate nucleotide exchange in EF-Tu (Zhang et al., 1998). Furthermore, substitution of $His118_{Tu}$ with alanine reduced the EF-Ts-stimulated nucleotide dissociation rates about 60 fold (Dahl et al., 2006). Adding to the list of potential nucleotide-destabilizing affects, structural changes were observed in the G-4 motif as well as in the P-loop of EF-Tu (Kawashima et al., 1996). These elements interact with the guanine base and β/γ-phosphates of bound GDP and GTP. It is difficult, however, to discriminate between cause and effect of nucleotide dissociation from the comparison of EF-Tu•nucleotide (reactant) and EF-Tu•EF-Ts (product) X-ray crystal structures. It is interesting to note that each amino acid substitution that has been found to affect EF-Ts-stimulated nucleotide dissociation has a relatively small effect (about 10-

fold) compared to the 60,000-fold stimulation of nucleotide dissociation. In comparison, removal of Mg^{2+} from the nucleotide-binding pocket, which may also be induced by EF-Ts binding, accelerates GDP dissociation only 150-300 fold (Gromadski et al., 2002). These results have led to the hypothesis that several interactions between EF-Tu and EF-Ts work synergistically to induce rapid nucleotide dissociation from EF-Tu (Dahl et al., 2006).

Elongation Factor Tu is the target of antibiotics

EF-Tu is the target of four different classes of antibiotics. Representative members from these classes are kirromycin, enacyloxin IIa, pulvomycin, and GE2270 A, which are reviewed in Parmeggiani and Nissen (2006). Both kirromycin and enacyloxin IIa share a binding site at the domain I/domain III interface, as shown in **Figure 1.6** (Parmeggiani et al., 2006b; Vogeley et al., 2001). The mode of action for these two antibiotics is to prevent the conformational change of EF-Tu from the 'on' to the 'off' state (Zuurmond et al., 1999). This results in an EF-Tu molecule bound at the ribosomal A-site in its 'on' conformation that will not release aa-tRNA for accommodation. This causes a roadblock in translation, as the A-site is no longer open to accept EF-G or other EF-Tu•GTP•aa-tRNA ternary complexes. The antibiotics pulvomycin and GE2279 A bind at the domain I/domain II interface, and the interface among all three domains of EF-Tu, respectively as shown in **Figure 1.6** (Parmeggiani et al., 2006a). These antibiotics prevent the stable binding of aa-tRNA, and thus reduce the concentration of EF-Tu•GTP•aa-tRNA in the cell (Anborgh and Parmeggiani, 1991; Wolf et al., 1974). All four classes of antibiotics either prevent aa-tRNA binding to or dissociation from EF-Tu. It is interesting to note that all four of the representative antibiotics discussed here

are synthesized by bacteria. Perhaps evolutionary pressures have been too strict to allow bacteria to synthesize antibiotics that act on EF-Tu•aa-tRNA interactions as well as explore antibiotics that inhibit the nucleotide exchange reaction on EF-Tu. Conversely, such antibiotics, which have not yet been identified, may exist in nature. An antibiotic that could prevent EF-Ts binding to EF-Tu, or slow EF-Ts-stimulated nucleotide dissociation from EF-Tu significantly, could be a potent antibacterial agent. Targeting the nucleotide exchange mechanism of EF-Tu by antibiotics is an attractive prospect given that the GEF for eEF1Bα is not homologous to EF-Ts and EF-Ts is essential in bacteria (Gerdes et al., 2003; Maessen et al., 1986). Thus, novel antibiotics targeting nucleotide exchange in EF-Tu have the potential to specifically target prokaryotes and not eukaryotes.

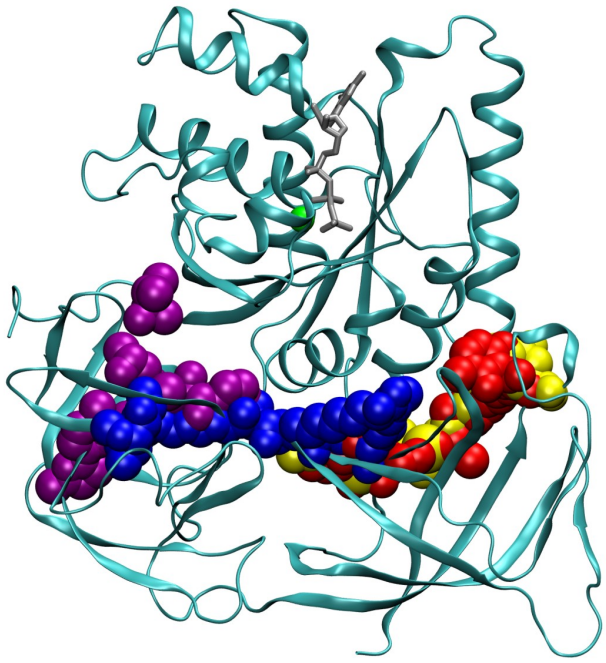

Figure 1.6. Location of antibiotic binding sites on EF-Tu. The binding sites of kirromycin (red), enacyloxin II a (yellow), pulvomuycin (blue), and GE 2270A (purple) are shown on EF-Tu based on superimpositions of EF-Tu•GDPNP (cyan, PDBID: 1EFT (Kjeldgaard et al., 1993)) with EF-Tu•GDP•kirromycin (PDBID: 1HA3 (Vogeley et al., 2001)), EF-Tu•GDPNP•enacyloxin IIa (PDBID: 2BVN (Parmeggiani et al., 2006b)), EF-Tu•GDNPN•pulvomycin (PDBID: 2C78 (Parmeggiani et al., 2006a)), and EF-Tu•GDPNP•GE2270A (PDBID: 2C77 (Parmeggiani et al., 2006a)).

In all, EF-Tu is an excellent model system for studying structural dynamics and intramolecular communication events. The wealth of structural and biochemical data on EF-Tu provides an ideal testing ground for hypotheses on this enzyme. The most attractive feature of EF-Tu towards studying structural dynamics is the variety of different signals to which EF-Tu must respond. The binding of GTP, GDP, EF-Ts, aa-tRNA, the ribosome, or several combinations thereof each has the potential to elicit different biochemical properties in EF-Tu. Since many of the different signals and properties have been studied biochemically and structurally in EF-Tu, it is now possible to begin to understand if these different signals are interrelated or how they are relayed in such a functionally diverse yet medium sized protein. Do these signals share common pathways or bottlenecks in EF-Tu? Alternatively, different signals may travel along mutually exclusive paths, each one subject to its own set of selection pressures. The answers to these types of questions likely require a time-resolved approach. Each binding partner seems to alter the conformation of EF-Tu, but these conformational changes occur as a function of time. Studying the structural dynamics of EF-Tu will provide valuable insight into how EF-Tu is 'wired' to perform a number of functions so efficiently.

1.3. Introduction to Molecular Dynamics

Molecular Dynamics (MD) involves simulation of the atomic motions in a given molecular system (Young, 2001a). Thus, MD has the ability to provide time-resolved information about molecular motion at atomic resolution. This is an attractive prospect in the field of biochemistry where protein function is often linked to conformational

changes (Tzeng and Kalodimos, 2012; Wolf-Watz et al., 2004). High-resolution structures available for many proteins and nucleic acids reveal snapshots of macromolecules in different conformations. These snapshots, however, fail to capture the time domain, which is fundamental in understanding the mechanisms that lead to conformational changes affecting protein function. However, the major caveat to MD is that it provides simulations not observations; MD should always be interpreted in the context of available experimental data.

MD comes in many flavours: different models can be used to represent molecular systems, and the forces driving atomic motion can be represented in different ways (Young, 2001a). Here the focus will be placed on the models used to conduct molecular dynamics simulations in this work. All-atom models of biomolecules are common in MD today, where each atom in the model is explicitly represented. These models make use of a 'balls and springs' approximation where each atom is treated as a mass, and the bonds behave as springs that hold the molecule together and influence atomic motions (MacKerell et al., 1998; Phillips et al., 2005). This is a gross approximation to a system in which molecular bonding is truly governed by electrons. A true quantum mechanical treatment of all but the smallest proteins, however, would be computationally expensive, if at all possible since computational time increases with the number of electrons in the molecule (EF-Tu, for example, has approximately 23,100 electrons).

An MD simulation is carried out in a stepwise manner (Young, 2001a). At each step (t) in the simulation, the net force acting on each atom in the molecular system is computed based on bonded and nonbonded interactions it participates in (*vide infra*). These forces are applied to their respective atoms over a defined time step (dt) based on Newton's

laws of motion to compute the position of each atom at time t+dt (Phillips et al., 2005). With new atomic coordinates the forces acting on each atom change and must be re-evaluated. Thus, the entire process is repeated iteratively with each round adding a new step to the simulation trajectory. In order to simulate bond vibrations accurately, the step size used in MD simulations must be on the order of femtoseconds (Young, 2001a). Many interesting motions within proteins such as loop movement and conformational changes, however, occur on the nanosecond to millisecond timescale (Benkovic and Hammes-Schiffer, 2003; Henzler-Wildman and Kern, 2007). In order to produce MD simulations that span timescales of nanoseconds to microseconds, millions or billions of steps must be computed. Reaching these timescales efficiently, therefore, requires that MD calculations be rapid (Phillips et al., 2005).

At the heart of an MD simulation is the ability to compute the potential energy of the molecular system (U) as a function of the atomic coordinates ($\vec{R}$). This is usually carried out using molecular mechanics: in the NAMD software package, this computation is performed based on **Equations 1.1-1.7** (Phillips et al., 2005).

$$U(\vec{R}) = U_{bond}(\vec{R}) + U_{angle}(\vec{R}) + U_{dihedral}(\vec{R}) + U_{improper}(\vec{R}) + U_{VdW}(\vec{R}) + U_{electrostatic}(\vec{R}) \quad (1.1)$$

$$U_{bond}(\vec{R}) = \sum_{bonds\ i} k_i^{bond}(r_i - r_{0i})^2 \quad (1.2)$$

$$U_{angle}(\vec{R}) = \sum_{angles\ i} k_i^{angle}(\theta_i - \theta_{0i})^2 \quad (1.3)$$

$$U_{dihedral}(\vec{R}) = \sum_{dihedrals\ i} k_i^{dihedral}\left[1 + \cos(n_i\phi_i - \gamma_i)\right] \quad (1.4)$$

$$U_{improper}(\vec{R}) = \sum_{impropers\ i} k_i^{improper}(\phi_i - \phi_{0i})^2 \quad (1.5)$$

$$U_{VdW}(\vec{R}) = \sum_i \sum_{j>i} 4\varepsilon_{ij}\left[\left(\frac{\sigma_{ij}}{r_{ij}}\right)^{12} - \left(\frac{\sigma_{ij}}{r_{ij}}\right)^{6}\right] \quad (1.6)$$

$$U_{electrostatic}(\vec{R}) = \sum_i \sum_{j>i} \frac{q_i q_j}{4\pi\varepsilon_0 r_{ij}} \quad (1.7)$$

The first four terms in the potential energy function (U_{bond}, U_{angle}, $U_{dihedral}$, and $U_{improper}$) represent interactions that are dependent on bonding within the molecular structure. Interactions between atoms that are separated by one, two, or three bonds are each computed by a different function (U_{bond}, U_{angle}, $U_{dihedral}$/$U_{improper}$, respectively). The $U_{improper}$ term represents out-of-plane bending in planar structures such as aromatic rings. The last two terms in the potential energy function represent the non-bonded interactions. These are the van der Waals energy, represented by the Lennard-Jones potential (**Equation 1.6**) and the Coulomb interaction energy (**Equation 1.7**). The minimum energy bonding distances, angles, and dihedrals (r_0, θ_0, and γ/φ_0 respectively); the spring constants (k^{bond}, k^{angle}, $k^{dihedral}$/$k^{improper}$); the multiplicity of each dihedral angle function (n_i); the Lennard-Jones parameters (σ_{ij}); and the atomic charges (q_i, q_j) are specific to atoms or atom combinations, and are contained in the molecular mechanics force field.

The force field is fundamental to all calculations in MD, and several different force fields are available (Duan et al., 2003; Foloppe and Mackerell, 2000; Oostenbrink et al.,

2004). Force field parameters are optimized in an iterative approach that relies on both experimental data and *ab initio* calculations (MacKerell et al., 1998). Initial estimates for parameters, equilibrium bond distances/angles and spring constants for example, are made based on available structures and vibrational data, respectively. Both structures and vibrational data can be obtained from *ab initio* calculations and wet-lab experiments. The initial force field is then used to perform calculations on a set of test molecules. These calculations include energy minimization of structures, the relative energy of conformers for a set of test molecules, and molecular vibrations. The results from these calculations are compared to *ab initio* and experimental data to assess the quality of the force field. The force field parameters are then adjusted and tested again until the test calculations are in satisfactory agreement with *ab initio* and experimental data.

The set of test molecules used and types of calculations performed during force field optimization will influence the utility of each force field. For example, force fields are not optimized against total energies computed from *ab initio* methods (MacKerell et al., 1998; Young, 2001b). Thus, molecular mechanics force fields will not compute energies comparable to *ab initio* calculations (Young, 2001b). One can, in principle, compute relative energies of similar molecular systems with some degree of accuracy assuming that the major errors associated with energy calculations cancel during comparison. In addition, the relative energies of some conformers are considered during force field optimization (MacKerell et al., 1998). Examples of comparisons between different molecular systems can be found in Eargle *et al.* (2008) and Pyrkosz *et al.* (2010). It is difficult to predict the error associated with energy comparisons, however, and comparisons should be made to available experimental data. The major purpose of MD is

not to compute energy; the intent is to simulate molecular motions. The motion of each atom in the system is computed based on the forces acting on it. These forces are obtained by differentiating the potential energy function with respect to atomic coordinates.

Over the last four decades, studies in molecular dynamics have progressed from simulations shorter than ten picoseconds (McCammon et al., 1977) to simulations that, for the privileged few, peer into the microsecond realm (Dror et al., 2011; Freddolino et al., 2008). This progression has been made possible by significant advancement in both computer hardware and software. Today, the majority of MD simulations published are on the order of tens of nanoseconds in length. The majority of biochemical experiments, on the other hand, are carried out on the timescale of milliseconds to minutes. This leaves a disparity between biochemical experiments and MD simulations. To overcome this disparity, some groups perform MD simulations using simplified models and/or include additional forces to accelerate simulations as in Whitford *et al*. (2010). A few studies have shown that some enzyme functions occurring on the millisecond to second timescale are dominated by faster (picosecond to millisecond) fluctuations within the proteins (Carroll et al., 2012; Henzler-Wildman et al., 2007). These studies make use of NMR to measure fast-timescale fluctuations within the protein. Comparison of NMR data and MD simulations has shown that backbone dynamics simulated by MD agree well with the picosecond/nanosecond fluctuations measured in NMR (Henzler-Wildman et al., 2007). Thus, MD can potentially provide insight into how protein dynamics correlate with protein function *in vitro* or even, *in vivo* (Henzler-Wildman et al., 2007; Levin et al., 2012; Whitford et al., 2010; Wieden et al., 2010).

At this point it becomes necessary to define the term ‘structural dynamics’. In this work, structural dynamics refers to time-dependent atomic motions within a structure. Conversely, a conformational change refers to the process of a molecule moving from one energy basin to another on a potential energy surface; each energy basin representing a distinct global conformation of the same molecule. For comparison, a conformational change in real-time is dependent on structural dynamics: atomic motions are required for the molecule to move from point A to point B on the potential energy surface. Structural dynamics, however, do not necessarily refer to a conformational change. In this context, structural dynamics can refer to sidechain rotations or small loop motions that correspond to different sub-conformations within the same energy basin.

Recent studies on allosteric regulation, which occurs on timescales similar to those of conformational change (Benkovic and Hammes-Schiffer, 2003), have yielded intriguing methods for studying structural dynamics. These methods involve constructing a network model to describe the protein (Gasper et al., 2012; Ma et al., 2012; Sethi et al., 2009). In the study of allostery, a network can describe how allosteric ligand binding at one site can elicit a signal that travels through the protein to the active site. The goal of constructing these networks was to describe the path traveled by the allosteric signal from input (allosteric binding site) to output (active site). The three-dimensional structure of a protein certainly contributes to shaping the topology of the corresponding network, but structural dynamics are likely involved given the timescale of allosteric regulation (microsecond to second), (Benkovic and Hammes-Schiffer, 2003). Some allosteric network models have incorporated structural dynamics based on short MD simulations (Dhulesia et al., 2008; Gasper et al., 2012; Ma et al., 2012; Sethi et al., 2009). This

approach to understanding structural dynamics holds a lot of promise for understanding the nature and timescale of the signals being transmitted through an allosteric network. This knowledge will significantly contribute to our understanding of the underlying structural principles in protein biochemistry.

MD simulations and X-ray crystallography provide complementary data towards investigating protein biochemistry. High-resolution structures provide essential starting points for structural studies, but provide limited dynamic information. An X-ray crystal structure will always favour the most populated protein conformation(s) in the crystal environment, but this conformation may not be the most insightful for the biochemist (Fraser et al., 2011; Wieden et al., 2010). As an example, biochemical reactions proceed along a reaction coordinate from reactants to products and important structural features may form or break throughout the course of a reaction. If these structural features are not present in the reactant or product state, they are not likely to be revealed by X-ray crystallography which likely favours the local minima (reactant or products) on the potential energy surface. MD can complement these structures by accessing sparsely populated conformations through simulation (Whitford et al., 2011). Within a protein, loop motions and sidechain rotations generally occur on the picosecond to nanosecond timescale (Henzler-Wildman and Kern, 2007; Wolf-Watz et al., 2004). These are the motions that will be tractable on the average MD timescale. MD simulations in the nanosecond range can, therefore, provide insight into which sidechain rotamers and loop conformations within a protein are accessible, but might not be represented in available X-ray crystal structures. Since MD simulations provide models of structural dynamics, they should be carefully interpreted in the context of the experimental data available.

Molecular dynamics simulations of EF-Tu have been reported previously. These studies reported on thermostability of the G-domain (Melchionna et al., 2006); a potential binding site for tetracycline (Aleksandrov and Simonson, 2008); comparison of structural dynamics in EF-Tu•GTP•aa-tRNA and EF-G (Kulczycka et al., 2011); and the stability of aa-tRNA bound to EF-Tu•GTP (Eargle et al., 2008). In addition, molecular dynamics were used to assist in modeling transition states for GTP hydrolysis on EF-Tu in the absence of the ribosome (Grigorenko et al., 2008), and fitting a model of EF-Tu into a single particle cryo-EM reconstruction of EF-Tu bound to the ribosome (Villa et al., 2009). In this work, **Chapters 2 and 4** will focus on the structural dynamics of EF-Ts catalyzed nucleotide exchange in EF-Tu. **Chapter 3** will investigate how the structural dynamics of the P-loop mediate nucleotide-binding properties of EF-Tu. Finally, **Chapter 5** will investigate an intraprotein communication network in EF-Tu that contributes to GTPase activation on the ribosome. In each chapter, MD simulations of EF-Tu are presented alongside simulations of other EF-Tu variants to allow direct comparison of structural dynamics on the nanosecond timescale. In addition, results from kinetics studies utilizing the same EF-Tu variants *in vitro* are reported to allow comparison of EF-Tu function on the timescale of milliseconds to minutes.

Objective

In order to provide insight into the structural dynamics that underlie functions of EF-Tu, differences in simulated dynamics are correlated with functional differences between enzyme variants. This approach helps elucidate the functional design of EF-Tu at atomic resolution.

Chapter 2

A combined molecular dynamics and rapid kinetics approach to identify conserved three-dimensional communication networks in Elongation Factor Tu

Reprinted with permission from

"A combined molecular dynamics and rapid kinetics approach to identify conserved three-dimensional communication networks in Elongation Factor Tu."

Biophysical Journal. **2010**. *11*, 3735-3743.

Hans-Joachim Wieden, Evan Mercier, John Gray, Brett Steed, Davis Yawney

Copyright 2010, Elsevier Limited

2.1 Foreword

The following chapter is a manuscript in the form in which it was accepted for publication in Biophysical Journal (2010). This manuscript was written by Hans-Joachim Wieden, Professor of Biochemistry at the University of Lethbridge and supervisor of this dissertation. I, Evan Mercier, coauthor of this published manuscript, generated and analyzed data therein, constructed figures, and assisted in writing and revising the written work. All of the (*in vitro*) biochemical experiments presented in this work were performed by Brett Steed, Davis Yawney, and Hans-Joachim Wieden. I constructed all *in silico* models, performed all MD simulations, and analyzed all of the MD data in this publication.

Structural studies have a significant impact on the field of biochemistry. Not only do they provide three-dimensional structures of biomolecules such as proteins, they enable researchers to extend the range of their hypotheses. With structures now available for many enzymes, studying point mutations *in vitro* or *in vivo* can lead to reasonable hypotheses about specific roles of particular amino acids in enzyme function. In concert with three-dimensional structures, biochemical assays of enzymes and their variants can provide significant insight into the role of many amino acids within the protein. In line with this idea, X-ray crystallography provides invaluable guidance for developing new testable hypotheses regarding the role of specific amino acids. However, this type of structural information provides limited dynamic information about proteins, and protein dynamics are often critical for function (Tzeng and Kalodimos, 2012; Wolf-Watz et al., 2004).

In the following chapter, all-atom models of *Escherichia coli* (*E. coli*) EF-Tu•GTP and EF-Tu•GDP were constructed based on available 3-dimensional structures (Kjeldgaard et al., 1993; Song et al., 1999). These models were each used to generate 10 ns MD simulations of the protein•nucleotide complexes in aqueous environments. Analysis of these simulations revealed that among the vibrations within the protein, the sidechain of $Asp109_{Tu}$ underwent multiple reorientations and formed a transient hydrogen bond with the adjacent sidechain of $His22_{Tu}$ in the P-loop. This was an interesting finding since the crystal structure of the EF-Tu•EF-Ts complex revealed a contact between the sidechain of the conserved $Arg12_{Ts}$, and the backbone carbonyl of $Asp109_{Tu}$, in addition to a conformational change in the P-loop (Kawashima et al., 1996). Identification of this hydrogen bond led to the hypothesis that the highly conserved $Arg12_{Ts}$ communicates with the P-loop of EF-Tu during the EF-Ts-catalyzed nucleotide exchange mechanism. The *in vitro* experiments presented in the following manuscript confirm that $Asp109_{Tu}$ contributes significantly to EF-Ts-catalyzed GDP dissociation from EF-Tu. Identification of a previously unknown $Arg12_{Ts}$•••$Asp109_{Tu}$•••$His22_{Tu}$ hydrogen-bonding network that potentially relays a signal from EF-Ts to the P-loop of EF-Tu relied on simulating the dynamic properties of EF-Tu with MD.

In order to characterize the transient hydrogen bond between $Asp109_{Tu}$ and $His22_{Tu}$, inspiration was drawn from single-molecule fluorescence microscopy (Cornish et al., 2009; Uphoff et al., 2010). The $N\text{-}H_{His22}$•••O_{Asp109} distances were measured over the course of each MD simulation and plotted as histograms to reveal both hydrogen-bonding and non-hydrogen-bonding populations. Fitting the histograms to Gaussian functions allowed for statistical analysis of the populations: average hydrogen bonding distances

and associated errors were computed in addition to the probability of hydrogen bond formation during each simulation. This approach proved to be a useful tool for analyzing metrics such as interaction distances or energies and is used throughout the work presented in this dissertation. One of the major advantages to this method of analyzing MD data is the focus on understanding the distribution of measured values. It is evident from the histograms in **Figure 2.2** that a mean $N\text{-}H_{His22}\bullet\bullet\bullet O_{Asp109}$ distance would be a poor representation of this hydrogen bond. In addition, the hydrogen-bonding distribution gives a clear description of the variance for the hydrogen-bonding distance during the MD simulation. The authors are not aware of this statistical approach being used in the analysis of MD simulations prior to the publication of this manuscript as most analyses focus exclusively on the time dependence of such metrics. Developing this analysis, therefore, represents a significant contribution to the field of molecular dynamics.

The *in vitro* results in this manuscript describe the rate constants for the complete kinetic mechanism of nucleotide exchange in wild type and $EF\text{-}Tu_{D109A}$. Using these rate constants, the relative activation barriers for several steps in the mechanism were compared. The slower EF-Ts-stimulated GDP dissociation from $EF\text{-}Tu_{D109A}$ compared to wild type is consistent with destabilization of the $[EF\text{-}Ts\bullet EF\text{-}Tu\bullet\bullet\bullet GDP]^{\ddagger}$ transition state upon D109A substitution, as depicted in **Figure 2.6**. The magnitude of this destabilization is consistent with the loss of a single hydrogen bond. Thus, it seems likely that an $Asp109_{Tu}\bullet\bullet\bullet His22_{Tu}$ hydrogen bond is involved in stabilization of the $[EF\text{-}Ts\bullet EF\text{-}Tu\bullet\bullet\bullet GDP]^{\ddagger}$ transition state. Since transition states are fleeting, they do not lend themselves to direct structural studies. The ability to make an informed hypothesis

about a transition state structure speaks to the power of combining *in vitro* experiments and MD simulations.

This study indentifies a conserved hydrogen bond in bacterial EF-Tu that likely contributes to EF-Ts-catalyzed GDP dissociation. This dissociation process is critical in all bacterial cells and is required to efficiently recycle EF-Tu•GTP for protein synthesis (Baba et al., 2006; Gerdes et al., 2003; Gromadski et al., 2002; Weissbach et al., 1970). As such, understanding the structural dynamics of how this process occurs is of significant interest to the scientific community. Given the high conservation of many amino acids in EF-Tu (DeLaurentiis et al., 2011) and the multitude of binding partners it communicates with, it is interesting to learn more about the role of specific amino acids within this protein. As more signal inputs, outputs, and interconnecting paths are identified, the 'communication map' within EF-Tu will become clearer. This map will contain interesting fundamental information about communication networks in general and shed light on the design principles underlying EF-Tu's functions. Understanding intramolecular signal communication in EF-Tu is particularly interesting since EF-Tu is the target of several antibiotics. The communication pathways identified in EF-Tu that regulate essential functions may be useful targets for novel antibiotics. The region surrounding $Asp109_{Tu}$ is of particular interest since this region is shown (in this chapter) to contribute to nucleotide exchange, and is not conserved in the eukaryotic homologue of EF-Tu (eEF1A). Thus, nucleotide exchange may prove to be an attractive target for new antibiotics in the future.

2.2 Introduction

During the elongation phase of translation, codon-dependent aminoacyl (aa)-tRNA delivery to the ribosome is catalyzed by Elongation Factor (EF) Tu in bacteria. The bound GTP is hydrolyzed upon correct codon-anticodon interaction in the ribosomal A-site. EF-Tu then undergoes a large conformational change into the inactive GDP-bound form of the factor, releasing the bound aa-tRNA, and dissociating from the ribosome. EF-Tu•GDP must be recycled from the inactive GDP-bound form to the active GTP complex before it can bind another aa-tRNA and enter the next cycle of elongation. However, the intrinsic rate of nucleotide exchange is too slow to sustain efficient protein synthesis observed *in vivo*. To overcome the tight binding of the GDP-nucleotide and to facilitate rapid nucleotide exchange, regeneration of EF-Tu•GTP is catalyzed by the nucleotide exchange factor EF-Ts. EF-Tu•GDP binds EF-Ts to form an unstable ternary complex that rapidly dissociates into EF-Tu•EF-Ts and GDP. Following GTP binding and the subsequent dissociation of EF-Ts from EF-Tu, EF-Tu•GTP binds another aa-tRNA and delivers it to the ribosome. All of the interactions between EF-Tu, EF-Ts and guanine nucleotides are reversible and occur in a steady-state environment *in vivo* (Dahl et al., 2006; Gromadski et al., 2002).

The crystal structure of the EF-Tu•EF-Ts complex (Kawashima et al., 1996) suggested that EF-Ts catalyzes nucleotide release by altering at least three of the crucial binding interactions between EF-Tu and guanine nucleotides. These crucial elements, common among GTPases, are: i) the conserved NKxD motif (residues 135-138, *E. coli* numbering) that binds the guanine base, ii) the bound magnesium ion that coordinates the β- and γ-phosphates, stabilizing their negative charges, iii) the P-loop containing the consensus

element GxxxGK(S/T) (residues 18-25) which coordinates the β-phosphate of the bound nucleotide. Previous analysis using rapid kinetic techniques revealed a 60,000-fold increase in the dissociation rate of GDP from the ternary complex EF-Tu•GDP•EF-Ts as compared to EF-Tu•GDP (Gromadski et al., 2002). Several aspects contributing to the mechanism of nucleotide exchange have been studied through a combination of mutational and kinetic analyses mainly based on molecular interactions identified in the structure of the binary EF-Tu•EF-Ts complex. These studies suggest a concerted process in which the interaction between the three major nucleotide interaction sites (including the phosphate and base moieties) are altered in a well coordinated fashion involving communication between these sites to achieve efficient dissociation of GDP (Dahl et al., 2006; Gromadski et al., 2002; Wieden et al., 2002). Although critical for efficient EF-Ts catalyzed nucleotide exchange in EF-Tu, nothing is known about how this coupling is achieved, requiring communication over more than 20 Å and involving amino acids separated by over 100 amino acids in the primary sequence of the protein. Experimental and computational studies of many protein/protein and protein/nucleic acid complexes strongly support the view that conformational transitions in these complexes are communicated by a 3-dimensional network of interresidue contacts (Boehr, 2009; Boehr et al., 2009; Eisenmesser et al., 2005; Sethi et al., 2009). Identification of the amino acids involved in this communication network is particularly difficult since this is a dynamic feature involving so called second-shell residues, which do not directly participate in interactions with the respective substrates like the nucleotide and EF-Ts in the case of EF-Tu. Nevertheless, these second-shell residues have been shown to be critical for the function and specificity of a number of enzymes due to their role in positioning of

catalytically active residues (Röthlisberger et al., 2008) or in providing critical flexibility to secondary structure elements involved in the respective reaction (Drawz et al., 2009; Tomatis et al., 2005). In order to identify second shell residues that participate in the 3-dimensional communications network, evolutionary conservation can provide valuable information (Gaucher et al., 2002; Gaucher et al., 2001).

Here we report a prime example of how a combined theoretical and experimental approach can be used to successfully identify and study these 3D communication networks. Previous studies reported slow evolutionary speeds for both $Asp109_{Tu}$ and $Glu152_{Tu}$ (Gaucher et al., 2002; Gaucher et al., 2001), where the latter is involved in a functionally important salt bridge with the N-terminal domain of EF-Ts and the former seems not to participate in any interactions with either EF-Tu or EF-Ts; these observations suggest an unknown functional role of the $Asp109_{Tu}$ side chain during the nucleotide exchange reaction that is specific for the bacterial protein. Our own molecular dynamics simulations of the EF-Tu•GDP and EF-Tu•GTP complex revealed that a transient hydrogen bond can be formed between the aspartate residue at position 109 and a residue in the P-loop, $His22_{Tu}$. The subsequent detailed kinetic analysis of an aspartate 109 to alanine substitution in EF-Tu revealed a functional role of this aspartate side chain specific for EF-Ts stimulated GDP but not for GTP dissociation. This is the first report of an MD guided design of EF-Tu mutants and is aimed at the identification of the functional role of second-shell residues that are members of the 3D communication network involved in the catalytic mechanism of nucleotide exchange in EF-Tu. In summary, combining the analysis of the dynamic properties of EF-Tu *in silico* with the rapid kinetic analysis *in vitro,* our results indicate an important role of $Asp109_{Tu}$ during

the nucleotide exchange reaction by stabilizing the EF-Tu•GDP•EF-Ts$^{\neq}$ transition state and linking the interactions of EF-Ts with the base side and the phosphate side in EF-Tu. These interactions seem to be specific for the acceleration of GDP dissociation in bacteria but not in eukaryotes.

2.3 Material and Methods

Molecular Dynamics Simulations

The initial model for *E. coli* EF-Tu in the GTP-bound conformation was obtained by constructing a homology model using the Swiss-Model server (Schwede et al., 2003) and the crystal structure of *T. aquaticus* EF-Tu•GDPNP as a template (PDB-ID: 1EFT). Transformation of the GDPNP molecule to GTP was done by hand. The model for *E. coli* EF-Tu in the GDP-bound conformation was obtained from the respective crystal structure (PDB-ID: 1EFC). As the 7 N-terminal residues were missing in this structure, conformations of these amino acids were assigned identically to those in the GTP-bound model. Hydrogen atoms were added to both models using psfgen in the NAMD software package (Phillips et al., 2005), and histidine sidechains were protonated at the ε-nitrogen only. Initial models were minimized in vacuum and then placed in a water box extending at least 10 Å from the protein in all directions. Water molecules present in the respective crystal structures were included in this box while all other water molecules were added at random using the Solvate package in NAMD (Phillips et al., 2005). Relaxation of the solvated system was achieved by minimizing the positions of water molecules, followed by protein and ligand atoms in two iterative rounds. Each of these minimizations was carried out for 10,000 steps. Following unconstrained minimization, sodium ions were

then added in random positions by the Autoionize package in VMD (Humphrey et al., 1996) to neutralize the total charge of the system. Finally, an all-atoms minimization was carried out until no change in energy was observed over 1,000 steps. All minimizations were performed using the NAMD software package. Molecular dynamics simulations were performed on solvated models with a step size of 0.5 fs using the CHARMM22 force field as implemented in the NAMD package (Phillips et al., 2005) while invoking periodic boundary conditions. Minimized models were initially equilibrated at 300 K and 350 K for 150 ps at constant pressure (1 atm). Production phase simulations were performed after crossing trajectories and were carried out for 10 ns. All simulations were performed in the NAMD software package, and visualization was carried out in VMD (Humphrey et al., 1996; Phillips et al., 2005). NAMD and VMD were developed by the Theoretical and Computational Biophysics Group in the Beckman Institute for Advanced Science and Technology at the University of Illinois at Urbana-Champaign.

Analysis of MD simulations was performed using data sampled every 0.5 ps. Calculations of RMSD and RMSF were performed using in-house scripts invoked with the VMD software package (Humphrey et al., 1996). For the RMSD calculations the first 10 N-terminal amino acids were excluded due to the high level of mobility exhibited throughout all simulations, consistent with the respective crystallographic studies in which the N-terminal amino acids were either not resolved or exhibited particularly large B-factors.

To assess whether hydrogen bond formation can occur between the side chains of $Asp109_{Tu}$ and $His22_{Tu}$, the distance between the two carboxylate oxygens ($O^{\alpha/\beta}$) of the aspartate side chain and the proton at the N^{ε} of the histidine residue were measured over

the last 5 ns of each simulation. Each oxygen atom of the carboxylate sidechain on $Asp109_{Tu}$ was considered independently. Histograms were generated from the $O^{\alpha/\beta}{}_{Asp}$•••H-$N^{\varepsilon}{}_{His}$ distances measured by subsequent binning using a 0.25 Å bin size and were plotted at the bin midpoint. For both simulations a bimodal distribution of counts was observed. To deconvolve the contribution of each state (mode), the data were fitted with a sum of two Gaussian functions (**Equation 2.1**) using the Table Curve (Jandel Scientific) and Prism (GraphPad) software packages, where A and D represent amplitudes of the first and second Gaussian functions, respectively; B and E represent the mean O•••H distances for the two functions; and C and F represent the distribution in O•••H distance around the respective mean distance.

$$g(x) = \mathrm{A}e^{\frac{-(x-\mathrm{B})^2}{2\mathrm{C}^2}} + \mathrm{D}e^{\frac{-(x-\mathrm{E})^2}{2\mathrm{F}^2}} \quad (2.1)$$

The occupancy of each hydrogen-bonded state was determined by integrating the Gaussian centered on 2 Å over the interval (-∞,∞) and expressing it as a percentage of the sum of both Gaussians integrated over the same interval.

Buffers and Reagents

Experiments were performed in buffer A (50 mM Tris-HCl, pH 7.5, 70 mM NH_4Cl, 30 mM KCl, 7 mM $MgCl_2$) at 20 °C. Chemicals were purchased from Sigma or VWR. Fluorescent mant-GDP and mant-GTP were from Molecular Probes (Oregon).

Mutagenesis - The plasmid pEECAHis (Wieden et al., 2002) containing the full-length *E. coli tufA* gene was obtained from M. V. Rodnina (Witten, Germany). The Quikchange™ method was then used for site-directed mutagenesis. Mutations were verified by sequencing.

Protein expression, purification and complex formation

Protein expression, purification and complex formation were performed similar to Gromadski *et al*. (Gromadski et al., 2002) and are described in the Materials and Methods section of **Appendix 1**.

Rapid Kinetic Measurements

Fluorescence stopped-flow measurements were performed on a KinTek SF-2004 stopped-flow instrument. Tryptophan fluorescence was excited at 280 nm and measured after passing a WG-305-F filter (Newport Filters). Mant-GDP/GTP fluorescence was excited indirectly using Fluorescence Resonance Energy Transfer (FRET) from the single tryptophan residue proximal to the nucleotide-binding site. Mant-GDP/GTP fluorescence was measured after passing a LG-400-F filter (Newport Filters). Experiments were carried out at 20 °C in buffer A by rapidly mixing equal volumes (25 µl each) of reactants and monitoring the time courses of the fluorescence change. Fluorescence time courses were evaluated by fitting to an exponential function with the characteristic apparent time constant (k_{app}), the amplitude (A), and the final signal (F_∞) according to **Equation 2.2**.

$$F = F_\infty + Ae^{-k_{app} \cdot t} \quad (2.2)$$

where F is the fluorescence at time t. Calculations were performed using TableCurve software (Jandel Scientific) and Prism (GraphPad Software). Standard deviations of k_{app} values were calculated using the same software. All elementary rate constants of nucleotide exchange except k_{-2} were measured directly. The value for k_{-2} was calculated from all other elementary rate constants based on the kinetic scheme depicted in **Scheme 2.1**. Standard deviations of the rate constants were estimated from the variation of values obtained in different experiments.

Calculation of k_{-2} for EF-Tu_{wt}, EF-Tu_{D109A} and EF-Tu_{E152A}

Calculation of k_{-2} was performed similarly to Gromadski *et al*. (2002) using the law of mass action. Based on the mechanism in **Scheme 2.1**, the rate constants k_{-2} were calculated from rate constants of the right, the GDP branch, [$k_{-2} = k_{-1}k_2k_{-3}k_4/(k_1k_3k_{-4})$] and left, the GTP branch, [$k_{-2} = k_{-5}k_2k_{-6}k_7/(k_5k_6k_{-7})$], yielding two independently calculated values for k_{-2}.

2.4 Results

Asp109 forms a transient hydrogen bond to His22

The observation that the aspartate side chain in position 109 of EF-Tu from *E. coli* is conserved in more than 99% of the bacterial EF-Tu sequences found in the SWISSPROT database suggests a functional requirement of aspartate at this position. However, inspection of the available crystal structures of EF-Tu bound to the respective nucleotide (GDP and GTP) as well as to its exchange factor (EF-Ts) did not reveal any direct interactions involving the $Asp109_{Tu}$ side chain. Interestingly the main chain oxygen of $Asp109_{Tu}$ participates in a hydrogen bond interaction with the side chain of the invariant arginine (Arg) in position 12 of EF-Ts, linking it with the equally conserved $Glu152_{Tu}$ in helix D of EF-Tu, which has previously been shown to be important for efficient EF-Ts-catalyzed nucleotide exchange (Wieden et al., 2002; Zhang et al., 1998). These observations suggest a role of the $Asp109_{Tu}$ side chain during a phase in the nucleotide exchange reaction that has not been trapped using X-ray crystallography. This most likely involves a highly dynamic transient intermediate, not accessible by crystallographic methods, such as the ternary complexes EF-Tu•GDP•EF-Ts and EF-Tu•GTP•EF-Ts or

their respective transition states (**Scheme 2.1**). We wanted to address the functional role of $Asp109_{Tu}$ by combining molecular dynamics simulations to describe the dynamic properties of the Asp side chain *in silico* with the subsequent analysis of the mechanistic role using rapid kinetics *in vitro*. In order to study the dynamic properties of $Asp109_{Tu}$ by molecular dynamics simulations and to circumvent effects due to sequence variations in the different organisms used for the determination of the respective X-ray structures, we have constructed two full-length structural models of *E. coli* EF-Tu in complex with GTP and GDP using homology modeling, followed by hydration with explicit waters and subsequent energy minimization. Inspection of these models revealed that the side chain of $Asp109_{Tu}$ is in close proximity to $His22_{Tu}$, which would be capable of accepting a hydrogen bond from one of the carboxylate oxygens of $Asp109_{Tu}$. However, in these energy minimized static models, the side chain of $Asp109_{Tu}$ is oriented in such a way that participation in a hydrogen bonding interaction is prevented. This is surprising since this hydrogen bond could be established through a few minor bond rotations, consistent with an evolutionarily conserved role of $Asp109_{Tu}$ as a hydrogen bond acceptor. We wanted to know if under more physiological conditions, which also take into account the overall dynamic properties of the enzyme in water, this hydrogen bond could indeed be formed in EF-Tu, thus providing an explanation for the high degree of conservation of $Asp109_{Tu}$.

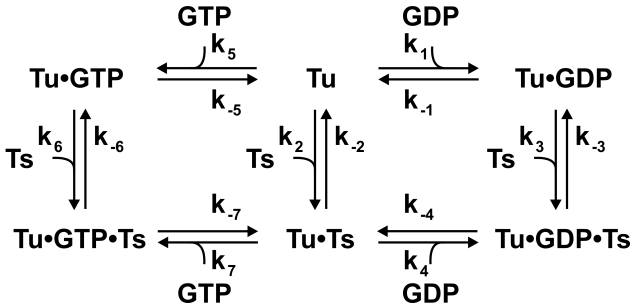

Scheme 2.1. Kinetic scheme of nucleotide exchange in EF-Tu

To address this question we performed, based on these models, 10 ns long MD simulations of the wild type enzyme and an *in silico* mutant carrying an alanine substitution at position 109 (EF-Tu$_{D109A}$), bound to GTP or GDP, at 300 K. The stability of EF-Tu during these simulations was judged by measuring the Root Mean Squared Deviation (RMSD) of the backbone atoms with respect to the initial structure throughout the whole simulation (**Figure 2.1.A** and **A.3**). All four simulations were stable after 2 ns following an initial increase in the RMSD of ~1.5 Å, yielding 8 ns of stable simulation time. When, both for the mutant and for the wild type, GDP-bound complexes were compared to the corresponding GTP-bound complexes, the two GDP-bound complexes exhibited slightly larger fluctuations in RMSD (**Figure 2.1.A**), in agreement with the more open conformation of EF-Tu•GDP, which provides less intramolecular stabilization compared to the EF-Tu•GTP complexes (**Figure A.1.2**).

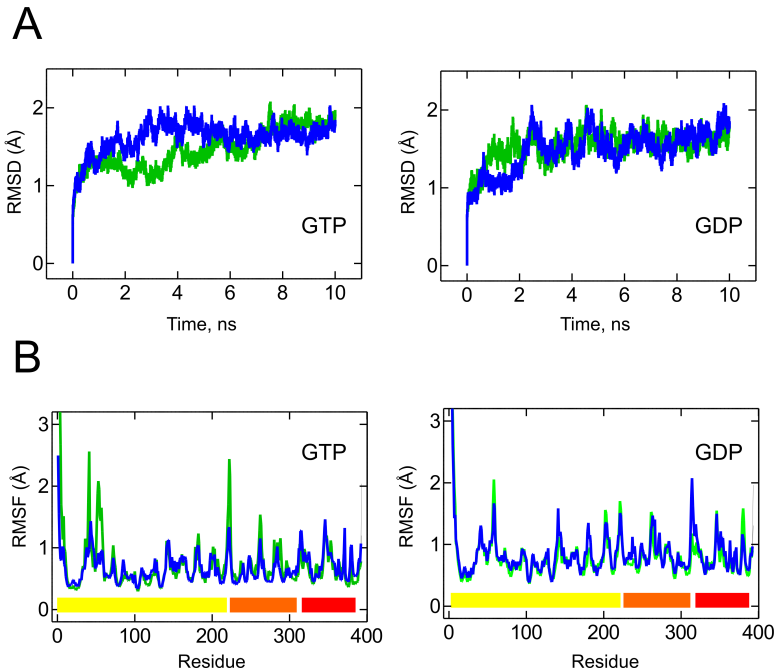

Figure 2.1. Conformational changes during MD simulation. (A) RMSDs of EF-Tu$_{wt}$ (green) and EF-Tu$_{D109A}$ (blue) from the starting conformation for the GTP and GDP conformations at 300 K. RMSDs were calculated using all backbone atoms and excluded the mobile N-terminus. (B) Cα RMSF for EF-Tu$_{wt}$ (green) and EF-Tu$_{D109A}$ (blue) in the GTP and GDP conformations. Colored bars in the bottom indicate the domain structure of the protein (Domains 1-3 in yellow, orange and red, respectively).

Interestingly, when comparing the Root Mean Square Fluctuation (RMSF) of each Cα in domain I of EF-Tu (**Figure 2.1.B**) between the wild type and the D109A mutant simulations, no significant increase in flexibility was observed for the P-loop including $His22_{Tu}$ in either the GTP- or the GDP-bound state, indicating that the aspartate side chain is not required for its stability in these complexes. However both complexes displayed lower RMSF values (decreased flexibility) for the majority of switch I residues (44 to 69) in the EF-Tu_{D109A} simulations, as well as consistently higher values (increased flexibility) for the N-terminal half of helix D (139 to 144) and the preceding nucleotide specificity motif (NKxD, 135 to 138) which is slightly more pronounced in the GDP complex (**Figure 2.1.B**).

In order to investigate if a transient hydrogen bond can form between $Asp109_{Tu}$ and $His22_{Tu}$ we monitored the $O^{\alpha/\beta}{}_{Asp}$•••H-$N^{\varepsilon}{}_{His}$ distance over 5 ns of the simulation (from 5-10 ns). The distances between the acidic hydrogen on $His22_{Tu}$ and both carboxylate oxygens of $Asp109_{Tu}$ ($O^{\alpha/\beta}{}_{Asp}$) were measured in the GDP- and GTP- bound simulations and plotted as histograms (**Figure 2.2**). The $O^{\alpha/\beta}{}_{Asp}$•••H-$N^{\varepsilon}{}_{His}$ distances observed exhibited a bimodal distribution with the first mode centered over 2 Å and the second over 4 Å. This suggests that two major states exist for the interactions between these two side chains. Based on the frequently applied distance criterion for assigning a hydrogen bond of < 3.5 Å for the O•••H distance (Andersen and Rost, 2009), we believe that the distribution at small $O^{\alpha/\beta}{}_{Asp}$•••$H^{\varepsilon}{}_{His}$ distances represents a population of conformations in which $Asp109_{Tu}$ and $His22_{Tu}$ are engaged in hydrogen bonding with each other. Thus, the population at longer O_{Asp}•••H_{His} distances and centered over 4 Å may represent non-hydrogen bonding conformations. This is supported by the observation that the

distributions representing hydrogen bonding conformations have mean $O^{\alpha/\beta}_{Asp}$•••H_{His} distances ranging from 2.1-2.3 Å. These distances are well below the more conservative cut-off distance for hydrogen bonding of 2.7 Å (sum of van der Waals radii for hydrogen and oxygen). In order to deconvolve the partitioning between each state and to provide a means for estimating the relative contribution of hydrogen bonding conformations at physiological temperatures (300 K), we have fit these histograms to functions with two Gaussian terms (**Figure 2.2.A & B**). In fact, depending on the respective oxygen (a or b) and simulation (GDP- or GTP-bound state), between 81.6% and 97.5% of the hydrogen bonding states (first mode) fall below the 2.7 Å cut-off. When compared to the non-hydrogen bonding state (second mode), considering both carboxylate oxygens of $Asp109_{Tu}$, $EF\text{-}Tu_{wt}$ exists in the hydrogen bonding states during 19.6% (GTP) or 30.5% (GDP) of the analyzed simulation. On the basis of these MD simulations it is likely that EF-Tu is indeed capable of forming an intramolecular hydrogen bond between $Asp109_{Tu}$ and $His22_{Tu}$, and that this hydrogen bond contributes significantly to the dynamics of the protein at 300 K. The fact that the hydrogen-bound state is only sampled between 20% and 30% of the simulation time suggests a minor functional role in these binary complexes. Together with the evolutionary conservation of $Asp109_{Tu}$, it is likely that the hydrogen-bound state contributes more significantly to one of the other complexes formed during the functional cycle of EF-Tu, e.g. the EF-Ts-catalyzed nucleotide exchange (**Scheme 2.1**). Together with the similar level of conservation of the functionally important $Glu152_{Tu}$ in helix D of EF-Tu, the hydrogen bond between $His22_{Tu}$ and $Asp109_{Tu}$ might be important for the three-dimensional communication

network in the two ternary complexes EF-Tu•GDP•EF-Ts / EF-Tu•GTP•EF-Ts, transiently formed during EF-Ts-catalyzed nucleotide exchange.

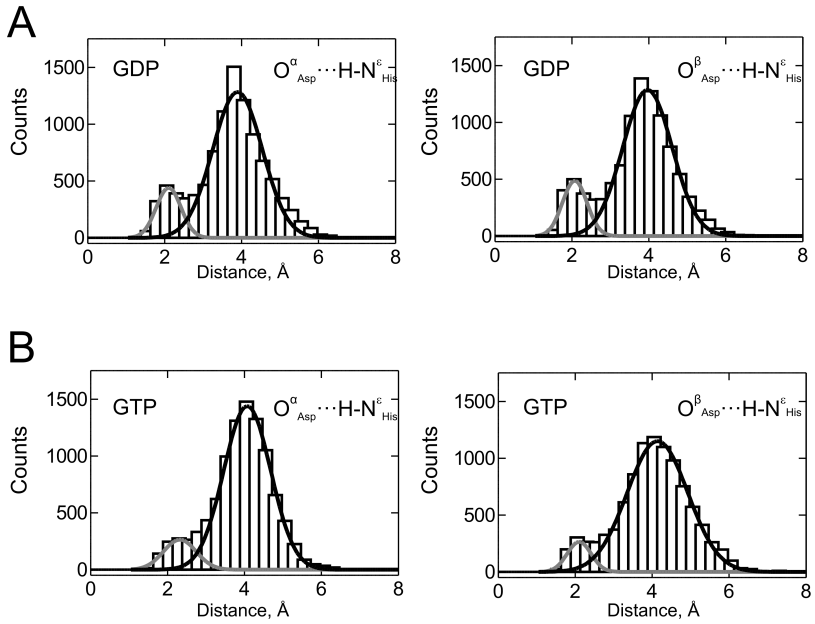

Figure 2.2. Hydrogen bonding between $Asp109_{Tu}$ and $His22_{Tu}$. Distances between the two terminal oxygen atoms (O^{α} and O^{β}) of the $Asp109_{Tu}$ residue and the hydrogen at the N^{ε} of $His22_{Tu}$ were measured during the second half of MD simulations (ns 5 - 10) for the EF-Tu_{wt}•GDP and EF-Tu_{wt}•GTP complexes and plotted as bars. Distances are shown for the O^{α} and O^{β} oxygen atoms of the aspartate side chain in the GDP (A) and the GTP (B) complexes. The superimposed Gaussian fits indicate the contribution of the hydrogen bonded (grey) and the non-bonded (black) states.

The mechanistic role of Asp109-His22 hydrogen bonding

We then wanted to know if a functional role for the $Asp109_{Tu}$-$His22_{Tu}$ hydrogen bonded state could be confirmed *in vitro*. To this end we have constructed a mutant version of EF-Tu containing a single amino acid substitution at position 109 replacing aspartate with alanine (EF-Tu_{D109A}, corresponding to our *in silico* mutant) to prevent the formation of the hydrogen bond to $His22_{Tu}$. We then performed a detailed kinetic analysis of the nucleotide exchange reaction (**Scheme 2.1**) for this mutant and the wild-type (WT) protein, along the lines of previous studies, using rapid kinetics (Gromadski et al., 2002). When compared to the WT data reported previously (Gromadski et al., 2002; Schümmer et al., 2007; Wieden et al., 2002), as well as the rate constants determined in

this study, we found that replacing Asp109 with alanine does affect the rate constant for EF-Ts-stimulated GDP dissociation (k_{-4}, 13-fold decrease) as well as the rate constant for EF-Ts association to nucleotide-free EF-Tu (k_2, 3-fold decrease). Experimental results for the wild type are in very good agreement with the results from previous studies (see **Table 2.1** for a summary of the obtained rate constants and **Figures 2.3 & 2.4** as well as **Figure A.1.4**).

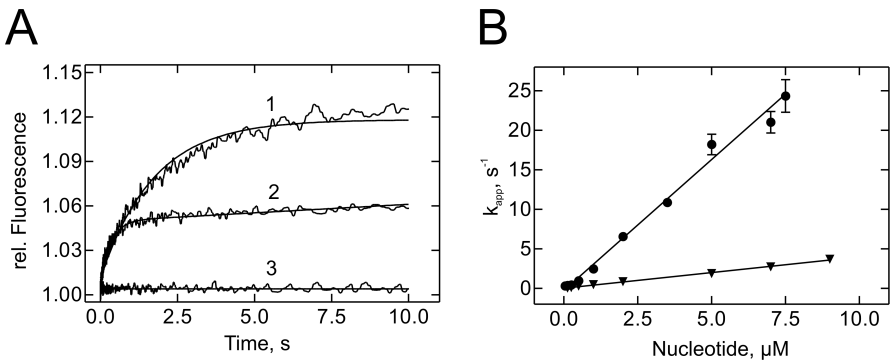

Figure 2.3. Interaction of guanine nucleotides with EF-Tu_{D109A} in the absence of EF-Ts. (A) Time courses of (1) mant-GTP (1 μM) or (2) mant-GDP (1 μM) binding to nucleotide-free EF-Tu_{D109A} (0.25 μM) measured by FRET between the single tryptophan in EF-Tu and the mant group; (3) control without EF-Tu. (B) Concentration dependence of k_{app}. k_{app} values were calculated by a single-exponential fitting from time courses in (A). Key: circles, mant-GDP; triangles, mant-GTP.

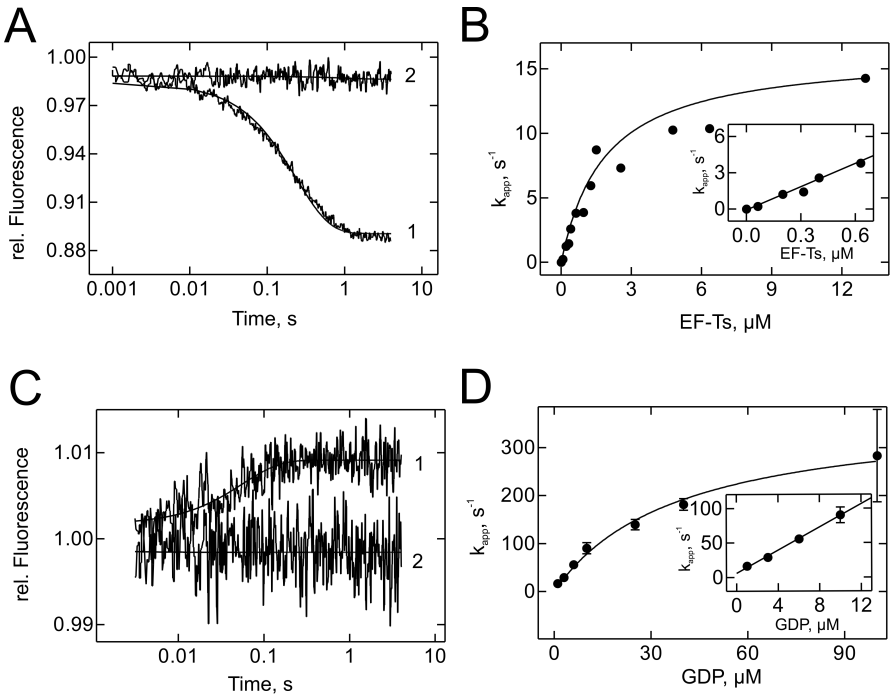

Figure 2.4. Interaction of EF-Tu$_{D109A}$ with EF-Ts and GDP. (A) Time courses of dissociation of EF-Tu$_{D109A}$•mant-GDP (0.15 μM) in the presence of EF-Ts (0.2 μM) and excess unlabeled GDP (25 μM) (1) or in the absence of EF-Ts (2). The fluorescence of the mant group was monitored. (B) Concentration dependence of k_{app} for EF-Tu$_{D109A}$•mant-GDP dissociation. The values of k_{app} were calculated by single-exponential fitting of the time courses in (A). (C) Time courses of the dissociation of EF-Tu$_{D109A}$•EF-Ts (0.5 μM) in the presence of GDP (1 μM) (1) or in the absence of GDP (2), as monitored by the fluorescence of Trp184 in EF-Tu. (D) Concentration dependence of k_{app} for EF-Tu$_{D109A}$•EF-Ts dissociation in the presence of GDP. The values of k_{app} were calculated by single-exponential fitting of the time courses in (C).

Table 2.1 Effect of mutations in EF-Tu on the experimentally determined rate constants of EF-Tu interaction with EF-Ts and guanine nucleotides

	WT[b]	WT[c]	D109A[b]	E152A[b/d]
k_1 /10^6 M^{-1}s^{-1}	2.8 ± 0.1	2.0 ± 0.5	3.3 ± 0.1	2.0[d]
k_{-1} /s^{-1}	0.002 ± 0.001	0.002 ± 0.001	0.004 ± 0.001	0.003[d]
k_2 /10^7 M^{-1}s^{-1}	1.3 ± 0.1	1 ± 0.2	0.3 ± 0.1	0.08 ± 0.01[b]
k_{-2} /s^{-1}	0.01	0.03	0.04	0.01[d]
k_3 /10^7 M^{-1}s^{-1}	3 ± 1	6 ± 1	4 ± 1	0.46[d]
k_{-3} /s^{-1}	438 ± 50	350 ± 50	408 ± 64	170 ± 30[d]
k_4 /10^6 M^{-1}s^{-1}	7 ± 1	14 ± 5	7 ± 1	7.6[d]
k_{-4} /s^{-1}	219 ± 25	125 ± 25	16 ± 1	9 ± 2[d]
k_5 /10^5 M^{-1}s^{-1}	4.3 ± 0.1	5.0 ± 1	3.9 ± 0.1	2.5 ± 0.1[b]
k_{-5} /s^{-1}	0.02 ± 0.01	0.03 ± 0.01	0.05 ± 0.01	0.05 ± 0.01[b]
k_6 /10^7 M^{-1}s^{-1}	12.4 ± 0.3	3 ± 0.5	3.3 ± 0.2	5.3 ± 1.6[b]
k_{-6} /s^{-1}	60 ± 10	60 ± 10	90 ± 10	390 ± 90[b]
k_7 /10^6 M^{-1}s^{-1}	3.9 ± 0.7	6 ± 1	1.8 ± 0.2	5.9 ± 2.7[b]
k_{-7} /s^{-1}	95 ± 10	85 ± 10	50 ± 5	8.5 ± 1[b]

[a] According to the mechanism of **Scheme 2.1**
[b] This study
[c] Gromadski *et al.* (2002)
[d] Wieden *et al.* (2002)

Glu152 is critical for the EF-Ts-catalyzed dissociation of both GTP and GDP.

Interestingly, $Asp109_{Tu}$ also forms a hydrogen bond via its main chain carbonyl to the highly conserved side chain of $Arg12_{Ts}$, which in turn participates in a salt bridge with the invariant $Glu152_{Tu}$ in helix D of EF-Tu. Since $Asp109_{Tu}$ and $Glu152_{Tu}$ seemed to be evolutionarily linked (Gaucher et al., 2002; Gaucher et al., 2001), we wanted to know if disrupting the salt-bridge between $Glu152_{Tu}$ and $Arg12_{Ts}$ is also specific for the acceleration of GDP dissociation (k_{-4}) and not the GTP (k_{-7}) dissociation from the ternary complex EF-Tu•GDP/GTP•EF-Ts. Previous studies (Wieden et al., 2002) have focused solely on the role of the highly conserved $Glu152_{Tu}$ on the GDP branch of the exchange mechanism and provided no information on the GTP branch. Values for the rate constants of the GDP branch (k_1, k_{-1}, k_2, k_{-2}, k_3, k_{-3}, k_4, k_{-4}, summarized in **Table 2.1**) revealed effects on both the EF-Ts-stimulated GDP dissociation (k_{-4}), as well as the interaction of EF-Ts with EF-Tu (k_2, k_{-2}, k_3, k_{-3}). In order to assess if these effects are also limited to the GDP bound forms of EF-Tu, we performed a similar kinetic analysis on the previously unstudied GTP branch of the nucleotide-exchange mechanism (**Figure A.1.5**) using the published alanine substitution mutant of EF-Tu (Wieden et al., 2002). When comparing the obtained rate constants for the GTP branch (k_2, k_{-2}, k_5, k_{-5}, k_6, k_{-6}, k_7, k_{-7}, summarized in **Table 2.1**) similar effects as for the GDP branch were observed.

2.5 Discussion

Past structural and biochemical studies on the mechanism of guanine nucleotide exchange in EF-Tu suggest that this process occurs through a three-part mechanism, involving breaking of the Mg^{2+} coordination, structural changes in the P-loop (the

phosphate side), and the disruption of interactions with nucleotide base (the base side). Little is known about the timing and the structural dynamics of these events. This is reflected by the somewhat surprising observation that the disruption of any of the putative key interactions in the EF-Tu•EF-Ts complex derived from the available X-ray structures of the binary complex resulted in only moderate changes in the efficiency of nucleotide exchange (Dahl et al., 2006; Wieden et al., 2002; Zhang et al., 1996; Zhang et al., 1998). EF-Ts-stimulated nucleotide exchange might therefore rely on a number of second-shell residues to induce and relay small rearrangements through a network of changes in EF-Tu contributing synergistically to the efficient exchange of guanine nucleotides. Identification of these intrinsically dynamic communication networks is of great interest for our understanding of the design principles underlying the function and structural dynamics of biomolecular activities. However, identifying the participants of these networks and assigning a specific function to them using only static structural information derived from X-ray crystallographic studies is inherently difficult. The use of a combination of MD simulations together with mutagenesis and kinetic analysis of the nucleotide exchange mechanism using rapid kinetics has allowed us to identify the second shell residue $Asp109_{Tu}$ as such a mechanistically important residue *in vivo*.

Role of $Asp109_{Tu}$ during EF-Ts-catalyzed nucleotide exchange

The highly conserved $Asp109_{Tu}$ interacts with $Arg12_{Ts}$ through the main chain carbonyl group. The strict conservation as an aspartate residue in bacterial and mitochondrial EF-Tu sequences indicates a functional role of the side chain during EF-Ts-mediated nucleotide exchange in bacteria, but not in eukaryotes. Although no direct interaction of the side chain with other residues has been reported (Kawashima et al., 1996; Kjeldgaard

et al., 1993; Song et al., 1999), mutation of $Asp109_{Tu}$ has a significant effect on the EF-Ts-mediated GDP (but not GTP) dissociation. In contrast, the disruption of the salt bridge between $Glu152_{Tu}$ and $Arg12_{Ts}$ affects the rate of nucleotide dissociation for GDP (Wieden et al., 2002) and GTP (this study), as well as significantly alters the association rates of EF-Ts to the respective binary complexes and nucleotide-free EF-Tu. $Arg12_{Ts}$ also interacts via a hydrogen bond with the main-chain carbonyl oxygen of $Asp109_{Tu}$, thereby connecting $Glu152_{Tu}$ and $Asp109_{Tu}$ in the EF-Tu•EF-Ts complex (**Figure 2.5**). The use of MD simulations reported in this study allowed us for the first time to identify and to assign a role of the highly conserved side chain $Asp109_{Tu}$. As part of the dynamic properties of EF-Tu, $Asp109_{Tu}$ is able to participate in a previously unidentified hydrogen bond with $His22_{Tu}$ located in the P-loop, thus connecting a secondary shell residue ($Asp109_{Tu}$) with residues at the phosphate side in the nucleotide-binding pocket ($His22_{Tu}$). This effectively establishes a communication path between helix D and the P-loop. However, this hydrogen bond is only observed for a fraction of the simulation time (20-30%) in either the EF-Tu•GDP or the EF-Tu•GTP complex suggesting sampling of a functional interaction between the two residues, which becomes important upon formation of the transient ternary complex (EF-Tu•nucleotide•EF-Ts) or an intermediate on the reaction path. This is supported by the close approach of the two side chains (3.09 Å) in the EF-Tu•EF-Ts complex (PDB-ID: 1EFU), and the reduced affinity of EF-Ts (K_2) for the nucleotide free $EF\text{-}Tu_{D109A}$, as well as the increased flexibility of the N-terminal half of helix D and the NKxD specificity motif in the $EF\text{-}Tu_{D109A}$ simulations.

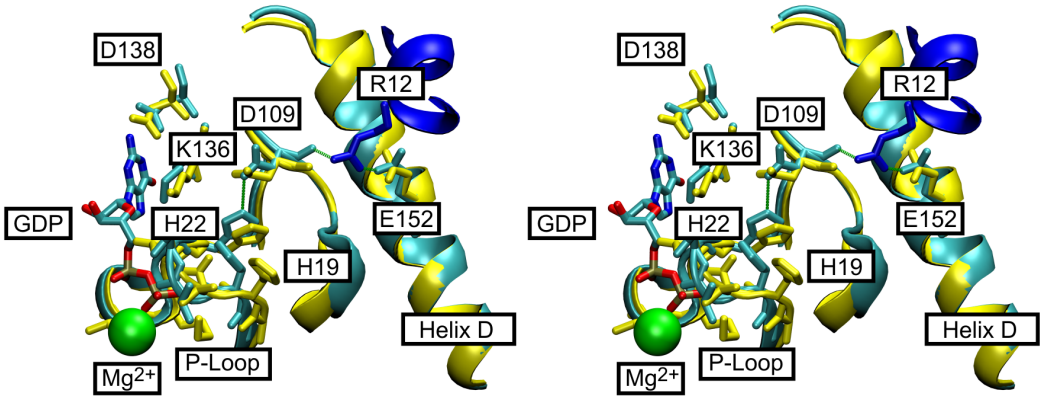

Figure 2.5. Structure of the nucleotide-binding pocket (Stereo View). (A) H-bonding interactions between $Asp109_{Tu}$ and $His22_{Tu}$: Detailed view of the nucleotide interactions in the EF-Tu•GDP (yellow) and EF-Tu•EF-Ts (cyan for EF-Tu and blue for EF-Ts) complexes. Residues involved in nucleotide binding are highlighted. $Arg12_{Ts}$ is depicted in dark blue, and Mg^{2+} is represented by a green sphere. Hydrogen bonds of the proposed hydrogen bond relay are indicated in green. The figure was prepared with the VMD (Humphrey et al., 1996) using coordinate sets 1EFC and 1EFU in the Protein Data Bank (Kawashima et al., 1996; Song et al., 1999).

The reported detailed kinetic analysis of the nucleotide exchange mechanism (**Scheme 2.1**) in the absence (D109A) and presence (WT) of the predicted hydrogen bond (**Table 2.1**) revealed that only the rate constants for GDP (and not GTP) dissociation from the EF-Tu•GDP•EF-Ts complex (k_{-4}, lowered 13-fold) and EF-Tu/EF-Ts association (k_2, lowered 3 fold) were affected. Based on these rate constants and the respective equilibrium dissociation constants (K_D), the change in Gibbs free energy (ΔG^0) of step 2 (interaction of EF-Tu and EF-Ts) and step 4 (interaction of GDP with the EF-Tu•EF-Ts complex) for both $EF\text{-}Tu_{wt}$ and $EF\text{-}Tu_{D109A}$ can be calculated: $\Delta G^0_{2,WT}$ = -51.1 kJ/mol and $\Delta G^0_{2,D109A}$ = - 44.2 kJ/mol; $\Delta G^0_{4,WT}$ = -25.3 kJ/mol and $\Delta G^0_{4,D109A}$ = -31.6 kJ/mol. The fact that only k_{-4} and k_2 differ (decreased) between $EF\text{-}Tu_{D109A}$ and $EF\text{-}Tu_{wt}$ can be explained by a destabilization of the transition states for the two reactions resulting in higher transition state energies upon removal of the hydrogen bond between $Asp109_{Tu}$ and $His22_{Tu}$ (depicted by the length of the arrows of the respective rate constants in **Figure 2.6**). On the other hand the rate constants for the

reverse reactions (k_4 and k_{-2}) are not changed, suggesting that the difference in the Gibbs free energies between the destabilized transition states and the mutant EF-Tu•EF-Ts complex is not affected. The latter can be explained by a destabilization of the EF-Tu•EF-Ts complex to a similar extent as the destabilization of the respective transition states (**Figure 2.6**). Consequently, the Gibbs free energy $\Delta G^0_{4,D109A}$ should be larger and $\Delta G^0_{2,D109A}$ should be smaller than in the WT case, respectively. This is consistent with the calculated values for these ΔG^0s (*vide supra*). It is furthermore reflected by the respective $\Delta\Delta G^0$s ($\Delta\Delta G^0_4$ = 6.4 kJ/mol and ΔG^0_2 = -7.0 kJ/mol) between WT and mutant, which correspond well with the energy contribution of a single hydrogen bond being removed. The fact that the observed changes in $\Delta\Delta G^0$s indeed reflect the removal of a single hydrogen bond demonstrate the power of this combined MD and experimental approach. It also indicates the importance of this hydrogen bond for the mechanism and the molecular dynamics of the protein (*vide infra*). Furthermore, if the hydrogen bond would be part of a degenerate communication network within the protein, other members of the network would compensate for its loss and it would have been difficult to measure the difference on a specific rate constant, further supporting the significance of this finding.

To understand the role of this hydrogen bond for the nucleotide exchange reaction, it is important to view the observed destabilization of the EF-Tu_{D109A} complexes as a stabilization of the respective complexes with the wild type protein. Recent kinetic analysis of the nucleotide exchange reaction in yeast supports a different mechanism of nucleotide exchange and moreover, different structural requirements for the nucleotide binding properties of the eukaryotic factor (eEF1A) compared to bacterial EF-Tu

(Gromadski et al., 2007). Dissociation of the bound nucleotide is up to 100 times faster for eEF1A than for EF-Tu (0.13 s^{-1} vs. 0.002 s^{-1} for GDP and 0.1 s^{-1} vs. 0.02 s^{-1} for GTP). These differences might also be reflected by the different mode of interaction between eEF1A and its nucleotide exchange factor eEF1B. $Asp109_{Tu}$ might therefore be important in overcoming the additional stabilizations of GDP-binding observed in the prokaryotic EF-Tu•GDP complex (as indicated by the lower dissociation constant) when compared to their eukaryotic counterparts eEF1A•GDP. This in turn suggests that prokaryotes require this hydrogen bond (and therefore have maintained it during evolution) to overcome the additional stabilization of GDP binding by stabilizing the EF-Tu•EF-Ts complex and in particular of the two transition states.

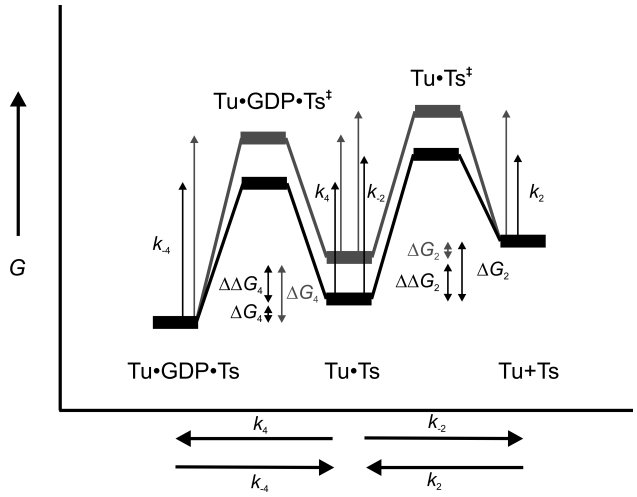

Figure 2.6. Gibbs Free Energy diagram depicting the transition state stabilizing effect of the hydrogen bond between $Asp109_{Tu}$ and $His22_{Tu}$. Gibbs free energy diagram for the two reactions described by the equilibrium constants K_2 and K_4 (**Scheme 2.1**) of $EF\text{-}Tu_{wt}$ (black) and $EF\text{-}Tu_{D109A}$ (grey), respectively. Removal of the hydrogen bond between $His22_{Tu}$ and $Asp109_{Tu}$ results (calculated from the experimentally determined rate constants summarized in **Table 2.1**) in a destabilization of the Tu•Ts complex and the two transition states ($Tu•Ts^{\neq}$ and $Tu•GDP•Ts^{\neq}$) to a similar extent, reflected by the comparable $\Delta\Delta G^0$s for the for both reactions ($\Delta\Delta G^0_4$ = 6.4 kJ/mol and $\Delta\Delta G^0_2$ = 7.0 kJ/mol), consistent with the energy for a single hydrogen bond. This increase in energy of the transition states and Tu•Ts complex results in decreased rates constants for k_{-1} and k_4 as well as no changes for the rates constants of k_2 and k_{-1} as indicated by the length of the respective arrows (grey vs. black).

Our combination of MD simulations in conjunction with the detailed rapid kinetics analysis reported here provide the first step toward unraveling the 3D communication network that, in the two transient ternary complexes EF-Tu•GDP•EF-Ts and EF-Tu•GTP•EF-Ts, facilitates a 60,000-fold and 3,000-fold acceleration of the nucleotide dissociation rates, respectively. This is of particular importance since the eukaryotic ternary complexes have been successfully crystallized (Andersen et al., 2001), but no structural information is available for the bacterial factors due to the low stability of these ternary complexes.

Role of histidine 22 for efficient nucleotide release

$His22_{Tu}$ is located two amino acid residues downstream of the crucial amino acids $Val20_{Tu}$ and $Asp21_{Tu}$, which are involved in flipping of the main chain carbonyl (between $Val20_{Tu}$ and $Asp21_{Tu}$, **Figure A.1.6**) in EF-Tu upon EF-Ts interaction (Kawashima et al., 1996). This main chain carbonyl is positioned in the EF-Tu•EF-Ts complex such that its partial negative charge as well as the resulting steric clash will disfavor the binding of the β-phosphate of GDP (**Figure A.1.6**). Hence, formation of the hydrogen bond between $Asp109_{Tu}$ and $His22_{Tu}$ implies a function in constraining the flexibility of the peptide backbone upstream of $His22_{Tu}$, effectively forming the pivot point that is required for flipping the peptide backbone upon intrusion of the conserved $Phe81_{Ts}$ and the subsequent displacement of helices B and C in EF-Tu. The N-terminal end of helix C contains the strictly conserved methionine $Met112_{Tu}$, a residue that is in close proximity to the conserved histidines 19 and 22 and that is moved by several Ångströms, providing additional flexibility for the P-loop between $His19_{Tu}$ and $His22_{Tu}$. Movement of these two helices results in widening of the crevice in which $Ile17_{Tu}$ is buried, the first amino

acid upstream of the P-loop sequence and that shows a different orientation in the EF-Tu•GDP and the EF-Tu•EF-Ts complexes. Relieving the spatial constraints on the N-terminal side of the P-loop, in particular at $Ile17_{Tu}$, will allow it to be more flexible and to explore a larger conformational space. Together with stabilizing the C-terminal side of the P-loop through additional hydrogen bonding interactions ($His22_{Tu}$-$Asp109_{Tu}$), this will ultimately lead to the flip of the peptide bond between $Val20_{Tu}$ and $Asp21_{Tu}$ and subsequently promote dissociation of the bound nucleotide. This is consistent with the observation that removal of this hydrogen bond destabilizes the transition state of step 4 of the nucleotide exchange mechanism (EF-Tu•EF-Ts•$GDP^{\neq}$), but not the ternary complex Tu•GDP•EF-Ts itself (*vide supra*).

2.6 Conclusions

By using evolutionary analysis in combination with molecular dynamics simulations, we were able to identify $Asp109_{Tu}$ as a second-shell residue that serves as a relay point (the $Glu152_{Tu}$-$Arg12_{Ts}$-$Asp109_{Tu}$-$His22_{Tu}$ relay) in the 3D communication network underlying the structural dynamics responsible for facilitating efficient nucleotide exchange in bacterial EF-Tus. Through the complementation of these computational approaches with the determination of the rate constants governing this interaction using rapid kinetic techniques, we were able to further define the role of $Asp109_{Tu}$ as a requirement for efficient GDP exchange in EF-Tu by contributing to the stabilization of the respective transition state in prokaryotes. We believe that $Asp109_{Tu}$ is important for linking of structural rearrangements in the base side of the binding pocket with structural rearrangements in the phosphate side of the binding pocket. The current study is an

example that very short MD simulations, which should be carefully interpreted with respect to energetics due to limitations in sampling and possible inaccuracies in the force field, can successfully be used to develop likely enzyme mechanisms when confirmed by experimental data. Our approach clearly demonstrates the power of combining *in silico* with *in vitro* studies to identify the dynamic 3D communication pathways underlying the efficient function of proteins.

Chapter 3

A conserved P-loop anchor limits the structural dynamics that mediate nucleotide dissociation in EF-Tu

3.1 Introduction

The phosphate-binding loop (P-loop) is a conserved sequence motif found in the superfamily of P-loop containing nucleoside triphosphate hydrolases (P-loop NTPases), (Wilson et al., 2007). The P-loop, also known as the Walker A motif, contributes to binding nucleotides in the members of this superfamily and has the consensus sequence GxxxxGKS/T (Walker et al., 1982; Wittinghofer and Vetter, 2011). Structural studies have revealed that this sequence wraps around the phosphates of the bound nucleotide and the amide hydrogens of the protein backbone form hydrogen bonds with the oxygen atoms of the γ- and/or β-phosphates (Kinoshita et al., 1999; Walker et al., 1982). Comparison of the X-ray structures of over 450 proteins from various functional backgrounds has revealed that the P-loop three-dimensional structure is conserved among 13 different superfamilies of mononucleotide-binding proteins although the sequence is not (Kinoshita et al., 1999). Thus, the P-loop appears to be a versatile evolutionary solution to mononucleotide binding.

In spite of the well-conserved three-dimensional structure of the P-loop in the presence of nucleotides, some P-loop NTPases have been crystallized with 'alternative' P-loop conformations in the absence of bound nucleotides. These structures include the ATPases adenylate kinase (Müller et al., 1996) and MutS (Lamers et al., 2000) as well as the G-proteins Rac1 (Chhatriwala et al., 2007), Ras (Boriack-Sjodin et al., 1998), EF-G (Ævarsson et al., 1994), Gs (Rasmussen et al., 2011), and Elongation Factor (EF) Tu (Kawashima et al., 1996). These findings suggest that structural dynamics of the P-loop may be a feature of at least some P-loop NTPases. The G-proteins Rac1, Ras, Gs, and EF-Tu are particularly interesting insofar as in each of these structures the G-protein is

bound to its respective Guanine nucleotide Exchange Factor (GEF), which stimulates nucleotide dissociation. Thus, conformational changes in the P-loop may be a common strategy contributing to GEF-stimulated nucleotide exchange in G-proteins. It is impossible to tell from these X-ray crystal structures, however, if P-loop conformational changes are the cause or effect of GEF-induced nucleotide dissociation. Understanding the relationship between P-loop conformational changes and nucleotide-binding properties requires an understanding of the structural dynamics in the P-loop.

Structural dynamics have been shown to contribute significantly to enzyme function in several instances.(Benkovic and Hammes-Schiffer, 2003; Boehr et al., 2006; Eisenmesser et al., 2005; Henzler-Wildman et al., 2007; Wolf-Watz et al., 2004) An interesting trend that has emerged from the study of protein dynamics is that some protein conformational changes or functions that occur on the microsecond to second timescale are slaved to shorter-timescale fluctuations within proteins (picosecond to millisecond), (Carroll et al., 2012; Henzler-Wildman et al., 2007; Nagel et al., 2011; Tzeng and Kalodimos, 2012). This suggests that nanosecond-timescale molecular dynamics (MD) simulations can provide insight into protein dynamics that proceed on the millisecond to seconds timescale. MD simulations are valuable tools for studying structural dynamics as they can simulate motions within proteins at atomic resolution. Since MD simulations are just that, *simulations*, they should be interpreted carefully in the context of available experimental data. To this end, I present an investigation of P-loop structural dynamics, using MD to provide atomic-resolution simulations of P-loop motions and rapid kinetics experiments to measure nucleotide-binding properties.

Two different P-loop conformations have been identified in EF-Tu: one in the presence of a bound nucleotide (Kjeldgaard et al., 1993; Schmeing et al., 2009; Song et al., 1999) and another in the presence of the GEF EF-Ts (Kawashima et al., 1996). In the transition from nucleotide-bound EF-Tu to the EF-Tu•EF-Ts complex, a flip occurs in the peptide backbone between $Val20_{Tu}$ and $Asp21_{Tu}$ (Kawashima et al., 1996). The rapid dissociation of nucleotides from EF-Tu•nucleotide•EF-Ts complexes (Gromadski et al., 2002) strongly implies a correlation between P-loop conformation and nucleotide binding properties as noted by others (Kawashima et al., 1996). Similarly, an H118A variant of EF-Tu, which lacks the His118•••Gly18 hydrogen bond between the P-loop and helix C, was previously shown to bind nucleotides ten times more weakly than wild type EF-Tu (Dahl et al., 2006). It was suggested that removal of this hydrogen bond might increase P-loop flexibility and result in lower nucleotide binding affinities. Here I test the hypothesis that P-loop structural dynamics mediate GTP-binding properties in EF-Tu and that adjacent amino acids can play a role in regulating P-loop structural dynamics.

I first sought to retro-engineer a highly dynamic P-loop to serve as a standard. To this end, an $EF\text{-}Tu_{H22G}$ was constructed in order to place an additional glycine in the P-loop (see **Figure 3.1**). Subsequently, attention focused on the secondary shell where amino acids were hypothesized to fine-tune P-loop properties. Adjacent to the P-loop is a six amino acid coil that is well conserved in bacterial EF-Tus and contains $Asp109_{Tu}$ which we have previously shown to communicate, via hydrogen bonding, with $His22_{Tu}$ of the P-loop (**Chapter 2**), (Wieden et al., 2010). The highly conserved (>99%) $Met112_{Tu}$ is in the same coil as $Asp109_{Tu}$ and is in close contact with $His22_{Tu}$ in X-ray crystal structures and throughout MD simulations (see **Figure 3.1**). Based on these observations I

hypothesized that interactions between the P-loop and the adjacent coil may limit P-loop dynamics. I have replaced $Met112_{Tu}$ with glycine or alanine in an attempt to increase the mobility of $His22_{Tu}$ and, in turn, P-loop flexibility. Substitution of $Met112_{Tu}$ with leucine served as a control for mutating position 112 without diminishing the contacts between this position and the P-loop.

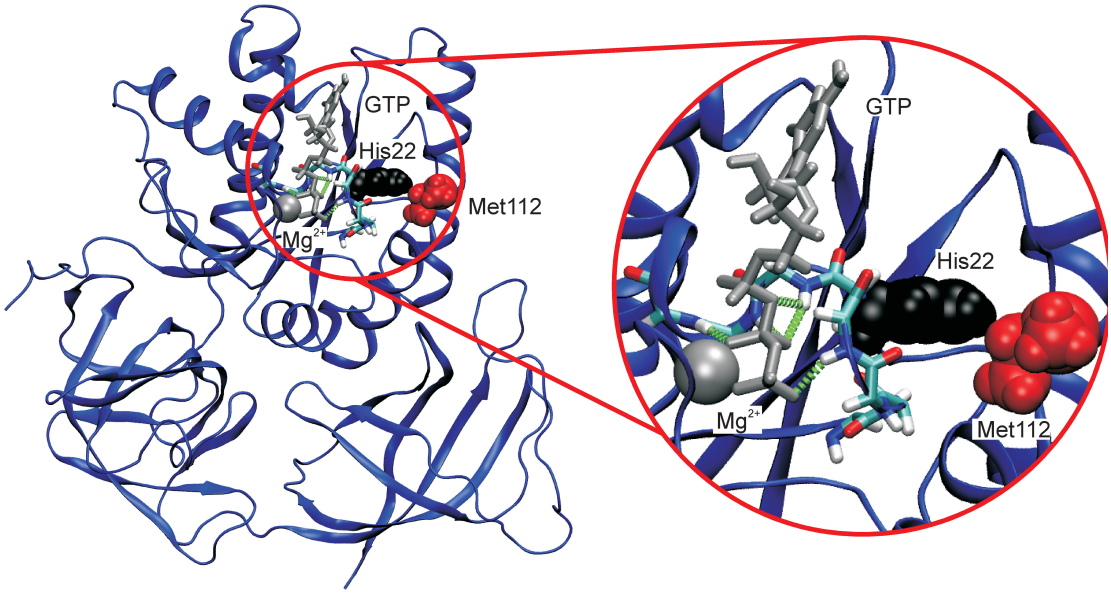

Figure 3.1. $His22_{Tu}$ and $Met112_{Tu}$ form close contacts in the secondary shell surrounding the P-loop of EF-Tu. The model of *E. coli* EF-Tu•GTP is shown in cartoon representation after 10 ns of molecular dynamics simulation. Bound GTP and Mg^{2+} are shown as sticks and space-filling, respectively, both coloured silver. The backbone atoms of the P-loop are shown as sticks and hydrogen bonds between P-loop amide hydrogen atoms and phosphate oxygen atoms of GTP are shown as green dashed lines. $His22_{Tu}$ (black) of the P-loop and $Met112_{Tu}$ (red) of the adjacent coil are shown in space-filling representation.

Here pre-steady state kinetics measurements were used to measure the effect of each substitution on the GTP-binding properties of EF-Tu. In order to assess effects on conformational sampling, the entropic barrier for EF-Tu•GTP dissociation was determined in each EF-Tu variant. All-atom MD simulations of wild type and mutant EF-Tus were performed in order to rationalize the *in vitro* results in the context of P-loop

structural dynamics. These results establish a direct correlation between high entropic barriers for GTP dissociation *in vitro* and P-loop structural dynamics *in silico*

3.2 Materials and Methods

Buffers and Reagents

Stopped-flow experiments were performed in Buffer A (50 mM Tris-HCl pH 7.5, 70 mM NH_4Cl, 30 mM KCl, 7 mM $MgCl_2$). GTP was purchased from Sigma and 2′-/3′-O-N′-methylantraniloyl (mant)-GTP from JenaBioScience or Molecular Probes. DNA primers were purchased from Integrated DNA Technologies.

Mutagenesis

The plasmid pEECAHis (Wieden et al., 2002), encoding for *E. coli* EF-Tu with a C-terminal hexahistidine tag, was used as the template for all mutagenesis reactions. The Quikchange™ method (Stratagene) employing two complementary primers was used in order to introduce each mutation. For construction of EF-Tu_{H22G}, the coding primer sequence was (5′)GTACTATCGGCCACGTTGA**CGGT**GGTAAAACAACGCTG(3′), where the codon encoding $Gly22_{Tu}$ is shown in bold, and the six nucleotide sequence corresponding to an NcoI restriction site in the wild type EF-Tu sequence is underlined. For construction of the EF-Tu_{M112L} variant, the coding primer sequence was (5′)ACGGCCCG**CTG**CCGCAGACTCGAGAGCACAT(3′), where the leucine codon is bolded and a novel XhoI restriction site, used in screening for successful mutagenesis, is underlined. The coding primers used in construction of the M112A and M112G substitutions were (5′)TGACGGCCCG**xxx**CCGCAGACTCGAGAGCACATC(3′), with **xxx** representing the GTG codon for glycine or the GCG codon for alanine. Again, a

novel XhoI restriction site is underlined. Mutagenesis of the template DNA was carried out in 25 μL reaction mixtures containing 0.4 mM of each dNTP, 0.4 μM of each primer, 2 mM $MgSO_4$, 1 μg of template pDNA, and 3 units of Pfu DNA polymerase (Fermentas) in 1x Pfu buffer (Fermentas). Reactions were carried out in a thermocycler using the following program: initial denaturation (368 K for 5 min); 18 cycles of denaturing (368 K for 45 s), annealing (1 min), and extension (341 K for 15 min); and final extension (341K for 15 min). The annealing temperatures were as follows: M112A 337 K, M112G 335 K, M112L 332 K, H22G 338 K. Template pDNA was then degraded in a DpnI restriction digestion: 15 μL mutagenesis reaction mixture, 10 units DpnI (Fermentas), 1x Buffer Tango (Fermentas) incubated at 310 K overnight. Mutagenized plasmids were transformed into competent *E. coli* NEB 5α cells (New England Biolabs) using heat shock (315 K for 45s). Following growth in LB medium for 1 hour at 310 K with shaking, transformed cells were plated on LB agar containing 0.1 mg/mL ampicillin and grown overnight. Single colonies were selected and grown in liquid LB medium containing 0.1 mg/mL ampicillin overnight and used to extract plasmid DNA via miniprep kit (EZ-10 spin column kit Bio Basic). Isolated plasmid DNA was sequenced (MacroGen) to confirm that the desired mutations, and only the desired mutations, were present.

Protein Overexpression and Purification

Plasmids bearing the desired mutations were each transformed into competent *E. coli* BL21 (DE3) cells (same protocol as for NEB 5α cells above) for overexpression of each EF-Tu variant. *E. coli* cells were grown in liquid LB media containing 0.1 mg/mL ampicillin and inoculated to an initial OD_{600} of 0.1. At an OD_{600} of 0.6, overexpression

was induced by the addition of isopropyl β-D-1-thiogalactopyranoside (IPTG) to a final concentration of 1 mM. Cells were harvested by centrifugation after three hours of overexpression. Cells (~10 g) were opened by lysozyme treatment (1 mg/mL) in 7mL Buffer B per gram of cells (Buffer B: 50 mM Tris-Cl pH 8.0 @ 4 °C, 60 mM NH_4Cl, 7 mM $MgCl_2$, 7 mM β-mercaptoethanol, 1 mM phenylmethane-sulfonylfluoride, 50 μM GDP, 300 mM KCl, 10 mM imidazole, 15% glycerol), followed by incubation with sodium deoxycholate (12.5 mg/g of cells), and sonication. Each His-tagged EF-Tu variant was purified by affinity chromatography using Ni^{2+} sepharose resin. Recombinant EF-Tu was bound to ~5 mL of nickel column material in Buffer B and eluted in Buffer C (50 mM Tris-Cl pH 8.0 @ 4 °C, 60 mM NH_4Cl, 7 mM $MgCl_2$, 7 mM β-mercaptoethanol, 1 mM phenylmethanesulfonylfluoride, 50 μM GDP, 300 mM KCl 250 mM imidazole, 15% glycerol). Affinity purified EF-Tu was further purified by size exclusion chromatography on a Superdex 75 column (XK26/100 column; Superdex 75 prep grade (GE Healthcare)) in Buffer A. Purified EF-Tu was concentrated using a VivaSpin centrifugal concentration device (Sartorius; 30 kDa molecular weight cutoff), flash frozen in liquid nitrogen and stored at -80 °C until use.

Component preparation for stopped-flow measurements

EF-Tu•mant-GTP complexes for use in pre-steady state kinetics experiments were formed by incubation of 0.3 μM EF-Tu with ten-fold excess mant-GTP in the presence of 3 mM phosphoenolpyruvate and 10 μg/mL pyruvate kinase at 37 °C for 30 minutes. Nucleotide-free EF-Tu was prepared by mixing EF-Tu with excess Buffer D (25 mM Tris-HCl pH 7.5 @ 37 °C, 50 mM NH_4Cl, 10 mM EDTA) and subsequent incubation at 37 °C for 30 minutes. EF-Tu was then separated from free nucleotide by size exclusion

chromatography on a 10/300 Superdex 75 column (GE Healthcare) in buffer E (25 mM Tris-Cl pH 7.5 @ room temperature, 50 mM NH_4Cl) prior to stopped-flow experiments. All solutions containing GTP or mant-GTP were incubated with phosphoenolpyruvate (3 mM) and pyruvate kinase (10 μg/mL) at 37 °C for 30 minutes prior to kinetic experiments to convert any GDP or mant-GDP to the respective tri-phosphate form.

Fluorescence Based Stopped-Flow

All stopped-flow experiments were carried out with a Kintek stopped-flow device (Model SF-2004). Fluorescence resonance energy transfer (FRET) from Trp184 in EF-Tu to bound mant-GTP was monitored through a 400 nm long-pass cut-off filter (LG-4000-F: Newport Filters) upon excitation at 280 nm. Dissociation of mant-GTP was monitored as a decrease in mant fluorescence upon mixing equal volumes of EF-Tu•mant-GTP complex with unlabelled GTP to final concentrations of 0.15 μM EF-Tu, 1.5 μM mant-GTP, and 25 μM unlabelled GTP. The presence of excess unlabeled nucleotide in the reaction ensured that the rebinding of mant-GTP was negligible. Thus, the system decays with the unimolecular rate constant k_{off}. The association of mant-GTP to EF-Tu was monitored upon mixing nucleotide-free EF-Tu (0.6 μM) with varying concentrations of mant-GTP (2-20 μM). The temperature was maintained constant during each experiment by circulating water from a refrigerated/heated water bath (VWR model 1156D) through a water jacket surrounding the observation cell and syringes of the stopped-flow apparatus. Temperature was measured in the water jacket with a built-in electronic thermometer.

Data Analysis

Single traces for all nucleotide dissociation experiments were fit using TableCurve software (Jandel Scientific), with single exponential equations as follows.

$$F = F_{\infty} + Ae^{-k_{app} \cdot t} + B \cdot t \qquad (3.1)$$

Here F represents fluorescence, F_{∞} is the final fluorescence, A is the amplitude, k_{app} is the apparent rate constant, and B represents the linear rate of photobleaching. The average k_{app} value obtained from at least 4 fits yielded the unimolecular dissociation rate constant k_{off}, and the error was represented by the corresponding standard deviation. For EF-Tu•mant-GTP association experiments, individual traces were fit to the single exponential **Equation 3.2** as follows.

$$F = F_{\infty} + Ae^{-k_{app} \cdot t} \qquad (3.2)$$

Under these pseudo-first order conditions, the apparent rate (k_{app}) of mant-GTP binding to EF-Tu was equal to k_{on}[mant-GTP]+k_{off}. The bimolecular rate constant k_{on} was determined by plotting the apparent rate of EF-Tu•mant-GTP formation as a function of initial mant-GTP concentration, post-mixing. The resulting titration curves were analyzed by linear regression in Prism (GraphPad Software) with the slope of the fitted line representing the association rate constant k_{on} and the error was provided by the standard error in the fit. The temperature dependence of mant-GTP dissociation was analyzed by constructing Eyring plots: ln(k_{off}/T) as a function of inverse absolute temperature (1/T). Linear regression was used to fit the resulting curves in Prism (GraphPad Software). The Eyring equation can be expressed as follows.(Tinoco et al., 2002)

$$\ln\left(\frac{k_{off}}{T}\right) = \frac{-\Delta H^{0\neq}}{R}\left(\frac{1}{T}\right) + \frac{\Delta S^{0\neq}}{R} + \ln\left(\frac{k_B}{h}\right) \qquad (3.3)$$

In **Equation 3.3**, R is the ideal gas constant (8.3145 J K^{-1} mol^{-1}), k_B is the Boltzman constant (1.3807 x10^{-23} J K^{-1}), h is Planck's constant (6.6261 x10^{-34} J s), $\Delta H^{0‡}$ is the enthalpy of activation for mant-GTP dissociation, $\Delta S^{0‡}$ is the entropy of activation for mant-GTP dissociation, and ^{0} indicates the molar standard state. The slope of the resulting fit was equal to $-\Delta H^{0‡}/R$, and the y-intercept was $\ln(k_B/h)+\Delta S^{0‡}/R$.

All-Atom Model Construction

In order to construct an all-atom model of *E. coli* EF-Tu•GTP, a homology model of *E. coli* EF-Tu was constructed using the SwissModel online server (Schwede et al., 2003). In this procedure, the X-ray crystal structure of *T. aquaticus* EF-Tu in complex with GDPNP was used as a template (PDBID: 1EFT) (Kjeldgaard et al., 1993). The high level of identity between EF-Tu amino acid sequences from *E. coli* and *T. aquaticus* (71%) provides high confidence in the resulting model. All water molecules in the crystal structure within 10 Å of the protein were placed in the *E. coli* EF-Tu model. To construct EF-Tu•Mg^{2+}•GTP models, the GDPNP and Mg^{2+} ligands from the crystal structure (1EFT) were manually inserted into the *E. coli* homology model and GDPNP was changed to GTP by hand. Both nucleotide and Mg^{2+} were omitted from the EF-Tu^{apo} models. Hydrogen atoms were added using the psfgen command in VMD (Humphrey et al., 1996) and the CHARMM27 topologies (Foloppe and Mackerell, 2000; MacKerell et al., 1998) Amino acid sidechains were protonated as expected for the isolated functional groups at pH 7.5. Histidine sidechains were protonated at the epsilon nitrogen only. The topology for GTP was constructed by modification of the existing topology for ATP.(Foloppe and Mackerell, 2000) The EF-Tu•Mg^{2+}•GTP or EF-Tu^{apo} model was

solvated using the Solvate package in VMD (Humphrey et al., 1996) in a box of TIP3 water molecules extending at least 10 Å from the protein in each direction. The solvated system was relaxed by iterative minimization moving the water, protein and ligands, water, protein and ligands, and finally, all atoms. The electrostatic charge of each minimized system was then neutralized by the addition of sodium ions using the Autoionize package in VMD (Humphrey et al., 1996) and all atoms in the model were then relaxed by minimization. Minimizations on water or protein and ligands were carried out for 10,000 steps, while all-atom minimizations were carried out until no change in total energy was seen over 1000 steps. EF-Tu variants were constructed using the Mutator plugin in VMD (Humphrey et al., 1996) starting from the minimized *E. coli* EF-Tu•Mg^{2+}•GTP or EF-Tu^{apo} model. Models of each EF-Tu variant were then solvated, minimized, and neutralized (*vide supra*).

Equilibrium Molecular Dynamics

All molecular dynamics calculations were performed using NAMD 2.6 (Phillips et al., 2005), the CHARM22 parameters for proteins (MacKerell et al., 1998), and CHARMM27 parameters for nucleic acids (Foloppe and Mackerell, 2000). MD simulations were performed with a 0.5 fs step size in an NPT ensemble with the use of periodic boundary conditions. The pressure was maintained at one atmosphere using a Nosé-Hoover Langevin piston, and the temperature was controlled using Langevin dynamics. Non-bonded interactions were computed with a 12 Å cutoff and a 10 Å switching distance. Van der Waals and short-range electrostatic interactions were computed every 0.5 fs, and long-range electrostatics were computed every 1 fs. Each EF-Tu model was equilibrated at 300 K and 350 K for 150 ps in two independent

simulations. After equilibration the model at 350 K was cooled to 300 K by applying the atomic velocities from the 300 K equilibration to the structure obtained from equilibration at 350 K. Production simulations were allowed to develop for 10 ns using velocity rescaling to stabilize the temperature at 300 K.

Steered Molecular Dynamics

Steered molecular dynamics (SMD) simulations were initiated using coordinates and velocities from equilibrium MD simulations after 6 ns, 7 ns, 8 ns, 9 ns, and 10 ns. The SMD driving force was attached to the magnesium ion and had a spring constant of 5 kcal/mol/Å^2. The spring was pulled at a rate of 0.1 Å/ps, in five different directions. Direction A was defined as the vector from C6 to N3 of GTP, so chosen because it was essentially 'straight out' of the nucleotide-binding pocket. Direction B was defined as the vector from C6 to C2 of GTP. Directions C, D, and E were defined by rotating direction B $\pi/2$, π, or $3\pi/4$ radians around an axis defined by direction A. Each SMD simulation was carried out for 0.5 ns.

Analysis of MD simulations

Snapshots of equilibrium MD simulations were saved every 0.5 ps and compiled using the software Carma (Glykos, 2006) to remove water molecules as well as the motion of the protein centre of mass. All metrics were measured using TCL scripts written in house, evoked in VMD. Ramachandran histograms were prepared and analyzed by running scripts in the software R (RCoreTeam, 2012). Two-dimensional histograms with bin sizes of $\pi/32 \times \pi/32$ radians^2 were constructed using the backbone φ and ψ data from each simulation. These metrics were measured every 0.5 ps for equilibrium MD simulations and 0.1 ps for SMD simulations. Each histogram was searched for local maxima, defined

as a bin or group of bins that is/are surrounded by 3 bins of decreasing occupancy in both the x- and y- directions. This definition allows for two local maxima to be as close as π/8 radians apart (centre to centre distance).

Potential hydrogen bonding distances were measured from the hydrogen atom of the hydrogen bond donor to the hydrogen bond acceptor. Distances were plotted as histograms for each simulation using a 0.1 Å bin size. **Equation 3.4** or **3.5** was fit to each histogram corresponding to a one Gaussian or two Gaussian fit, respectively (Brase and Brase, 2003b).

$$\text{counts} = \mathrm{A}e^{\frac{-(x-\bar{x}_\mathrm{a})}{2\sigma_\mathrm{a}^2}} \qquad (3.4)$$

$$\text{counts} = \mathrm{A}e^{\frac{-(x-\bar{x}_\mathrm{a})}{2\sigma_\mathrm{a}^2}} + \mathrm{B}e^{\frac{-(x-\bar{x}_\mathrm{b})}{2\sigma_\mathrm{b}^2}} \qquad (3.5)$$

Here A and B represent the peak heights of populations A and B, $\bar{x}_\mathrm{a}$ and $\bar{x}_\mathrm{b}$ are the average distances for populations A and B, and σ_a and σ_b are the standard deviations for populations A and B.

3.3 Results and Discussion

H22G substitution increases the entropy barrier for GTP dissociation in vitro.

In an attempt to retro-engineer a highly dynamic P-loop, an EF-Tu variant was constructed by replacing the conserved $\mathrm{His22_{Tu}}$ with glycine, reasoning that the more flexible glycine would promote P-loop motion. The GTP-binding properties of the EF-$\mathrm{Tu_{H22G}}$ were investigated in a purified *in vitro* system by the pre-steady state kinetics approach described elsewhere (Gromadski et al., 2002; Wieden et al., 2010). The dissociation and association rate constants for EF-$\mathrm{Tu_{H22G}}$•mant-GTP were measured as $(0.0116 \pm 0.0004)\ \mathrm{s^{-1}}$ and $(1.37 \pm 0.07)\times10^{6}\ \mathrm{M^{-1}\ s^{-1}}$, respectively (**Figure 3.2, Table 3.1**)

compared to (0.030 ± 0.010 s^{-1}) and (4.20 ± 0.20)$\times 10^5$ M^{-1} s^{-1} for wild type EF-Tu. Surprisingly, the rate of GTP dissociation is approximately 3-fold slower in EF-Tu_{H22G} compared to wild type, and a similar difference was observed in the rate of mant-GTP association. Therefore, if H22G substitution in EF-Tu does indeed increase the flexibility of the P-loop, it does not result in an accelerated rate of GTP dissociation. The approximately 10-fold higher affinity of EF-Tu_{H22G} for mant-GTP compared to EF-Tu_{wt} (K_D/nM = 8.5 ± 0.5 vs. 70 ± 30 respectively) is also inconsistent with the expectation that replacing the histidine sidechain in position 22 with a hydrogen would increase P-loop backbone conformational freedom and reduce the GTP-binding affinity of EF-Tu.

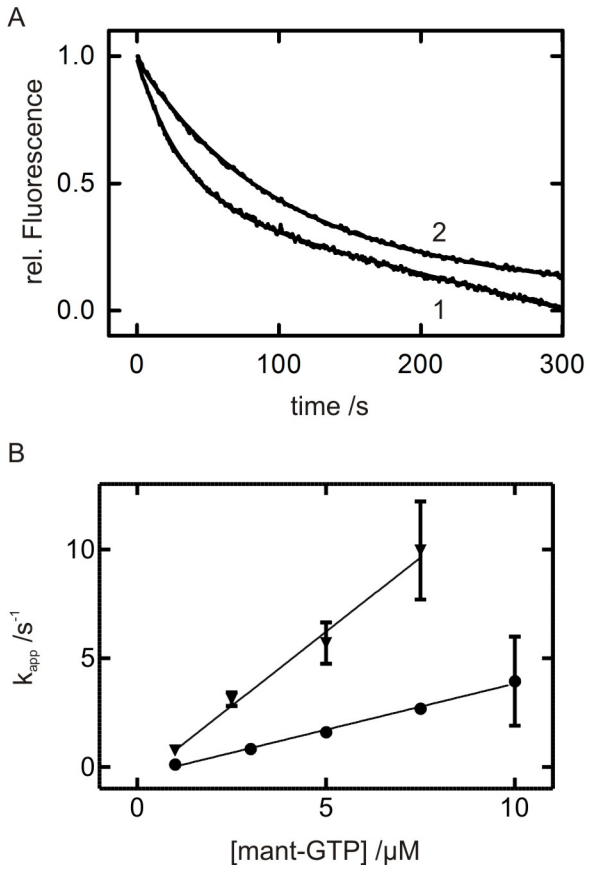

Figure 3.2. Interaction of EF-Tu_{H22G} with mant-GTP. All experiments were performed using fluorescence-based stopped-flow with excitation of the tryptophan residue in EF-Tu at 280nm. Fluorescent emissions from bound mant-GTP were monitored through a 400nm cut-off filter. Dissociation of mant-GTP (A) was monitored upon mixing equal volumes of EF-Tu•mant-GTP complex with unlabelled GTP to final concentrations of 0.15μM and 25μM, respectively. Single traces using (1) wild type EF-Tu and (2) H22G EF-Tu are plotted along with the fitted exponential functions (smooth curves). Mant-GTP association was monitored after mixing nucleotide free wild type (●) or H22G (▼) EF-Tu (0.3μM final concentration) with varying concentrations of mant-GTP (B). Data points represent the average of k_{app} values obtained from fits of individual traces and error bars represent the corresponding standard deviations. The trendlines were produced by linear regression using Prism software (GraphPad).

Table 3.1. Kinetic rate constants governing the interaction between EF-Tu and mant-GTP.

EF-Tu	k_{off} /s^{-1}	k_{on} /($10^5 M^{-1}s^{-1}$)	K_D /nM
wt	0.030 ± 0.010	4.20 ± 0.20	70 ± 30
H22G	0.0116 ± 0.0004	13. 7 ± 0.7	8.5 ± 0.5
M112G	0.0200 ± 0.0010	2.2 ± 0.1	91 ± 9
M112A	0.075 ± 0.003	1.0 ± 0.2	750 ± 180
M112L	0.150 ± 0.010	2.1 ± 0.2	700 ± 100

To identify the reason for the observed (and unexpected) difference between EF-Tu_{wt} EF-Tu_{H22G}, the activation entropy for EF-Tu•mant-GTP dissociation was determined. The dissociation of EF-Tu•mant-GTP was monitored by fluorescence based stopped-flow at temperatures ranging from 4°C to 37°C (**Figure 3.3**). These data were used to construct Eyring plots, with ln(k_{off}/T) plotted on the *y*-axis, and 1/T plotted on the *x*-axis. These plots exhibited the expected linear behaviour for both EF-Tu_{wt} and EF-Tu_{H22G}. A linear equation was fit to the data points for each EF-Tu variant, providing a slope equivalent to $-\Delta H^{0\ddagger}/R$ and a y-intercept equal to $\ln(k_B/h)+\Delta S^{0\ddagger}/R$. The differences in activation entropy and enthalpy between wild type and mutant EF-Tus are summarized in **Table 3.2**. Interestingly, the entropy of activation is higher for EF-Tu_{H22G}•mant-GTP dissociation compared to wild type ($T\Delta S^{0\ddagger}_{H22G}$ - $T\Delta S^{0\ddagger}_{wt}$ = (18 ± 4) kJ/mol at 20°C). This higher activation entropy is consistent with more conformational sampling in EF-Tu_{H22G} during the GTP dissociation mechanism as initially expected. While the increased entropic barrier would tend to increase the rate of EF-Tu_{H22G}•mant-GTP dissociation, this effect is counteracted by an enthalpic contribution. Based on the slopes of the temperature dependence in **Figure 3.3**, the enthalpic barrier for EF-Tu•mant-GTP dissociation is (19 ± 4) kJ/mol higher for EF-Tu_{H22G} compared to EF-Tu_{wt}. The overall difference in $\Delta\Delta G^{0\ddagger}$, calculated from the mant-GTP dissociation rates at 20 °C, is 2.3 kJ/mol which is

within the error of the entropy and enthalpy calculations reported here. At this point it is tempting to interpret the difference in $T\Delta S^{0‡}$ between EF-Tu_{wt} and EF-Tu_{H22G} in the context of expected changes in P-loop structural dynamics. Experimentally measured changes in entropy, however, reflect changes to the whole system and cannot be assigned to a small subset of atoms in the system.

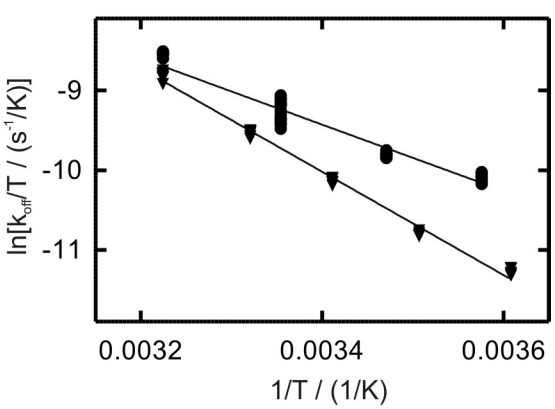

Figure 3.3. Eyring plots of mant-GTP dissociation from EF-Tu_{wt} and EF-Tu_{H22G}. Rate constants of EF-Tu•mant-GTP dissociation were determined at different temperatures using the fluorescence-based stopped-flow experiments described in **Figure 3.2** and **Section 3.2**. Data points represent rates obtained from fitting individual traces in replicate experiments; EF-Tu_{wt} (●), EF-Tu_{H22G} (▼). Trendlines were obtained by linear regression using Prism software (GraphPad).

Table 3.2. Thermodynamic parameters for mant-GTP dissociation from EF-Tu variants obtained from Eyring plots. Values for $\Delta\Delta H^{0‡}$ and $\Delta\Delta S^{0‡}$ represent differences relative to wild type EF-Tu. Values for $T•\Delta\Delta S^{0‡}$ were computed at 20°C.

EF-Tu	$\Delta\Delta H^{0‡}$ (kJ/mol)	$T•\Delta\Delta S^{0‡}$ (kJ/mol)
wt	0	0
H22G	19 ± 4	18 ± 4
M112G	1 ± 5	2 ± 5
M112A	0 ± 4	2 ± 4
M112L	1.2 ± 2.4	6.1 ± 2.5

Molecular Dynamics simulations reveal an additional hydrogen bond between GTP and the P-loop in EF-Tu_{H22G} .

In order to provide some insight into *where* the measured differences in activation entropy and enthalpy for wild type and H22G EF-Tu•mant-GTP dissociation might be localized, all-atom MD simulations were performed. Equilibrium MD simulations were carried out on wild type and H22G models of EF-Tu•GTP and EF-Tu^{apo} (no nucleotide or magnesium ion bound). Comparison of nucleotide-bound and nucleotide-free simulations

should be directly related to the equilibrium binding constant for GTP, ($K_{D,GTP}$), which describes the free energy difference between EF-Tu•GTP and EF-Tu + GTP. In addition, the transition state for GTP dissociation [EF-Tu•••GTP]‡ is expected to possess some properties of EF-Tu•GTP and some properties of EF-Tu^{apo} (Hammond, 1953). Thus, analysis of these two simulations should provide insight into the measured differences in $\Delta H^{0‡}$ and $T\Delta S^{0‡}$ for EF-Tu_{wt}•GTP and EF-Tu_{H22G}•GTP dissociation. Interactions between EF-Tu and bound nucleotide in simulations of EF-Tu_{wt}•GTP and EF-Tu_{H22G}•GTP are shown in **Figure 3.4**. For the wild type simulation, interactions between EF-Tu and GTP were consistent with available X-ray crystal structures throughout the 10 ns simulation: $Asn135_{Tu}$, $Lys136_{Tu}$, $Asp138_{Tu}$ of the NKxD motif formed the guanine base-specific interactions; the magnesium ion as well as the backbone amide bonds of four P-loop amino acids interacted with the β- and γ-phosphates of GTP (**Figure 3.4.A**), (Kjeldgaard et al., 1993). In simulations of EF-Tu_{H22G}•GTP, these same interactions were present. Interestingly, an additional hydrogen bond between the P-loop and GTP was observed in the EF-Tu_{H22G}•GTP simulation. This hydrogen bond formed between the backbone amide bond of $Gly22_{Tu}$ and an oxygen atom of the β-phosphate (**Figure 3.4.B**).

In order to assess P-loop/GTP hydrogen bonds on a quantitative level, the N-H•••O distances of each potential hydrogen bond was measured in snapshots throughout the simulations. These distances were used to construct histograms, to which Gaussian functions were fit as previously described (Wieden et al., 2010), (**Figure 3.4.C and D; Table 3.3**). The N_{22}-H•••$O_{β1}$ distances for EF-Tu_{wt}•GTP and EF-Tu_{H22G}•GTP were fit well by single Gaussian distributions centred at (3.1 ± 0.3) Å and (2.0 ± 0.2) Å, respectively. Although a small tail at higher distances was observed in the

EF-Tu_{H22G}•GTP simulation, the fit was not improved by addition of a second Gaussian function. This analysis demonstrates that while the N_{His22}-H•••$O_{\beta1}$ distance does not constitute a hydrogen bond under a conservative criterion of 2.7 Å (Wieden et al., 2010) in the wild type simulation, it does for EF-Tu_{H22G}. This hydrogen bond is expected to contribute to the higher binding affinity for EF-Tu_{H22G}•GTP compared to EF-Tu_{wt}•GTP. More specifically, this hydrogen bond is expected to contribute to the measured increase in activation enthalpy for EF-Tu_{H22G}•GTP dissociation compared to wild type. This is consistent with the slower GTP dissociation from EF-Tu_{H22G}, compared to wild type, measured *in vitro* at 20 °C.

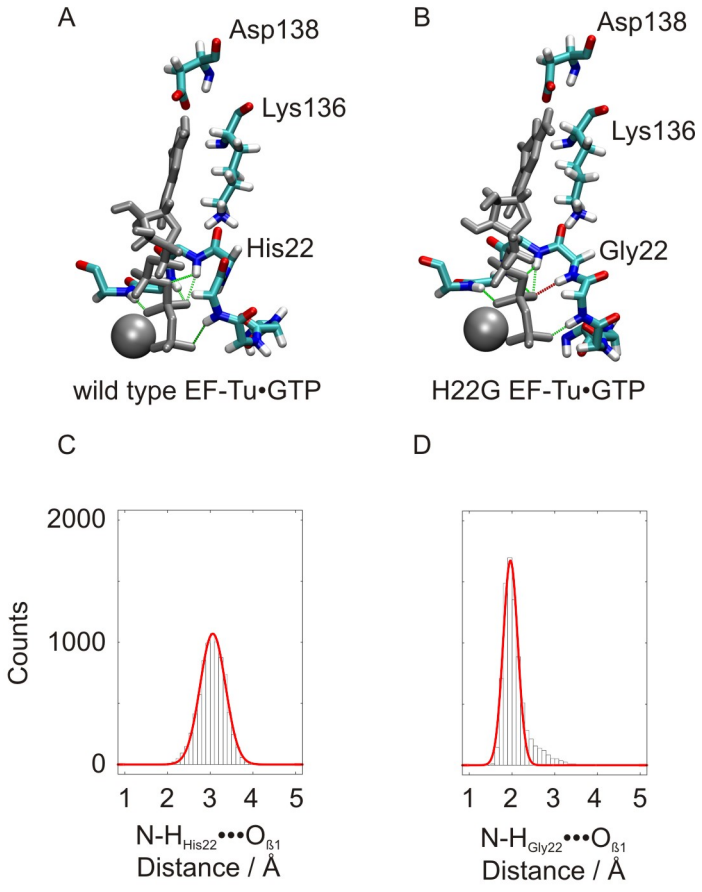

Figure 3.4. The EF-Tu_{H22G} variant forms an additional hydrogen bond between the P-loop and bound GTP during molecular dynamics simulations. The snapshots presented in (A) and (B) were taken after 10 ns of equilibrium MD simulations of EF-Tu_{wt}•GTP (A) and EF-Tu_{H22G}•GTP (B). Backbone atoms of the P-loop are shown as sticks as are $Lys136_{Tu}$ and $Asp138_{Tu}$ of the NKxD motif. GTP and the Mg^{2+} ion are shown as sticks and a van der Waals sphere, respectively (coloured silver). Hydrogen bonds identified between P-loop amino acids and GTP phosphates in both wt and H22G models are indicated by green dashed lines. The N-H_{His22}•••Oβ1 hydrogen bond found in the EF-Tu_{H22G}•GTP model is shown as a red dashed line. The N-H_{22}•••$O_{\beta1}$ distances were measured in snapshots during MD simulation of EF-Tu_{wt}•GTP (C) and EF-Tu_{H22G}•GTP (D), and plotted in histograms. The solid red lines represent fits of the histograms to single Gaussian functions.

Table 3.3 Distances between N-H bonds of the P-loop backbone and oxygen atoms of GTP phosphates during MD simulations. Average values and errors are reported as determined by Gaussian fits to histograms of N-H•••O distances.

Distance Measured	EF-Tu_{wt}•GTP	EF-Tu_{H22G}•GTP
$N\text{-}H_{Asp21}\bullet\bullet\bullet O_{\gamma 2}$	(2.3 ± 0.3) Å	(1.96 ± 0.21) Å
$N\text{-}H_{His22}\bullet\bullet\bullet O_{\beta 1}$	**(3.1 ± 0.3) Å**	**(1.97 ± 0.17) Å**
$N\text{-}H_{Gly23}\bullet\bullet\bullet O_{\beta 1}$	(2.19 ± 0.19) Å	(1.97 ± 0.19) Å
$N\text{-}H_{Gly23}\bullet\bullet\bullet O_{\alpha 3}$	(2.63 ± 0.23) Å	(2.55 ± 0.25) Å
$N\text{-}H_{Lys24}\bullet\bullet\bullet O_{\beta 1}$	(1.97 ± 0.14) Å	(2.01 ± 0.15) Å
$N\text{-}H_{Thr25}\bullet\bullet\bullet O_{\beta 2}$	(1.95 ± 0.12) Å	(1.98 ± 0.12) Å

Substitution of Histidine 22 with Glycine increases backbone conformational freedom in the P-loop.

Replacement of $His22_{Tu}$ with glycine appears to increase the conformational freedom of the P-loop backbone at position 22 allowing for the formation of an additional hydrogen bond to GTP. This apparent increase in allowed backbone conformations in EF-Tu_{H22G}, compared to EF-Tu_{wt} could account for the measured increase in entropy of activation for EF-Tu_{H22G}•GTP dissociation. In order to directly compare differences in backbone structural dynamics, the backbone φ and ψ angles of every amino acid were measured in snapshots throughout MD simulations. These values were used to construct a 'Ramachandran histogram' for each amino acid in each simulation, such that the conformational space explored by the backbone of each amino acid could be visualized (**Figure 3.5**). Each Ramachandran histogram was then searched for distinct conformations using a computer script described in **Section 3.2**. The amino acids that occupied multiple conformations on the Ramachandran histogram were identified as 'hot' amino acids. These 'hot' amino acids are likely to make significant contributions to the global entropy of EF-Tu, as entropy is proportional to the multiplicity of microstates in the system. The hot amino acids in each simulation were identified and represented in

blue in **Figure 3.5.B**. In the simulation of EF-Tu$_{H22G}$•GTP, Asp21$_{Tu}$ in the P-loop was identified as hot, while no amino acids that interact with GTP were hot in the wild-type simulation. In simulations of EF-Tu$^{apo}_{H22G}$, P-loop amino acids Gly22$_{Tu}$ and Gly23$_{Tu}$ were hot while, once again, no amino acids that would interact with GTP were hot in the EF-Tu$^{apo}_{wt}$ simulation. These simulations suggest that progression from EF-Tu•GTP to EF-Tu^{apo} causes a larger increase in P-loop structural dynamics for EF-Tu$_{H22G}$ than EF-Tu$_{wt}$. This is consistent with the measurably larger $T\Delta S^{0\ddagger}$ for EF-Tu$_{H22G}$•GTP dissociation compared to wild type *in vitro*. In addition, it appears that the differences in P-loop structural dynamics identified in **Figure 3.5** based on *in silico* simulation provide

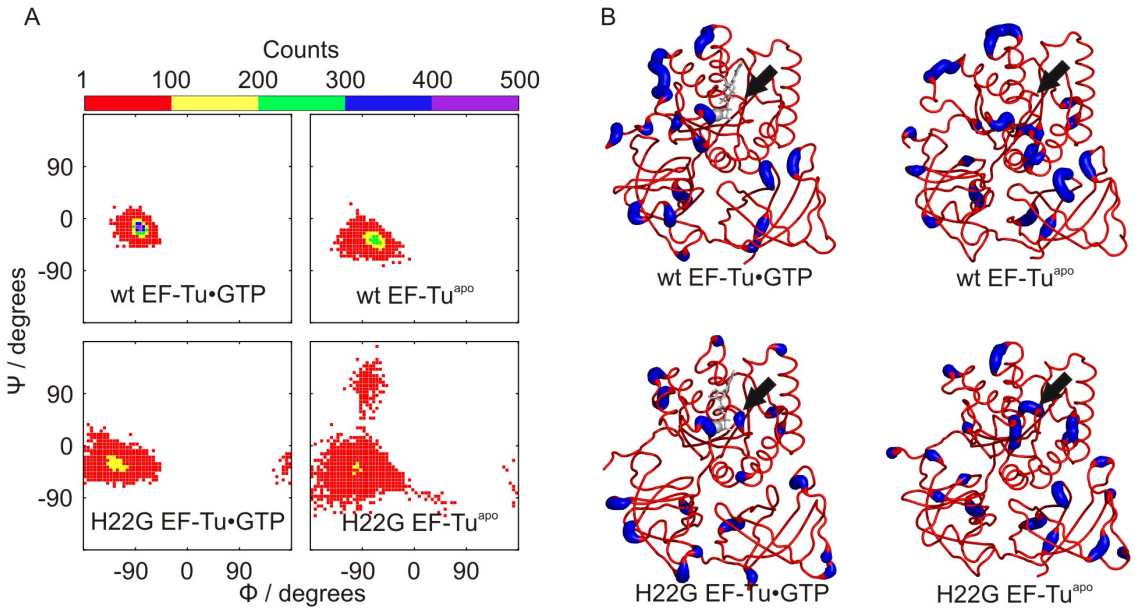

Figure 3.5. The P-loop has higher entropy in MD simulations of EF-Tu$_{H22G}$ compared to EF-Tu$_{wt}$. The backbone φ and ψ dihedral angles of amino acid 22 were measured in snapshots of 10 ns equilibrium MD simulations of EF-Tu•GTP, EF-Tu^{apo}, EF-Tu$_{H22G}$•GTP, and EF-Tu$_{H22G}^{apo}$, and plotted in 2-D histograms of φ vs. ψ (A). Each histogram is divided into bins with dimensions π/32 x π/32. Each bin was coloured based on the occupancy as defined in the colour legend. Each 2-D histogram was searched for local maxima (see **Section 3.2**) that were separated by at least 3π/32, indicative of amino acids that occupy multiple conformations. Amino acids that occupied multiple conformations in histograms analogous to those in (A) were identified as 'hot' and coloured blue on the structures presented in (B). Each structure presented in (B) is a snapshot taken after 10 ns of the respective MD simulation. The arrows in (B) are each directed at amino acid 22 in the P-loop as a reference point.

a reasonable indication of P-loop entropy. The comparison of EF-Tu_{H22G} and EF-Tu_{wt} *in vitro* and *in silico* demonstrates that higher P-loop dynamics are correlated with a measurably higher entropy of activation for EF-Tu•GTP dissociation. This suggests that P-loop structural dynamics contribute significantly to EF-Tu•GTP dissociation and constitutes a structural element that can be used to fine-tune nucleotide-binding properties.

Amino acid 112 modulates GTP binding in EF-Tu in vitro.

Next I sought to establish if and how P-loop dynamics are fine-tuned in EF-Tu. Previous work has shown that amino acids adjacent to the P-loop can influence nucleotide-binding properties of EF-Tu. Specifically, a ten-fold reduction in nucleotide binding affinities upon substitution of $His118_{Tu}$ with alanine was proposed to result from removal of a $His118_{Tu}$•••$Gly18_{Tu}$ hydrogen bond between the P-loop and helix C (Dahl et al., 2006). Furthermore, D109A substitution in EF-Tu, which removes a transient $Asp109_{Tu}$•••$His22_{Tu}$ hydrogen bond with the P-loop, was shown to reduce the EF-Ts-stimulated GDP-dissociation ten-fold (Wieden et al., 2010). Methionine 112 in EF-Tu is close to $Asp109_{Tu}$ in primary sequence and forms close contacts with $His22_{Tu}$ of the P-loop in X-ray crystal structures (Kawashima et al., 1996) and MD simulations (**Figure 3.1**). In addition, $Met112_{Tu}$ is conserved in 124 of 125 aligned bacterial EF-Tu sequences suggesting that function has significantly limited the evolution-accessible sequence space at this position (DeLaurentiis et al., 2011). Thus, $Met112_{Tu}$ was selected as a promising candidate for fine-tuning P-loop structural dynamics. Based on its location relative to the P-loop, $Met112_{Tu}$ could act as a 'door stop', limiting the motion of the $His22_{Tu}$ sidechain and, subsequently, limiting P-loop conformational freedom. To test this hypothesis, three

EF-Tu variants were constructed with glycine, alanine, or leucine at position 112. Replacement of $Met112_{Tu}$ with the smallest amino acids (glycine or alanine) was expected to provide more conformational freedom for the P-loop, increase the rate of EF-Tu•GTP dissociation, and reduce the affinity of the EF-Tu•GTP complex without providing additional hydrogen bonding opportunities for the P-loop backbone (*vide supra*). Replacement of $Met112_{Tu}$ with leucine, however, was expected to have little effect on P-loop dynamics, and little effect on EF-Tu•GTP binding. These EF-Tu variants were constructed, expressed, purified, and the rate constants for nucleotide binding and dissociation were subsequently determined.

Surprisingly, little difference in GTP-binding properties was observed between $EF\text{-}Tu_{wt}$ and $EF\text{-}Tu_{M112G}$. The only significant difference was a modest (2-fold) decrease in k_{on} for $EF\text{-}Tu_{M112G}$•GTP complex formation (**Table 3.1**). The M112A substitution reduced the affinity of EF-Tu•GTP by about 10-fold (**Table 3.1**), due to opposite affects on k_{on} and k_{off}. Intriguingly, the M112L substitution showed the most dramatic effects on EF-Tu/GTP interactions. Substitution of Met112 with the similarly sized leucine reduced the affinity of EF-Tu for GTP by approximately ten-fold (**Table 3.1**). This effect was the result of an approximate 5-fold increase in k_{off} and ~2-fold decrease in k_{on}. These observations clearly demonstrate that an amino acid in position 112 can modulate nucleotide-binding properties in EF-Tu, but how this modulation is conferred from the secondary shell to the P-loop remained unclear.

M112L substitution increases the entropy barrier for GTP dissociation in vitro.

To better understand how position 112 modulates GTP-binding properties in EF-Tu, the temperature dependence of mant-GTP dissociation was investigated in a manner similar

to EF-Tu_{H22G} (**Figure 3.6**). The obtained Eyring plots clearly demonstrate that the slopes, and consequently $\Delta H^{0‡}$, for EF-Tu_{M112X}•mant-GTP dissociation are identical to wild type within the error of the method. In regards to entropy, only the EF-Tu_{M112L} shows a statistically significant difference in $T\Delta S^{0‡}$ when compared to EF-Tu_{wt}•GTP dissociation. Substitution of $Met112_{Tu}$ with leucine increases the entropy of activation for EF-Tu•GTP dissociation by (6.1 ± 2.5) kJ/mol at 20°C and, consequently, accelerates dissociation.

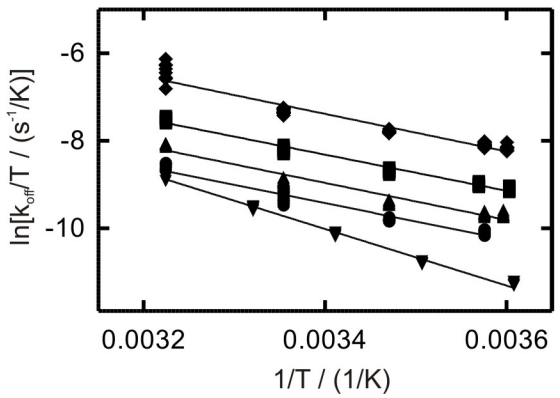

Figure 3.6. Eyring plots of mant-GTP dissociation from EF-Tu variants. Mant-GTP dissociation was monitored as described in **Section 3.2** and **Figure 3.2**. Data points represent rates obtained from fitting individual traces in replicate experiments; wild type EF-Tu (●), H22G (▼), M112G (▲), M112A (■), M112L (♦). Trendlines were obtained by linear regression using Prism software (GraphPad).

M112L substitution weakens P-loop/helix C interactions and increases P-loop flexibility.

In order to investigate the reason for the increased entropy of activation observed during dissociation of EF-Tu_{M112L}•GTP, MD simulations of EF-Tu_{wt} and EF-Tu_{M112L} were compared. As for EF-Tu_{H22G}, equilibrium simulations of the EF-Tu_{M112L}•GTP complex and EF-Tu^{apo}_{M112L} were carried out, and amino acids occupying multiple backbone conformations were identified. No amino acids that could potentially interact with the bound GTP were identified as 'hot' in any of the simulations. It seemed possible that these short equilibrium MD simulations were unable to capture the effect of M112L substitution on the [EF-Tu•••GTP]‡ transition state. This was not entirely surprising since transition states are necessarily distinct from conformations that lie at energy minima on

the potential energy surface (the starting points for the equilibrium MD simulations). Steered molecular dynamics (SMD) simulations were applied to evoke GTP dissociation *in silico* and explore the structural dynamics of these models outside the energy basins sampled during equilibrium MD simulations.

This SMD approach introduces a spring with one end attached to the ligand and the other end attached to a point in space that moves at a constant velocity throughout the simulation.(Phillips et al., 2005) To minimize systematic errors of this strict biasing force, five different 'pulling' directions were investigated (**Figure 3.7**) and five different starting conformations (6, 7, 8, 9, or 10 ns old equilibrium MD simulations) were tested for each model. In total, 25 different SMD simulations were performed for each model. The resulting trajectories were not interpreted as likely GTP-dissociation pathways due to the bias imposed by a constant pulling direction in SMD relative to the natural process of GTP dissociation *in vitro* or *in vivo*. Instead, the SMD simulations were interpreted as models perturbed out of potential energy minima. In this context perturbed models were analyzed to identify the 'hot' amino acids. The backbone conformation of each amino acid was investigated on a Ramachandran histogram as in **Figure 3.5.A**, and the 'hot' amino acids were identified. The probability of each amino acid being hot in an SMD simulation was expressed as a percentage of the 25 total SMD simulations and represented as a colour on the respective EF-Tu•GTP model in **Figure 3.7**. The 'hot' amino acids identified in **Figure 3.7** reveal that P-loop amino acids do undergo backbone conformational changes during these SMD simulations. Each P-loop amino acid has an equal or higher probability of being hot in EF-Tu_{M112L}•GTP compared to wild type (**see Table 3.4**). These results suggests that the P-loop is able to explore more conformations

during EF-Tu•GTP dissociation in the M112L variant compared to wild type. This is expected to contribute to the increased entropy of activation (and a faster rate constant) for EF-Tu_{M112L}•GTP dissociation.

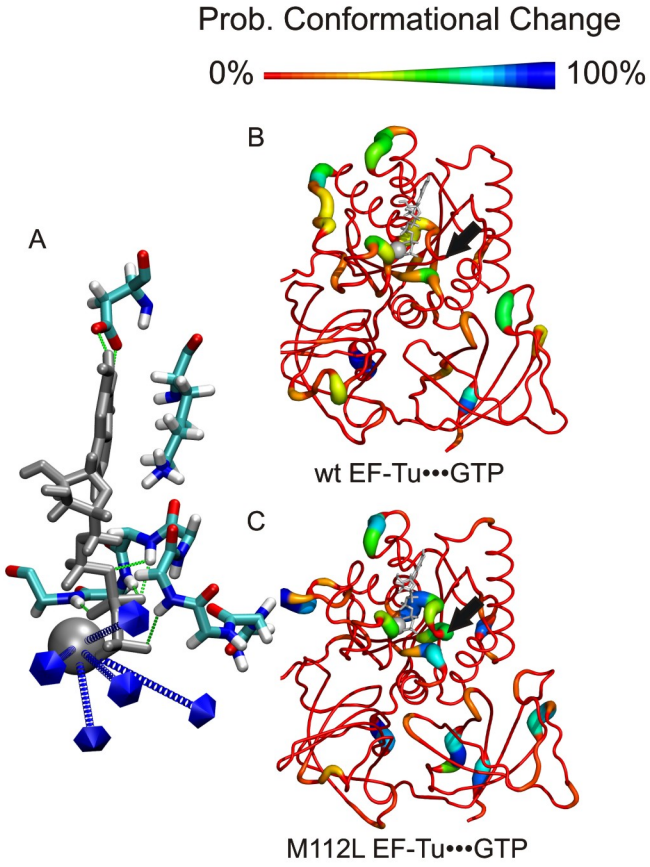

Figure 3.7. The P-loop has higher entropy in steered MD simulations of EF-Tu_{M112L} compared to EF-Tu_{wt}. The five different directions used to pull GTP•Mg^{2+} out of the nucleotide binding pocket of EF-Tu are shown as blue arrows in A. The nucleotide-binding pocket is represented as in **Figure 3.4 A, B**, and the snapshot was taken after 10ns of equilibrium MD simulation of EF-Tu_{wt}•GTP. The probability of a backbone conformational change during SMD simulation was computed in percent for each amino acid in EF-Tu_{wt}•GTP (B) and EF-Tu_{M112L}•GTP (C), and represented as a different colour and thickness on the corresponding structure. The structures in B and C are snapshots taken after 10 ns of the respective equilibrium MD simulation.

Table 3.4. Probability of P-loop amino acids undergoing backbone conformational changes during steered MD. Probabilities (in percent) were computed based on the fractions of SMD simulations in which the respective amino acid occupied multiple backbone conformations.

Amino Acid	wt	H22G	M112G	M112A	M112L
Gly18	**0**	28	4	4	**64**
His19	**0**	28	16	8	**64**
Val20	4	12	8	4	4
Asp21	12	80	72	12	48
His22	20	72	56	24	56
Gly23	40	52	56	52	88
Lys24	44	40	56	52	88
Thr25	4	8	4	8	16

Comparing the P-loop amino acids in **Table 3.4** revealed that the largest differences between EF-Tu_{wt} and EF-Tu_{M112L} were found in the two amino acids at the N-terminus of the P-loop: $Gly18_{Tu}$ and $His19_{Tu}$. Each of these amino acids was hot in zero SMD simulations for the wild type model and 64% of SMD simulations for the M112L model. In order to better understand the structural basis of these differences, equilibrium MD simulations of EF-Tu_{wt}•GTP and EF-Tu_{M112L}•GTP were compared. In EF-Tu_{wt}•GTP, $Gly18_{Tu}$ and $His19_{Tu}$ are stabilized by hydrogen bonds to $His118_{Tu}$ and $Gln114_{Tu}$, respectively (**Figure 3.8**). In simulations of EF-Tu_{M112L}•GTP, however, the His19•••Gln114 hydrogen bond was not present while the Gly18•••His118 hydrogen bond was only transiently stable (43.9% of the analyzed simulation; **Figure 3.8**). This effect appears to result from the slightly higher space requirements of the leucine sidechain compared to methionine; in order to accommodate the branched leucine sidechain, the N-terminal tip of helix C is displaced approximately 3.6 Å away from the P-loop (**Figure 3.8.B**). This displacement was measured between the nitrogen atom of $Pro113_{Tu}$ in each model following alignment EF-Tu_{wt}•GTP and EF-Tu_{M112L}•GTP via the P-loop backbone atoms after 10 ns of equilibrium simulation. These results suggest that hydrogen bonds between His19/Gly18 of the P-loop and Gln114/His118 of helix C limit the structural dynamics of the P-loop and mediate the entropy of activation for EF-Tu•GTP dissociation.

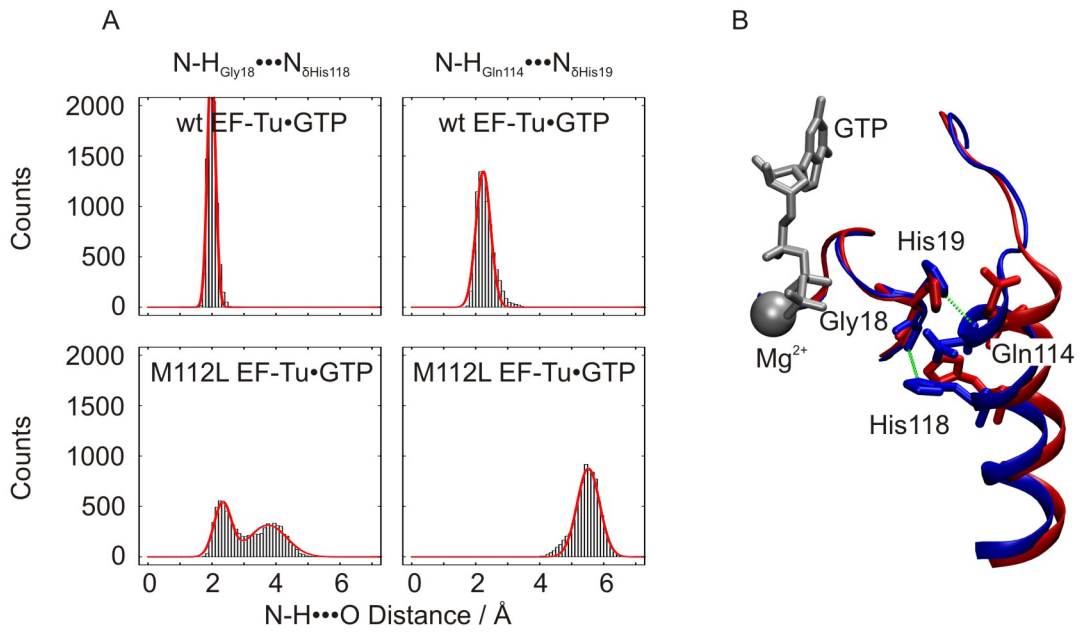

Figure 3.8. Substitution of methionine 112 with leucine disrupts two P-loop/helix C interactions in equilibrium MD simulations of EF-Tu•GTP. Distances between N and H atoms of potential hydrogen bonds were measured in snapshots during equilibrium MD simulations of EF-Tu$_{wt}$•GTP and EF-Tu$_{M112L}$•GTP. Distances were plotted as histograms in A which were subsequently fitted to single- or double-Gaussian functions (red lines in A). Comparison of EF-Tu$_{wt}$•GTP (blue) and EF-Tu$_{M112L}$•GTP (red) after 10ns of equilibrium MD simulations reveals that displacement of helix C is concomitant with disruption of Gly18•••His118 and His19•••Gln114 interactions (B). The P-loop and helix C from each protein are represented as cartoons, and pertinent sidechains are shown as sticks. The GTP molecule and Mg^{2+} from the wild type simulation are coloured silver and shown as sticks and van der Waals representation, respectively. All hydrogen atoms are omitted for clarity, and green dashed lines represent N•••N distances of the hydrogen bonds analyzed.

Table 3.5. Summary of 'hot' P-loop amino acids in MD simulations of all EF-Tu variants. Amino acids listed for SMD were 'hot' in 20% or more of SMD simulations.

	wild type	H22G	M112G	M112A	M112L
K_D/nM [a]	70 ± 30	8.5 ± 0.5	91 ± 9	750 ± 180	700 ± 100
$T\Delta S^{0‡}$ @ 20°C [b] /kJmol^{-1}	-46 ± 1	-29 ± 2	-45 ± 5	-44 ± 3	-40 ± 1
EF-Tu•GTP 'Hot' amino acids	none	Asp21	Asp21 His22	none	none
SMD 'Hot amino acids'	His22 Gly23 Lys24	Gly18 His19 Asp21 Gly22 Gly23 Lys24	Asp21 His22 Gly23 Lys24	His22 Gly23 Lys24	Gly18 His19 Asp21 His22 Gly23 Lys24
EF-Tu^{Apo} 'Hot' amino acids	none	Gly22 Gly23	Asp21	none	none

a computed from kinetic analysis of the EF-Tu•GTP complex
b computed for EF-Tu•GTP dissociation

Global comparison of P-loop dynamics in EF-Tu variants

In order to assist in the direct comparison of P-loop structural dynamics between all EF-Tu variants studied here, SMD and equilibrium MD simulations were performed on models of all EF-Tu variants. The hot amino acids identified in all SMD and equilibrium MD simulations are summarized in **Table 3.5**. For comparison, amino acids that were hot in 20% of SMD simulations or more are included as hot amino acids in this summary. The P-loop dynamics of EF-Tu_{M112A} are similar to those of EF-Tu_{wt}. Neither variant shows any hot amino acids in equilibrium MD simulations, and $His22_{Tu}$, $Gly23_{Tu}$, and $Lys24_{Tu}$ are hot in 20% or more of SMD simulations. This is consistent with the lack of measureable difference in the entropy barrier for EF-Tu•GTP dissociation. EF-Tu_{M112A} does, however, have a ten-fold lower binding affinity for GTP than EF-Tu_{wt} (K_D/nM = 750 ± 180 vs. 70 ± 30 for M112A vs. wild type). When snapshots from equilibrium MD simulations of EF-Tu_{wt}^{apo} and EF-Tu_{M112A}^{apo} were compared, an obvious difference in P-loop conformations was observed. The P-loop of EF-Tu_{wt}•GTP was similar to that in EF-Tu_{wt}^{apo} simulations, while for the EF-Tu_{M112A}^{apo}, the P-loop forms a single helical turn from amino acids 19 to 23 as shown in **Figure 3.9.I**. This P-loop conformation, which is not observed in simulations of any other variants, should stabilize the EF-Tu^{apo} conformation. This stabilization likely contributes to the smaller change in free energy upon GTP binding to EF-Tu_{M112A} compared to EF-Tu_{wt} that is evident from the larger K_D determined experimentally.

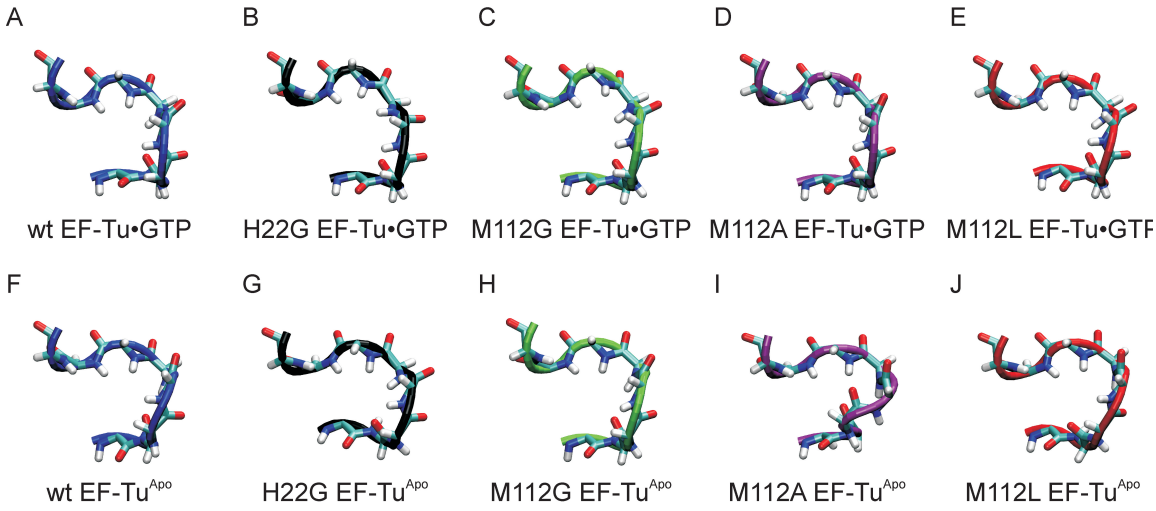

Figure 3.9. The P-loop forms a helical turn in simulation of EF-Tu_{M112A}^{apo}. P-loop backbone conformations are shown for wild type (A&F), H22G (B&G), M112G (C&H), M112A (D&I), and M112L (E&J) after 10ns of simulation of EF-Tu•GTP (A-E) or $EF\text{-}Tu^{apo}$ (F-J).

The $EF\text{-}Tu_{H22G}$ variant, which has the largest entropy of activation for EF-Tu•GTP dissociation, is the only variant that has more hot amino acids in $EF\text{-}Tu^{apo}$ compared to EF-Tu•GTP. If the transition state of EF-Tu•GTP dissociation possesses some dynamic properties of the EF-Tu•GTP complex, and some dynamic properties of $EF\text{-}Tu^{apo}$, then there the P-loop of the $[EF\text{-}Tu_{H22G}\bullet\bullet\bullet GTP]^{\ddagger}$ transition state likely moves more freely compared to wild type. As stated previously, this is consistent with the higher $T\Delta S^{0\ddagger}$ for $EF\text{-}Tu_{H22G}$•GTP dissociation compared to wild type. In comparison, there are two hot amino acids in the $EF\text{-}Tu_{M112G}$•GTP simulation ($Asp21_{Tu}$ and $His22_{Tu}$) indicating that substitution of Met112 with glycine does, in fact, increase P-loop conformational freedom relative to wild type. In the $EF\text{-}Tu_{M112G}^{apo}$ simulation, however, only $Asp21_{Tu}$ is hot, indicating a net loss in hot amino acids progressing from $EF\text{-}Tu_{M112G}$•GTP to $EF\text{-}Tu_{M112G}^{apo}$. While one might expect a smaller activation entropy for $EF\text{-}Tu_{M112G}$•GTP dissociation compared to wild type, this change may be too small to be measured using

the kinetic approach employed here. The M112G substitution demonstrates that increased P-loop motion does not necessarily result in accelerated nucleotide dissociation.

When hot amino acids are compared in SMD simulations of the different EF-Tu variants (**Table 3.6**) it is evident that $Gly18_{Tu}$ and $His19_{Tu}$ are hot in 20% of SMD simulations or more for EF-Tu_{H22G} and EF-Tu_{M112L} variants only. While 20% is an arbitrary cutoff, from **Table 3.5** it is clear that $Gly18_{Tu}$ and $His19_{Tu}$ are more likely to be hot in SMD simulations of EF-Tu_{H22G} and EF-Tu_{M112L}, than any other variant tested. These are the two EF-Tu variants that demonstrate the largest entropies of activation for EF-Tu•GTP dissociation. Thus, there is a clear correlation between backbone dynamics at positions 18 and 19 in the P-loop of EF-Tu, and nucleotide dissociation rates. Despite the finding that $Gly18_{Tu}$ and $His19_{Tu}$ are hot in more SMD simulations of EF-Tu_{M112L} than EF-Tu_{H22G}, the entropy of activation for EF-Tu•GTP dissociation is smaller for EF-Tu_{M112L} than EF-Tu_{H22G}. This inconsistency may reflect the limitation of SMD in predicting relative entropy barriers during ligand dissociation; indeed pulling a ligand out of a binding pocket in a constant direction is likely an unnatural approximation. Conversely, the increase in P-loop backbone dynamics observed in EF-$Tu_{H22G}{}^{Apo}$compared to EF-Tu_{H22G}•GTP may reflect a more significant contribution to activation entropy than the SMD experiments.

3.4 Conclusions

The results presented here demonstrate that increased P-loop mobility in EF-Tu does not necessarily alter nucleotide-binding properties (eg: EF-Tu_{M112G} vs. EF-Tu_{wt}). Increased backbone flexibility at $Gly18_{Tu}$ and $His19_{Tu}$, the two amino acids at the N-terminus of the P-loop, however, correlates with larger entropies of activation for EF-Tu•GTP dissociation, and rapid GTP dissociation. This suggests that the structural dynamics at these two positions in the P-loop make a significant contribution to mediating nucleotide binding in EF-Tu. For EF-Tu_{M112L}, increased backbone conformational freedom of $Gly18_{Tu}$ and $His19_{Tu}$ compared to wild type appears to result from disruption of $His19_{Tu}$•••$Gln114_{Tu}$ and $His118_{Tu}$•••$Gly18_{Tu}$ sidechain•••backbone hydrogen bonds. Disruption of these stabilizing interactions between the P-loop and the adjacent helix C likely increases the entropy of the [EF-Tu•••GTP]‡ transition state, lowering its free energy and accelerating nucleotide dissociation. This interpretation is consistent with the measured entropies of activation and rates of EF-Tu•mant-GTP dissociation presented here. A previous study of the EF-Tu_{H118A} variant showed that upon elimination of the $His118_{Tu}$•••$Gly18_{Tu}$ hydrogen bond between helix C and the P-loop, the rates of GTP and GDP dissociation were ten-fold faster than wild type (Dahl et al., 2006). This is in complete agreement with the data presented here and the subsequent interpretation. The importance of the $His19_{Tu}$•••$Gln114_{Tu}$ and $His118_{Tu}$•••$Gly18_{Tu}$ hydrogen bonds is highlighted by the finding that these amino acids are invariant in the 125 EF-Tu sequences investigated by De Laurentiis *et al*. (2011). This raises the question: are these interactions also important in other P-loop NTPases? To address this question, P-loop/helix C interactions were identified in structures of the G-proteins EF-G

(PDBID: 2BV3), FtsY (PDBID: 2Q9B), Ffh (PDBID: 2CO4), Ras (PDBID: 3L8Z), Rac1 (PDBID: 1MH1), and Ran (PDBID: 1MH1), along with the ATPases adenylate kinase (PDBID: 1AKE) and MutS (PDBID: 1E3M). Sequence alignments of the same structural elements, shown in **Appendix A.2.1**, reveal that interactions between helix C and one or both of the two N-terminal P-loop amino acids are highly conserved in each of these P-loop NTPases. I hypothesize that these conserved interactions between the P-loop and helix C form a 'P-loop anchor' that regulates P-loop entropy and, subsequently, nucleotide binding properties in P-loop NTPases. These P-loop anchors can take the form of hydrogen bonds as in EF-Tu, EF-G, Rac1, and Ran or hydrophobic interactions as in Ras, FtsY, Ffh, adenylate kinase, and MutS. While the latter class appears weak in nature, it was previously identified as part of a conserved 'glycine brace' in some Ras family G-proteins (Neuwald, 2009), supporting the functional relevance of a P-loop anchor as a conserved element in P-loop NTPases.

Conformational changes in the P-loop of EF-Tu, induced by EF-Ts binding, have been proposed to stimulate EF-Tu•nucleotide dissociation (Kawashima et al., 1996). Increased P-loop mobility would likely accelerate these conformational changes and, therefore, promote nucleotide dissociation. Interestingly, the P-loop anchor in EF-Tu is broken in the crystal structure of the EF-Tu•EF-Ts complex (Kawashima et al., 1996) as shown in **Figure 3.10.A**, suggesting that EF-Ts may have evolved to act on this conserved element to increase P-loop mobility during nucleotide dissociation. Similarly, X-ray crystal structures of Ran in complex with GDPNP or its GEF RCC1 reveals that GEF binding is concomitant with breaking the P-loop anchor in this G-protein as well (**Figure 3.10.B**) (Renault et al., 2001). Crystal structures of Ras and Rac1 bound to their respective GEFs

demonstrate that breaking P-loop/helix C interactions is not a requirement for GEF binding (Chhatriwala et al., 2007; Margarit et al., 2003), but it seems likely that some GEFs have evolved in the context of this P-loop anchor in order to mediate P-loop structural dynamics and promote nucleotide dissociation.

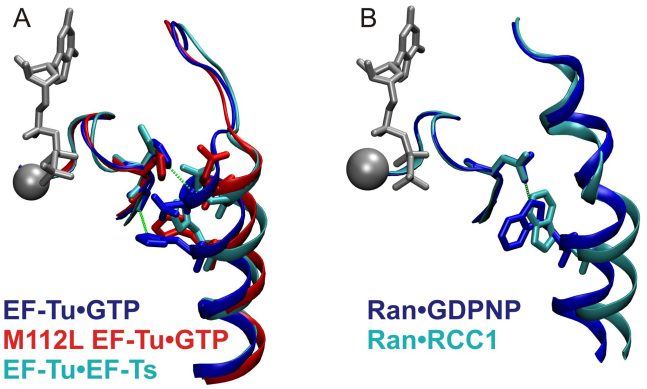

Figure 3.10. Interactions between the P-loop and helix C are broken by guanine nucleotide exchange factors for EF-Tu and Ran. Interactions between the P-loop and Helix C in EF-Tu_{wt}•GTP after 10 ns of MD simulation are compared to EF-Tu_{M112L}•GTP and the crystal structure of the EF-Tu•EF-Ts complex in (A). A similar interaction between the P-loop and adjacent helix of Ran is compared in X-ray structures of Ran•GDPNP (PDBID: 1IBR) and Ran•RCC1 (PDBID: 1I2M) (B). The P-loops and helices are shown in cartoon representation; sidechain and/or backbone atoms of amino acids participating in hydrogen bonds are shown as sticks; GTP and Mg^{2+} are represented as in **Figure 3.7**. All hydrogen atoms are omitted for clarity, and green dashed lines connect heavy atoms involved in each hydrogen bond. All superimpositions were performed using P-loop backbone atoms.

Chapter 4

Structural dynamics of switch II are critical for efficient guanine nucleotide exchange in Elongation Factor Tu

4.1 Introduction

During protein synthesis, the translation of mRNA relies on different aminoacyl-tRNAs (aa-tRNA) sampling the mRNA codon in the ribosomal A-site before the correct aa-tRNA is selected by codon/anticodon base pairing (Thompson and Stone, 1977). The first step in the selection of aa-tRNA is carried out by the universally conserved Elongation Factor (EF) which is thermally unstable (Tu), that binds to the ribosomal A-site as an EF-Tu•GTP•aa-tRNA ternary complex (Pape et al., 1998; Ravel et al., 1968). Following recognition of the correct anticodon in the ribosomal decoding centre, the GTPase activity of EF-Tu is activated (Pape et al., 1999). Hydrolysis of GTP and release of phosphate by EF-Tu are prerequisites for release of the aa-tRNA into the A-site of the ribosome (Kothe and Rodnina, 2006; Yokosawa et al., 1975). Thus, irreversible GTP hydrolysis acts as a barrier to separate codon-independent aa-tRNA binding, and codon-dependent aa-tRNA delivery to the A-site of the ribosome (Pape et al., 1998; Thompson and Stone, 1977).

During delivery of each aa-tRNA, EF-Tu is converted from its active GTP-bound form, which is capable of binding aa-tRNA with high affinity, to its inactive GDP-bound form (Yokosawa et al., 1975). Recycling of EF-Tu therefore requires the exchange of GDP for GTP and must be rapid in order to sustain in vivo protein synthesis rates (10-20 amino acids per second in *E. coli*) (Forchhammer and Lindahl, 1971; Proshkin et al., 2010). As the rate of spontaneous GDP dissociation from EF-Tu is too slow to ensure efficient recycling of EF-Tu ($k_{off} = 0.002\ s^{-1}$), bacteria rely on the conserved protein EF-Ts, which accelerates GDP dissociation by 60,000 fold (Gromadski et al., 2002). The complete kinetic mechanism of nucleotide exchange on EF-Tu has been solved by Rodnina's

research group (**Scheme 4.1**) and reveals an overall rate of about 30 s^{-1} for nucleotide exchange (Gromadski et al., 2002) which is rapid enough to sustain *in vivo* rates of protein synthesis.

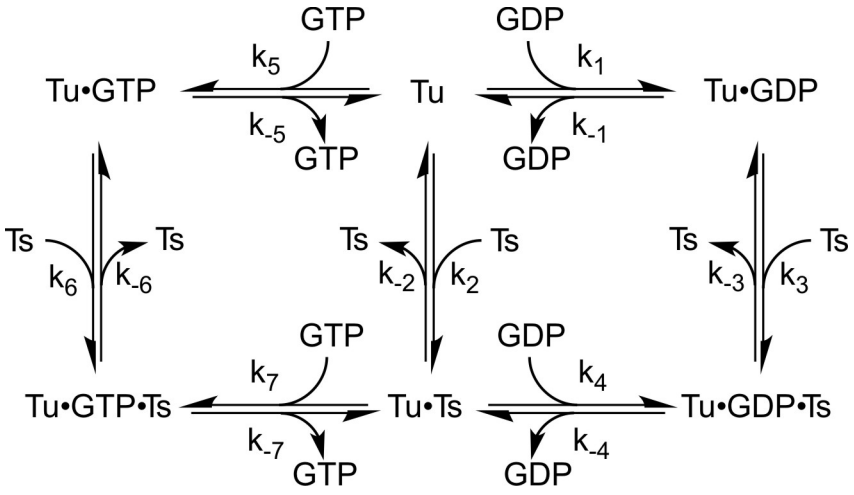

Scheme 4.1. Complete kinetic scheme of nucleotide exchange in EF-Tu.

An X-ray crystal structure of the EF-Tu•EF-Ts complex from *E. coli*, along with biochemical studies of numerous EF-Tu and EF-Ts variants, has highlighted several amino acids that are important for nucleotide exchange. The EF-Tu•EF-Ts complex (Kawashima et al., 1996) shows that EF-Ts binds to the 'side' of EF-Tu formed by domains I & III where it contacts both of these domains (**Figure 4.1**). Mutational analyses of amino acids along the EF-Tu/EF-Ts interface demonstrated that many of the contacts identified in the X-ray crystal structure indeed stabilize the EF-Tu•EF-Ts complex (Wieden et al., 2002; Zhang et al., 1998). The structural differences between EF-Tu•nucleotide complexes and EF-Tu•EF-Ts have prompted hypotheses about the mechanism of EF-Ts-stimulated nucleotide dissociation in EF-Tu. Contacts between EF-Ts and the phosphate-binding loop (P-loop) of EF-Tu appear to stabilize a 'flipped' conformation of the P-loop that is incompatible with nucleotide binding (Kawashima et

al., 1996). Previous work has revealed that $Asp109_{Tu}$ forms a transient hydrogen bond with $His22_{Tu}$ of the P-loop in Molecular Dynamics (MD) simulations and that D109A substitution in EF-Tu reduces the EF-Ts-stimulated rate of GDP dissociation over ten-fold (Wieden et al., 2010). Based on available biochemical data, it appears that EF-Ts-modulated conformational dynamics of the P-loop promote GDP dissociation in EF-Tu.

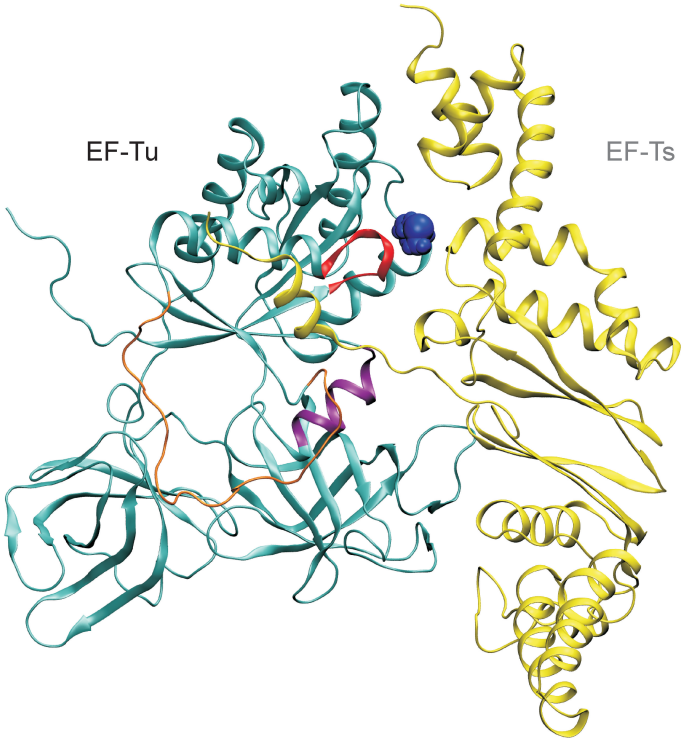

Figure 4.1. Model for the structure of the EF-Tu•EF-Ts complex (*E. coli).* EF-Tu (cyan) bound to EF-Ts (yellow) is shown in a cartoon representation after 20ns of MD simulation. The switch I region of EF-Tu which was modeled by simulated annealing is shown in orange, switch II is shown in purple and the P-loop is shown in red. The >99% conserved methionine 112 is shown in blue van der Waals representation.

In the EF-Tu•EF-Ts complex (**Figure 4.1**), insertion of $Phe81_{Ts}$ between $His84_{Tu}$ and $His118_{Tu}$ is accompanied by displacement of helix B, which contains $His84_{Tu}$ (Kawashima et al., 1996). Since helix B includes the conserved switch II element, which contributes to coordinating Mg^{2+} in the nucleotide-binding pocket of EF-Tu, it seems likely that EF-Ts binding destabilizes Mg^{2+} and accelerates nucleotide dissociation. This is consistent with the lower nucleotide exchange efficiencies of $EF\text{-}Ts_{F81A}$ (Zhang et al.,

1998), and slower EF-Ts-stimulated nucleotide dissociation rates from EF-Tu$_{H118A}$ (Schümmer et al., 2007).

The current understanding of the EF-Ts-catalyzed nucleotide exchange mechanism is limited by a lack of structural knowledge about the labile EF-Tu•nucleotide•EF-Ts complexes. Dissociation of EF-Tu•GDP•EF-Ts along k_{-4} and EF-Tu•GTP•EF-Ts along k_{-6} is critical to efficiently regenerate EF-Tu•GTP, but no crystal structures of these complexes are available, probably owing to their kinetic instability. X-ray crystal structures of EF-Tu•GDP (Song et al., 1999), EF-Tu•GDPNP (Kjeldgaard et al., 1993), and EF-Tu•EF-Ts (Kawashima et al., 1996) have been solved at atomic resolution, but these snapshots are of limited use for understanding the structural dynamics underlying the nucleotide exchange processes. Conversely, the kinetic schemes of nucleotide exchange in different EF-Tu variants allow for comparison of relative complex stabilities and relative activation barriers as shown in **Chapter 2**, but provide limited structural information.

To bridge this gap and gain insight into the structural dynamics of nucleotide exchange in EF-Tu, pre-steady state kinetic experiments were carried out *in vitro* and MD simulations were carried out *in silico*. Since the timescales of the MD simulations reported here (20 ns) are orders of magnitude shorter than the timescales measured in the performed experiments (ms-s timescale), directly predicting *in vitro* behaviour from the MD simulations is challenging. To meet this challenge, EF-Tu variants were constructed and compared to the wild type enzyme *in vitro* and *in silico*. In this manner, the differences between kinetics of nucleotide exchange in different EF-Tu variants can be compared to differences in MD simulations of the same variants. The kinetic schemes for

nucleotide exchange were solved for three EF-Tu variants. MD simulations allow for the comparison of stabilizing interactions at the EF-Tu/EF-Ts interface, which were compared to the measured stabilities of EF-Tu•EF-Ts complexes. While analyzing specific contacts present in MD simulations is fairly straightforward, describing the global dynamic behaviour of a molecular system can be a significant challenge. In order to compare the global dynamics of EF-Tu•EF-Ts complexes containing different EF-Tu variants, communication networks were constructed from each MD simulation using a method similar to those reported previously (Pyrkosz et al., 2010; Sethi et al., 2009). These networks highlight amino acid pairs that tend to move in the same direction at the same time and thus, interact significantly during MD simulation. The differences in structural dynamics evident in these networks were used to explain measured differences in nucleotide exchange mechanisms of different EF-Tu variants.

4.2 Materials and Methods

Buffers and Reagents

All stopped-flow experiments were performed in Buffer A (50 mM Tris-HCl, pH 7.5, 70 mM NH_4Cl, 30 mM KCl, 7 mM $MgCl_2$). Unlabeled guanine nucleotides were purchased from Sigma and mant-nucleotides were purchased from JenaBioScience or Invitrogen.

Mutagenesis

EF-Tu variants were constructed via Quikchange^{TM} mutagenesis of the pEECAHis plasmid (Wieden et al., 2002) encoding *E. coli* EF-Tu with a C-terminal hexahistidine

tag. A more detailed description of the mutagenesis procedure, including primer sequences, can be found in **Chapter 3**.

Protein Overexpression and Purification

Proteins were overexpressed and purified essentially as described in Wieden *et al.* (2010). Details for overexpression and purification of EF-Tu variants are outlined in **Chapter 3**. *E. coli* EF-Ts was overexpressed in *E. coli* BL21 (DE3) cells from the pHK1Ts plasmid (a kind gift of Charlotte Knudsen, Aarhus University, Denmark) as an N-terminal fusion to a chitin-binding intein. Cells were grown from a starting OD_{600} of 0.1 to 0.6 at 37 °C in LB media containing 0.1mg/mL ampicillin prior to inducing overexpression by the addition of isopropyl β-D-1-thiogalactopyranoside (IPTG) to a final concentration of 1 mM. Following the addition of IPTG, cultures were grown for two hours at 25°C and subsequently overnight at 16 °C. Cells were harvested by centrifugation, flash frozen in liquid nitrogen, and stored at -80 °C until cell opening. Cells (~10 g) were opened by lysozyme treatment (1 mg/mL) in 7 mL/g of cells Buffer B (25 mM Tris-HCl pH 7.5 @ 4 °C, 50 mM NH_4Cl, 10 mM $MgCl_2$, 0.1% phenylmethanesulfonylfluoride, 50 μM GDP), followed by incubation with sodium deoxycholate (12.5 mg/g of cells), and sonication. The EF-Ts/chitin-binding intein fusion was purified by affinity chromatography using ~5 mL of chitin resin (New England Biolabs). Fusion protein was bound to the resin in Buffer B and non-specifically bound proteins were separated by washing in Buffer C (20 mM Tris-HCl pH 8.0 @ 4°C, 0.1 mM EDTA, 50 mM NaCl, 50 μM GDP). EF-Ts was removed from the chitin resin via cleavage of the intein tag in Buffer D (20 mM Tris-HCl pH 8.0 @ room temperature, 0.1 mM EDTA, 50 mM NaCl, 400 mM KCl, and 60 mM dithiothreitol) overnight at room

temperature and subsequent elution in Buffer E (20 mM Tris-HCl pH 8.0 @ 4 °C, 0.1 mM EDTA, 50 mM NaCl, 400 mM KCl, and 50 μM GDP). To optimize recovery of EF-Ts, two consecutive rounds of cleavage and elution were performed. Affinity-purified EF-Ts was rebuffered and separated from co-purifying proteins via size exclusion chromatography through Superdex 75 resin (XK26/100 column; Superdex 75 prep grade (GE Healthcare)). Fractions containing purified EF-Ts were pooled and concentrated using a VivaSpin centrifugal concentration device (10 kDa molecular weight cutoff), flash-frozen in liquid nitrogen and stored at -80 °C until use.

Protein Concentration Determination

Protein concentrations were determined spectrophotometrically based on the absorbance at 280 nm for EF-Tu (ε_{280} = 32900 $M^{-1}cm^{-1}$) (Gromadski et al., 2002; Wieden et al., 2010) or 210 nm for EF-Ts (ε_{210} = 1,190,000 $M^{-1}cm^{-1}$). All protein preparations were determined to be >95% pure by 12% SDS-PAGE and Coomassie brilliant blue staining.

EF-Ts-induced EF-Tu•nucleotide dissociation

EF-Ts-stimulated EF-Tu•mant-nucleotide dissociation was monitored using fluorescent stopped-flow based methods previously described (Wieden et al., 2010). All stopped-flow experiments were carried out with a Kintek stopped-flow device (Model SF-2004). EF-Tu•mant-nucleotide complexes were formed by incubation of EF-Tu (0.3 μM) with a ten-fold excess of mant-nucleotide (3 μM) in Buffer A for 30 minutes at 37 °C. Nucleotide dissociation from EF-Tu was induced by rapid mixing with solutions containing various EF-Ts concentrations (0.3-60 μM). Presence of 50 μM unlabelled nucleotide in all EF-Ts solutions ensured that rebinding of mant-nucleotides was not

observed. Fluorescence Resonance Energy Transfer (FRET) from $Trp184_{Tu}$ to bound mant-nucleotides was observed by exciting the mixed samples at 280 nm and measuring fluorescence emissions through a 400 nm long-pass cutoff filter (LG-400-F: Newport Filters). Dissociation of mant-nucleotide from each EF-Tu•mant-nucleotide•EF-Ts complex was observed as a decrease in fluorescence over time. A plot of k_{app} versus EF-Ts concentration revealed hyperbolic behaviour, consistent with a two-step mechanism (Gromadski et al., 2002). At saturating concentrations of EF-Ts, nucleotide dissociation is rate limiting and decays with rate $k_{app} = k_{-4}$ (for the GDP branch) or k_{-7} (for the GTP branch). At low concentrations of EF-Ts, k_{app} increased linearly with [EF-Ts] as previously reported (Gromadski et al., 2002). The slope of this linear phase is equal to $k_3/(1+k_{-3}/k_{-4})$ for GDP dissociation or $k_6/(1+k_{-6}/k_{-7})$ for GTP dissociation (Gromadski et al., 2002).

Nucleotide induced EF-Tu•EF-Ts dissociation

Nucleotide-free EF-Tu•EF-Ts complexes were prepared by mixing equimolar quantities of EF-Tu and EF-Ts (10,000 pmol each) in excess Buffer F (25 mM Tris-HCl pH 7.5 @ 37 °C, 50 mM NH_4Cl, 10 mM EDTA) and incubating at 37 °C for 30 minutes. EF-Tu•EF-Ts complexes were separated from free nucleotides by gel filtration on a 10/300 Superdex 75 column (GE Healthcare) in Buffer G (25 mM Tris-HCl pH 7.5, 50 mM NH_4Cl) and used directly for fluorescence stopped-flow experiments. EF-Tu•EF-Ts complex was quantified in each fraction using its absorbance at 280 nm (ε_{280} = 32,900 $M^{-1}cm^{-1}$), (Gromadski et al., 2002). Dissociation of the protein complex was induced by rapid mixing of EF-Tu•EF-Ts (0.6 μM) with solutions containing various concentrations of unlabelled nucleotide (1-1000 μM). Dissociation was monitored as a

fluorescence increase using excitation at 280 nm and monitoring emissions through a 305nm long-pass cutoff filter (WG-305-F: Newport Filters) as published previously (Wieden et al., 2010). The apparent rate of fluorescence change increased hyperbolically with increasing nucleotide concentrations, consistent with a two-step reaction mechanism (**Scheme 4.1**) (Gromadski et al., 2002). At saturating concentrations of nucleotide, EF-Ts dissociation is rate limiting and decays with rate $k_{app} = k_{-3}$ (for the GDP branch) or k_{-6} (for the GTP branch). At low concentrations of nucleotide, k_{app} increased linearly with nucleotide concentration as previously reported (Gromadski et al., 2002). The slope of this linear section of the curve was equal to $k_4/(1+k_{-4}/k_{-3})$ for the GDP branch or $k_7/(1+k_{-7}/k_{-6})$ for the GTP branch (**Scheme 4.1**).

Analysis of kinetic data

Solving the kinetic scheme for nucleotide exchange in EF-Tu was performed as described in Gromadski *et al.* (2002) and Wieden *et al.* (2010). Single time courses (mant-nucleotide dissociation) or (when necessary) averages of multiple time-courses (EF-Tu•EF-Ts dissociation) were fit with single exponential functions (**Equation 4.1**) using TableCurve software.

$$F(t) = F_{\infty} + Ae^{-k_{app}t} \qquad (4.1)$$

In **Equation 4.1**, F represents the observed fluorescent signal, F_{∞} is the endpoint of the signal, A is the signal amplitude, k_{app} is the apparent rate, and t is time in seconds. For $EF\text{-}Tu_{M112L}$, due to low signal change during EF-Tu•EF-Ts dissociation, ten or more traces were averaged prior to fitting **Equation 4.1**. Data from each kinetic experiment was used to construct a plot of k_{app} versus final concentration of titrant (EF-Ts or

nucleotide). A hyperbolic equation was fitted to each kinetic titration and the initial (linear) phase of the graph was fit by a linear equation using GraphPad software.

For all EF-Tu variants, formation of the EF-Tu•EF-Ts complex could not be studied directly as in Gromadski *et al.* (2002) due to a low signal change upon complex formation. As a result, the dissociation constants for the EF-Tu•EF-Ts complexes were calculated based on one branch of the kinetic cycle when possible. For each EF-Tu variant analyzed, one of the unimolecular rate constants was too fast (~500 s^{-1}) to measure using the fluorescence stopped-flow apparatus. These rate constants were k_{-4} for EF-Tu_{M112L} (horizontal asymptote in **Figure 4.2.A**), k_{-6} for EF-Tu_{M112G} (horizontal asymptote in **Figure 4.3.G**), and k_{-3} for EF-Tu_{M112A} (horizontal asymptote in **Figure 4.4.G**). As a result, the bimolecular association rate constants for the reverse reactions could not be calculated, and lower bounds are reported for these constants. When a dissociation rate constant could not be measured directly, the bimolecular rate constant for EF-Tu•nucleotide•EF-Ts formation from the opposite direction in the kinetic scheme was assumed to be pseudo first-order. For example, if k_{-4} was too fast to measure precisely, k_3 was determined from the linear portion of the apparent rate for EF-Ts-stimulated EF-Tu•mant-GDP dissociation using the approximation in **Equation 4.2**.

$$\text{slope} = \frac{k_3}{1 + k_{-3}/k_{-4}} \approx k_3 \qquad (4.2)$$

Using the above approximation provided a rate constant that was within 10% of that computed using a value of 500 s^{-1} for k_{-4} and the relationship slope=$k_3/(1+k_{-3}/k_{-4})$. This indicates that the error inherent in **Equation 4.2** is no more than 10%.

Construction of EF-Tu•EF-Ts models in silico

A model of the *E. coli* EF-Tu•EF-Ts complex was constructed using the X-ray structure of this complex solved by Leberman and co-workers (Kawashima et al., 1996). This model lacked atomic coordinates for the N-terminus (amino acids 1 to 8) and switch I regions of EF-Tu, which were presumably disordered in the crystal. A model for the N-terminus of EF-Tu was obtained from the crystal structure of EF-Tu•GDPNP solved by Kjeldgaard *et al.* (1993). The conformation of the switch I region in EF-Tu has been resolved in complexes of EF-Tu•GDP (Song et al., 1999), EF-Tu•GDPNP (Kjeldgaard et al., 1993), and EF-Tu•GDPNP•aa-tRNA (Nissen et al., 1995). None of these conformations, however, are compatible with the C-terminal module of EF-Ts which binds near the nucleotide binding pocket of EF-Tu and presumably promotes reorientation of switch I (amino acids 42-63) (Kawashima et al., 1996).

The only conformation of EF-Tu's switch I available in the protein data bank that is compatible with the presence of the C-terminal module of EF-Ts is in a model of EF-Tu bound to the ribosome constructed by Villa *et al.* 2009. This model of EF-Tu was constructed using molecular dynamics flexible fitting of EF-Tu into cryo-EM electron density of EF-Tu bound to the ribosome (Villa et al., 2009). Manually grafting this switch I model to the EF-Tu•EF-Ts complex provided a poor model with several close contacts between switch I and the C-terminal module of EF-Ts. This model was solvated in a box of water molecules that extended 10 Å from the protein in each direction, and the aqueous system was minimized by relaxing the coordinates of protein, water, protein, water in sequential energy minimization calculations for 10,000 steps each. A final all-atom minimization was performed until no change in total energy was measured over

1,000 steps. To alleviate close contacts with the switch I region and generate a disordered conformation, the switch I and N-terminal regions were subjected to simulated annealing. During simulated annealing only the water molecules, the N-terminus, and switch I region of EF-Tu were allowed to move. The melting phase involved heating the system from 100 K to 1000 K by increasing the temperature 100 K every 5 ps. The system was maintained at 1000 K for 150 ps before the system was cooled to 300 K by decreasing the temperature 10 K every 5 ps. All simulated annealing was performed with constant volume in order to maintain close proximity of water molecules and the protein elements. Following simulated annealing, the protein complex was solvated in a new box of water molecules, and the aqueous system was again minimized as before (*vide supra*). The electrostatic charge of the model was then neutralized by addition of 24 Na^+ ions using the autoionize module in VMD (Humphrey et al., 1996).

EF-Tu_{M112L}, EF-Tu_{M112G}, and EF-Tu_{M112A}variants were constructed from the charge-neutralized model using the Mutator plugin in VMD (Humphrey et al., 1996). Each model (wild type and mutants) was then subjected to all-atoms energy minimization until no change in the total energy was computed over 1,000 consecutive steps. Each aqueous, neutral starting structure was equilibrated in two independent simulations: at 300 K and 350 K for 150 ps at 1 atm pressure using an NPT ensemble wherein the number of atoms, pressure, and temperature were kept constant. During equilibration the temperature was maintained using Langevin dynamics, and pressure was controlled by a Nosé-Hoover Langevin piston. At the start of each production phase simulation, the coordinates from the 350 K equilibration were cooled to 300 K by supplying the atomic velocities from the final step in the 300 K equilibration. Production phase simulations were carried out for 20

ns on each EF-Tu•EF-Ts model in an NPT ensemble; temperatures were maintained at 300 K by rescaling atomic velocities every 100 steps, and the Nosé-Hoover Langevin piston was used to maintain 1 atm pressure. All molecular dynamics simulations were carried out using the NAMD (Phillips et al., 2005) software with a conservative step size of 0.5 fs/step and the CHARMM27 forcefield (Foloppe and Mackerell, 2000; MacKerell et al., 1998).

Analysis of molecular dynamics simulations

Snapshots of each MD simulation were saved every 2 ps, and trajectories were fitted by the software Carma (Glykos, 2006) in order to remove water molecules as well as any rotations of the protein complex or translation of the centre of mass. All metrics in the simulation were measured in VMD (Humphrey et al., 1996) using scripts written in house. Further processing of MD data and subsequent plotting were performed using the software R (RCoreTeam, 2012). For quantitative analysis of hydrogen bonds or van der Waals interactions, a histogram of each interaction distance or energy (respectively) was plotted. Each histogram was fitted to a Gaussian function based on **Equation 4.3** where x was the midpoint of each bin, A is the height of the distribution, $\bar{x}$ is the centre of each distribution, and σ is the standard deviation of each distribution.

$$\text{counts} = \text{A}e^{\frac{-(x-\bar{x})^2}{2\sigma^2}} \qquad (4.3)$$

For some metrics, multiple Gaussian functions were included in the non-linear least squares fitting procedure. For some hydrogen bonding interactions, up to four distributions were fitted. The hydrogen bonds or interactions were reported as $\bar{x} \pm \sigma$, where $\bar{x}$ and σ were each obtained from the fitted equation.

Construction of communication networks

Construction of a communication network for each EF-Tu•EF-Ts complex was inspired by work of the Luthey-Schulten research group (Sethi et al., 2009). Each node in a network represents an amino acid and edges were drawn between nodes that were in contact *and* communicated significantly (based on statistical criteria) during the simulation. Contact criteria were the same used in Sethi *et al.* (2009); contacting amino acids were those whose heavy atoms were within 4.5 Å for 75% of the simulation or more.

In order to identify communication between amino acids, each simulation was searched for Cα atoms that moved in the same direction at the same time. This method is similar to computing covariance between Cα atoms in the Carma software package (Glykos, 2006) which was employed for network construction by Luthey-Schulten and coworkers (Pyrkosz et al., 2010; Sethi et al., 2009). The covariance metric computes a time-averaged measure of Cα motion relative to an average position (Glykos, 2006). The present work focuses on the distribution of angles describing relative displacement for each Cα pair. In order to accomplish this, each Cα pair in the MD simulation was used to compute the relative angle of displacement, $\theta(t)$,

$$\theta(t) = \arccos\left(\frac{v_i(t) \bullet v_j(t)}{|v_i(t)||v_i(t)|}\right) \qquad (4.4)$$

where • represents a dot product, || indicates a magnitude, and $v_i(t)$ is the vector of motion for Cα *i* at time *t*, computed in **Equation 4.5**.

$$v_i(t) = r_i(t) - r_i(t - dt) \qquad (4.5)$$

In **Equation 4.5**, $r_i(t)$ are the Cartesian coordinates of Cα *i* at time *t* and d*t* = 2 ps is the step size. Rather than computing a time-averaged relative angle of displacement, the values of $\theta_{ij}(t)$ were used to plot a histogram for each pair *ij* where $i \neq j$. Each histogram was analyzed to identify which Cα pairs moved in random directions relative to one another and which pairs deviated significantly from random behaviour. A random distribution of $\theta(t)$, which is expected if the motions of amino acids *i* and *j* are not correlated, should resemble the expectation function in **Equation 4.6**.

$$E(\theta) = C_{total} \frac{1}{2} \sin(\theta) d\theta \qquad (4.6)$$

The expected number of counts, $E(\theta)$, is a function of the total counts, C_{total}, the relative angle of displacement vectors (θ, the midpoint of each bin in the histogram), and the width of each bin ($d\theta = \pi/100$). In order to identify significant deviations from the expected random distribution, a chi-squared analysis was performed (Brase and Brase, 2003a).

Contacting amino acids that demonstrated significant propensities to move in the same direction at the same time were connected by edges in the corresponding communication network. All edges in the communication networks were given equal weights. Graphs were constructed in R, and transferred to the software Gephi (Bastian et al., 2009) for analysis and visualization. Each node in a network was given a size proportional to its betweenness centrality. The betweenness centrality metric quantifies the importance of each node to global communication within the network (Freeman, 1977). Each network was then organized using the 'Force Atlas' algorithm implemented in Gephi which causes all nodes to repel one another with nodes being held together only by edges within the network.

4.3 Results and Discussion

In order to correlate results from pre-steady state kinetics experiments (millisecond to second timescale) with MD simulations (nanosecond timescale), different EF-Tu variants were compared *in vitro* and *in silico*. In an attempt to rationally alter the kinetics of nucleotide exchange in EF-Tu, the >99% conserved $Met112_{Tu}$ was substituted with leucine, glycine, or alanine. Position 112 was chosen because of its location at the EF-Tu/EF-Ts interface (**Figure 4.1**) as well as its proximity to $Asp109_{Tu}$ and $His118_{Tu}$, both of which have been shown to be important for nucleotide exchange (Dahl et al., 2006; Kawashima et al., 1996; Wieden et al., 2010). Furthermore, substitution of $Met112_{Tu}$ with glycine was shown to have no affect on the affinity of EF-Tu for guanine nucleotides (**Chapter 3**). This finding suggests that another functional property of EF-Tu is responsible for selection against glycine at position 112_{Tu}. Given the location of $Met112_{Tu}$ on the EF-Tu/EF-Ts interface, position 112 may be involved in EF-Ts-catalyzed nucleotide exchange on EF-Tu. Interestingly, in the EF-Tu•EF-Ts X-ray structure, $Met112_{Tu}$ occupies a cavity on the surface of EF-Ts (**Figure 4.1**), but makes no specific contacts with EF-Ts (Kawashima et al., 1996). Substitution of $Met112_{Tu}$ with glycine and alanine was expected to reduce the stability of the EF-Tu•EF-Ts complex since it would remove the 112_{Tu} sidechain from the cavity in EF-Ts and might allow for more movement of EF-Ts relative to EF-Tu. The stability of $EF\text{-}Tu_{M112L}$•EF-Ts was expected be similar to that of the wild-type complex since both methionine and leucine are hydrophobic amino acids that should occupy the same cavity on the surface of EF-Ts. Predicting the effect of each substitution on the rates of EF-Tu•nucleotide•EF-Ts dissociation is extremely difficult since the three-dimensional structures of the respective

ternary complexes are unknown. The rate constants governing interactions of EF-Tu•EF-Ts with guanine nucleotides, however, are related to the free energy barriers separating different complexes in **Scheme 4.1**. Thus, these rate constants provide some insight into differences between the kinetically unstable EF-Tu•nucleotide•EF-Ts ternary complexes of different EF-Tu variants. The individual rate constants for EF-Ts-catalyzed guanine nucleotide exchange in each EF-Tu variant were determined and are summarized in **Table 4.1**. The associated kinetic titrations are shown in **Figures 4.2** (M112L), **4.3** (M112G), and **4.4** (M112A).

Interactions of guanine nucleotides with EF-Tu•EF-Ts (k_4,k_{-4},k_7,k_{-7})

Kinetic analysis of EF-Ts-stimulated nucleotide dissociation revealed significant differences between EF-Tu_{wt} and each EF-Tu variant. Substitution of $Met112_{Tu}$ with leucine resulted in faster dissociation rates for GDP and GTP (k_{-4}/s^{-1}> 500 vs. 130; k_{-7}/s^{-1}= 460 vs. 90 for M112L vs. wild type(Gromadski et al., 2002)). This effect is consistent with the faster nucleotide dissociation of EF-Tu_{M112L}•GTP compared to EF-Tu_{wt}•GTP, discussed in **Chapter 3**. Substitution of $Met112_{Tu}$ with glycine or alanine, however, reduced the rate of EF-Ts-stimulated nucleotide dissociation (k_{-4}/s^{-1} = 14.9, 27.0; k_{-7}/s^{-1}= 9.4, 26 for EF-Tu_{M112G} and EF-Tu_{M112A}, respectively). While slower nucleotide dissociation from EF-Tu•nucleotide•EF-Ts, compared to wild type, is a trend for EF-Tu_{M112G} and EF-Tu_{M112A}, the effects are notably larger for EF-Tu_{M112G}. It should be noted that these differences cannot be explained by lower binding affinities for EF-Ts to the EF-Tu•nucleotide complexes, since the rate constants k_{-4} and k_{-7} are obtained by extrapolating to saturating concentrations of EF-Ts (**Figures 4.3.A & C, 4.4.A & C**). Furthermore, the bimolecular rate constant for GTP association to EF-Tu_{M112G}•EF-Ts or

EF-Tu_{M112A}•EF-Ts is smaller than that of wild type (k_7 /$\mu M^{-1}s^{-1}$ = 0.26, 0.09, 6 for M112G, M112A, and wild type respectively). The corresponding rate constant of the GDP-branch (k_4) is only two-fold smaller when EF-Tu_{M112G} or EF-Tu_{M112A} is compared with EF-Tu_{wt}. This creates an interesting kinetic bias; the wild type EF-Tu•EF-Ts complex (and M112L for comparison) binds GDP and GTP at similar rates when the nucleotides are in equal concentration. The EF-Tu_{M112G}•EF-Ts and EF-Tu_{M112A}•EF-Ts complexes, however, bind GDP 10 to 100 times faster than GTP under the same conditions. This result suggests that differences in the wild type and M112G/M112A EF-Tu•GTP complexes might involve one or more of the nucleotide sensing elements in EF-Tu.

Table 4.1. Kinetic parameters governing the mechanism of EF-Ts-catalyzed nucleotide exchange in EF-Tu variants. Constants correspond to the reactions in **Scheme 4.1**.

	wt[a]	M112L	M112G	M112A
k_1 /($\mu M^{-1}s^{-1}$)	2.0 ± 0.5	0.81 ± 0.02	0.73 ± 0.02	0.54 ± 0.04
k_{-1} /(10^{-3} s^{-1})	2 ± 1	11 ± 5	3 ± 1	3 ± 1
K_{D1} /(nM)	1.0 ± 0.8	14 ± 7	4 ± 1	6 ± 2
K_{D2} /(nM)	0.7[b]	n.d.	40[b]	10[c]
k_3 /($\mu M^{-1}s^{-1}$)	60 ± 1	70 ± 1[d]	9 ± 2	> 100
k_{-3} /(s^{-1})	350 ± 50	80 ± 10	170 ± 30	> 500
K_{D3} /(μM)	6 ± 2	1.2 ± 0.2	18 ± 7	8[e]
k_4 /($\mu M^{-1}s^{-1}$)	14 ± 5	> 7	7.4 ± 0.7	6.2 ± 0.9[d]
k_{-4} /(s^{-1})	130 ± 30	> 500	14.9 ± 0.3	27.0 ± 0.7
K_{D4} /(μM)	9 ± 5	n.d.	2.0 ± 0.2	4.3 ± 0.8
k_5 /($\mu M^{-1}s^{-1}$)	0.5 ± 0.1	0.21 ± 0.02	0.22 ± 0.01	0.10 ± 0.02
k_{-5} /(s^{-1})	0.03 ± 0.01	0.15 ± 0.01	0.020 ± 0.001	0.075 ± 0.003
K_{D5} /(nM)	60 ± 30	700 ± 100	91 ± 9	800 ± 200
k_6 /($\mu M^{-1}s^{-1}$)	30 ± 5	71 ± 4	>46	22 ± 19
k_{-6} /(s^{-1})	60 ± 10	10 ± 2	>200	80 ± 20
K_{D6} /(μM)	2.0 ± 0.7	0.14 ± 0.03	10[e]	4 ± 4
k_7 /($\mu M^{-1}s^{-1}$)	6 ± 1	n.d.	0.26 ± 0.02[d]	0.09 ± 0.01
k_{-7} /(s^{-1})	90 ± 10	460 ± 20	9.4 ± 0.4	26 ± 2
K_{D7} /(μM)	14 ± 4	n.d.	37 ± 4	270 ± 60

a From Gromadski *et al.*
b Computed from GDP branch of kinetic cycle
c Computed from GTP branch of kinetic cycle
d Computed assuming a one-step, irreversible reaction mechanism.
e Computed using entire kinetic mechanism.
n.d. Not determined.

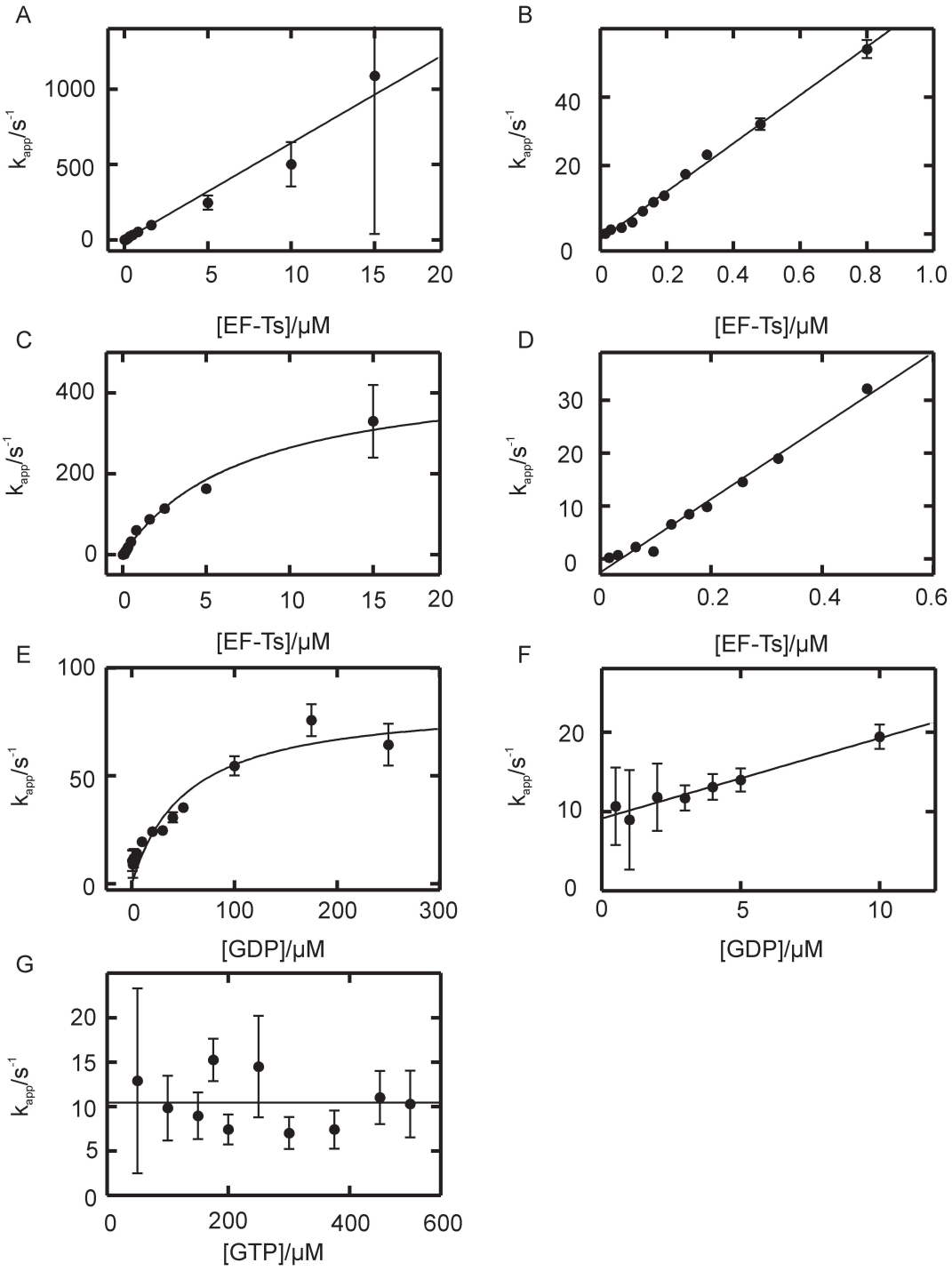

Figure 4.2. The kinetics of interaction between EF-Tu_{M112L}, EF-Ts, and guanine nucleotides. The apparent rate of EF-Tu_{M112L}•mant-GDP/GTP dissociation is shown at various concentrations of EF-Ts in A and C, respectively. The apparent rates of EF-Tu_{M112L}•EF-Ts dissociation in the presence of various concentrations of GDP or GTP are shown in E and G, respectively. The right panels (B, D, and F) show zoom-ins of the low titrant ranges for the corresponding titration curves in the left panels (A, C, and E respectively). Each symbol represents a mean obtained from multiple fitted traces (A, B, C, D) or the k_{app} value obtained from fitting the average of over 12 traces (E, F, G).The y-error bars represent standard deviations of multiple fitted parameters (A, B, C, D) or standard error obtained from the fit (E, F, G).

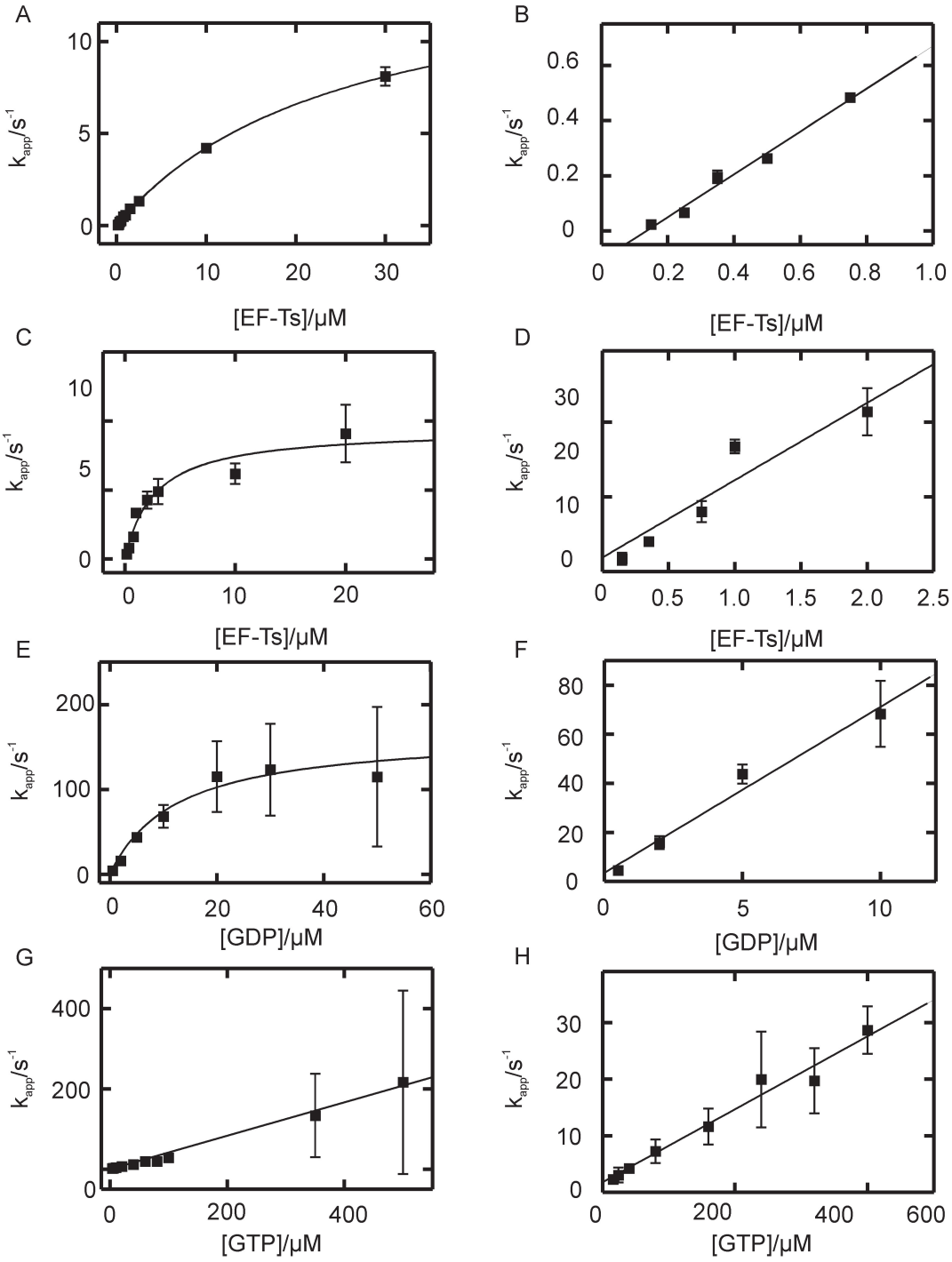

Figure 4.3. The kinetics of interaction between EF-Tu_{M112G}, EF-Ts, and guanine nucleotides. The apparent rates of EF-Tu_{M112G}•mant-GDP/GTP dissociation are shown at various concentrations of EF-Ts in A and C, respectively. The apparent rates of EF-Tu_{M112G}•EF-Ts dissociation in the presence of various concentrations of GDP or GTP are shown in E and G, respectively. The right panels (B, D, F, and H) show zoom-ins of the low titrant ranges for the corresponding titration curves in the left panels (A, C, E, and G respectively). Each symbol represents a mean obtained from multiple fitted traces and the y-error bars represent standard deviations.

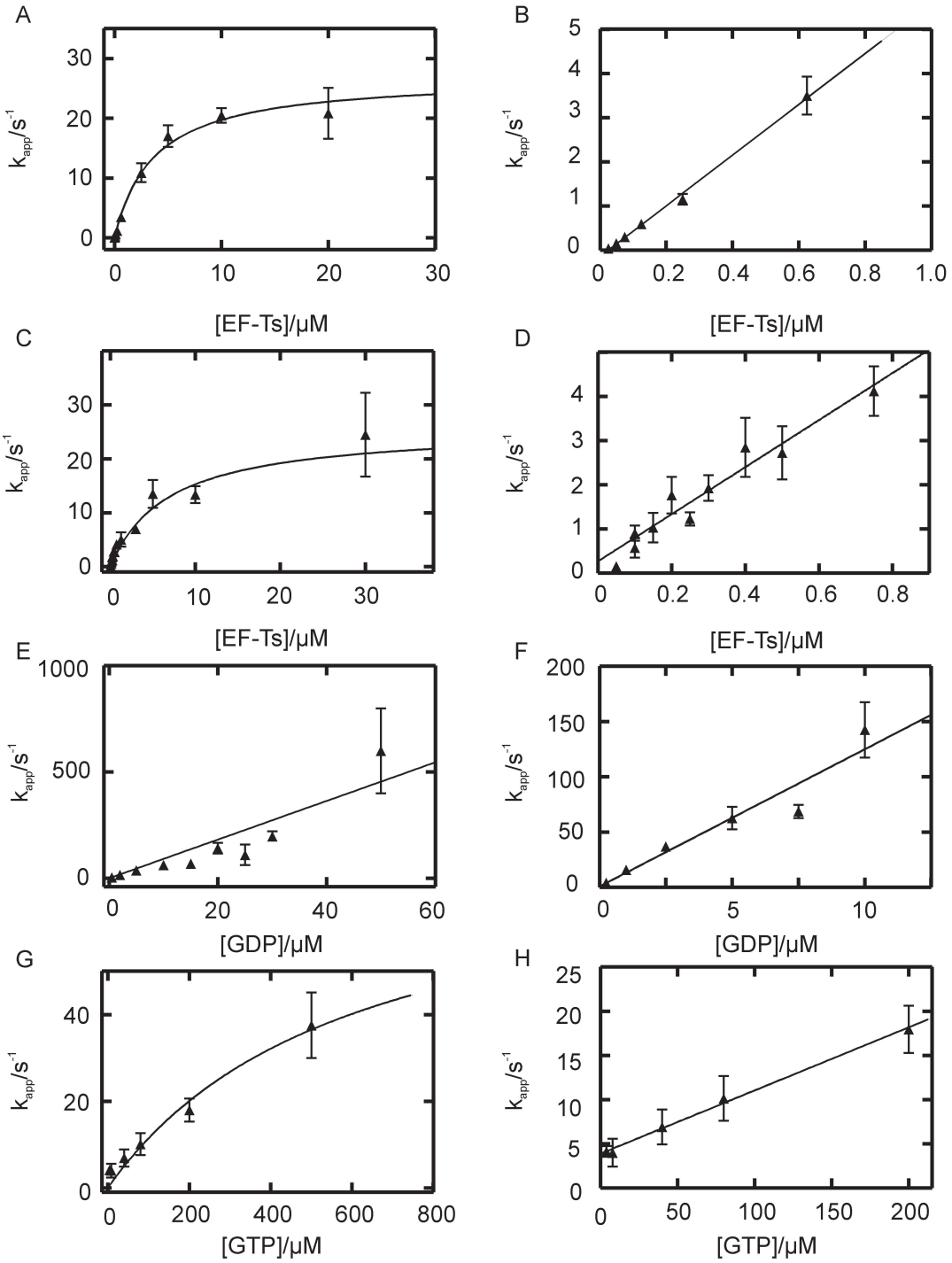

Figure 4.4. The kinetics of interaction between EF-Tu_{M112A}, EF-Ts, and guanine nucleotides. The apparent rates of EF-Tu_{M112A}•mant-GDP/GTP dissociation are shown at various concentrations of EF-Ts in A and C, respectively. The apparent rates of EF-Tu_{M112A}•EF-Ts dissociation in the presence of various concentrations of GDP or GTP are shown in E and G, respectively. The right panels (B, D, F, and H) show zoom-ins of the low titrant ranges for the corresponding titration curves in the left panels (A, C, E, and G respectively). Each symbol represents a mean obtained from multiple fitted traces and the y-error bars represent standard deviations.

Interaction of EF-Ts with EF-Tu•nucleotide (k_3, k_{-3}, k_6, k_{-6})

Dissociation of EF-Ts from EF-Tu•nucleotide•EF-Ts complexes was monitored by an increase in tryptophan fluorescence upon rapid mixing of EF-Tu•EF-Ts with unlabelled guanine nucleotides. At high GDP or GTP concentrations, the apparent rate of EF-Ts dissociation saturates at the unimolecular rate constant k_{-3} or k_{-6}, respectively. Surprisingly, no apparent concentration dependence of GTP-induced EF-Tu•EF-Ts dissociation was observed for EF-Tu_{M112L} variant. This reaction was, therefore, presumed to proceed with the rate-limiting unimolecular rate constant k_{-6} = 10 s^{-1}, slower than wild type (60 s^{-1}), (Gromadski et al., 2002). This interpretation assumes a rapid equilibrium between EF-Tu_{M112L}•EF-Ts + GTP and EF-Tu_{M112L}•GTP•EF-Ts. The rapid equilibrium assumption is supported by the large value of k_{-7} for M112L compared to wild type but, unfortunately, k_7 could not be determined for EF-Tu_{M112L} since there was no concentration dependence evident in **Figure 4.2.G**. The linear phase of **Figure 4.2.G** could not be analyzed since no change in tryptophan fluorescence was observed when EF-Tu_{M112L}•EF-Ts was mixed with GTP concentrations lower than 50 μM (final concentration). This may be due to a minimal increase in free EF-Ts concentrations when GTP was present in concentrations below 50 μM. The equilibrium constant governing conversion of EF-Tu•EF-Ts + GTP to EF-Tu•GTP + Ts, and consequently the signal amplitude during this experiment, is equal to K_{D6}/K_{D7}. Under the same experimental conditions for the M112L and wild type systems, lower signal amplitude for the M112L variant compared to wild type is supported by the larger k_{-7} for M112L (which increases K_{D7}) and smaller K_{D6} (see **Table 4.1**). While this tends to support the assignment of k_{-6} at 10 s^{-1}, this is not unequivocal proof since K_{D7} cannot be calculated for EF-Tu_{M112L}. Thus,

EF-Ts dissociation from EF-Tu_{M112L}•nucleotide•EF-Ts complexes is proposed to be slower than wild type (k_{-3} /s^{-1}= 80 vs. 350 and k_{-6} /s^{-1}= 10 vs. 60 for M112L vs. wild type). It is noteworthy that assignment of the slow k_{-6} for EF-Tu_{M112L} is consistent with the slow k_{-3} compared to wild type obtained from the GDP branch.

For EF-Tu_{M112A} the rate constants governing interactions of EF-Tu•nucleotide with EF-Ts were not largely different from those of wild type EF-Tu. While the rate of EF-Ts dissociation from EF-Tu_{M112A}•GDP was too fast to measure, the reported rate constant k_{-3} for wild type EF-Tu is close to the limit for the experimental setup used in this work. EF-Ts association to EF-Tu_{M112G}•GDP was found to be slower than wild type (k_3 /$\mu M^{-1}s^{-1}$ = 9 vs. 60 for M112G vs. wild type (Gromadski et al., 2002)), while EF-Ts dissociation from EF-Tu_{M112G}•GTP•EF-Ts was much faster than wild type (k_{-6} /s^{-1}>200 vs. 60 for M112G vs. wild type (Gromadski et al., 2002)).

Interactions of EF-Tu and EF-Ts in the absence of nucleotides

For each of the EF-Tu variants studied, formation of the EF-Tu•EF-Ts complex could not be monitored directly due to a low signal change upon complex formation. As a result, the dissociation constants for EF-Tu_{M112A}•EF-Ts and EF-Tu_{M112G}•EF-Ts complexes were computed based on the branch of the kinetic cycle for which all rate constants were determined. The affinities of the EF-Tu_{M112A}•EF-Ts and EF-Tu_{M112G}•EF-Ts complexes were found to be lower than wild type (K_{D2} /nM= 40 and 70 for M112G and M112A EF-Tu, respectively). As expected, substitution of $Met112_{Tu}$ with the smallest amino acids glycine or alanine reduced the affinity of the EF-Tu•EF-Ts complex. Due to the lack of concentration dependence of k_{-6} and its impact on the rest of the rate constants in the kinetic cycle of EF-Tu_{M112L}, no corresponding K_{D2} is available.

Given the higher affinities of EF-Ts for EF-Tu_{M112L}•nucleotide complexes compared to wild type, it seems likely that the affinity of EF-Tu_{M112L}•EF-Ts complex is similar, if not higher, than wild type.

Molecular dynamics simulations of EF-Tu•EF-Ts

In order to interpret the measured differences between the different EF-Tu variants, structural dynamics were investigated using molecular dynamics simulations. To this end the wild type EF-Tu•EF-Ts complex as well as models containing M112L, M112G, and M112A EF-Tu variants were simulated for 20 ns each. A plot of backbone root-mean squared deviation (RMSD) vs. time, shown in **Figure 4.5.A**, revealed that each structure was stable after 10ns of simulation time. The following analyses use the last half of each simulation. The Root-Mean Squared Fluctuations (RMSF) of the Cα atoms, shown in **Figure 4.5.B**, reveal that the dynamics of the EF-Tu•EF-Ts complexes are largely the same for all EF-Tu variants. Some notable differences are the varied RMSF profiles in the switch I region of EF-Tu (amino acids 42_{Tu}-63_{Tu}) and helices 10 and 11 of EF-Ts (amino acids 180_{Ts}-230_{Ts}). These regions are largely dynamic throughout the course of each simulation. The high flexibility of switch I in EF-Tu is consistent with the observation that this structural element is disordered in the EF-Tu•EF-Ts complex (Kawashima et al., 1996). The high RMSF values computed for helices 10 and 11 of EF-Ts is also not surprising given that these structural elements do not make any stabilizing contacts with EF-Tu or other regions of EF-Ts during the simulations. Differences in flexibility between EF-Tu variants in these highly flexible regions do not likely result from substitution of $Met112_{Tu}$ since these structural elements make no contacts with other regions of the proteins.

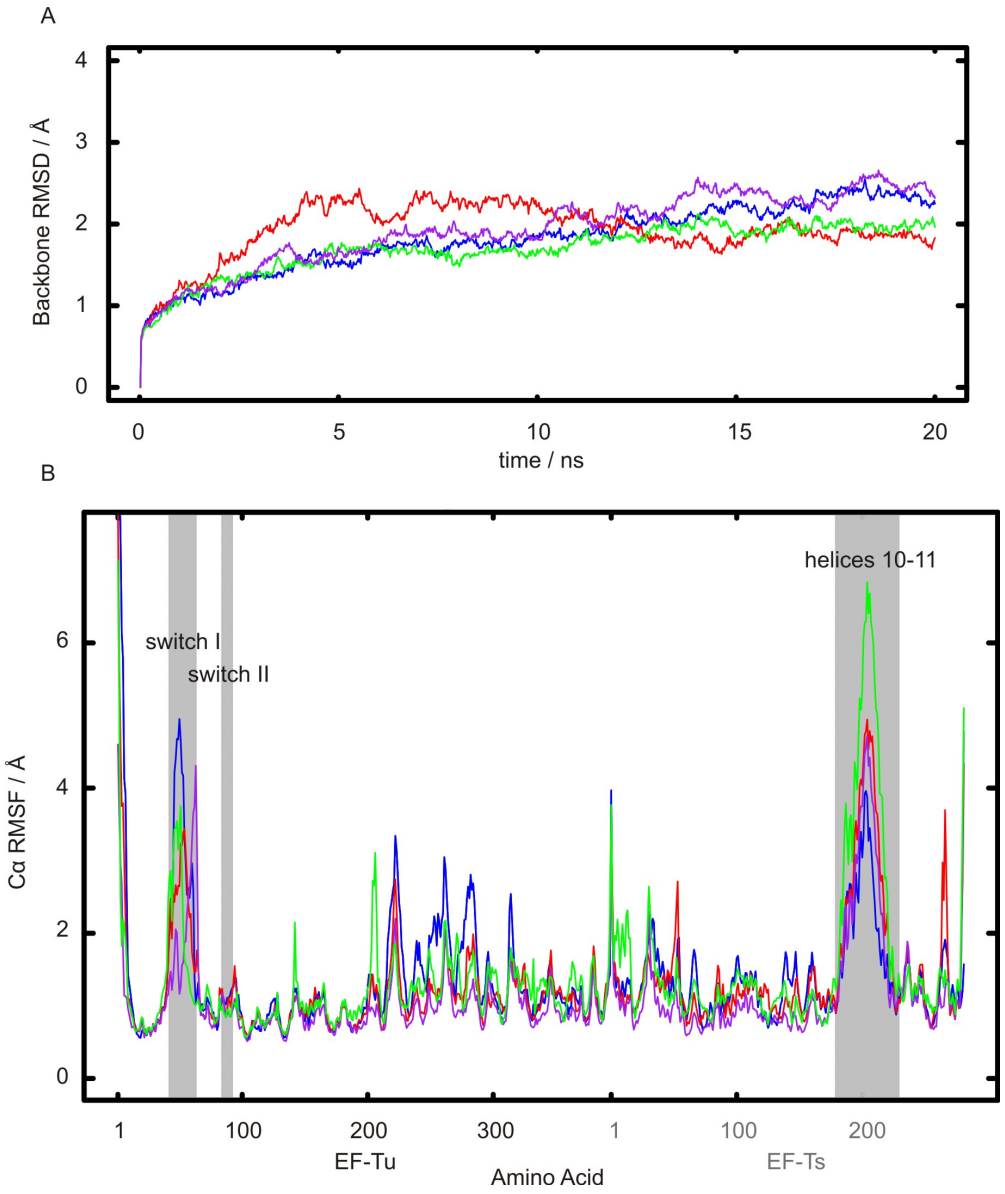

Figure 4.5. General properties of each EF-Tu•EF-Ts complex during 20 ns MD simulations. The backbone RMSD of each EF-Tu•EF-Ts model is shown in panel A, wild type (blue), M112L (red), M112G (green), M112A (purple). Panel B shows the RMSF values calculated for each Cα atom in the EF-Tu•EF-Ts model over the last ten nanoseconds of each MD simulation (10-20 ns). The lines are coloured as in A.

Examining differences in EF-Tu•EF-Ts complex stability

The relative stabilities of EF-Tu•EF-Ts complexes containing different EF-Tu variants can likely be explained by different contacts in the respective complexes. To visualize the overall differences between EF-Tu•EF-Ts complexes, **Figure 4.6** shows snapshots of the structures aligned with the wild type complex (blue). These snapshots indicate that helix 4 and the N-terminal region of EF-Ts are closer to EF-Tu_{M112G} and EF-Tu_{M112A} than EF-Tu_{wt} or EF-Tu_{M112L}. In order to accommodate this closer approach, the orientation of bound EF-Ts differs for EF-Tu_{M112G} or EF-Tu_{M112A} relative to EF-Tu_{wt}. This difference is best described as a slight rotation of EF-Ts relative to EF-Tu about an axis perpendicular to the EF-Tu•EF-Ts interface. This causes a notable change in the orientation of the N-terminal region of EF-Ts relative to helix D of EF-Tu as shown in **Figure 4.6**. This change is largest for the EF-Tu_{M112G} variant, which has the lowest binding affinity for EF-Ts. Closer inspection of the contacts between EF-Tu variants and EF-Ts revealed differences in the hydrogen bonds linking helix D in domain I of EF-Tu with the N-terminal domain of EF-Ts. As shown in **Figure 4.7**, the EF-Tu_{wt}•EF-Ts complex is stabilized by a hydrogen bond network centred on $Arg12_{Ts}$. In the X-ray crystal structure

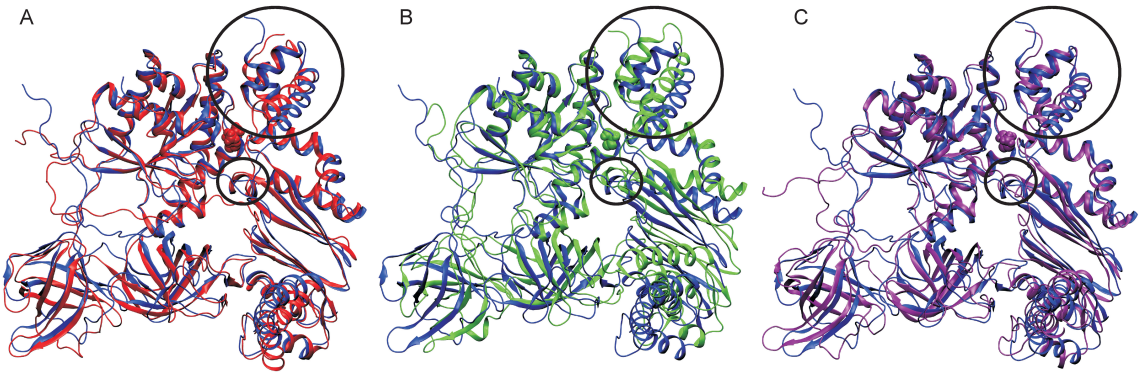

Figure 4.6. Substitution of $Met112_{Tu}$ alters the binding mode of EF-Ts. Structural alignments of EF-Tu•EF-Ts complexes are shown for snapshots after 20 ns of MD simulation. Alignments were performed using the backbone atoms in domain I of EF-Tu (more specifically, backbone atoms of β1, α1, P-loop, helix B, and helix D) and are shown for wild type EF-Tu•EF-Ts (blue) with M112L (A), M112G (B), and M112A (C). The N-terminal region (top) and helix 4 (middle) of EF-Ts are circled.

of the EF-Tu•EF-Ts complex from *E. coli*, $Arg12_{Ts}$ forms a salt bridge with $Glu152_{Tu}$ (Kawashima et al., 1996). This interaction is a bifurcated hydrogen bond system in the simulation of the wild type complex, which is present for 84% of the simulation from 10-20 ns. In addition, the $Arg12_{Ts}$ sidechain also interacts with the backbone carbonyl of $Ala17_{Ts}$, and $Glu13_{Ts}$ in this simulation (**Figure 4.7**, **Table 4.2**). These Ts/Ts interactions are present in 37% and 40% of the simulation analyzed, respectively. Hydrogen-bonding interactions between $Glu152_{Tu}$ and the long, flexible $Arg12_{Ts}$ sidechain will provide limited stability to the EF-Tu•EF-Ts complex. Additional hydrogen bonds from $Arg12_{Ts}$ to $Ala17_{Ts}$ and $Glu13_{Ts}$ should assist in anchoring $Arg12_{Ts}$, further stabilizing the contacts between helix D of EF-Tu and the N-terminal domain of EF-Ts.

In the simulation of EF-Tu_{M112L}•EF-Ts, the $Arg12_{Ts}$ sidechain makes a single hydrogen bond with $Glu152_{Tu}$ of helix D in EF-Tu (90% of 10-20 ns), and forms a stable (100% of simulation analyzed) bridging interaction with the sidechain of $Glu13_{Ts}$. This is shown in **Figure 4.7.B**. In contrast, simulations of EF-Tu_{M112G}•EF-Ts or EF-Tu_{M112A}•EF-Ts contain $Arg12_{Ts}$•••$Glu152_{Tu}$ interactions, but vanishingly few bridging interactions between the sidechain of $Arg12_{Ts}$ and other amino acids of the N-terminal domain in EF-Ts (**Figure 4.7.C & D, Table 4.2**). In fact, the $Arg12_{Ts}$•••$Ala17_{Ts}$ interaction is only present in 7% of frames analyzed for EF-Tu_{M112A}•EF-Ts and is absent entirely in EF-Tu_{M112G}•EF-Ts. No hydrogen-bonding interactions between $Arg12_{Ts}$ and $Glu13_{Ts}$ were identified in EF-Tu_{M112G}•EF-Ts or EF-Tu_{M112A}•EF-Ts simulations. These differences relative to the wild type simulation likely contribute to the lower affinities of EF-Tu_{M112G}•EF-Ts and EF-Tu_{M112A}•EF-Ts complexes compared to EF-Tu_{wt}•EF-Ts measured *in vitro*. Furthermore, the lower affinity of EF-Tu_{M112G}•EF-Ts compared to

EF-Tu$_{M112A}$•EF-Ts *in vitro* might be explained by the weaker interaction of Arg12$_{Ts}$ and Glu152$_{Tu}$ observed in MD simulations. These results are supported by previous observations that substitution of Glu152$_{Tu}$ with alanine reduces the affinity of the EF-Tu•EF-Ts complex by ~10 fold (Wieden et al., 2002). The results from simulation of

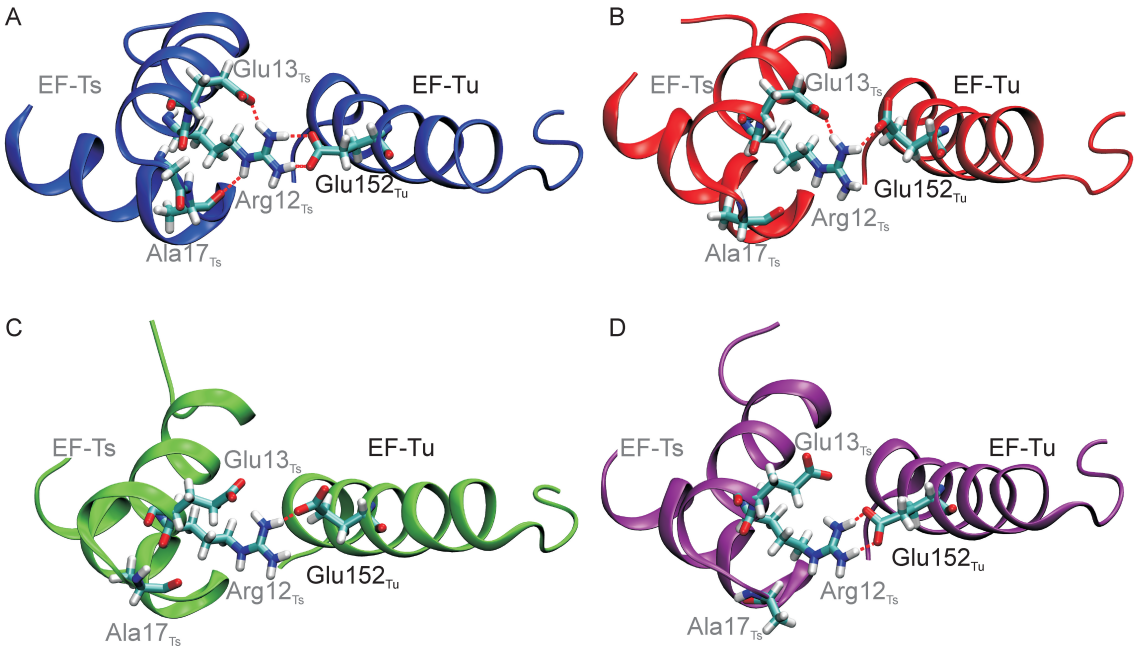

Figure 4.7. M112G or M112A substitution in EF-Tu breaks bridging interactions of Arg12$_{Ts}$ with EF-Ts. Snapshots of MD simulations from wild type (A), M112L (B), M112G (C), and M112A (D) EF-Tu•EF-Ts are used to show interactions between the N-terminal region of EF-Ts (left) with helix D of EF-Tu (right). Hydrogen bonds between Arg12$_{Ts}$ and Glu152$_{Tu}$, Ala17$_{Ts}$, or Glu13$_{Ts}$ are indicated by dashed red lines when present. Hydrogen bonding distances and probabilities for each hydrogen bond are indicated in **Table 4.2**.

Table 4.2. Hydrogen bonding distances and probabilities for interactions between helix D of EF-Tu and the N-terminal domain of EF-Ts. Probabilities represent the number of frames in 10-20 ns of simulation for which the indicated hydrogen bond was observed.

Donor	Acceptor	Wild Type	M112L	M112G	M112A
N-H$_{Arg12,Ts}$	O$_{Glu152,a,Tu}$	(1.73 ± 0.13) Å 84%	(1.81 ± 0.16) Å 90%	(1.75 ± 0.15) Å 40%	(1.72 ± 0.12) Å 80%
N-H$_{Arg12,Ts}$	O$_{Glu152,b,Tu}$	(1.72 ± 0.13) Å 90%	0%	0%	(1.71 ± 0.12) Å 62%
N-H$_{Arg12,Ts}$	O$_{Ala17,Ts}$	(1.95 ± 0.17) Å 37%	0%	0%	(1.81 ± 0.14) Å 7%
N-H$_{Arg12,Ts}$	O$_{Glu13,a,Ts}$	(1.7 ± 0.1) Å 9%	(1.7 ± 0.1) Å 100%	0%	0%
N-H$_{Arg12,Ts}$	O$_{Glu13,b,Ts}$	(1.71 ± 0.12) Å 31%	0%	0%	0%

EF-Tu$_{M112L}$•EF-Ts demonstrate that Arg12$_{Ts}$ is capable of making bridging interactions between EF-Tu and EF-Ts for this EF-Tu variant. This would suggest that EF-Tu$_{M112L}$•EF-Ts might have a similar affinity to the wild type complex, consistent with what is expected *in vitro*. Without a value for K_{D2}, however, this prediction cannot be confirmed.

Communication networks within the EF-Tu•EF-Ts complex

We have previously proposed that EF-Ts-stimulated nucleotide dissociation involves a conserved three-dimensional communication network between EF-Tu and EF-Ts rather than a few key interactions responsible for catalytic activity (Wieden et al., 2010). In order to better understand this network, data from MD simulations of each EF-Tu•EF-Ts complex were used to construct the communication networks shown in **Figure 4.8**. These networks were generated using a method similar to that employed by Luthey-Schulten's research group (Sethi et al., 2009). In the networks presented here, each amino acid is represented by a node (circle) and edges are drawn between nodes that a) are in contact during 75% of the simulation or more, and b) if the corresponding alpha carbons have a significant propensity to move in the same direction at the same time. A complete description of network construction including the significance criteria employed can be found in Materials and Methods (**section 4.2**) and **Appendix A.3**. Each network in **Figure 4.8** clearly resembles the three-domain structure of EF-Tu and the elongated structure of EF-Ts (Kawashima et al., 1996). The network for EF-Tu$_{wt}$•EF-Ts (**Figure 4.8.A**) clearly highlights the contacts between Domain I of EF-Tu and the N-terminal domain of EF-Ts (top); interaction of helix 4 of EF-Ts (containing Asp80$_{Ts}$ and Phe81$_{Ts}$) with helix C of EF-Tu (middle); contacts between the C-terminal region of EF-Ts and

domain III of EF-Tu (bottom); and the extended structure of the C-terminal motif of EF-Ts that interacts in the middle of domain I in EF-Tu near the P-loop.

The importance of these different interactions has been proposed and discussed at length by Kawashima *et al* (1996) based on the X-ray crystal structure of the EF-Tu•EF-Ts complex from *E. coli*. Biochemical studies have highlighted the importance of some of these interactions as well. When amino acids $Met19_{Ts}$ and $Met20_{Ts}$ are both substituted with alanine, for example, the EF-Tu•EF-Ts affinity decreases more than five fold (Zhang et al., 1998). These amino acids interact with EF-Tu amino acids $Thr108_{Tu}$ and $Asp109_{Tu}$ in all EF-Tu•EF-Ts networks presented here (see **Table A.3.3** for a complete list of interprotein edges). The interaction between helix 4 of EF-Ts and helix C of EF-Tu was highlighted in the discussion of the EF-Tu•EF-Ts X-ray structure; the intrusion of $Phe81_{Ts}$ between helix C and switch II of EF-Tu and interaction with $His118_{Tu}$ was proposed to contribute to EF-Ts-catalyzed nucleotide release from EF-Tu (Kawashima et al., 1996). Communication between $Phe81_{Ts}$ and helix C of EF-Tu is clearly evident in all EF-Tu•EF-Ts networks, consistent with the observation that EF-Ts stimulates nucleotide dissociation from all the EF-Tu variants tested here.

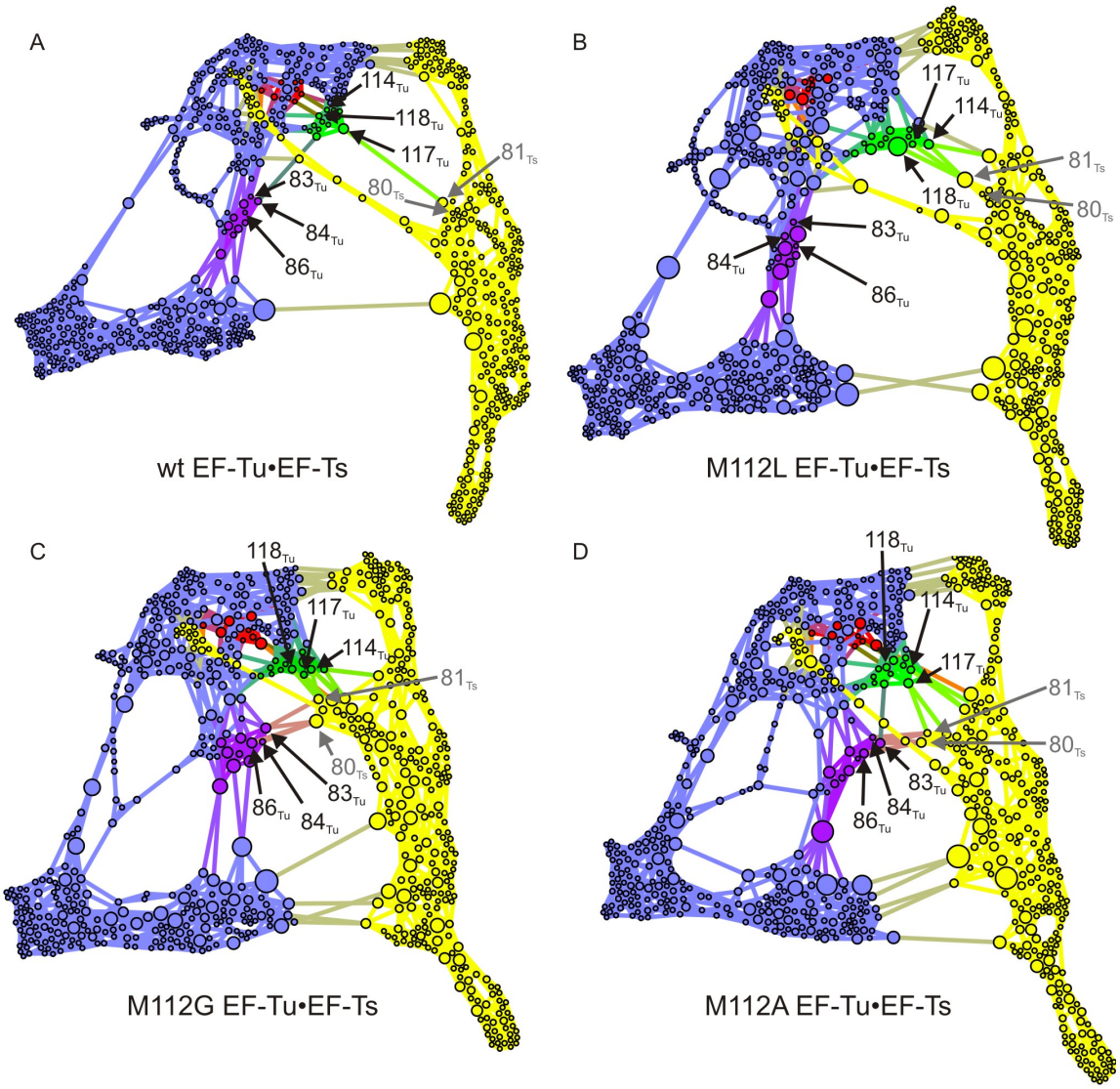

Figure 4.8. Communication networks of different EF-Tu•EF-Ts complexes reveal differential communication with switch II of EF-Tu. Each amino acid is represented by a node (circle) and amino acids that are in contact and communicate during MD simulations are connected by an edge (line). Amino acids of EF-Ts are represented in yellow, those of EF-Tu in blue, and various elements of EF-Tu are coloured as follows: P-loop (red), switch II (purple), and helix C (green). The edges are coloured by mixing the colours of the connected nodes. Networks are based on data from MD simulations of wild type (A), M112L (B), M112G (C), and M112A (D) EF-Tu•EF-Ts complexes. Specific amino acids in each network are indicated by arrows.

Reduced P-loop/helix C communication accelerates EF-Ts-stimulated nucleotide dissociation from EF-Tu$_{M112L}$.

When the network of EF-Tu$_{M112L}$•EF-Ts (**Figure 4.8.B**) is compared to the wild type complex (**Figure 4.8.A**), some differences emerge. In the wild type network, helix C (Pro113$_{Tu}$ to Val125$_{Tu}$, green) is connected to the P-loop (Gly18$_{Tu}$ to Lys25$_{Tu}$, red) of EF-Tu by two edges, while no edges connect these structural elements in the EF-Tu$_{M112L}$•EF-Ts network. By comparison, edges connecting the P-loop and helix C were also found in EF-Tu$_{M112G}$•EF-Ts and EF-Tu$_{M112A}$•EF-Ts networks (**Figure 4.8.C & D**). The findings presented in **Chapter 3** and elsewhere (Dahl et al., 2006) indicate that interactions between helix C and the P-loop regulate structural dynamics of the P-loop and limit nucleotide dissociation rates. The lack of P-loop/helix C communication in the EF-Tu$_{M112L}$•EF-Ts network suggests that a decrease in P-loop stabilization may similarly increase the rate of EF-Ts-catalyzed EF-Tu•nucleotide dissociation for EF-Tu$_{M112L}$ compared to wild type. In line with this hypothesis, the faster rate of EF-Ts-catalyzed nucleotide release in EF-Tu$_{M112L}$ is not nucleotide specific. Interestingly, the Gln114$_{Tu}$•••His19$_{Tu}$, His118$_{Tu}$•••Gly18$_{Tu}$ hydrogen bonds that were found to stabilize the P-loop in simulations of EF-Tu•GTP in **Chapter 3** were not present in any EF-Tu•EF-Ts simulations (not shown). Despite the absence of these hydrogen bonds, P-loop/helix C communication was still identified in EF-Tu$_{wt}$•EF-Ts, EF-Tu$_{M112G}$•EF-Ts and EF-Tu$_{M112A}$•EF-Ts networks.

EF-Ts communicates with switch II of EF-Tu$_{M112G}$ and EF-Tu$_{M112A}$.

One of the clear differences between networks of EF-Tu$_{M112G}$•EF-Ts or EF-Tu$_{M112A}$•EF-Ts (**Figures 4.8.C & D**) and EF-Tu$_{wt}$•EF-Ts is the presence of edges

between switch II ($Gly83_{Tu}$ to $Ile92_{Tu}$) of EF-Tu and $Phe81_{Ts}$/$Asp80_{Ts}$. By comparison, no such edges are present in networks of wild type or M112L EF-Tu•EF-Ts complexes. The communication observed between EF-Ts and switch II of EF-Tu_{M112G} or EF-Tu_{M112A} likely reduces the mobility of this structural element. This is supported by the lower mean RMSF values (wild type: 1.1 Å; M112L: 1.1 Å; M112G: 0.92 Å; M112A: 0.95 Å) for Cα atoms of the switch II region in simulations of M112G and M112A EF-Tu•EF-Ts complexes compared to M112L and wild type (**Figure 4.5.B**). The snapshots shown in **Figure 4.9.E & G** show that helix 4 of EF-Ts (including $Phe81_{Ts}$) forms close contacts with switch II of EF-Tu_{M112A} and EF-Tu_{M112G} that are primarily hydrophobic in nature. In contrast, the contacts appear less favourable for EF-Tu_{wt} and EF-Tu_{M112L} (**Figure 4.9.A & C**). This is likely the result of differences in overall orientations of EF-Ts relative to EF-Tu_{M112A} and EF-Tu_{M112G} compared to EF-Tu_{wt} and EF-Tu_{M112L}. These differences (visible in the domain I backbone alignments shown in **Figure 4.6**) allow helix 4 of EF-Ts to penetrate deeper into the cleft between helix C and switch II of EF-Tu_{M112G} or EF-Tu_{M112A} as opposed to EF-Tu_{M112L} or EF-Tu_{wt}.

The van der Waals interaction energy between switch II of EF-Tu and helix 4 of EF-Ts was computed for each EF-Tu•EF-Ts complex throughout 10 - 20 ns of simulation. This provides a useful metric for studying interaction as it includes contact distances between all the atoms in each structural element. The van der Waals energies were plotted as histograms in **Figures 4.9.B, D, F, & H**. The EF-Tu_{wt}•EF-Ts complex shows a single distribution centred at -3.5 kcal/mol. The other EF-Tu variants, however, have an additional distribution centred near -6 kcal/mol. This 'close approach' population constitutes 57%, 77%, and 86% of the frames for M112L, M112A, and M112G EF-Tu

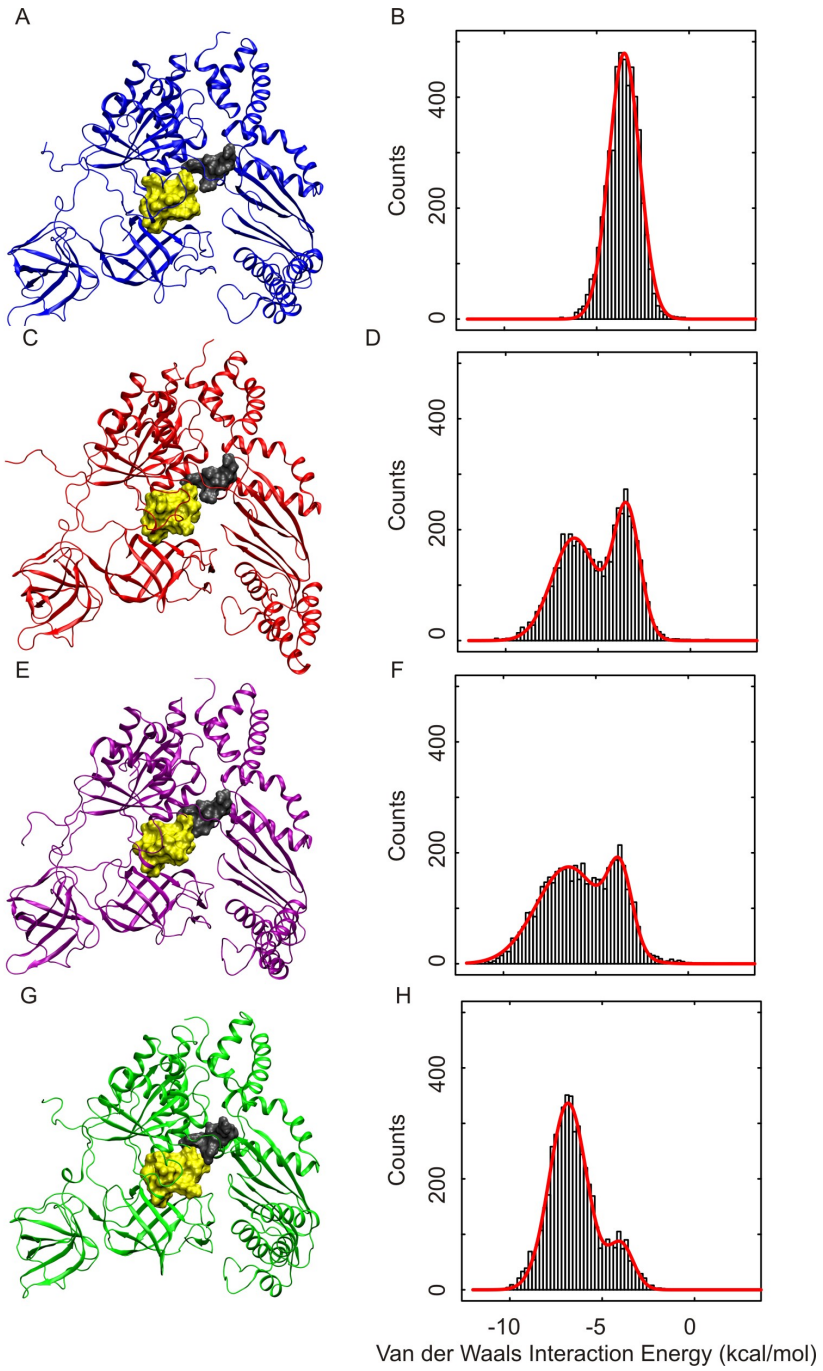

Figure 4.9. EF-Tu$_{M112G}$ and EF-Tu$_{M112A}$ variants form close interactions between switch II of EF-Tu and heix 4 of EF-Ts. Snapshots of MD simulations from wild type (A), M112L (C), M112A (E), and M112G (G) EF-Tu•EF-Ts complexes are shown with surface representations of switch II in EF-Tu (yellow) and helix 4 of EF-Ts (grey). The van der Waals interaction energy between switch II of EF-Tu and helix 4 of EF-Ts was computed during each MD simulation and is plotted as histograms in B (wild type), D (M112L), F (M112A), and G (M112G). The red line in each histogram indicates a one- or two-Gaussian function fitted to the respective data.

variants, respectively. The population of the close approach state increases with decreasing sidechain length at position 112: for close approach populations Met < Leu < Ala < Gly. This is consistent with a role of $Met112_{Tu}$ in acting as a 'keystone' for EF-Ts binding. With shorter sidechains at position 112, EF-Ts approaches EF-Tu closer, and helix 4 of EF-Ts penetrates deeper into the cleft between helix C and switch II of EF-Tu. The stabilizing van der Waals interaction energy for switch II of EF-Tu and helix 4 of EF-Ts likely reflects the same interactions that give rise to the communication identified in the $EF\text{-}Tu_{M112G}$•EF-Ts and $EF\text{-}Tu_{M112A}$•EF-Ts networks.

Table 4.3 Mean van der Waals interaction energies between switch II of EF-Tu and helix 4 of EF-Ts in simulations of EF-Tu•EF-Ts from each distribution observed in histograms (**Figure 4.9.B, D, F, H)**. Means and standard deviations were obtained from fitting each histogram to a one- or two-Gaussian function. The relative population of each state is shown in parentheses as a percentage of frames analyzed.

	Wild Type	M112L	M112G	M112A
High Energy State (kcal/mol)	-3.5 ± 0.8 (100%)	-3.5 ± 0.7 (43%)	-4.0 ± 0.7 (14%)	-3.7 ± 0.7 (23%)
Low Energy State (kcal/mol)	-	-6.3 ± 1.3 (57%)	-6.8 ± 1.0 (86%)	-6.5 ± 1.8 (77%)

Despite the population at low van der Waals interaction energy observed for $EF\text{-}Tu_{M112L}$•EF-Ts, no communication between switch II and helix 4 was identified in this network. The $EF\text{-}Tu_{wt}$•EF-Ts network reveals communication between $His84_{Tu}$ of switch I and helix C of EF-Tu that is not present in the M112L network. This effect likely results from displacement of helix C in $EF\text{-}Tu_{M112L}$•EF-Ts relative to the wild type complex, similar to the MD simulations of EF-Tu•GTP in **Chapter 3**. Disruption of switch II/helix C communication in $EF\text{-}Tu_{M112L}$•EF-Ts may increase the mobility of switch II and prevent communication with helix 4 of EF-Ts despite the close approach state observed for these two structural elements.

Stabilization of switch II in EF-Tu reduces the rates of EF-Ts-stimulated nucleotide dissociation.

The displacement of switch II upon EF-Ts binding has been implicated, both by structural and biochemical studies, to contribute to EF-Ts-catalyzed nucleotide dissociation (Dahl et al., 2006; Kawashima et al., 1996; Zhang et al., 1998). The intrusion of $Phe81_{Ts}$ between $His118_{Tu}$ and $His84_{Tu}$ of helix C and switch II in EF-Tu, respectively, was proposed to displace switch II (Kawashima et al., 1996). This displacement was suggested to break interactions between $Asp80_{Tu}$ and the magnesium ion bound in the nucleotide-binding pocket, thus promoting nucleotide exchange. Consistent with this hypothesis, substitution of $Phe81_{Ts}$ with alanine reduces the ability of EF-Ts to displace GDP from EF-Tu (Zhang et al., 1998). In addition, substitution of $His118_{Tu}$ with alanine reduces the rates of EF-Ts-catalyzed nucleotide dissociation by 25- to 100-fold (Dahl et al., 2006). Work of Schümmer *et al.* (2007), however, revealed that EF-Ts-stimulated nucleotide dissociation from $EF\text{-}Tu_{H84A}$ was 4-fold faster than wild type. This result contradicted the expectation that H84A substitution would impair the ability of $Phe81_{Ts}$ to displace switch II of EF-Tu, and could not be explained. In the $EF\text{-}Tu_{wt}$•EF-Ts network presented in **Figure 4.8.A**, $His84_{Tu}$ in switch II communicates with helix C. Since communication reports on correlated motion of Cα atoms, it reflects ordered motion of communicating amino acids relative to one another. As $His84_{Tu}$ contacts helix C via sidechain interactions (not shown), it seems likely that H84A substitution in EF-Tu eliminates switch II/helix C communication. This would promote more random motion of switch II in the EF-Tu•EF-Ts complex and, since switch II contributes to binding Mg^{2+}, it would likely accelerate nucleotide dissociation as shown experimentally (Schümmer et

al., 2007). The available structural and biochemical data, taken together with the communication networks presented here, suggest that the structural dynamics of switch II, not merely its position, mediates the kinetics of nucleotide release from EF-Tu.

Comparing interactions between different EF-Tu•EF-Ts complexes and guanine nucleotides in **Scheme 4.2** highlights some of the major differences observed in the kinetics experiments presented here. The rate constants for GTP and GDP binding to wild type EF-Tu•EF-Ts are similar and, in the cell, this equilibrium is driven towards GTP binding by the ten-fold excess of GTP over GDP (Bochner and Ames, 1982). For M112G and M112A variants, however, GDP binding is kinetically favoured over GTP, even at the cellular GTP/GDP ratio of 10:1 (Bochner and Ames, 1982). This difference results from a decrease in the bimolecular rate constant for GTP-binding (k_7) relative to wild type, while the rates for GDP binding are similar for wild type, M112G, and M112A EF-Tu variants. In light of the communication networks presented in **Figure 4.8**, this difference can be explained if GTP-binding to the EF-Tu•EF-Ts complex requires reorientation of switch II. For EF-Tu_{M112G} and EF-Tu_{M112A}, reorientation of switch II would require stabilizing interactions between EF-Ts and switch II to break and could contribute to increasing the energy barrier for GTP-binding and, consequently, decreasing k_7. The conformation of switch II in the EF-Tu•GTP•EF-Ts ternary complex may resemble the conformation in the EF-Tu•GTP binary complex, where $Gly83_{Tu}$ interacts with the γ-phosphate of GTP. In contrast, the switch II region of EF-Tu does not interact with bound GDP, and its conformation in the EF-Tu•GDP complex more closely resembles that of the EF-Tu•EF-Ts complex (Kawashima et al., 1996; Song et al., 1999). Smaller structural rearrangements in switch II during GDP binding to EF-Tu•EF-Ts

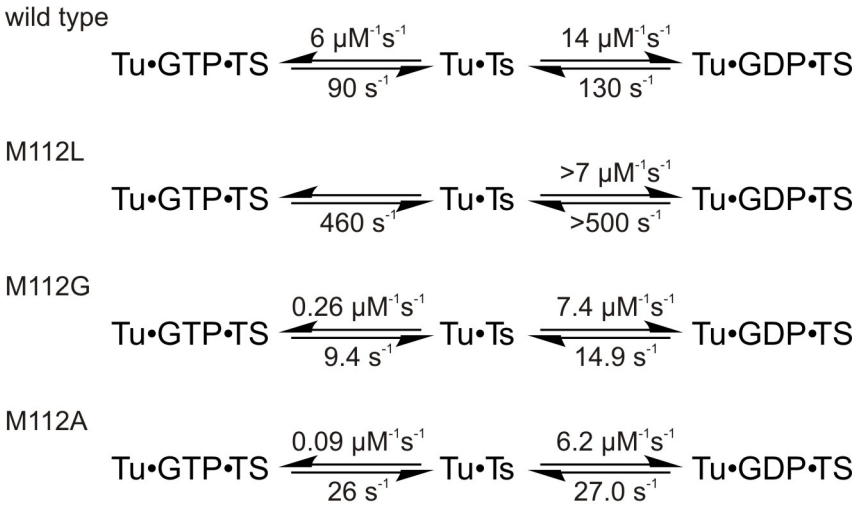

Scheme 4.2. Subsets of the kinetic schemes for nucleotide exchange in wild type, M112L, M112G, and M112A EF-Tu variants. These steps show the kinetic rate constants for interconversion between EF-Tu•EF-Ts and EF-Tu•nucleotide•EF-Ts.

would explain the similar k_4 rate constants in wild type, M112G, and M112A EF-Tu variants. It seems likely that some structural rearrangements of switch II occur upon EF-Tu•EF-Ts binding GDP since the rate of the reverse reaction (GDP dissociation from the ternary complex) is significantly slower for M112G and M112A variants compared to wild type. Consistent with this hypothesis, $Asp80_{Tu}$, which is just upstream of switch II ($Gly83_{Tu}$ to $Ile92_{Tu}$), assists in coordinating the Mg^{2+} ion in EF-Tu•GDP and EF-Tu•GTP complexes (Kjeldgaard et al., 1993; Song et al., 1999). The significantly higher activation free energies for nucleotide dissociation from M112G or M112A EF-Tu•nucleotide•EF-Ts complexes, compared to wild type, likely reflect the higher energy barriers required for close contacts observed between switch II and EF-Ts to form. Since helix 4 of EF-Ts penetrates deeper into the groove between helix C and switch II of $EF\text{-}Tu_{M112G}$ and $EF\text{-}Tu_{M112A}$ compared to $EF\text{-}Tu_{wt}$, these variants are likely more sensitive to reorientation of switch II. Thus, the measured decreases in k_{-4}, k_{-5}, and k_5

relative to wild type (**Scheme 4.2**) likely reflect higher energy barriers for switch II rearrangement in these variants.

4.4 Conclusions

This study of interactions between EF-Ts and three different EF-Tu variants has revealed that EF-Ts-stimulated nucleotide dissociation rates increase as communication with the switch II region of EF-Tu decreases. Since larger rate constants correlate with smaller free energy barriers for dissociation, this trend likely reflects an energetic contribution to forming interactions between switch II and EF-Ts. Similarly, increased communication with switch II is correlated with slower rates of nucleotide association to EF-Tu•EF-Ts complexes. Thus, breaking interactions with switch II and increasing its mobility likely occurs when nucleotides bind to form an EF-Tu•nucleotide•EF-Ts ternary complex. This suggests that switch II of EF-Tu undergoes conformational rearrangements upon GTP or GDP binding to the EF-Tu•EF-Ts complex.

Interestingly, the above hypothesis is in contrast to the available structures of the eukaryotic Elongation Factor (eEF) 1A, a homologue of EF-Tu, bound to its guanine nucleotide exchange factor eEF1Bα (Andersen et al., 2001). These structures reveal that the switch II structural element is in the same position in the eEF1A•eEF1Bα complex when GDPNP, GDP, GDP•Mg^{2+}, or no ligand is bound. The position of switch II in the eEF1A•eEF1Bα complexes is not conducive to making contacts with bound Mg^{2+} in the nucleotide-binding pocket, which led to the hypothesis that the nucleotide exchange factor for eEF1A acts via a mechanism similar to EF-Ts: disruption of switch II and the magnesium binding site (Andersen et al., 2001).

Several differences between the EF-Tu•EF-Ts system and the eEF1A•eEF1Bα system published by Andersen and coworkers might reconcile the contradictory hypotheses regarding switch II reorientation. Firstly, when crystals of eEF1A•GDPNP•eEF1Bα were soaked with magnesium, the crystals diffracted X-rays poorly (Andersen et al., 2001). This result suggests that GTP•Mg^{2+} binding, rather than GTP alone, is the signal which triggers rearrangement of switch II within the protein complex. Secondly, and perhaps most importantly, while eEF1A is a homologue of EF-Tu, the guanine nucleotide exchange factor eEF1Bα is not a homologue of EF-Ts (Maessen et al., 1986). Aside from sharing no sequence homology with EF-Ts, eEF1Bα binds in a different location on eEF1A than EF-Ts does on EF-Tu (Andersen et al., 2001; Kawashima et al., 1996). The binding site for eEF1Bα is at the interface of domains I and II in eEF1A, while EF-Ts binds at the interface of domains I and III, making no contacts with domain II. The two guanine nucleotide exchange factors have different strategies, EF-Ts binds on the 'side' of EF-Tu and disrupts interactions with bound nucleotide, while eEF1Bα binds over top of the nucleotide binding pocket in eEF1A and occupies the binding site of magnesium as well as the β- (and γ-) phosphates of GDP (and GTP). In the eukaryotic system, eEF1Bα does interact with switch II of eEF1A and appears to stabilize its position, but the orientation of switch II is different in the EF-Tu•EF-Ts complex (Andersen et al., 2001; Kawashima et al., 1996). In light of these differences it is possible that the structural dynamics of switch II differ between the EF-Tu/EF-Ts and eEF1A/eEF1Bα systems.

It seems that EF-Tu has evolved to maintain more mobility in switch II when bound to its guanine nucleotide exchange factor than its eukaryotic counterpart. In the yeast system, nucleotide binding stimulates eEF1A•eEF1Bα dissociation by less than 100-fold

(Gromadski et al., 2007) whereas EF-Tu•EF-Ts dissociation is stimulated by over 10,000-fold in *E. coli* upon GTP or GDP binding (Gromadski et al., 2002). Switch II structural dynamics in the EF-Tu•EF-Ts complex may, therefore, be critical for stimulating rapid EF-Ts dissociation and efficiently regenerating EF-Tu•GTP. The requirement for switch II mediated dissociation of the eEF1A•eEF1Bα complex may be less critical in *S. cerevisiae* where intrinsic dissociation of the complex is fast (k_{off} = 1.5 s^{-1}), (Gromadski et al., 2007) in comparison to that of *E. coli* (k_{off} = 0.03 s^{-1}) (Gromadski et al., 2002). Rapid dissociation of the guanine nucleotide exchange factor is, however, critical in both systems, as it is the last step in regenerating the 'on' state of the respective G-proteins.

Chapter 5

Conserved interdomain bridges in EF-Tu transmit a codon-independent GTPase activation signal from the 16S rRNA/domain II interaction site to the G-domain

All wet-lab experiments presented in this chapter were performed by Fan Mo, M.Sc.

5.1 Introduction

The ribosome carries out protein synthesis in all living cells. During the elongation phase of protein synthesis, Elongation Factor (EF) Tu is responsible for delivering aminoacyl-tRNAs (aa-tRNAs) to the ribosome in bacteria, while its respective homologues perform this task in eukaryotes and archaea. Since EF-Tu binds all aa-tRNAs with nanomolar affinity (Louie et al., 1984; Ott et al., 1990), EF-Tu•GTP•aa-tRNA ternary complexes bearing different aa-tRNAs will constantly sample the empty A-sites of elongating ribosomes. When a correct codon/anticodon interaction between mRNA and tRNA occurs in the decoding centre of the 30S ribosomal subunit, the GTPase activity of EF-Tu is stimulated (Pape et al., 1998). Following rapid GTP hydrolysis and P_i release, a correct aa-tRNA can accommodate into the A-site (Pape et al., 1998). Through separating A-site binding and delivery of aa-tRNAs by the irreversible hydrolysis of GTP, EF-Tu acts as the first checkpoint for incorporation of a correct amino acid. GTPase activation, which is rate limiting for GTP hydrolysis, is between 10 and 650-fold faster (depending on experimental conditions) in the presence of cognate compared to near-cognate aa-tRNA, thus contributing significantly to the fidelity of translation (Gromadski and Rodnina, 2004; Pape et al., 1998). GTPase activation of EF-Tu must, therefore, be specific enough to contribute to fidelity while still being fast enough to support rapid protein synthesis (a rate of ~10 amino acids per second) (Forchhammer and Lindahl, 1971; Proshkin et al., 2010). Here we investigate the ability of EF-Tu to transmit GTPase-activating signals from the ribosome to the catalytic components of EF-Tu.

Several different factors appear to contribute to GTPase activation of EF-Tu on the ribosome. The ribosomal protein L7/L12 has been shown to interact with helix D in domain I of EF-Tu (Villa et al., 2009) and to stimulate the rate of GTP hydrolysis on the ribosome ~2,500-fold (Mohr et al., 2002). The highly conserved sarcin-ricin loop is an element of the 23S rRNA that has also been shown to interact with domain I of EF-Tu as shown in **Figure 5.1** (Villa et al., 2009; Voorhees et al., 2010). A direct interaction between A2662 of the sarcin-ricin loop and the catalytic $His84_{Tu}$ was observed in X-ray structures of EF-Tu bound to the ribosome and was proposed to contribute to GTPase activation (Voorhees et al., 2010). Despite this contact, *in vitro* experiments carried out with ribosomes bearing a two-nucleotide deletion in the sarcin-ricin loop revealed a less than 2-fold decrease in the rate of GTP-hydrolysis (Shi et al., 2012). In general, contacts between the ribosome and domain I of EF-Tu are thought to align the GTPase machinery, including switch I and switch II, to facilitate GTP hydrolysis.

The regulation of GTPase activation in EF-Tu has been extensively studied using structural and biochemical techniques. Hydrolysis of GTP by EF-Tu is thought to be catalyzed by the conserved amino acid $His84_{Tu}$, which probably aligns/activates a water molecule for in-line attack of the γ-phosphate (Daviter et al., 2003; Grigorenko et al., 2008). The slow rate of intrinsic GTP hydrolysis by EF-Tu has been explained by the occlusion of the catalytic $His84_{Tu}$ from GTP by a hydrophobic gate comprised of amino acids $Val20_{Tu}$ and $Ile60_{Tu}$ (Berchtold et al., 1993). Stimulation of GTP hydrolysis by the antibiotic kirromycin (Wolf et al., 1974) or by programmed ribosomes in the presence of cognate aa-tRNA (Pape et al., 1998; Thompson and Stone, 1977) has been rationalized by conformational changes in the switch I and switch II regions (including $Ile60_{Tu}$ and

$His84_{Tu}$ respectively) (Schmeing et al., 2009; Vogeley et al., 2001; Voorhees et al., 2010). These conformational changes open the hydrophobic gate and reposition $His84_{Tu}$ although the precise conformations differ between the complexes studied.

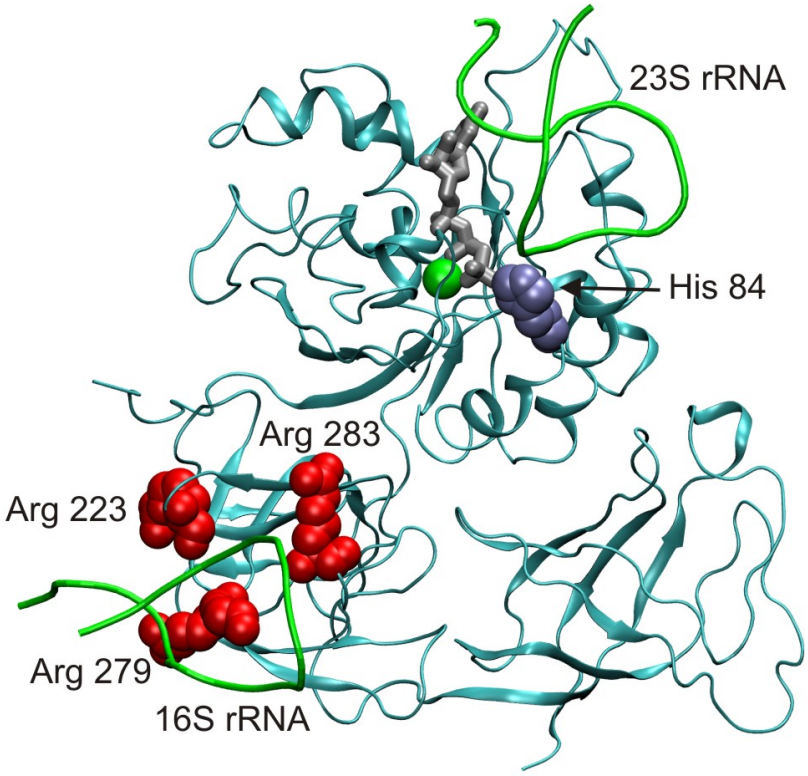

Figure 5.1. Interactions between rRNA elements and EF-Tu. The structure of *Thermus thermophilus* EF-Tu bound to GDPCP and Trp-$tRNA^{Trp}$ on the 70S ribosome from *Thermus thermophilus* is shown based on the crystal structure 2XQD/2XQE (Voorhees et al., 2010). The protein structure is shown in cyan (cartoon representation), rRNA is shown in green (tubes), GDPNP is shown in grey (sticks), and Mg^{2+} is shown as a green sphere. Amino acids $His84_{Tu}$ (blue), $Arg223_{Tu}$, $Arg279_{Tu}$, and $Arg283_{Tu}$ (red), are shown in space-filling representation and numbering is based on *E. coli* EF-Tu.

Intriguingly, contacts between helix 5 of the 16S rRNA and domain II of EF-Tu were also hypothesized to contribute to GTPase activation of EF-Tu on the ribosome (Agirrezabala et al., 2011; Schmeing et al., 2009). In line with this hypothesis, substitution of $Gly222_{Tu}$ with aspartate in domain II of EF-Tu was shown to render

GTPase activation of EF-Tu on the ribosome undetectable (Vorstenbosch et al., 1996). This substitution introduces an additional negative charge in domain II of EF-Tu that might disrupt interactions with the 16S rRNA. Single nucleotide substitutions in helix 5 of the 16S rRNA were shown to reduce overall translation activity *in vivo*, but no mechanistic basis for this effect was reported (McClory et al., 2010). Understanding the structural basis of the GTPase activation mechanism is not straightforward since the 16S rRNA/domain II contact is over 30 Å away from GTP bound in domain I of EF-Tu (**Figure 5.1)**. The first crystal structure of EF-Tu on the ribosome led to the proposal that movements in domain II were linked to conformational changes in switch I through the acceptor stem of bound tRNA (Schmeing et al., 2009). Since the aa-tRNA directly contacts both the decoding centre and EF-Tu, it has the potential to mediate codon-dependent signaling to EF-Tu. Intriguingly, the interaction between helix 5 and domain II of EF-Tu was also present in a cryo-EM reconstruction of EF-Tu bound to the ribosome with a near-cognate aa-tRNA in the A-site (Agirrezabala et al., 2011). This feature in the latter structure suggests that the direct 16S rRNA/domain II interaction is independent of codon recognition.

We herein report three single amino acid substitutions in domain II of EF-Tu that significantly reduce the GTPase activity of EF-Tu on the ribosome in the absence of tRNA. The omission of aa-tRNA from our experiments demonstrates that domain II in EF-Tu relays a GTP hydrolysis-activating signal from the ribosome to EF-Tu even in the absence of a codon/anticodon signal. These results also suggest that active communication pathways are present in EF-Tu•GTP that can transmit a GTPase stimulating signal from domain II to domain I in the absence of tRNA. We have carried

out molecular dynamics simulations of the EF-Tu•GTP complex in order to investigate these potential communication pathways. Simulations of EF-Tu_{wt} and two variants bearing single amino acid substitutions in domain I reveal that breakdown in communication between domains I and II is concomitant with rearrangement of the switch I and switch II regions. The results presented here demonstrate that domain II of EF-Tu contributes to GTP hydrolysis on the ribosome, and that a GTPase-activating signal likely travels from domain II to domain I in order to promote rearrangement of switch I and switch II.

5.2 Materials and Methods

Buffers and Reagents

All *in vitro* experiments were performed in Buffer A (50 mM Tris-HCl, pH 7.5, 70 mM NH_4Cl, 30 mM KCl, 7 mM $MgCl_2$). [γ-^{32}P]GTP was purchased from MP Biomedicals and DNA primers were purchased from Integrated DNA Technologies.

Mutagenesis

The plasmid pEECAHis (Wieden et al., 2002), encoding for *E. coli* EF-Tu with a C-terminal hexahistidine tag, was used as the template for all mutagenesis reactions. The Quikchange^{TM} method (Stratagene) employing two complementary primers was used in order to introduce the respective mutation. The coding primer sequences (5′→3′) were as follows: (R223A) CGTGTAGAA**GCA**GGTATCATCAAAGTTGG, (R279A) GGTGT-TCTGCTG**GCA**GGTATCAAACG, (C81A) CGCACACGTAGAC**GCA**CCGGGGCA-CGCC, (C81S) CGCACACGTAGAC**AGT**CCGGGGCACGCC, where the codon encoding the substituted amino acid is shown in bold. A more detailed description of

mutagenesis reactions is provided in **Chapter 3**. Reaction mixtures were treated with DpnI (Fermentas) to degrade template pDNA and subsequently used to transform competent *E. coli* NEB 5α cells (New England Biolabs). Plasmid DNA was isolated from a single colony in each NEB 5α strain and the presence of the desired mutation was confirmed by sequencing (MacroGen). The R283A EF-Tu construct was a gift from Marina Rodnina.

Protein Overexpression and Purification

Protein overexpression and purification was carried out as described in **Chapter 3**.

Ribosome Purification

Highly purified ribosomes and ribosomal subunits for use in *in vitro* assays were prepared as previously described (Milon et al., 2007). *E. coli* MRE600 cells were crushed by motar and pestle in the presence of alumina and DNAse I in a cold room. The resulting paste was suspended in Buffer D (20 mM Tris-HCl pH 7.6 @ 4°C, 100 mM NH_4Cl, 10.5 mM $MgCl_2$, 0.5 mM EDTA, 3 mM β-mercaptoethanol). The lysate was cleared by sequential centrifugation in a JA-14 rotor (Beckman) at 3,000 rpm for 10 minutes and 9,000 rpm for 30 minutes. The supernatant was filtered and centrifuged at 20,000 rpm in a Ti 45 rotor (Beckman) for 30 minutes. Twenty millilitre aliquots of the resulting supernatant were overlaid onto 20 mL sucrose cushions (Buffer E: 20 mM Tris-HCl pH 7.6 @ 4°C, 500 mM NH_4Cl, 10.5 mM $MgCl_2$, 0.5 mM EDTA, 1.1 M sucrose, 3 mM β-mercaptoethanol), and ribosomes were pelleted by centrifugation at 40,000 rpm in a Ti 45 rotor for 16 hours. Following resuspension of ribosomes in Buffer F (20 mM Tris-Hcl pH 7.6 @ 4°C, 500 mM NH_4Cl, 10.5 mM $MgCl_2$, 0.5 mM EDTA, 7 mM β-mercaptoethanol), 50 mL aliquots of ribosome solution were pelleted through 4 mL

sucrose cushions (Buffer E) by centrifugation in a Ti 45 rotor at 40,000 rpm for 16 hours. The ribosome pellets were again resuspended in Buffer F and 10 mL aliquots were pelleted through 1.5 mL sucrose cushions (Buffer E) by centrifugation in a Beckman SW28 rotor at 28,000 rpm for 16 hours. The pellets containing ribosomes were resuspended in Buffer G (20 mM Tris-Hcl pH 7.6 @ 4°C, 60 mM NH_4Cl, 5.25 mM $MgCl_2$, 0.25 mM EDTA, 3 mM β-mercaptoethanol, 5% sucrose) and 70S ribosomes, 50S ribosomal subunits, and 30S ribosomal subunits were separated on a 10% - 40% sucrose gradient via zonal centrifugation at 28,000 rpm in a Ti 15 rotor (Beckman) for 19 hours. 70S ribosomes, 50S ribosomal subunits, and 30S ribosomal subunits were harvested from the respective zones by centrifugation at 45,000 rpm in a Ti 45 rotor for 46 hours. Each pellet was resuspended in Buffer H (20 mM Tris-HCl pH 7.6 @ 4 °C, 50 mM NH_4Cl, 5 mM $MgCl_2$), flash frozen in liquid nitrogen, and stored at -80 °C until use. All centrifugation was performed at 4 °C.

Ribosome-stimulated GTPase activity of EF-Tu

Ribosome-stimulated GTP hydrolysis by EF-Tu was measured in multiple turnover Michaelis-Menten assays where EF-Tu•GTP was treated as substrate and 70S ribosomes or 50S ribosomal subunits were treated as enzyme. Prior to the reaction, [γ-^{32}P]GTP was charged at 37 °C for 15 min in a mixture containing 3 mM phosphoenolpyruvate and 0.25 mg/mL pyruvate kinase. EF-Tu•[γ-^{32}P]GTP complex was formed by incubation of 80 μM GTP with 1.2-60 μM EF-Tu and 0.1 μM EF-Ts followed by incubation for another 15 minutes. GTP hydrolysis reactions, initiated by the addition of 70S ribosomes or 50S ribosomal subunits to a final concentration of 0.1 μM, contained 0.3-15 μM EF-Tu, 0.025 μM EF-Ts, and 20 μM GTP. Reactions were carried out at 37 °C and 5 μL

aliquots were quenched in perchloric acid at various time points. Phosphate ions in the quenched reaction mixture were complexed with molybdate, separated from unhydrolyzed GTP via liquid/liquid extraction, and quantified by liquid scintillation counting. Each reaction was performed in triplicate.

Kinetic Analysis

Time points from replicate trials were used to construct time courses (pmol GTP hydrolyzed plotted as a function of time.) The linear phase of each GTP hydrolysis time course was fitted with a linear function, the slope of which provided the initial rate for GTP hydrolysis. The standard error in the fitted slope was reported as the error for the initial rate of GTP hydrolysis. Michaelis-Menten graphs were constructed by plotting the initial rate of GTP hydrolysis as a function of EF-Tu concentration. These plots were fitted to hyperbolic functions to provide the respective v_{max} and K_M parameters. The errors reported for these parameters were the standard errors for the fits. All plotting and fitting of these data was performed using Prizm software (GraphPad).

Molecular dynamics simulations

All-atom models of EF-Tu_{wt}•GTP, EF-Tu_{C81A}•GTP, and EF-Tu_{C81S}•GTP in electrostatically neutral aqueous systems were constructed as described in **Section 3.2**. Equilibration and production phase MD simulations were carried out with NAMD2.6 (Phillips et al., 2005) in NPT ensembles using a step size of 0.5 fs as described in **Section 3.2**. Each simulation was carried out for 20 ns. The simulation of EF-Tu_{wt}•GTP presented in this chapter is an extension to the trajectory presented in **Chapter 3** for the same model.

Analysis of MD simulations

Snapshots of equilibrium MD simulations were saved every 1 ps and compiled using the software Carma (Glykos, 2006) to remove water molecules as well as whole-body translations and rotations of the protein. The final ten nanoseconds of each simulation were used for analysis. In order to trace long-range communication in EF-Tu, communication networks were constructed in a manner similar to that described by Sethi *et al.* (2009). In order to trace a signal pathway in EF-Tu as a sequence of discrete steps between contacting amino acids that communicate with one another, contact information and 'communication information' were incorporated into each network. Each Cα in EF-Tu is represented by a node in the network and nodes are connected by edges if a) the two amino acids are in contact and b) the Cα atoms 'communicate' significantly during the MD simulation. Amino acids were defined as in contact if the subsuming heavy atoms were separated by < 4.5 Å for > 75 % of the simulation analyzed, as performed in Sethi *et al*. (2009). Communication between Cα atoms was assessed using a covariance analysis performed in the software Carma (Glykos, 2006). The normalized covariance between amino acids *i* and *j* (c_{ij}) is calculated as a time-averaged value according to **Equation 5.1.** (Glykos, 2006).

$$C_{ij} = \frac{\left\langle \left(v_{i,t} - \overline{v}_i\right) \bullet \left(v_{j,t} - \overline{v}_j\right) \right\rangle}{\left(\left\langle \left(v_{i,t} - \overline{v}_i\right) \right\rangle^2 \left\langle \left(v_{j,t} - \overline{v}_j\right) \right\rangle^2 \right)^{1/2}} \qquad (5.1)$$

In **Equation 5.1**, $v_{i,t}$ are the Cartesian coordinates for the Cα of amino acid *i* at frame *t*, $\overline{v}_i$ are the time-averaged Cartesian coordinates for the Cα of amino acid *i*, • indicates a dot product, and $\langle\ \rangle$ indicates time-averaging of the quantities within the brackets. The normalized covariance matrix is thus normalized with respect to the diagonal such that

C_{ij}=1 when *i*=*j*. The resulting matrix C is symmetric with values of 1 along the diagonal. Covariance values range from -1 (moving in opposite directions) to 1 (moving in the same direction) and most covariance values computed for these simulations were close to zero. In part, covariance describes the time-averaged tendency for a pair of amino acids to move in the same direction at the same time relative to their respective average positions. Information about the relative magnitude of motion is also involved, however.

In order to simplify the communication network and reduce noise, an edge connecting a pair of contacting amino acids was kept if and only if the covariance between these amino acids was significant. Significance was defined separately for each amino acid (*i*) based on the distribution of normalized covariance values c_{ij}, where *j* is any other amino acid. A covariance (c_{ij}) was defined as significant if it met the criteria in **Equations 5.2** and **5.3**.

$$\left|c_{ij}\right| > \bar{c}_i + 3\sigma_i \qquad (5.2)$$

$$\left|c_{ij}\right| > \bar{c}_j + 3\sigma_j \qquad (5.3)$$

Here $\bar{c}_i$ and σ_i are the average and standard deviation for covariance of amino acid *i* respectively, each obtained by fitting a normal distribution to the histogram of normalized covariances for amino acid *i*. Analysis of contact and covariance data as well as graph construction was performed in the statistical analysis software R (RCoreTeam, 2012) and the igraph package (Csardi, 2009) using scripts written in house. Following construction, each communication network was visualized and analyzed in the software Gephi (Bastian et al., 2009). Each network was organized using the Force Atlas algorithm, which causes all nodes to repel one another. The edges act as springs to keep

communicating nodes in close proximity. The resulting representations are shown in **Figures 5.3** and **5.4**.

The 'importance' of each node to global communication within the network was computed using the betweenness measure. Betweenness is defined as the number of shortest paths within the network that pass through a given node (Freeman, 1977). A shortest path is the route connecting two nodes that passes through the smallest number of intervening nodes. The betweenness of node v (B_v) can be expressed mathematically as follows:

$$B_v = \sum_{i \neq j, i \neq v, j \neq v} g_{ivj} / g_{ij} \qquad (5.4)$$

where v, i, and j are nodes in the network, g_{ij} is number of shortest paths connecting nodes i and j, and g_{ivj} is the number of shortest path connecting nodes i and j which passes through node v (Csardi, 2009; Freeman, 1977).

5.3 Results and Discussion

Arginine residues in domain II of EF-Tu are important for GTP hydrolysis on the ribosome.

If specific contacts between domain II in EF-Tu and 16S rRNA indeed participate in GTPase activation of EF-Tu, substitution of the amino acids involved should reduce the 70S-stimulated GTPase activity rather than just changing the affinity of EF-Tu for the ribosome. To this end, several EF-Tu variants were designed bearing single amino acid substitutions in domain II. By examining the available X-ray structures of EF-Tu bound to the ribosome (PDB IDs: 2QXD and 2WRN) (Schmeing et al., 2009; Voorhees et al., 2010), $Arg279_{Tu}$ and $Arg223_{Tu}$ in domain II, which directly interact with 16S rRNA and

are 100% conserved in EF-Tu (DeLaurentiis et al., 2011), were identified as promising candidates. Both of these amino acids were proposed by Schmeing *et al*. (2009) to be involved in a communication pathway between the ribosome and the GTP binding site in EF-Tu. Arginine 283 was also selected for mutagenesis since it is in close proximity (< 5.5 Å) to the 16S rRNA when EF-Tu is bound to the ribosome and could contact helix 5 upon sidechain rotation (Schmeing et al., 2009; Voorhees et al., 2010). In addition, $Arg283_{Tu}$ is conserved as an arginine or lysine in all bacterial EF-Tus (DeLaurentiis et al., 2011). The positions of $Arg279_{Tu}$, $Arg223_{Tu}$, and $Arg283_{Tu}$ relative to helix 5 are shown in **Figure 5.1** based on an X-ray structure of EF-Tu•GDPCP•aa-tRNA bound to the ribosome (PDBID: 2XQD), (Voorhees et al., 2010).

The ability of each EF-Tu variant to hydrolyze GTP on ribosomes was tested using Michaelis-Menten steady-state kinetics. In these experiments, ribosomes (Rb) were treated as the enzyme and EF-Tu•GTP was treated as substrate, according to **Scheme 5.1**. Here, the k_{cat} parameter, which is essentially independent of EF-Tu•GTP•Rb affinity, represents the rate of EF-Tu•GTP•Rb turnover, which includes GTPase activation, GTP hydrolysis, and dissociation of EF-Tu•GDP from the ribosome.

$$\text{EF-Tu•GTP + Rb} \rightleftharpoons \text{EF-Tu•GTP•Rb} \xrightarrow{k_{cat}} \text{EF-Tu•GDP + Rb + } P_i$$

Scheme 5.1. Michaelis-Menten mechanism for ribosome stimulated GTP hydrolysis by EF-Tu.

The results in **Figure 5.2**, summarized in **Table 5.1**, demonstrate that wild type EF-Tu•GTP turns over on the ribosome with a k_{cat} of 2.0 ± 0.2 min^{-1}. This rate is similar to the rate shown for GTP hydrolysis by EF-Tu bound to an aminoacylated-acceptor stem fragment of tRNA on the ribosome under single turnover conditions (4 min^{-1}) (Piepenburg et al., 2000). Since the single turnover experiment is independent of EF-Tu

release, the k_{cat} measured in the present report likely reflects the rate of GTPase activation and/or GTP hydrolysis. This is also consistent with the rapid rate of EF-Tu•GDP dissociation from the ribosome (240 min^{-1}) previously reported. The H84A variant of EF-Tu, previously shown to be deficient in GTP hydrolysis (Daviter et al., 2003), is shown as a negative control (**Figure 5.2.A**). Each arginine substitution (R223A, R279A, or R283A) resulted in a 4-5-fold reduction in the k_{cat} for EF-Tu•GTP turnover (**Figure 5.2.A**, **Table 5.1**). This effect could result from changes in GTPase activation, GTP hydrolysis, or EF-Tu•GDP dissociation from the ribosome (*vide supra*). In order for EF-Tu•GDP dissociation to become rate limiting under these conditions, however, its rate would have to decrease about 100-fold (Pape et al., 1998). This seems unlikely given that substitution of arginine for alanine would likely weaken the interaction between EF-Tu and the ribosome and increase the rate of EF-Tu dissociation. In the presence of aa-tRNA, the rate of GTP hydrolysis has been shown to be limited by the rate of the preceding GTPase activation step on the ribosome (Pape et al., 1999). Thus, the lower k_{cat} values measured here for $EF\text{-}Tu_{R223A}$, $EF\text{-}Tu_{R279A}$, and $EF\text{-}Tu_{R283A}$ likely reflect smaller rates of GTPase activation compared to $EF\text{-}Tu_{wt}$. In line with this hypothesis, substitution of $Gly222_{Tu}$, which is in domain II and in close proximity to positions 223, 279, and 283, with aspartate was shown to render GTPase activation of EF-Tu on the ribosome undetectable (Vorstenbosch et al., 1996). Thus, our results support the hypothesis that interactions between domain II of EF-Tu and 16S rRNA contribute a GTPase activation signal to EF-Tu, even in the absence of a codon/anticodon interaction.

GTPase activation via domain II is dependent on the small ribosomal subunit.

If interactions between 16S rRNA and $Arg223_{Tu}$, $Arg279_{Tu}$, and $Arg283_{Tu}$ contribute to GTPase stimulation of EF-Tu, then omitting 30S ribosomal subunits from the experiments should result in similar rates of EF-Tu•GTP turnover for wild type, R223A, R279A, and R283A EF-Tus. The results of these experiments, shown in **Figure 5.2.B** and summarized in **Table 5.1**, clearly support this hypothesis. Turnover of EF-Tu•GTP in the presence of 50S ribosomal subunits occurs with a k_{cat} of about 0.4 min^{-1} for wild type, R279A, and R283A EF-Tus. The substitution of $Arg223_{Tu}$ with alanine results in a slight (less than 2-fold) but significant increase in k_{cat} (0.63 ± 0.07 min^{-1}) compared to $EF\text{-}Tu_{wt}$. Thus, the 4-fold difference in k_{cat} observed in the presence of 70S ribosomes for these variants compared to wild type clearly results from an effect specific to the 30S ribosomal subunit. Based on the available X-ray structures of EF-Tu bound to the ribosome, substitution of $Arg223_{Tu}$, $Arg279_{Tu}$, or $Arg283_{Tu}$ with alanine likely results in loss of an interaction between domain II of EF-Tu and helix 5 of the 16S rRNA. Our results suggest that this interaction likely contributes a GTPase activating signal to EF-Tu as proposed by Ramakrishnan and coworkers (Schmeing et al., 2009). Interestingly, omission of the 30S ribosomal subunit from the GTPase reactions reduces the turnover of $EF\text{-}Tu_{wt}$•GTP by the same factor (4-fold) as alanine substitution of $Arg223_{Tu}$, $Arg279_{Tu}$, or $Arg283_{Tu}$. This suggests that in the absence of a codon/anticodon interaction, the primary contribution of the 30S ribosomal subunit to GTPase activation of EF-Tu is through the domain II/helix 5 interaction.

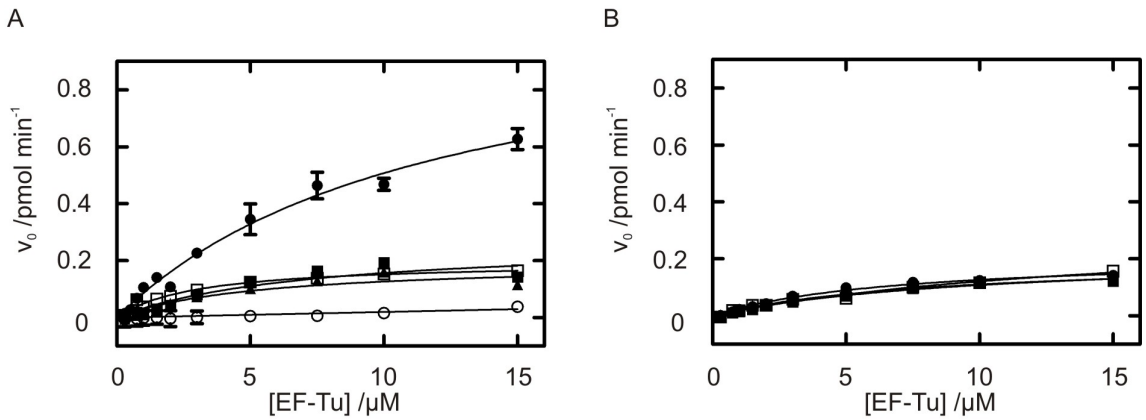

Figure 5.2. Michaelis-Menten analysis of EF-Tu domain II variants. (A) 70S ribosomes or (B) 50S ribosomal subunits (0.1 µM) were incubated with increasing concentrations of EF-Tu•GTP (0.3-15 µM) in the presence of EF-Ts (0.025 µM). Linear fits to the initial phase of GTP hydrolysis time courses (triplicate experiments) provided initial reaction velocities (v_0). The error bars are derived from the linear regression and lines represent fitted hyperbolic functions. Symbols represent EF-Tu variants (•) wild-type, (◦) H84A, (□) R279A, (■) R283A, and (□) R223A.

Table 5.1. Michaelis-Menten kinetic parameters for 70S ribosome- and 50S ribosomal subunit-stimulated EF-Tu•GTP hydrolysis using EF-Tu variants. Parameters were determined based on the hyperbolic fits shown in **Figures 5.2** and **5.4**. The reported errors were obtained from standard errors of the fits. Parameters that could not be determined due to large standard errors in the fits are indicated (-) in addition to experiments that were not performed (n/d).

	70S		50S	
	k_{cat} /min^{-1}	K_M /µM	k_{cat} /min^{-1}	K_M /µM
wt	2.0±0.2	12±2	0.43±0.03	7±1
H84A	-	-	n/d	n/d
R279A	0.39±0.05	5±1	0.41±0.03	8±1
R283A	0.54±0.07	7±2	0.44±0.03	10±1
R223A	0.40±0.02	3±1	0.63±0.07	16±3
C81A	0.53±0.09	8±3	0.6±0.4	60±40
C81S	0.5±0.1	19±8	-	-

Conserved bridges can communicate signals between domain II and the GTP-binding site in domain I of EF-Tu

In order to understand how a GTPase activating signal can be transmitted from domain II in EF-Tu to the GTP binding pocket in domain I, approximately 30 Å from the interaction with helix 5, a 20 ns MD simulation was performed on the wild-type EF-Tu•GTP complex. The last ten nanoseconds of the simulation were used to construct

a communication network similar to those presented in Sethi *et al.* (2009). In the network shown in **Figure 5.3.A**, each amino acid is represented by a node. Two nodes are connected by an edge if they are in contact during at least 75% of the simulation and show significant correlated motion during the MD simulation. Details of network construction and the criteria used to identify significant correlated motion are described in Materials and Methods (**Section 5.2**) as well as **Appendix A.3**. The network shown in **Figure 5.3.A** represents the collection of pathways that allow contacting amino acids to communicate by influencing each other's motion. This network representation was prepared using a force-based algorithm in the software Gephi (Bastian et al., 2009) that causes all nodes to repel one another, while edges maintain close proximity of communicating amino acids. It is noteworthy that the resulting network topology reflects the expected three-domain structure of EF-Tu. The EF-Tu•GTP network clearly demonstrates dense communication between amino acids within a given domain, and limited communication between domains.

The EF-Tu•GTP network can be used to identify communication pathways connecting any two amino acids in EF-Tu. Our biochemical results indicate that signals originating at $Arg223_{Tu}$, $Arg279_{Tu}$, and $Arg283_{Tu}$ need to be communicated to the GTPase machinery. However, it is unclear where exactly these signals terminate. Since the GTPase machinery is located in domain I, the network shown in **Figure 5.3.A** was used to identify potential 'bridges' that would allow a signal to be transmitted from domain II in EF-Tu, to domain I. Three bridges were identified: His11/Glu272, Gln97/Arg230, and Thr93/Glu215. The amino acids that form these bridges are highly conserved in 125 aligned bacterial EF-Tu sequences: $Glu215_{Tu}$ is invariant, $Gln97_{Tu}$ and $Thr93_{Tu}$ are each

>99% conserved, $Arg230_{Tu}$ is >96% conserved, $Glu272_{Tu}$ is > 99% conserved as Glu (26%) or Asp (73%), and $His11_{Tu}$ is invariant in the 121 sequences for which the N-terminal sequence was available. Interestingly, although each of these four amino acids is polar or charged, interactions within each pair are hydrophobic in nature (**Figure 5.3.B**).

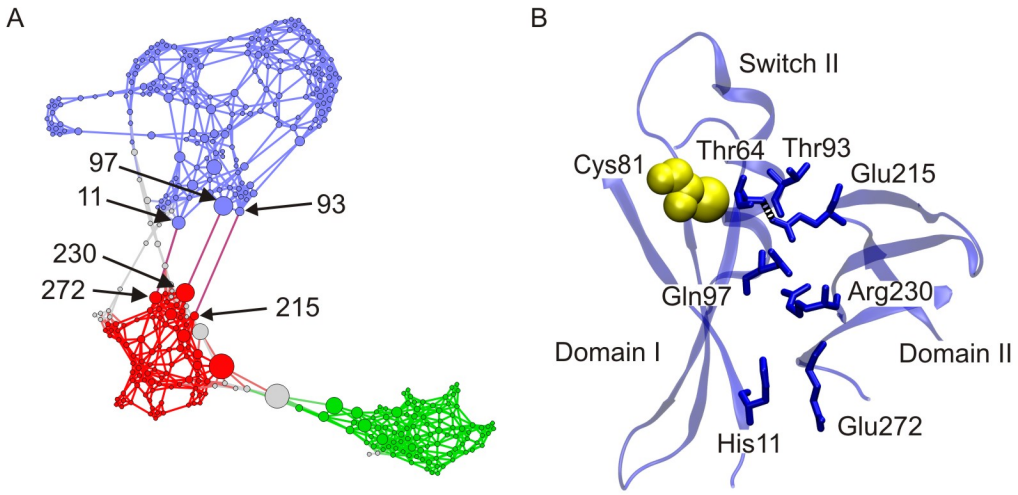

Figure 5.3. Intramolecular communication network of EF-Tu•GTP *in silico* reveals three interdomain bridges. (A) Each node in the network represents an amino acid in EF-Tu and is coloured according to domain (blue: domain I, red: domain II, green: domain III, grey: linker or N/C-terminus). Edges were drawn between nodes that were in contact for 75% or more of MD simulation from 10-20ns and had significant covariance with one another. Networks were prepared with Gephi, and organized using the Force Atlas algorithm based on data from MD simulations of EF-Tu•GTP. (B) Snapshot of EF-Tu after 20 ns of MD simulation is shown with protein in cartoon representation, $Cys81_{Tu}$ shown in yellow space-filling representation, and selected sidechains are shown as sticks. The hydrogen bond between $Thr64_{Tu}$ and $Glu215_{Tu}$ in wild-type EF-Tu is indicated by a dashed black line.

Communication within a network is assumed to be most efficient along shortest paths, i.e. pathways that travel through the minimum number of nodes from source to target (Freeman, 1977). In order to quantify the importance of each amino acid to global communication within the EF-Tu network, a betweenness analysis was carried out and the results are summarized in **Table A.4.1**. This analysis quantifies the number of shortest paths that each amino acid participates in within the network. An amino acid with a high betweenness is therefore capable of relaying communication between many pairs of amino acids. These amino acids may play important roles in regulating global

communication within the network. Not surprisingly, amino acids that participate in interdomain bridges show high betweenness since they are necessary for communication between domains. The Glu272/His11, Gln97/Arg230, and Thr93/Glu215 bridges are included in the top 10% of amino acids ranked by betweenness (**Table A.4.1**).

In order to validate these bridges as pathways capable of transmitting GTPase activating signals, an EF-Tu variant was sought with impaired domain II/domain I communication for analysis *in vitro* and *in silico*. The highly conserved $Cys81_{Tu}$ (89 % identity) is ranked 28^{th} in betweenness out of 393 amino acids. This analysis places $Cys81_{Tu}$ in the top 8% of amino acids and suggests an important role in intramolecular communication in EF-Tu. Position 81 in EF-Tu has previously been studied using site directed mutagenesis (DeLaurentiis et al., 2011) and covalent modification with N-tosyl-L-phenylalanyl chloromethylketone (TPCK) (Jonák et al., 1982). Modification with TPCK has been shown to impair the binding of aa-tRNA to EF-Tu (Richman and Bodley, 1973) as well as reduce GTP hydrolysis by EF-Tu on the ribosome in the absence of aa-tRNA (Sedláček et al., 1974). The reported effect on ribosome-stimulated GTP hydrolysis might reflect a lower affinity of EF-Tu•GTP for the ribosome, disruption of the active site in EF-Tu, and/or an impaired ability to transmit GTPase activation signals following $Cys81_{Tu}$ modification. Previous studies of EF-Tu variants bearing single amino acid substitutions at position 81 have revealed that C81S substitution compromises the ability of EF-Tu to bind aa-tRNA, while C81A does not (DeLaurentiis et al., 2011). Since the C81S substitution is a seemingly conservative substitution and aa-tRNA interacts with the domain II/domain I interface, it seemed possible that domain II/domain I communication was disrupted in this variant.

To address this hypothesis, EF-Tu_{C81A} and EF-Tu_{C81S} variants were simulated *in silico* and the corresponding communication networks shown in **Figure 5.4.A & B** were constructed. Strikingly, the interdomain bridges present in the wild type network (His11/Glu272, Gln97/Arg230, and Thr93/Glu215) are not present in the network of either variant. In fact, communication from domain II to domain I must pass through the N-terminus or linker region in each of the variant networks. These results suggest that communication between domains II and I is altered by C81A or C81S substitution. A close inspection of the MD simulations reveals the origin of breakdown in communication across the interdomain bridges. Substitution of $Cys81_{Tu}$ with alanine or serine causes an approximate 10° rotation in the Switch II helix, which includes $Thr93_{Tu}$ and $Gln97_{Tu}$. As a result of this rotation, the Gln97/Arg230 and Thr93/Glu215 interactions are disrupted (**Figure 5.4 C & D**). Disruption of the His11/Glu272 bridge appears to result from increased separation between the backbone atoms of $His11_{Tu}$ and $Glu272_{Tu}$. Although each bridge was identified as a contact in MD simulations of EF-Tu_{C81A} and EF-Tu_{C81S}, none of the amino acid pairs in these bridges showed significant covariance.

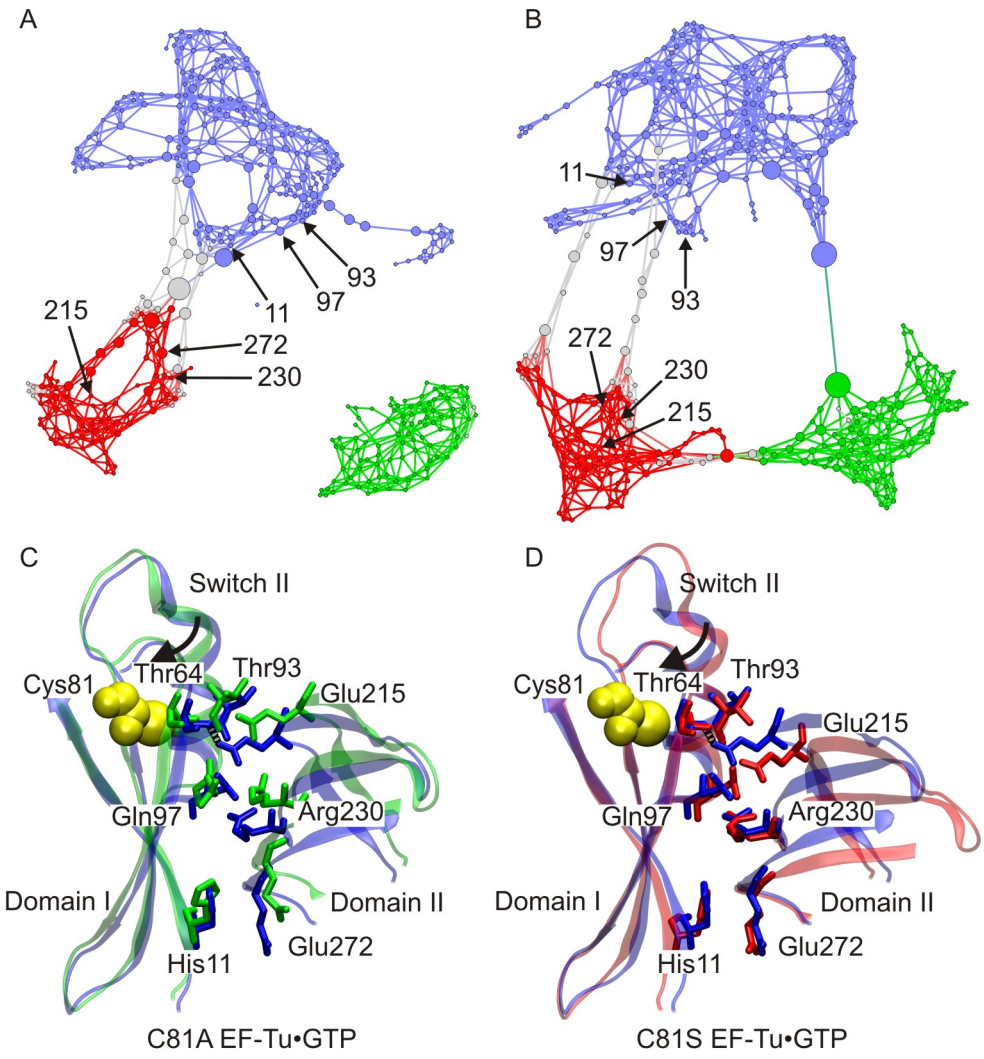

Figure 5.4. Substitution of $Cys81_{Tu}$ alters communication between domain II and domain I *in silico*. Communication networks for C81A (A) and C81S (B) EF-Tu are drawn as described in **Figure 5.3**. domain I is coloured blue, domain II coloured red and domain III coloured green. (C & D) Snapshots of EF-Tu after 20 ns of MD simulation are shown with protein in cartoon representation, $Cys81_{Tu}$ shown in yellow space-filling representation, and sidechains of selected amino acids are shown as sticks. The hydrogen bond between $Thr64_{Tu}$ and $Glu215_{Tu}$ in wild-type EF-Tu is indicated by a dashed black line. Wild-type EF-Tu (blue) is superimposed with C81A EF-Tu (green) in (C) or C81S EF-Tu (red) in (D). The ~10° rotation in the switch II helix is indicated by curved arrows in (C) and (D).

Breakdown of domain II/domain I communication in EF-Tu reduces GTP hydrolysis on the ribosome

If C81A or C81S substitution in EF-Tu disrupts communication between domain II and domain I as the *in silico* results suggest, the ability of these variants to have their GTPase activity stimulated by 70S ribosomes should be compromised. This hypothesis was tested *in vitro* by monitoring the 70S- and 50S- stimulated rates of GTP hydrolysis by EF-Tu_{C81A} and EF-Tu_{C81S} variants as shown in **Figure 5.5**, summarized in **Table 5.1**. The results demonstrate that in the presence of 70S ribosomes, the rates of EF-Tu_{C81A}•GTP or EF-Tu_{C81S}•GTP turnover (k_{cat}/min^{-1} = 0.53 ± 0.09 and 0.5 ± 0.1 respectively) are reduced four-fold relative to wild type. Thus, substitution of $Cys81_{Tu}$ with alanine or serine reduces the rate of GTP hydrolysis to that observed for EF-Tu_{wt} in the absence of 30S ribosomal subunits (the 50S-stimulated k_{cat} reported in **Table 5.1**). These results are consistent with the hypothesis that $Cys81_{Tu}$ plays a central role in communicating GTPase activating signals in EF-Tu. The rate of 50S-stimulated EF-Tu_{C81A}•GTP turnover (k_{cat} 0.6 ± 0.4 min^{-1}) is similar to that observed in the presence of 70S ribosomes (0.53 ± 0.09 min^{-1}), although the uncertainty in this number is quite large. The K_M for this process (K_M = 60 ± 40 μM), however, was significantly higher than with EF-Tu_{wt} (K_M = 7 ± 1 μM), suggesting a lower affinity of EF-Tu_{C81A}•GTP for the ribosome compared to the wild type complex. GTP hydrolysis by EF-Tu_{C81S} was detected in the presence of 50S ribosomal subunits, but the k_{cat} and K_M values obtained from the fit to data in **Figure 5B** were not significantly different from zero. This suggests a low affinity of EF-Tu_{C81A}•GTP for the ribosome and, consequently, a higher K_M value.

The larger apparent K_M values for EF-Tu_{C81A} and EF-Tu_{C81S} compared EF-Tu_{wt} could reflect increases in k_{cat}, or lower affinities of EF-Tu•GTP for 50S subunits. An increase in k_{cat} is unlikely as it would be inconsistent with the smaller k_{cat} values measured in the presence of 70S ribosomes (**Table 5.1**). Thus, EF-Tu_{C81A}•GTP and EF-Tu_{C81S}•GTP likely have lower affinities for 50S subunits compared to wild type. This is in contrast to the similar K_M values reported in the presence of 70S ribosomes that suggest similar affinities of EF-Tu_{wt}, EF-Tu_{C81A}, and EF-Tu_{C81S} for 70S. The lack of evidence to suggest that C81S or C81A substitutions affect the rate of 50S-stimulated GTP hydrolysis by EF-Tu implies that the four-fold smaller k_{cat} observed for EF-Tu_{C81A} and EF-Tu_{C81S} in the presence of 70S ribosomes is specific to the 30S ribosomal subunit. This is in line with the hypothesis that $Cys81_{Tu}$ is important for communication of GTPase activating signals from domain II to domain I in EF-Tu, consistent with the networks constructed using *in silico* data.

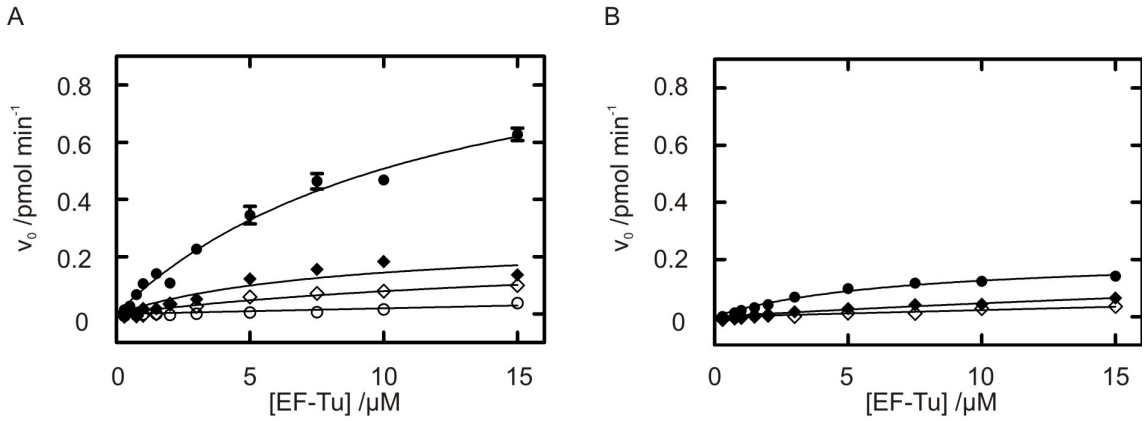

Figure 5.5. Substitution of $Cys81_{Tu}$ affects ribosome-stimulated GTP hydrolysis *in vitro*. (A) 70S ribosomes or (B) 50S ribosomal subunits (0.1 μM) were incubated with increasing concentrations of EF-Tu•GTP (0.3-15 μM) in the presence of EF-Ts (0.025 μM). Linear fits to the initial phase of GTP hydrolysis time courses (triplicate experiments) provided initial reaction velocities (v_0). The error bars are derived from the linear regression and lines represent fitted hyperbolic functions. Symbols represent EF-Tu variants (•) wild-type, (◦) H84A, (□) C81A, (□) C81S.

Intersubunit bridges in EF-Tu are directly linked to movements of switch I and switch II.

In order to understand how $Cys81_{Tu}$ substitution alters GTP hydrolysis in the presence of 70S ribosomes, MD simulations of EF-Tu_{wt}•GTP, EF-Tu_{C81A}•GTP, and EF-Tu_{C81S}•GTP complexes were compared. The plot of backbone Root Mean Squared Deviation (RMSD) over simulation time, shown in **Figure 5.6.A**, reveals that each simulation is stable after 10 ns. While the simulation of EF-Tu_{wt}•GTP appears to stabilize at a backbone RMSD of 1.8 Å, simulations of EF-Tu_{C81A}•GTP and EF-Tu_{C81S}•GTP stabilize at 2.3 Å. This indicates that during simulation, EF-Tu_{C81A} and EF-Tu_{C81S} models deviate more from their respective starting structures than EF-Tu_{wt}. To compare the overall structural dynamics of these different models, the Root Mean Squared Fluctuation (RMSF) of each Cα was calculated over the last half of each simulation. The resulting plot, shown in **Figure 5.6.B** indicates higher flexibility in the switch I (42_{Tu}-63_{Tu}), helix C (113_{Tu}-125_{Tu}), and helix D (143_{Tu}-159_{Tu}) regions of EF-Tu_{C81A} and EF-Tu_{C81S} compared to EF-Tu_{wt}. In addition, the switch II region of EF-Tu_{C81A}•GTP was notably more flexible than wild type or the C81S variant.

To understand the structural basis of the measured RMSD and RMSF differences, the MD simulations were visualized. Clear differences were observed in the switch I and switch II regions of EF-Tu_{C81S} and EF-Tu_{C81A} compared to EF-Tu_{wt}, as shown in **Figure 5.7**. During simulation of EF-Tu_{C81A}•GTP the switch I region becomes disordered, as shown in **Figure 5.7.A**. During the course of the simulation of this variant, a hydrogen bond breaks between the conserved amino acids $Glu215_{Tu}$ and $Thr64_{Tu}$. Since $Thr64_{Tu}$ is adjacent to the C-terminal end of switch I, breakage of the Glu215/Thr64 interaction, and subsequently the Glu215/Thr93 interdomain bridge, likely increases switch I motion.

Similarly, in the simulation of EF-Tu_{C81S}•GTP the helix A″ of Switch I is more mobile than in the wild type simulation (**Figure 5.6.B**) and repositions itself as shown in **Figure 5.7.B**. In this simulation, the Glu215/Thr64 hydrogen bond is also broken. In addition, the switch II region undergoes a conformational change in the simulation of EF-Tu_{C81S}•GTP (**Figure 5.6.B**). When the backbone hydrogen bond between $Tyr87_{Tu}$ and $Met91_{Tu}$ breaks in this simulation, the first half turn of helix B melts. This affect appears to originate from the ~10° rotation in helix B. Thus, the increased flexibilities of switch I and switch II identified in **Figure 5.6.B** appear to result from the same changes in helix B that cause breakage of the domain II/domain I intersubunit bridges.

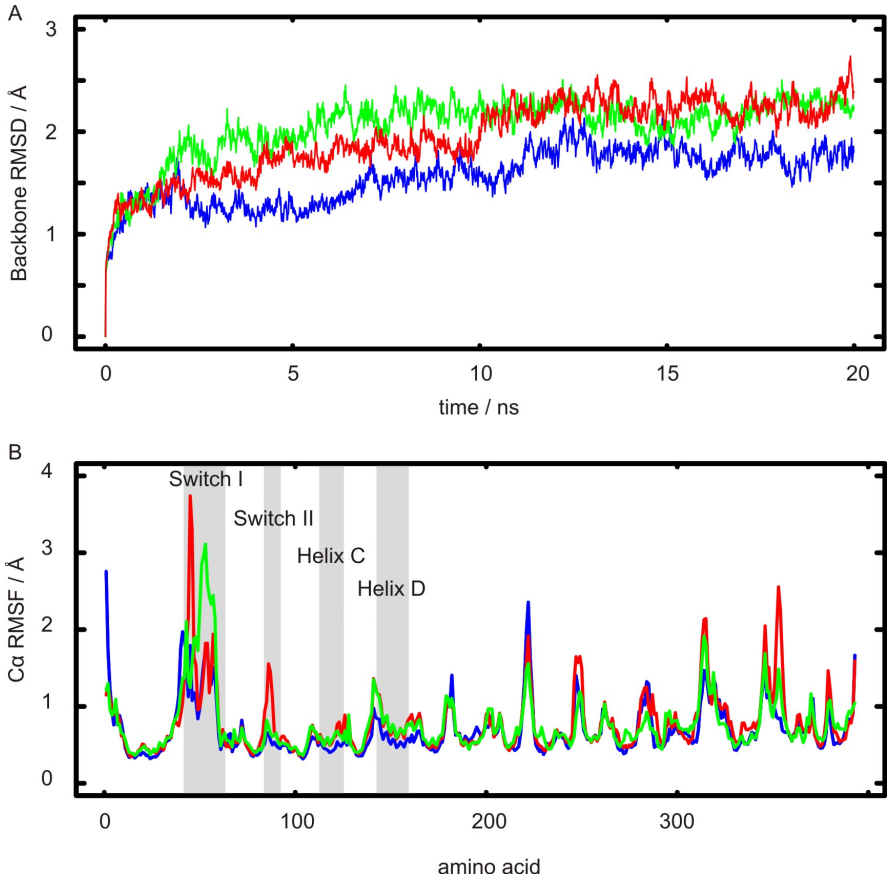

Figure 5.6. Specific regions of EF-Tu_{C81A} and EF-Tu_{C81S} are more flexible than EF-Tu_{wt} during 20 ns MD simulations. The backbone RMSD of each EF-Tu•GTP model is shown in panel A, wild type (blue), C81A (green), C81S (red). Panel B shows the RMSF values calculated for each Cα atom in the EF-Tu•GTP model over the last ten nanoseconds of each MD simulation (10-20ns). The lines are coloured as in A.

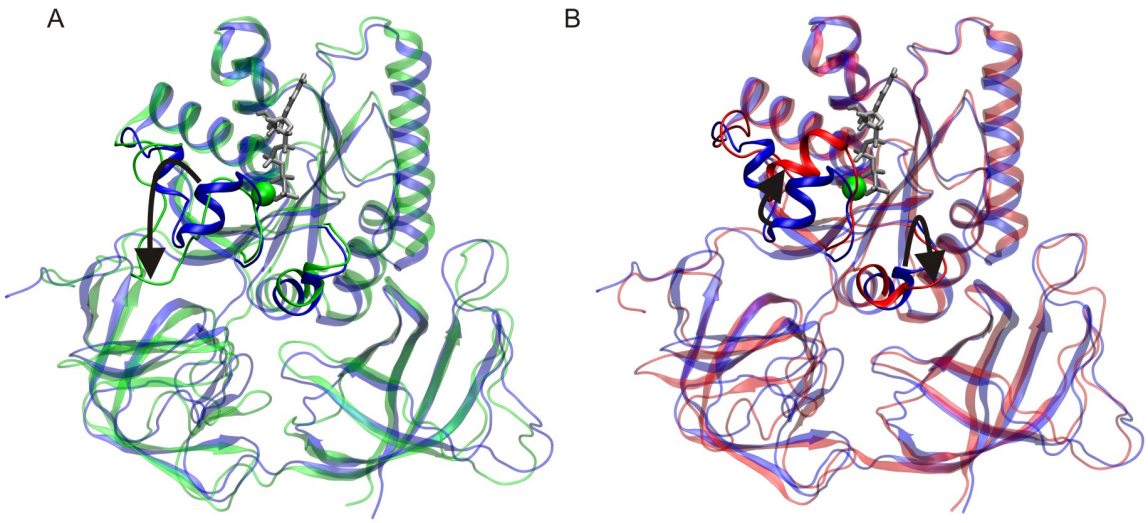

Figure 5.7. Conformational changes in switch I and switch II are correlated with domain II/domain II communication. Snapshots after 20 ns of MD simulation are shown in cartoon representation for wild type (blue), superimposed with C81A (green) in A or C81S (red) EF-Tu•GTP in B. The GTP molecule and Mg^{2+} ion in the wild type model are shown as grey sticks and green sphere, respectively. Conformational changes in the EF-Tu variants, relative to wild type, are indicated by curved arrows.

Increased mobility in the G-domain impairs interactions with the 50S ribosomal subunit.

The structural basis of higher RMSF values in helix C and helix D for EF-Tu_{C81A} and EF-Tu_{C81S} variants compared to wild type is not clearly evident from structural comparisons. In the X-ray crystal structure of EF-Tu•GDPNP, helix B is adjacent to helix C is adjacent to helix D (Kjeldgaard et al., 1993). Each of these helices is on the perimeter of the G-domain and packs around the central core of β-sheets. Thus, it seems likely that the structural changes in helix B upon C81S or C81A substitution discussed above leads to changes in the structural dynamics of helix C and, consequently, helix D. Interestingly, mutations in helix D of EF-Tu have been shown to reduce the rate of EF-Tu•GTP•aa-tRNA ternary complex binding to the ribosomal A-site by up to four-fold (Kothe et al., 2004). This effect is thought to result from compromised interactions between helix D of EF-Tu and ribosomal protein L7/12 in the large ribosomal subunit. Thus, the higher flexibility of helix D observed in EF-Tu_{C81A} and EF-Tu_{C81S} compared to

EF-Tu_{wt} could contribute to the higher K_M values reported for these variants in 50S-stimulated GTPase assays *in vitro* (**Figure 5.5.B**). In addition, the conserved sarcin/ricin loop (SRL) element of 23S rRNA of the large ribosomal subunit has been shown to contact both switch I and switch II of EF-Tu in X-ray crystal structures (Schmeing et al., 2009; Vorstenbosch et al., 1996). Weakening of these interactions due to increased structural dynamics of switch I may also contribute to higher K_M's in the 50S-stimulated GTPase reactions for EF-Tu_{C81A} and EF-Tu_{C81S} compared to wild type. This is consistent with the larger RMSF values and structural rearrangements observed in switch I of these EF-Tu variants compared to EF-Tu_{wt}. Interactions between the SRL and switch II may contribute to further weakening of interactions between EF-Tu_{C81A} and the 50S ribosomal subunit. The higher RMSF values and notable structural changes of switch II that are unique to EF-Tu_{C81A} *in silico* are consistent with a higher K_M compared to EF-Tu_{wt} and EF-Tu_{C81S} in 50S-stimulated GTPase reactions. Interestingly, the K_M values determined in the presence of 70S ribosomes were statistically indistinguishable for EF-Tu_{wt}, EF-Tu_{C81A}, and EF-Tu_{C81S}. This can be explained if EF-Tu•GTP binding to the 70S ribosome occurs via a different mechanism than 50S binding. Conversely, contacts between the 30S ribosomal subunit and EF-Tu could act to stabilize the conformations of switch I, switch II, and/or helix D and thus stabilize EF-Tu/50S interactions.

5.4 Conclusions

The results reported here support the hypothesis that a direct interaction between the 30S ribosomal subunit and domain II of EF-Tu promotes GTP hydrolysis. X-ray structures of EF-Tu bound to the ribosome reveal two specific hydrogen-bonding interactions between the 16S rRNA and domain II of EF-Tu, $U368_{16S}$/$Arg223_{Tu}$ and $U367_{16S}$/$Arg279_{Tu}$ (Schmeing et al., 2009). Our results demonstrate that disruption of either of these two interactions via R223A or R279A substitution reduces the ability of the 70S ribosome to stimulate EF-Tu•GTP turnover. While it appears that Arg283 is important for 70S-stimulated GTP hydrolysis, this amino acid interacts with aa-tRNA in the aforementioned crystal structure. It is possible that the Arg283/16S rRNA is a transient interaction when EF-Tu is bound to the ribosome, and/or that the absence of tRNA facilitates this additional interaction between domain II and 16S rRNA. Consistent with the hypothesis that these amino acids interact with the 16S rRNA, R223A, R279A, and R283A substitutions have no effect on the 50S-stimulated GTPase reactions. Previous work demonstrated that G222D substitution in EF-Tu abolishes GTPase activation of EF-Tu•GTP•aa-tRNA on mRNA-programmed ribosomes (Vorstenbosch et al., 1996). The G222D substitution was hypothesized to inhibit formation of specific interactions between rRNA and EF-Tu due to electrostatic repulsion. Interestingly, wild type-like activity can be restored to $EF\text{-}Tu_{G222D}$ *in vitro* in high Mg^{2+} conditions (10 mM) (Vorstenbosch et al., 1996). High Mg^{2+} concentrations may assist in shielding electrostatic repulsion between $EF\text{-}Tu_{G222D}$ and the 16S rRNA and lower the energy barrier for formation of GTPase-activating domain II/helix 5 contacts. Since arginines

223, 279, and 283 are all clustered around position 222, the low k_{cat} values presented here for EF-Tu_{R223A}, EF-Tu_{R279A}, and EF-Tu_{R283A} likely reflect inefficient GTPase activation.

A general role for helix 5/domain II interactions in GTPase activation of ribosome-associated G-proteins

The importance of helix 5 in 16S rRNA has been investigated by Kurt Fredrick's group using *in vivo* experiments (McClory et al., 2010). This study reveals that single nucleotide substitutions in helix 5 at positions A55, G357, or U367 each reduce β-galactosidase expression *in vivo* by 20-100 fold compared to wild-type ribosomes (McClory et al., 2010). Although this work suggests an important physiological role of helix 5, it relies on overall measures of gene expression and cannot discriminate between effects on one particular partial reaction during protein synthesis (EF-Tu and EF-G or initiation, elongation, or termination). However, the results presented here support a role for helix 5 in GTPase activation of EF-Tu in line with models proposed by Ramakrishnan (Schmeing et al., 2009) and Fredrick (McClory et al., 2010). Helix 5 of the 16S rRNA might play a more general role in GTPase activation since several G-proteins (EF-Tu, EF-G, RF3, IF-2, LepA, and TetM) each bind to the same location near the A-site of the ribosome. X-ray structures of EF-G or RF3 bound to ribosomes have revealed similar contacts between helix 5 and domain II which have been proposed to participate in GTPase activation of these G-proteins (Gao et al., 2009; Jin et al., 2011). In addition, cryo-EM reconstructions of IF-2, LepA, or TetM bound to ribosomes also suggest contacts between helix 5 and domain II (Allan et al., 2005; Connell et al., 2008; Dönhöfer et al., 2012).

Alignment of domain II in three-dimensional structures of each of the abovementioned G-proteins revealed basic amino acids in each protein that are on the correct surface to interact with helix 5 of the 16S rRNA. Alignment of 5-11 amino acid sequences for each G-protein indicated that at least one position in domain II of each protein has the potential to interact with helix 5 and is conserved as a basic amino acid between the respective aligned sequences (summarized in **Table A.4.2**). This comparison suggests that helix 5/domain II interactions may be a conserved feature of G-proteins that bind near the ribosomal A-site. In addition, the positions in three-dimensional structures of EF-G, RF3, LepA, IF-2, and TetM that correspond to the interdomain bridges identified in EF-Tu (this work) are summarized in **Table A.4.2**. Of the three potential interdomain bridges in EF-G, RF3, LepA or TetM, at least one is composed of amino acids whose chemical properties (hydrophobic, polar, acidic, or basic) are conserved in each alignment. This hints at the potential for conserved interdomain bridges to communicate GTPase activating signals from domain II to domain I in EF-Tu, EF-G, RF3, LepA, or TetM upon interaction with helix 5 of the 16S rRNA. While the potentially bridging amino acids in EF-G, RF3, LepA, and TetM are different than those in EF-Tu, it is interesting to note that each of these G-proteins has at least one invariant arginine at a bridging position. The potential interdomain bridges of IF-2, however, are poorly conserved. This may indicate that a different GTPase activating signal, or none at all, is passed to domain II of IF-2. Conversely, the nature of a signal communicated from domain II to domain I may be different in IF-2 compared to the other G-proteins considered above.

A pathway for GTPase activating signals from 16S rRNA to the G-domain of EF-Tu.

Based on the first X-ray structure of EF-Tu bound to the ribosome, a GTPase activating signal was proposed to travel from helix 5 of the 16S rRNA, to domain II of EF-Tu, through the acceptor stem of aa-tRNA, and into domain I (Schmeing et al., 2009). In this hypothesis, interactions between helix 5 and domain II were suggested to promote distortion of the acceptor stem of aa-tRNA that would break interactions between the acceptor stem and switch I of EF-Tu. Loss of aa-tRNA interactions with switch I was proposed to result in disordering of switch I which would open the hydrophobic gate and allow the catalytic $His84_{Tu}$ of switch II to align a water molecule for attack on the γ-phosphate of GTP. Since the experiments presented in the present work were performed in the absence of aa-tRNA, our results suggest that a GTPase activating signal can be transferred from domain II to domain I without passing through the acceptor stem of aa-tRNA. This finding is supported by similar rates of GTP hydrolysis by EF-Tu on the ribosome in the absence of aa-tRNA (this work), and in the presence of unlinked aa-tRNA acceptor stem and anticodon stem fragments (4 min^{-1}, (Piepenburg et al., 2000)). Together with the finding that R223A, R279A, or R283A substitutions in EF-Tu reduce the 70S-stimulated k_{cat} by 4-5 fold, it appears that a GTPase activating signal can be passed from the 16S rRNA to the GTPase machinery in domain I of EF-Tu in the absence of the aa-tRNA acceptor stem.

The communication network of EF-Tu•GTP presented in **Figure 5.3** highlights three highly conserved interdomain bridges in EF-Tu that are capable of communicating a signal from domain II to domain I even in the absence of aa-tRNA. It is interesting to note that the antibiotic pulvomycin binds at the interface among all domains disrupting

all of these interdomain bridges (Parmeggiani et al., 2006a). The presence of pulvomycin stimulates GTP hydrolysis in EF-Tu by ~10-fold, and no further stimulation was observed when ribosomes were present (Anborgh et al., 2004). These results suggest that pulvomycin binding to EF-Tu may essentially 'short circuit' this communication network. An EF-Tu_{R230C} variant was previously identified to result in pulvomycin resistance as it disrupts the binding site for this antibiotic and reduces pulvomycin-binding affinity. Consistent with the prediction that R230C substitution should also disrupt one of the domain II/domain I bridges, *E. coli* expressing this variant as the sole source of EF-Tu have ~20% longer doubling time (Zeef et al., 1994).

We hypothesize that off the ribosome, the interdomain bridges identified here prevent GTP hydrolysis on EF-Tu by limiting the mobility of switch I and switch II, acting analogously to the safety on a firearm. This is consistent with the low measured rates of GTP hydrolysis by EF-Tu in the absence of ribosomes, (Wolf et al., 1974) as well as the importance of the switch regions to GTP hydrolysis (Berchtold et al., 1993; Daviter et al., 2003; Villa et al., 2009; Vogeley et al., 2001). In the context of the hydrophobic gate hypothesis of Hilgenfield (*vide supra*), (Berchtold et al., 1993), changes in the structural dynamics and/or conformation of domain II in EF-Tu may be relayed across the interdomain bridges to drive rearrangement of the switch I and switch II regions. This proposal is consistent with the simulations of EF-Tu_{C81A}•GTP and EF-Tu_{C81S}•GTP, which show that disruption of the interdomain bridges in EF-Tu is concomitant with structural rearrangements in switch I and switch II. In fact, both of these simulations show increased motion of switch I that, in contrast to EF-Tu_{wt}, open the hydrophobic gate as shown in **Figure 5.6**. In addition, rearrangement of switch II in the simulation of

EF-Tu$_{C81S}$•GTP demonstrates that the interdomain bridges can also be linked to structural dynamics of switch II. During the simulations of EF-Tu•GTP reported here, His84$_{Tu}$ is not positioned to properly align a water molecule for attack of the γ-phosphate. Proper positioning of this catalytic amino acid is likely facilitated by direct interaction with the sarcin-ricin loop of 23S rRNA as observed by Voorhees *et al.* (2010).

Since the biochemical experiments presented in this work were carried out in the absence of a codon/anticodon signal, the GTPase activating communication network proposed here is independent of codon recognition. This is in contrast to Ramakrishnan's hypothesis that interactions between helix 5 of the 16S rRNA and domain II of EF-Tu are formed upon codon-dependent "30S subunit domain closure" (Schmeing et al., 2009). Codon-independence of the helix 5/domain II interactions is supported by evidence for these same contacts in cryo-EM structures of EF-Tu bound to near-cognate aa-tRNA on the ribosome (Agirrezabala et al., 2011). We propose that interactions between helix 5 of the 16S rRNA and domain II of EF-Tu act to 'arm' EF-Tu for GTPase activation in a codon-independent manner. As illustrated in the model presented in **Figure 5.8**, the 'arming signal' likely travels from domain II, through one or more of the interdomain bridges to increase the structural dynamics of switch I and switch II. This should lower the activation barrier for the SRL of the large ribosomal subunit to organize the catalytic machinery in domain I of EF-Tu for GTP hydrolysis. Codon-independent 'arming' of the GTPase machinery in EF-Tu may be either independent of or amplified by codon-dependent GTPase activation.

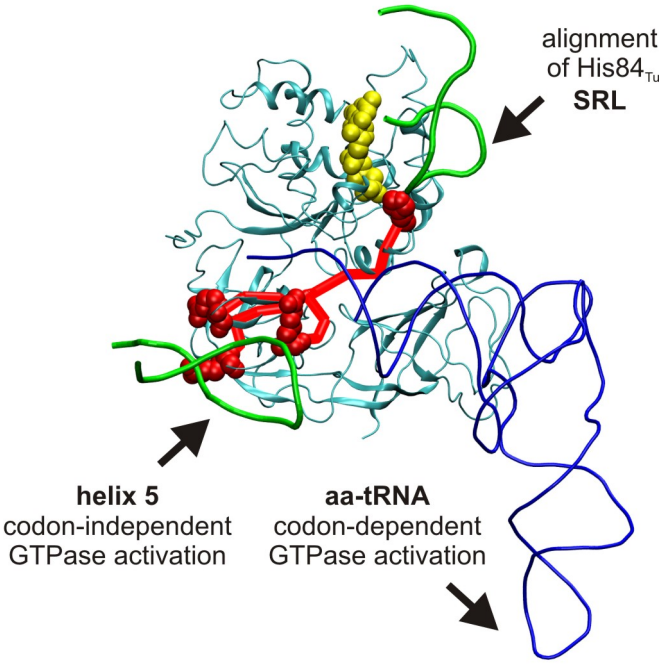

Figure 5.8. A model for GTPase activation of EF-Tu on the ribosome. The structure of *Thermus thermophilus* EF-Tu (cyan) bound to GDPCP (yellow) and Trp-tRNA^{Trp} (blue) on the 70S ribosome from *Thermus thermophilus* is shown based on the crystal structure 2XQD/2XQE (Voorhees et al., 2010). Potential communication pathways from Arg223$_{Tu}$, Arg279$_{Tu}$, and Arg283$_{Tu}$ in domain II to His84$_{Tu}$ in domain I are shown as red cylinders. The sources and target for these pathways are shown in space-filling representations. Helix 5 of the 16S rRNA, and the SRL of the 23S rRNA are shown at green tubes. The codon-independent helix 5/domain II interactions are proposed to 'arm' EF-Tu for GTPase activation. Codon-dependent GTPase activation signals are contributed by aa-tRNA, and the SRL assists in aligning His84$_{Tu}$ into a catalytically competent conformation.

Contribution of codon-dependent GTPase activation signals

The nature of the codon-dependent GTPase activation signal that travels over 70 Å from the decoding centre on the small ribosomal subunit to domain I of EF-Tu is poorly understood. Several studies suggest an important role for the aa-tRNA body in transmitting this codon-dependent signal. When aa-tRNA is supplied in two disconnected halves (*i.e.* an anticodon stem-loop half and an acceptor stem half), the GTPase activity of EF-Tu is extremely low (4 min^{-1}), (Piepenburg et al., 2000). While this rate is in line with the codon-independent GTP hydrolysis observed in this work (k_{cat} = 2 min^{-1}), it is 1,000-10,000-fold slower than the rate of GTPase activation and hydrolysis observed in the presence of intact cognate aa-tRNA (Pape et al., 1998). A role of aa-tRNA dynamics

in transmission of the codon-dependent signal is also supported by fluorescence changes observed in aa-tRNAs bearing a fluorescent label in the D-loop during codon-recognition on the ribosome (Rodnina et al., 1994). These fluorescent studies suggest partial unfolding of the D-loop during the codon-recognition process (Rodnina et al., 1994). X-ray structures of EF-Tu bound to aa-tRNA on the ribosome indeed show distortion of the tRNA elbow relative to its conformation in free EF-Tu•GDPNP•aa-tRNA ternary complex, as shown in **Figure 5.9** (Schmeing et al., 2009; Schmeing et al., 2011). This distortion suggests that upon codon recognition the anticodon stem of aa-tRNA might act as a lever to exert torque on the acceptor stem. As shown in **Figure 5.9**, if the tRNA behaves as a rigid body this torque would tend to 'squeeze' arginines 223, 279, and 283 between helix 5 of the 16S rRNA and the CCA end of aa-tRNA. In this context aa-tRNA may act to increase the helix 5/domain II GTPase activating signal. Conversely codon-dependent lever motion of the aa-tRNA anticodon stem may stimulate a distinct GTPase signal, perhaps through domain III of EF-Tu which appears to rotate along with the acceptor stem. These structural hypotheses are limited by the lack of knowledge surrounding aa-tRNA flexibility. Flexibility within the tRNA molecule will tend to limit the torque that can be applied to EF-Tu but may play a significant role in providing the correct codon-dependent signal.

One outstanding question is what role does the 16S rRNA/domain II interaction play in protein synthesis? These interactions were observed in X-ray structures of EF-Tu on the ribosome in the presence of cognate aa-tRNA in the A-site (Schmeing et al., 2009; Voorhees et al., 2010) as well as a cryo-EM reconstruction of near-cognate aa-tRNA in the A-site (Agirrezabala et al., 2011). Together with our findings, these results suggest

that the 16S rRNA/domain II interaction should promote GTP hydrolysis by EF-Tu regardless of the signal originating from the ribosomal decoding centre. In the context of our 'safety switch' hypothesis, direct interaction of the 30S ribosomal subunit with domain II of EF-Tu may be a codon-independent prerequisite for GTP hydrolysis by EF-Tu. We therefore hypothesize that the 16S rRNA/domain II interaction contributes significantly to GTP hydrolysis by EF-Tu during elongation, but not to aa-tRNA selection, which occurs after codon recognition. Addressing this hypothesis directly requires that R223A, R279A, and R283A EF-Tu variants be tested for GTPase activity in the presence of tRNAs and mRNA, work which is currently underway.

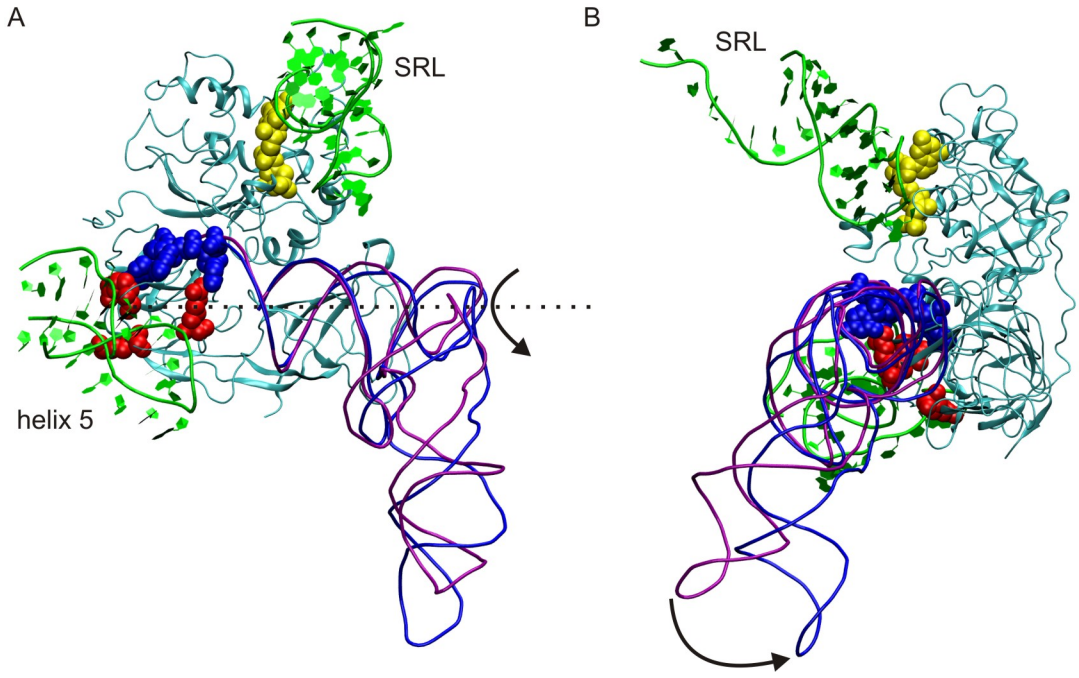

Figure 5.9. Conformational changes in the anticodon stem of aa-tRNA might cause torque on its acceptor stem. The structure of EF-Tu (cyan) bound to GDPCP (yellow) and aa-tRNA (blue) on the ribosome is shown (PDBID: 2XQD). The conformation of aa-tRNA in the EF-Tu•GDPNP•aa-tRNA (PDBID: 1TTT) is shown in purple, aligned by backbone atoms of the acceptor stem. A) is a 'front on view' while B) is a 'side view', rotated 90° relative to A. The change in aa-tRNA conformation upon ribosome binding is indicated by the arrow in B. The apparent torque on the acceptor stem of aa-tRNA is indicated by the arrow in A about the approximate axis of the acceptor stem (dashed line). Such torque would have the potential to cause the CCA-end of aa-tRNA (blue spheres) for force Arg223, Arg279, and Arg283 (red spheres) into helix 5 of the 16S rRNA.

Chapter 6

Conclusions

6.1. Structural dynamics of G-proteins

Proteins are inherently flexible and their evolution is constrained by the requirement to be flexible enough to perform a specific function while still being able to fold stably under cellular conditions. Members of the GTPase superfamily, to which EF-Tu belongs, contain a G-domain based on a Rossmann fold topology (Bourne et al., 1991). Not surprisingly, the functional elements of G-proteins are found in the loops that connect secondary structure elements composing the core of this domain (Bourne et al., 1991). Each of these functional elements (the G-motifs) contributes to switching between GTP/GDP-bound states and/or to binding guanine nucleotides. Crystal structures of EF-Tu and other G-proteins demonstrate that the P-loop, switch I, and switch II regions each undergo notable conformational changes depending on which factor, (GEF, GTP, or GDP), is bound (Boriack-Sjodin et al., 1998; Bourne et al., 1991; Chhatriwala et al., 2007; Kawashima et al., 1996; Kjeldgaard et al., 1993; Kjeldgaard et al., 1996; Song et al., 1999; Wittinghofer and Vetter, 2011). Hydrolysis of GTP and subsequent P_i release results in loss of interactions between the γ-phosphate and conserved threonine/glycine amino acids in the switch I/switch II elements. This presumably triggers the structural rearrangements in switch I and switch II that accompany the GTP to GDP conformational change (Bourne et al., 1991; Wittinghofer and Vetter, 2011). Conformational changes in the P-loop, however, are likely triggered by the absence of nucleotide and/or GEF binding (Ævarsson et al., 1994; Boriack-Sjodin et al., 1998; Chhatriwala et al., 2007; Kawashima et al., 1996). Furthermore, NMR experiments have revealed that in the GDPNP-bound form, the switch I, switch II, and P-loop regions of the small G-proteins RalB and Ras are more flexible than other elements of the G-domain (Araki et al., 2011;

Fenwick et al., 2009). Based on the conformational changes and flexibility of the switch I, switch II, and P-loop elements, the structural dynamics of these regions are likely to be essential for their functions.

Structural dynamics in the P-loop, switch I, and switch II regions may be conserved features of G-proteins in general. It is not clear, however, if structural dynamics would be conserved within the sequences of the P-loop, switch I, and switch II regions as the amino acid sequences diverge significantly between different GTPases. In GTPases, the P-loop contains the conserved, GxxxxGKS/T sequence, switch I (usually) contains a conserved threonine residue, and switch II (usually) contains a conserved glycine (Bourne et al., 1991; Wittinghofer and Vetter, 2011). These sparse, conserved positions may be all that is required for conserved structural dynamics of their subsuming elements. Conversely, the structural dynamics of these elements may be conserved in contacting positions and/or the overall fold. The results in the present work support the hypothesis that specific elements in EF-Tu, EF-Ts, and the ribosome have evolved to fine-tune structural dynamics of the P-loop, switch I, and switch II regions as a means of regulating EF-Tu's function.

6.2. Structural dynamics of the P-loop

The results presented in this work suggest that structural dynamics in the P-loop of EF-Tu are important for nucleotide-binding properties and EF-Ts-stimulated nucleotide dissociation. In **Chapter 2**, removal of the transient Asp109•••His22 hydrogen bond between the P-loop and the adjacent loop, by substitution of $Asp109_{Tu}$ with alanine, was shown to reduce the efficiency of EF-Ts-stimulated GDP dissociation from EF-Tu.

Interestingly, no direct link between this hydrogen bond and the structural dynamics of the P-loop was evident in simulations of EF-Tu•GTP. This hydrogen bond is proposed to stabilize the EF-Tu•EF-Ts complex which has a 'flipped' P-loop conformation in the corresponding X-ray structure. Thus, the $Asp109_{Tu}$•••$His22_{Tu}$ hydrogen bond may contribute to the structural dynamics of the P-loop by stabilizing the 'flipped' P-loop conformation. Communication between EF-Ts and the P-loop of EF-Tu via the $Asp109_{Tu}$•••$His22_{Tu}$ hydrogen bond has been mapped in grey in **Figure 6.1**. The *in vitro* and *in silico* results presented in **Chapter 3** suggest that a conserved P-loop anchor mediates P-loop entropy and nucleotide-binding properties in EF-Tu. P-loop anchors appear to be conserved in other P-loop NTPases (**Appendix A.2.2**), although the interacting amino acids differ between proteins. Thus, different NTPases may have evolved different P-loop anchors in order to fine-tune the structural dynamics of the P-loop and, ultimately, nucleotide binding properties. For example, binding of the GEFs EF-Ts and RCC1 to their respective G-proteins, EF-Tu and Ran, breaks the sidechain/backbone interactions of the P-loop anchors as revealed by the respective X-ray structures (Kawashima et al., 1996; Renault et al., 2001). Thus, some GEFs seem to have evolved to act on the P-loop anchor to modulate P-loop structural dynamics and facilitate nucleotide dissociation. Communication between EF-Ts and the P-loop anchors in EF-Tu are mapped on the structure of EF-Tu•GTP in black in **Figure 6.1**.

6.3. Structural dynamics of switch I and switch II

The structural dynamics of the switch I and switch II regions were found to be influenced by the orientation of helix B in the MD simulations presented in **Chapter 5**.

The influence of helix B on switch I and switch II is likely regulated by interactions between domain II and the ribosome during GTPase activation of EF-Tu. Communication pathways from the conserved arginines in domain II to helix B and switch I are mapped on EF-Tu•GTP in purple in **Figure 6.1**. Interestingly, communication between helix B and domain II may be a 'two way street' since reorientation of helix B during the GTP to GDP transition is concomitant with a significant reorientation of domain II (Berchtold et al., 1993; Song et al., 1999). Regulation of switch I and switch II dynamics by helix B is likely common to other G-proteins based on structural considerations; switch I and switch II interact in the 'on' state of G-proteins and switch II makes up the N-terminal portion of helix B (Kjeldgaard et al., 1996). However, regulation of switch I and switch II structural dynamics by domain II is unlikely to be a common feature of small GTPases which are each composed of a single domain. It would be interesting to investigate the functional relationship between domain II of EF-Tu and GTPase Activating Proteins (GAPs), which associate with small G-proteins.

Results presented in **Chapter 4** reveal that EF-Ts is able to regulate the structural dynamics of switch II in EF-Tu. Structural dynamics of the switch II region in EF-Tu appear to be important for efficient GTP binding to the EF-Tu•EF-Ts complex and nucleotide dissociation from EF-Tu•nucleotide•EF-Ts ternary complexes. Alterations in the structural dynamics of switch II upon nucleotide binding may also facilitate EF-Ts dissociation as part of the functional cycle of EF-Tu. Communication between switch II and EF-Ts is drawn in yellow on a model of EF-Tu•GTP in **Figure 6.1**. Conformational changes in switch II appear to be a common mechanism of GEF-induced nucleotide dissociation in G-proteins (Bos et al., 2007; Margarit et al., 2003; Renault et al., 2001).

However, it is unclear if nucleotide-dependent modulation of switch II structural dynamics in G-protein•GEF complexes is common to G-proteins in general. X-ray structures of eEF1A (Andersen et al., 2001) and Arf1 (Mossessova et al., 2003) bound to their respective GEFs *and* guanine nucleotides demonstrate that the switch II element does not directly interact with the bound nucleotide. These structures seem to suggest that switch II does not directly respond to the presence of nucleotides in these G-protein•nucleotide•GEF ternary complexes. Investigation of the structural dynamics of other G-proteins is required to assess if switch II structural dynamics is a general design feature of G-proteins that facilitates GEF-induced nucleotide exchange.

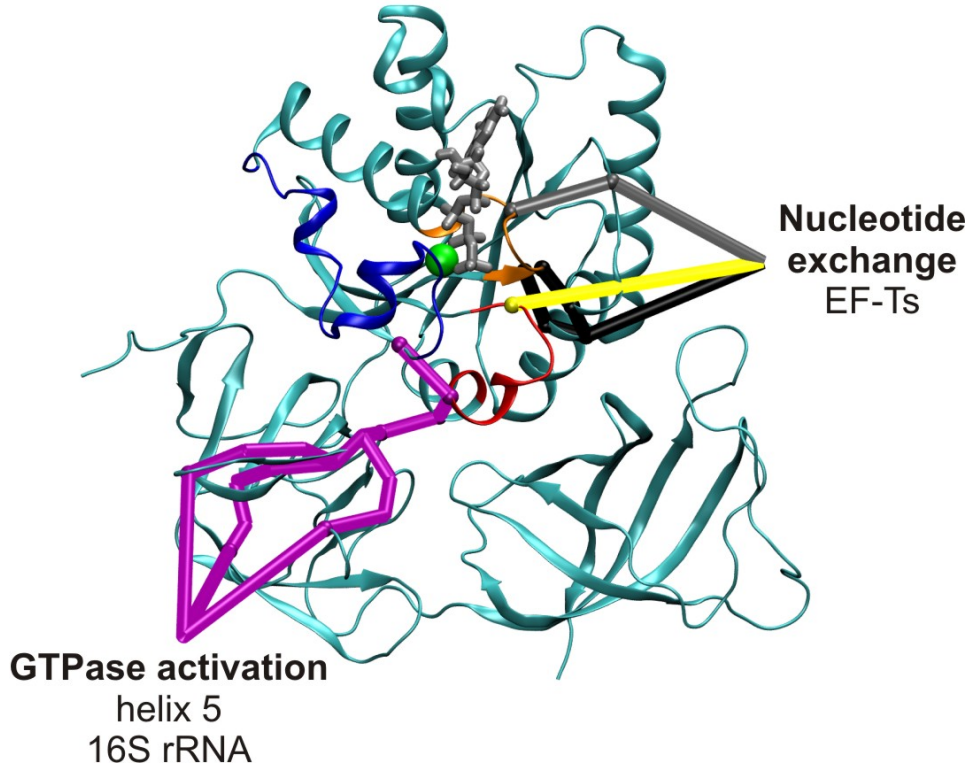

Figure 6.1. Regulating the structural dynamics of the P-loop, switch I, and switch II elements of EF-Tu. A model of EF-Tu•GTP is shown after 20 ns of MD simulation with EF-Tu in cyan, GTP in silver and Mg^{2+} in green. The P-loop is coloured orange, switch I blue, and switch II red. Possible communication pathways from helix 5 of the 16S rRNA to switch I and switch II (purple) or from EF-Ts to the P-loop (grey and black) or switch II (yellow) were determined from communication networks of EF-Tu•GTP or EF-Tu•EF-Ts.

6.4. A structural dynamics 'roadmap' of Elongation Factor Tu

Figure 6.1 is a first approach to mapping multiple communication pathways on EF-Tu based on the experiments and simulations presented in this work. This 'roadmap' is likely incomplete and does not account for additional contributions to EF-Ts-catalyzed nucleotide exchange (by C-terminal extension of EF-Ts for example) or GTPase activation on the ribosome (by aa-tRNA for example). Shortcomings aside, two trends are clearly evident in **Figure 6.1**. Firstly, the communication pathways appear to converge in the centre of EF-Tu. It is possible that EF-Tu acts as a funnel to direct signals into the centre of the protein where the P-loop, switch I, and switch II elements are located. This work provides specific examples of how the signals highlighted in **Figure 6.1** modulate the structural dynamics of these conserved motifs by altering flexibility and/or mobility. The second trend in **Figure 6.1** is that the pathways investigated are non-overlapping; i.e. GTPase activating signals take distinct pathways relative to nucleotide exchange signals. In order to clearly establish this trend the contributions of individual amino acids within a communication pathway need to be experimentally verified. Development of experimental approaches to study communication networks will allow a large variety of different proteins to be studied. This should ultimately lead to a better understanding of the relationships between communication networks, protein structure, structural dynamics, and protein evolution.

6.5. The role of methionine 112 in Elongation Factor Tu

Several EF-Tu variants bearing single amino acid substitutions at position 112 were studied in this work. Position 112 was chosen for investigation since it is conserved as

methionine in 124 of 125 bacterial EF-Tu sequences (DeLaurentiis et al., 2011), but not in the eukaryotic homologue eEF1A (**Figure A.2.1**). The loop bearing $Met112_{Tu}$ is replaced by an α helix in eEF1A (Andersen et al., 2001), suggesting that $Met112_{Tu}$ may contribute to properties specific to the bacterial enzyme. Analysis of the nucleotide-binding properties of eEF1A from yeast revealed micromolar affinities for GDP and GTP ($K_{D,GDP}$ = 0.4 μM; $K_{D,GTP}$ = 1 μM) (Gromadski et al., 2007). In comparison, EF-Tu from *E. coli* has higher (nanomolar) affinities for guanine nucleotides with 60-fold preference for GDP binding over GTP ($K_{D,GDP}$ = 1 nM; $K_{D,GTP}$ = 60nM) (Gromadski et al., 2002). Substitution of $Met112_{Tu}$ with glycine showed little effect on the guanine nucleotide-binding properties of EF-Tu, while substitution with alanine and leucine reduced the GDP- *and* GTP-binding affinities by five to ten fold. Thus, $Met112_{Tu}$ does not appear to be solely responsible for higher nucleotide binding affinities of EF-Tu compared to eEF1A or the preference for GDP binding in the bacterial system.

Each substitution of $Met112_{Tu}$ tested in this work had a significant effect on EF-Ts-stimulated nucleotide dissociation from EF-Tu. Both M112G and M112A substitutions slowed EF-Ts-stimulated nucleotide dissociation five to ten fold. It appears that position 112 is a keystone for EF-Tu/EF-Ts binding. When this keystone is substituted with a smaller amino acid, EF-Ts does not sit 'properly' on EF-Tu, and the nucleotide exchange efficiency is reduced. While EF-Tu and eEF1A are homologues, their respective GEFs, EF-Ts and eEF1Bα, are not (Maessen et al., 1986). In fact, the exchange factors EF-Ts and eEF1Bα bind to different surfaces of EF-Tu and eEF1A, respectively (Andersen et al., 2001; Kawashima et al., 1996). Although $Met112_{Tu}$ is located at the Tu/Ts interface in the EF-Tu•EF-Ts complex, its corresponding location in eEF1A is not on the

eEF1A/eEF1Bα interaction interface. Thus, divergence in the primary and secondary structures of EF-Tu and eEF1A in the region surrounding $Met112_{Tu}$ likely results from a significant change in evolutionary pressures associated with binding the respective GEF.

7. References

Ævarsson, A., Brazhnikov, E., Garber, M., Zheltonosova, J., Chirgadze, Y., Al-Karadaghi, S., Svensson, L.A., and Liljas, A. (1994). Three-dimensional structure of the ribosomal translocase: elongation factor G from *Thermus thermophilus*. The EMBO Journal *13*, 3669-3677.

Agirrezabala, X., Schreiner, E., Trabuco, L.G., Lei, J., Ortiz-Meoz, R.F., Schulten, K., Green, R., and Frank, J. (2011). Structural insights into cognate versus near-cognate discrimination during decoding. The EMBO Journal *30*, 1497-1507.

Aleksandrov, A., and Simonson, T. (2008). Binding of tetracyclines to Elongation Factor Tu, the Tet represssor, and the ribosome: a molecular dynamics simulation study. Biochemistry *47*, 13594-13603.

Allan, G.S., Zavialov, A., Gurskey, R., Ehrenberg, M., and Frank, J. (2005). The cryo-EM structure of a translation initiation complex from *Escherichia coli*. Cell *121*, 703-712.

Alto, N.M. (2008). Mimicking small G-proteins: an emerging theme from the bacterial virulence arsenal. Cellular Microbiology *10*, 566-575.

Anborgh, P.H., Okamura, S., and Parmeggiani, A. (2004). Effects of the antibiotic pulvomycin on the elongation factor Tu-dependent reactions. Comparison with other antibiotics. Biochemistry *43*, 15550-15556.

Anborgh, P.H., and Parmeggiani, A. (1991). New antibiotic that acts specifically on the GTP-bound form of elongation factor Tu. The EMBO Journal *10*, 779-784.

Andersen, C.A., and Rost, B. (2009). Secondary structure assignment. In Structural Bioinformatics, J. Gu, and P.E. Bourne, eds. (Hoboken N.J., John Wiley & Sons), pp. 419-484.

Andersen, G.R., Valente, L., Pedersen, L., Kinzy, T.G., and Nyborg, J. (2001). Crystal structures of nucleotide exchange intermediates in the eEF1A-eEF1Bα complex. Nature Structural Biology *8*, 531-534.

Anderson, J.S., Bretscher, M.S., Clark, B.F.C., and Marcker, K.A. (1967). A GTP requirement for binding initiator tRNA to ribosomes. Nature *215*, 490-492.

Araki, M., Shima, F., Yoshikawa, Y., Muraoka, S., Ijiri, Y., Nagahara, Y., Shirono, T., Kataoka, T., and Tamura, A. (2011). Solution structure of the state 1 conformer of GTP-bound H-Ras protein and distinct dynamic properties between the state 1 and state 2 conformers. Journal of Biological Chemistry *286*, 39644-39653.

Baba, T., Ara, T., Hasegawa, M., Takai, Y., Okumura, Y., Baba, M., Datsenko, K.A., Tomita, M., Wanner, B.L., and Mori, H. (2006). Construction of *Escherichia coli* K-12 in-frame, single-gene knockout mutants: the Keio collection. Molecular Systems Biology.

Bastian, M., Heymann, S., and Jacomy, M. (2009). Gephi: an open source software for exploring and manipulating networks. Paper presented at: International AAAI Conference on Weblogs and Social Media.

Becker, M., Gzyl, K.E., Altamirano, A.M., Vuong, A., Urbahn, K., and Wieden, H.-J. (2012). The 70S ribosome modulates the ATPase activity of *Escherichia coli* YchF. RNA Biology *9*, 1288-1301.

Benkovic, S.J., and Hammes-Schiffer, S. (2003). A perspective on enzyme catalysis. Science *301*, 1196-1202.

Berchtold, H., Reshetnikova, L., Reiser, C.O.A., Schirmer, N.K., Sprinzi, M., and Hilgenfeld, R. (1993). Crystal structure of active elongation factor Tu reveals major domain rearrangements. Nature *365*, 126-132.

Berger, L., Slein, M.W., Colowick, S.P., and Cori, C.F. (1945). Isolation of pure hexokinase from yeast. Journal of General Physiology *29*, 141-142.

Block, W., and Pingoud, A. (1981). The identification and analysis of nucleotides bound to the elongation factor Tu from *Escherichia coli*. Analytical Biochemistry *114*, 112-117.

Bochner, B.R., and Ames, B.N. (1982). Complete analysis of cellular nucleotides by two-dimensional thin layer chromatography. The Journal of Biological Chemistry *257*, 9759-9769.

Boehr, D.D. (2009). During transitions proteins make fleeting bonds. Cell *139*, 1049-1051.

Boehr, D.D., McElheny, D., Dyson, H.J., and Wright, P.E. (2006). The dynamic energy landscape of dihydrofolate reductase catalysis. Science *313*, 1638-1642.

Boehr, D.D., Nussinov, R., and Wright, P.E. (2009). The role of dynamic conformational ensembles in biomolecular recognition. Nature Chemical Biology *5*, 789-796.

Boriack-Sjodin, P.A., Margarit, S.M., Bar-Sagi, D., and Kuriyan, J. (1998). The structural basis of the activation of Ras by Sos. Nature *394*, 337-343.

Bos, J.L., Rehmann, H., and Wittinghofer, A. (2007). GEFs and GAPs: critical elements in the control of small G proteins. Cell *129*, 865-877.

Bourne, H.R., Sanders, D.A., and McCormick, F. (1991). The GTPase superfamily: conserved structure and molecular mechanism. Nature *309*, 117-127.

Brase, C.H., and Brase, C.P. (2003a). Chi-Square and F Distributions. In Understandable Statistics, L. Schultz, ed. (Boston, Jack Shira), pp. 635-715.

Brase, C.H., and Brase, C.P. (2003b). Normal Distributions. In Understandable Statistics, L. Schultz, ed. (Boston, Jack Shira), pp. 270-331.

Cabrer, B., San-Millan, M.J., Vazquez, D., and Modolell, J. (1976). Stoichiometry of polypeptide chain elongation. The Journal of Biological Chemistry *251*, 1718-1722.

Carroll, M.J., Mauldin, R.V., Gromova, A.V., Singleton, S.F., Collins, E.J., and Lee, A.L. (2012). Evidence for dynamics in proteins as a mechanism for ligand dissociation. Nature Chemical Biology *8*, 246-252.

Changeux, J.-P. (2011). 50th anniversary of the word "allosteric". Protein Science *20*, 1119-1124.

Chhatriwala, M.K., Betts, L., Worthylake, D.K., and Sondek, J. (2007). The DH and PH domains of Trio coordinately engage Rho GTPases for their efficient activation. Journal of Molecular Biology *368*.

Ciferri, O., and Tiboni, O. (1973). Elongation factors for chloroplast and mitochondrial protein synthesis in *Chlorella vulgaris*. Nature *245*, 209-211.

Cohn, S.A., Ingold, A.L., and Scholey, J.M. (1987). Correlation between the ATPase and microtubule translocating activities of sea urchin egg kinesin. Nature *328*, 160-163.

Connell, S.R., Topf, M., Qin, Y., Wilson, D.N., Mielke, T., Fucini, P., Nierhaus, K.H., and Spahn, C.M.T. (2008). A new tRNA intermediate revealed on the ribosome during EF4-mediated back-translocation. Nature Structural and Molecular Biology *15*, 910-915.

Cooper, E.L., Carćia-Lara, J., and Foster, S.J. (2009). YsxC, an essential protein in *Staphylococcus aureus* crucial for ribosome assembly/stability. BMC Microbiology *9*, 266.

Cornish, P.V., Ermolenko, D.E., Staple, D.W., Hoang, L., Hickerson, R.P., Noller, H.F., and Ha, T. (2009). Following movements of the L1 stalk between three functional states in single ribosomes. Proceedings of the National Academy of Sciences of the United States of America *106*, 2571-2576.

Csardi, G. (2009). Routines for simple graphs, network analysis. In igraph, pp. Routines for simple graphs and network analysis. igraph can handle large graphs very well and provides functions for generating random and regular graphs, graph visualization, centrality indices and much more.

Dahl, L.D., Wieden, H.-J., Rodnina, M.V., and Knudsen, C.R. (2006). The importance of P-loop and domain movements in EF-Tu for guanine nucleotide exchange. The Journal of Biological Chemistry *281*, 21139-21146.

Daviter, T., Wieden, H.-J., and Rodnina, M.V. (2003). Essential role of histidine 84 in elongation factor Tu for the chemical step of GTP hydrolysis on the ribosome. Journal of Molecular Biology *332*, 689-699.

DeLaurentiis, E.I., Mo, F., and Wieden, H.-J. (2011). Construction of a fully active Cys-less elongation factor Tu: Functional role of conserved cysteine 81. Biochimica et Biophysica Acta *1814*, 684-692.

Dell, V.A., Miller, D.L., and Johnson, A.E. (1990). Effects of nucleotide- and aurodox-induced changes in Elongation Factor Tu conformation upon its interactions with aminoacyl transfer RNA. A fluorescence study. Biochemistry *29*, 1757-1763.

Dhulesia, A., Gspooner, J., and Vendruscolo, M. (2008). Mapping of two networks of residues that exhibit structural and dynamical changes upon binding in a PDZ domain protein. Journal of the American Chemical Society *130*, 8931-8939.

Dönhöfer, A., Franchenberg, S., Wickles, S., Berninghausen, O., Beckmann, R., and Wilson, D.N. (2012). Structural basis for TetM-mediated tetracycline resistance. Proceedings of the National Academy of Sciences of the United States of America *109*, 16900-16905.

Drawz, S.M., Bethel, C.R., Hujer, K.M., Hurless, K.N., Distler, A.M., Caselli, E., Prati, F., and Bonomo, R.A. (2009). The role of a second-shell residue in modifying substrate and inhibitor interactions in the SHV β-lactamase: a study of ambler position Asn276. Biochemistry *48*, 4557-4566.

Dror, R.O., Pan, A.C., Arlow, D.H., Borhani, D.W., Maragakis, P., Shan, Y., Xu, H., and Shaw, D.E. (2011). Pathway and mechanism of drug binding to G-protein-coupled receptors. Proceedings of the National Academy of Sciences of the United States of America *108*, 13118-13123.

Duan, Y., Wu, C., Chowdhury, S., Lee, M.C., Xiong, G., Zhang, W., Yang, R., Cieplak, P., Luo, R., Lee, T.*, et al.* (2003). A point-chage force field for molecular mechanics simulations of proteins based on condensed-phase quantum mechanical calculations. Journal of Computational Chemistry *24*, 1999-2012.

Eargle, J., Black, A.A., Sethi, A., Trabuco, L.G., and Luthey-Schulten, Z. (2008). Dynamics of recognition between tRNA and elongation factor Tu. Journal of Molecular Biology *377*, 1382-2405.

Eisenmesser, E.Z., Millet, O., Labeikovsky, W., Korzhnev, D.M., Wolf-Watz, M., Bosco, D.A., Skalicky, J.J., Kay, L.E., and Kern, K. (2005). Intrinsic dynamics of an enzyme underlies catalysis. Nature *438*, 117-121.

Fenwick, R.B., Prasannan, S., Campbell, L.J., Nietlispach, D., Evetts, K.A., Camonis, J., Mott, H.R., and Owen, D. (2009). Solution structure and dynamics of the small GTPase RalB in its active conformation: significance for effector protein binding. Biochemistry *48*, 2192-2206.

Fersht, A. (1999). Structure and mechanism in protein science (New York, W. H. Freeman and Company).

Feuerstein, J., Goody, R.S., and Webb, M.R. (1989). The mechanism of guanosine nucleotide hydrolysis by p21 c-Ha-ras. The Journal of Biological Chemistry *264*, 6188-6190.

Fischer, J.J., Coatham, M.L., Bear, S.E., Brandon, H.E., Laurentiis, E.I.D., Shields, M.J., and Wieden, H.-J. (2012). The ribosome modulates the structural dynamics of the conserved GTPase HflX and triggers tight nucleotide binding. Biochimie *94*, 1647-1659.

Foloppe, N., and Mackerell, A.D. (2000). All-atom emperical force field for nucleic acids: I. Parameter optimization based on small molecule and condensed phase macromolecular target data. Journal of Computational Chemistry *21*, 86-104.

Forchhammer, J., and Lindahl, L. (1971). Growth rate of polypeptide chains as a function of the cell growth rate in a mutant of *Escherichia coli* 15. Journal of Molecular Biology *55*, 563-568.

Fraser, J.S., Bedem, H.v.d., Samelson, A.J., Lang, P.T., Holton, J.M., Echols, N., and Alber, T. (2011). Accessing protein conformational ensembles using room-temperature X-ray crystallography. Proceedings of the National Academy of Sciences of the United States of America *108*, 16247-16252.

Freddolino, P.L., Liu, F., Gruebele, M., and Schulten, K. (2008). Ten-microsecond molecular dynamics simulation of a fast-folding WW domain. Biophysical Journal *94*, L75-L77.

Freeman, L.C. (1977). A set of measures of centrality based on betweenness. Sociometry *40*, 35-41.

Fung, B.K.-K., and Stryer, L. (1980). Photolyzed rhodopsin catalyzes the exchange of GTP for bound GDP in retinol rod outer segments. Proceedings of the National Academy of Sciences of the United States of America *77*, 2500-2504.

Gao, Y.-G., Selmer, M., Dunham, C.M., Weixlbaumer, A., Kelley, A.C., and Ramakrishnan, V. (2009). The structure of the ribosome with elongation factor G trapped in the posttranslocational State. Science *326*.

Gasper, P.M., Fuglestad, B., Komives, E.A., Markwick, P.R.L., and McCammon, J.A. (2012). Allosteric networks in thrombin distinguish procoagulant vs. anticoagulant activities. Proceedings of the National Academy of Sciences of the United States of America *109*, 21216-21222.

Gaucher, E.A., Das, U.K., Miyamoto, M.M., and Benner, S.A. (2002). The crystal structure of eEF1A refines the functional predictions of an evolutionary analysis of rate changes among elongation factors. Molecular Biology and Evolution *19*, 569-573.

Gaucher, E.A., Miyamoto, M.M., and Benner, S.A. (2001). Function-structure analysis of proteins using covarion-based evolutionary approaches: Elongation factors. Proc Natl Acad Sci U S A *98*, 548-552.

Gerdes, S.Y., Scholle, M.D., Campbell, J.W., Balázsi, G., Ravasz, E., Daugherty, M.D., Somera, A.L., Kyrpides, N.C., Anderson, I., Gelfand, M.S*., et al.* (2003). Experimental determination and system level analysis of essential genes in *Escherichia coli* MG1655. Journal of Bacteriology *185*, 5673-5684.

Gideon, P., John, J., Frech, M., Lautwein, A., Clark, R., Scheffler, J.E., and Wittinghofer, A. (1992). Mutational and kinetic analysis of the GTPase-activating protein (GAP)-p21 interaction: the C-terminal domain of GAP is not sufficient for full activity. Molecular and Cellular Biology *12*, 2050-2056.

Glykos, N.M. (2006). Carma: A molecular dynamics analysis program. Journal of Computational Chemistry *27*, 1765-1768.

Grigorenko, B.L., Shadrina, M.S., Topol, I.A., Collins, J.R., and Nemukhin, A.V. (2008). Mechanism of the chemical step for the guanosine triphosphate (GTP) hydrolysis catalyzed by elongation factor Tu. Biochimica et Biophysica Acta *1784*, 1908-1917.

Gromadski, K.B., and Rodnina, M.V. (2004). Kinetic determinants of high-fidelity tRNA discrimination on the ribosome. Molecular Cell *13*, 191-200.

Gromadski, K.B., Schümmer, T., Strømgaard, A., Knudsen, C.R., Kinzy, T.G., and Rodnina, M.V. (2007). Kinetics of the interaction between yeast Elongation Factors 1A and 1Bα, guanine nucleotides, and aminoacyl-tRNA. The Journal of Biological Chemistry *282*, 35629-35637.

Gromadski, K.B., Wieden, H.-J., and Rodnina, M.V. (2002). Kinetic mechanism of elongation factor Ts-catalyzed nucleotide exchange in elongation factor Tu. Biochemistry *41*, 162-169.

Haenni, A.-L., and Lucas-Lenard, J. (1968). Stepwise synthesis of a tripeptide. Proceedings of the National Academy of Sciences of the United States of America *61*, 1363-1369.

Hammond, G.S. (1953). A correlation of reaction rates. Journal of the American Chemical Society *77*, 334-338.

Hausner, T.-P., Atmadja, J., and Nierhaus, K.H. (1987). Evidence that the G2661 region of the 23S rRNA is located at the ribosomal binding sites of both elongation factors. Biochimie *69*, 911-923.

Henzler-Wildman, K., and Kern, D. (2007). Dynamic personalities of proteins. Nature *450*, 964-972.

Henzler-Wildman, K.A., Lei, M., Thai, V., Kerns, S.J., Karplus, M., and Kern, D. (2007). A hierarchy of timescales in protein dynamics is linked to enzyme catalysis. Nature *450*, 913-916.

Humphrey, W., Dalke, A., and Schulten, K. (1996). VMD: visual molecular dynamics. Journal of Molecular Graphics *13*, 33-38.

Inoue-Yokosawa, N., Ishikawa, C., and Kaziro, Y. (1974). The role of guanosine triphosphate in translocation reaction catalyzed by elongation factor G. The Journal of Biological Chemistry *249*, 4321-4323.

Ishihama, Y., Schmidt, T., Rappsilber, J., Mann, M., Hartl, F.U., Kerner, M.J., and Frishman, D. (2008). Protein abundance profiling of the *Escherichia coli* cytosol. BMC Genomics *9*.

Iwasaki, K., Motoyoshi, K., Nagata, S., and Kaziro, Y. (1976). Purification and properties of a new polypeptide chain elongation factor, EF-1β from pig liver. The Journal of Biological Chemistry *251*, 1843-1845.

Jagath, J.R., Rodnina, M.V., Lentzen, G., and Wintermeyer, W. (1998). Interaction of guanine nucleotides with the signal recognition particle from *Escherichia coli*. Biochemistry *37*, 15408-15413.

Jin, H., Kelley, A.C., and Ramakrishnan, V. (2011). Crystal structure of the hybrid state of ribosome in complex with the guanosine triphosphatase release factor 3. Proceedings of the National Academy of Sciences of the United States of America *108*, 15798-15803.

John, J., Sohmen, R., Feuerstein, J., Linke, R., Wittinghofer, A., and Goody, R.S. (1990). Kinetics of interaction of nucleotides with nucleotide-free H-ras p21. Biochemistry *29*, 6058-6065.

Jonák, J., Petersen, T.E., Clark, B.F.C., and Rychlík, I. (1982). N-tosyl-L-phenylalanylchloromethane reacts with cysteine 81 in the molecules of elongation factor Tu from *Escherichia coli*. FEBS Letters *150*, 484-488.

Jones, S., Vignais, M.-L., and Broach, J.R. (1991). The CDC25 protein of *Saccharomyces cerevisiae* promotes exchange of guanine nucleotides bound to Ras. Molecular and Cellular Biology *11*, 2641-2646.

Karnoub, A.E., and Weinberg, R.A. (2008). Ras oncogenes: split personalities. Nature Reviews Molecular Cell Biology *9*, 517-531.

Katunin, V.I., Savelsbergh, A., Rodnina, M.V., and Wintermeyer, W. (2002). Coupling of GTP hydrolysis by elongation factor G to translocation of factor recycling on the ribosome. Biochemistry *41*, 12806-12812.

Kawashima, T., Berthet-Colominas, C., Wulff, M., Cusack, S., and Leberman, R. (1996). The structure of the *Escherichia coli* EF-Tu•EF-Ts complex at 2.5 Å resolution. Nature *379*, 511-518.

Kinoshita, K., Sadanami, K., Kidera, A., and Go, N. (1999). Structural motif of phosphate-binding site common to various protein superfamilies: all-against-all structural comparison of protein-mononucleotide complexes. Protein Engineering *12*, 11-14.

Kjeldgaard, M., Nissen, P., Thirup, S., and Nyborg, J. (1993). The crystal structure of elongation factor EF-Tu from Thermus aquaticus in the GTP conformation. Structure *1*, 35-50.

Kjeldgaard, M., Nyborg, J., and Clark, B.F.C. (1996). The GTP binding motif: variations on a theme. The FASEB Journal *10*, 1347-1368.

Klebe, C., Prinz, H., Wittinghofer, A., and Goody, R.S. (1995). The kinetic mechanism of Ran-nucleotide exchange catalyzed by RCC1. Biochemistry *34*, 12543-12552.

Konieczny, A., and Safer, B. (1983). Purification of the Eukaryotic initiation factor 2-Eukaryotic initiation factor 2B complex and characterization of its guanine nucleotide exchange activity during protein synthesis initiation. The Journal of Biological Chemistry *258*, 3420-3408.

Kothe, U., and Rodnina, M.V. (2006). Delayed release of inorganic phosphate from elongation factor Tu following GTP hydrolysis on the ribosome. Biochemistry *45*, 12767-12774.

Kothe, U., Wieden, H.-J., Mohr, D., and Rodnina, M.V. (2004). Interaction of helix D of elongation factor Tu with helices 4 and 5 of protein L7/12 on the ribosome. Journal of Molecular Biology *336*, 1011-1021.

Kulczycka, K., Długosz, M., and Trylska, J. (2011). Molecular dynamics of ribosomal elongation factors G and Tu. European Biophysics Journal *40*, 289-303.

Lamers, M.H., Perrakis, A., Enzlin, J.H., Winterwerp, H.H.K., Wind, N.d., and Sixma, T.K. (2000). The crystal structure of DNA mismatch repair protein MutS binding to a G•T mismatch. Nature *407*, 711-717.

LaRiviere, F.J., Wolfson, A.D., and Uhlenbeck, O.C. (2001). Uniform binding of aminoacyl-tRNAs to elongation factor Tu by thermodynamic compensation. Science *294*, 165-158.

Larkin, M.A., Blackshields, G., Brown, N.P., Chenna, R., McGettigan, P.A., McWilliam, H., Valentin, F., Wallace, I.M., Wilm, A., Lopez, R.*, et al.* (2007). Clustal W and Clustal X version 2.0. Bioinformatics *23*, 2947-2948.

Lenzen, C., Cool, R.H., Prinz, H., Kuhlmann, J., and Wittinghofer, A. (1998). Kinetic analysis by fluorescence of the interaction between Ras and the catalytic domain of the guanine nucleotide exchange factor $Cdc25^{Mm}$. Biochemistry *37*, 7420-7430.

Levin, A.M., Bates, D.L., Ring, A.M., Krieg, C., Lin, J.T., Su, L., Moraga, I., Raeber, M.E., Bowman, G.R., Novick, P.*, et al.* (2012). Exploiting a natural conformational switch to engineer an interleukin-2 'superkine'. Nature *484*, 529-533.

Louie, A., Ribeiro, N.S., Reid, B.R., and Jurnak, F. (1984). Relative affinities of all *Escherichia coli* aminoacyl-tRNAs for elongation factor Tu-GTP. The Journal of Biological Chemistry *259*.

Ma, C.-W., Xiu, Z.-L., and Zeng, A.-P. (2012). Discovery of intramolecular signal transduction network based on a new protein dynamics model of energy dissipation. PLoS One *7*, e31529.

MacKerell, A.D., Bashford, D., Bellott, M., Jr., R.L.D., Evanseck, J.D., Field, M.J., Kuczera, K., Lau, F.T.K., Mattos, C., Michnick, S.*, et al.* (1998). All-atom emperical potential for molecular modeling and dynamics studies of proteins. Journal of Physical Chemistry B *102*, 3586-3616.

Maessen, G.D.F., Amons, R., Maassen, J.A., and Möller, W. (1986). Primary structure of elongation factor 1β from *Artemia*. FEBS Letters *208*, 77-83.

Margarit, S.M., Sondermann, H., Hall, B.E., Nagar, B., Hoelz, A., Pirruccello, M., Bar-Sagi, D., and Kuriyan, J. (2003). Structural evidence for feedback activation by Ras•GTP of the Ras-specific nucleotide exchange factor SOS. Cell *112*, 685-695.

Marshall, R.A., Aitken, C.E., and Publisi, J. (2009). GTP hydrolysis by IF2 guides progression of the ribosome into elongation. Molecular Cell *35*, 37-47.

McCammon, J.A., Gelin, B.R., and Karplus, M. (1977). Dynamics of folded proteins. Nature *267*, 585-590.

McClory, S.P., Leisring, J.M., Qin, D., and Fredrick, K. (2010). Missense supressor mutations in the 16S rRNA reveal the importance of helices h8 and h14 in aminoacyl-tRNA selection. RNA *16*, 1925-1934.

Melchionna, S., Sinibaldi, R., and Briganti, G. (2006). Explanation of the stability of thermophilic proteins based on unique morphology. Biophysical Journal *90*, 4204-4212.

Milburn, M.V., Tong, L., deVos, A.M., Brünger, A., Yamaizumi, Z., Nishimura, S., and Kim, S.-H. (1990). Molecular switch for signal transduction: structural differences

between active and inactive forms of protooncogenic ras proteins. Science *247*, 939-945.
Milon, P., Konevega, A.L., Peske, F., Fabbretti, A., Gualerzi, C.O., and Rodnina, M.V. (2007). Transient kinetics, fluorescence, and FRET in studies of initiation of translation in Bacteria. In Methods in Enzymology, pp. 1-30.
Moazed, D., Robertson, J.M., and Noller, H.F. (1988). Interaction of elongation factors EF-G and EF-Tu with a conserved loop in 23S RNA. Nature *334*, 362-364.
Mohr, D., Wintermeyer, W., and Rodnina, M.V. (2002). GTPase activation of elongation factors Tu and G on the ribosome. Biochemistry *41*, 12520-12528.
Moore, M.S., and Blobel, G. (1993). The GTP-binding protein Ran/TC4 is required for protein import into the nucleus. Nature *365*, 661-663.
Mossessova, E., Corpina, R.A., and Goldberg, J. (2003). Crystal structure of ARF1•Sec7 complexed with brefeldin A and its implications for the guanine nucleotide exchange mechanism. Molecular Cell *12*, 1403-1411.
Mulcahy, L.S., Smith, M.R., and Stacey, D.W. (1985). Requirement for ras proto-oncogene function during serum-stimulated growth of NIH 3T3 cells. Nature *313*, 241-243.
Müller, C.W., Schlauderer, G.J., Reinstein, J., and Schulz, G.E. (1996). Adenylate kinase motions during catalysis: an energetic counterweight balancing substrate binding. Structure *4*, 147-156.
Nagata, S., Tsunetsugo-Yokota, Y., Naito, A., and Kaziro, Y. (1983). Molecular cloning and sequence determination of the nuclear gene coding for mitochondrial elongation factor Tu of *Saccharomyces cerevisiae*. Proceedings of the National Academy of Sciences of the United States of America *80*, 6192-6196.
Nagel, Z.D., Dong, M., Bahnson, B.J., and Klinman, J.P. (2011). Impaired protein conformational landscapes as revealed in anomalous Arrhenius prefactors. Proceedings of the National Academy of Sciences of the United States of America *108*, 10520-10525.
Neal, S.E., Eccleston, J.F., Hall, A., and Webb, M.R. (1988). Kinietic analysis of the hydrolysis of GTP by $p21^{N\text{-}ras}$. The Journal of Biological Chemistry *263*, 19718-19722.
Neuwald, A.F. (2009). The glycine brace: a component of Rab, Rho, and Ran GTPases associated with hinge regions of guanine- and phosphate-binding loops. BMC Structural Biology *9*.
Nissen, P., Kjeldgaard, M., Thirup, S., Plekhina, G., Reshetnikova, L., Clark, B.F., and Nyborg, J. (1995). Crystal structure of the ternary complex of Phe-tRNAPhe, EF-Tu, and a GTP analog. Science *270*, 1464-1472.
Ogle, J.M., Brodersen, D.E., Jr., W.M.C., Tarry, M.J., Carter, A.P., and Ramakrishnan, V. (2001). Recognition of cognate transfer RNA by the 30S ribosomal subunit. Science *292*, 897-902.
Oostenbrink, C., Villa, A., Mark, A.E., and VanGunsteren, W.F. (2004). A biomolecular force field based on the free enthalpy of hydration and solvation: the GROMOS force-field parameter set 53A5 and 53A6. Journal of Computational Chemistry *25*, 1656-1676.
Ott, G., Schiesswohl, M., Kiesewetter, S., Förster, C., Arnold, L., Erdmann, V.A., and Sprinzl, M. (1990). Ternary complexes of *Escherichia coli* aminoacyl-tRNAs with the

elongation factor Tu and GTP: thermodynamic and structural studies. Biochimica et Biophysica Acta *1050*, 222-225.

Pape, T., Wintermeyer, W., and Rodnina, M. (1999). Induced fit in initial selection and proofreading of aminoacyl-tRNA on the ribosome. The EMBO Journal *18*, 3800-3807.

Pape, T., Wintermeyer, W., and Rodnina, M.V. (1998). Complete kinetic mechanism of elongation factor Tu-dependent binding of aminoacyl-tRNA to the A site of the *E. coli* ribosome. The EMBO Journal *17*, 7490-7497.

Parmeggiani, A., Krab, I.M., Okamura, S., Nielsen, R.C., Nyborg, J., and Nissen, P. (2006a). Structural basis of the action of pulvomycin and GE2270 A on elongation factor Tu. Biochemistry *45*, 6846-6857.

Parmeggiani, A., Krab, I.M., Watanabe, T., Nielsen, R.C., Dahlberg, C., Nyborg, J., and Nissen, P. (2006b). Enacyloxin IIa pinpoints a binding pocket of elongation factor Tu for development of novel antibiotics. Journal of Biological Chemistry *281*, 2893-2900.

Phillips, J.C., Braun, R., Wang, W., Gumbart, J., Tajkhorshid, E., Villa, E., Chipot, C., Skeel, R.D., Kalé, L., and Schulten, K. (2005). Scalable molecular dynamics with NAMD. Journal of Computational Chemistry *26*, 1781-1802.

Piepenburg, O., Pape, T., Pleiss, J.A., Wintermeyer, W., Uhlenbeck, O.C., and Rodnina, M.V. (2000). Intact aminoacyl-tRNA is required to trigger GTP hydrolysis by elongation factor Tu on the ribosome. Biochemistry, 1734-1738.

Powers, T., and Walter, P. (1997). Co-translational protein targeting catalyzed by the *Escherichia coli* signal recognition particle and its receptor. The EMBO Journal *16*, 4880-4886.

Proshkin, S., Rahmouni, A.R., Mironov, A., and Nudler, E. (2010). Cooperation between translating ribosomes and RNA polymerase in transcription elongation. Science *328*, 504-508.

Pyrkosz, A.B., Eargle, J., Sethi, A., and Luthey-Schulten, Z. (2010). Exit strategies for charged tRNA from GluRS. Journal of Molecular Biology *397*, 1350-1371.

Rasmussen, S.G.F., DeVree, B.T., Zou, Y., Kruse, A.C., Chung, K.Y., Kobilka, T.S., Thian, F.S., Chae, P.S., Pardon, E., Calinski, D*., et al.* (2011). Crystal structure of the β_2 adrenergic receptor-Gs protein complex. Nature *477*, 549-555.

Ravel, J.M., and Shorey, R.L. (1969). Formation and properties on an aminoacyl-tRNA•GTP•protein complex. Journal of Cellular Physiology *74*, 103-116.

Ravel, J.M., Shorey, R.L., and Shive, W. (1968). The composition of the active intermediate in the transfer of aminoacyl-RNA to ribosome. Biochemical and Biophysical Research Communication *32*, 9-14.

RCoreTeam (2012). R: A Language and Environment for Statistical Computing (Vienna, Austria).

Renault, L., Kuhlmann, J., Henkel, A., and Wittinghofer, A. (2001). Structural basis for guanine nucleotide exchange on Ran by the regulator of chromosome condensation (RCC1). Cell *105*, 245-255.

Richman, N., and Bodley, J.W. (1973). Irreversible inhibition of the interaction between elongation factor Tu and phenylalanyl transfer ribonucleic acid by L-1-tosylamido-2-phenylethyl chromethyl ketone. The Journal of Biological Chemistry *248*, 381-383.

Rodnina, M.V., Fricke, R., and Wintermeyer, W. (1994). Transient conformational states of aminoacyl-tRNA during ribosome binding catalyzed by elongation factor Tu. Biochemistry *33*, 12267-12275.

Rodnina, M.V., Pape, T., Fricke, R., Kuhn, L., and Wintermeyer, W. (1996). Initial binding of the elongation factor Tu•GTP•aminoacyl-tRNA complex preceding codon recognition on the ribosome. The Journal of Biological Chemistry *271*, 646-652.

Röthlisberger, D., Khersonsky, O., Wollacott, A.M., Jiang, L., DeChancie, J., Betker, J., Gallaher, J.L., Althoff, E.A., Zanghellini, A., Dym, O.*, et al.* (2008). Kemp elimination catalysts by computational enzyme design. Nature *453*, 190-195.

Sanderson, L.E., and Uhlenbeck, O.C. (2007). Directed mutagenesis identifies amino acid residues involved in elongation factor Tu binding to yeast Phe-tRNA^{Phe}. Journal of Molecular Biology *368*, 119-130.

Schmeing, T.M., Voorhees, R.M., Kelley, A.C., Gao, Y.-G., Murphy, F.V., Weir, J.R., and Ramakrishnan, V. (2009). The crystal structure of the ribosome bound to EF-Tu and aminoacyl-tRNA. Science *326*, 688-694.

Schmeing, T.M., Voorhees, R.M., Kelley, A.C., and Ramakrishnan, V. (2011). How mutations in tRNA distant from the anticodon affect the fidelity of decoding. Nature Structural and Molecular Biology *18*, 432-436.

Schnell, R., Abdulkarim, F., Kálmán, M., and Isaksson, L.A. (2003). Functional EF-Tu with large C-terminal extension in an *E. coli* strain with a precise deletion of both chromosomal *tuf* genes. FEBS Letters *538*, 139-144.

Schrader, J.M., Chapman, S.J., and Uhlenbeck, O.C. (2011). Tuning the affinity of aminoacyl-tRNA to elongation factor Tu for optimal decoding. Proceedings of the National Academy of Sciences of the United States of America *108*, 5215-5220.

Schümmer, T., Gromadski, K.B., and Rodnina, M.V. (2007). Mechanism of EF-Ts-catalyzed guanine nucleotide exchange in EF-Tu: contribution of interactions mediated by helix B of EF-Tu. Biochemistry *46*, 4977-4984.

Schwede, T., Kopp, J., Guex, N., and Peitsch, M.C. (2003). SWISS-MODEL: an automated protein homology-modeling server. Nucleic Acids Research *31*, 3381-3385.

Scopes, R.K. (1974). Measurement of protein by spectrophotometry at 205nm. Analytical Biochemistry *59*, 277-252.

Sedláček, J., RychlÍk, I., and Jonák, J. (1974). The role of aminoacyl-tRNA binding site on the factor EF-T in uncoupled GTPase reaction. Biochimica et Biophysica Acta *349*, 78-83.

Sethi, A., Eargle, J., Black, A.A., and Luthey-Schulten, Z. (2009). Dynamical networks in tRNA:protein complexes. Proceedings of the National Academy of Sciences of the United States of America *106*, 6620-6625.

Shi, X., Khade, P.K., Sanbonmatsu, K.Y., and Joseph, S. (2012). Functional role of the sarcin-ricin loop of the 23S rRNA in the elongation cycle of protein synthesis. Journal of Molecular Biology *419*, 125-138.

Shields, M.J., Fischer, J.J., and Wieden, H.-J. (2009). Toward understanding the function of the universally conserved GTPase HflX from *Escherichia coli*: a kinetic approach. Biochemistry *48*, 10793-10802.

Siderovski, D.P., and Willard, F.S. (2005). The GAPs, GEFs, and GDIs of heterotrimeric G-protein alpha subunits. International Journal of Biological Sciences *1*, 51-66.

Simon, M.I., Strathmann, M.P., and Gautam, N. (1991). Diversity of G proteins in signal transduction. Science *252*, 802-808.

Song, H., Parsons, M.R., Rowsell, S., Leonard, G., and Phillips, S.E.V. (1999). Crystal structure of intact elongation factor EF-Tu from *Escherichia coli* in GDP conformation at 2.05 Å resolution. Journal of Molecular Biology *285*, 1245-1256.

Thompson, J.D., Higgins, D.G., and Gibson, T.J. (1994). Clustal W: improving the sensitivity of progressive multiple sequence alignment through sequence weighting, position-specific gap penalties and weight matrix choice. Nucleic Acids Research *22*, 4673-4680.

Thompson, R.C., and Stone, P.J. (1977). Proofreading of the codon-anticodon interaction on ribosomes. Proceedings of the National Academy of Sciences of the United States of America *74*, 198-202.

Tinoco, I., Sauer, K., Wang, J.C., and Puglisi, J.D. (2002). Kinetics: rates of chemical reactions. In Physical Chemistry, priciples and applications in biological sciences, J. Challice, ed. (Upper Saddle River, Prentice Hall), pp. 315-388.

Tomatis, P.E., Rasia, R.M., Segovia, L., and Vila, A.J. (2005). Mimicking natural evolution in metallo-β-lactamases through second-shell ligand mutations. Proceedings of the National Academy of Sciences of the United States of America *102*, 13761-13766.

Tombs, M.P., Souter, F., and MacLagan, N.F. (1959). The spectrophotometric determination of protein at 210mμ. Biochemical Journal *73*, 167-171.

Trahey, M., and McCormick, F. (1987). A cytoplasmic protein stimulates normal N-ras p21 GTPase, but does not affect ocogenic mutants. Science *238*, 542-545.

Tzeng, S.-R., and Kalodimos, C.G. (2012). Protein activity regulation by conformational entropy. Nature *488*, 236-240.

Uphoff, S., Holden, S.J., Reste, L.L., Periz, J., Linde, S.v.d., Heilemann, M., and Kapanidis, A.N. (2010). Monitoring multiple distances within a single molecule using switchable FRET. Nature Methods *7*, 831-836.

Verstraeten, N., Fauvart, M., Versées, W., and Michiels, J. (2011). The universally conserved prokaryotic GTPases. Microbiology and Molecular Biology Reviews *75*, 507-542.

Villa, E., Sengupta, J., Trabuco, L.G., LeBarron, J., Baxter, W.T., Shaikh, T.R., Grassucci, R.A., Nissen, P., Ehrenberg, M., Schulten, K.*, et al.* (2009). Ribosome-induced changes in elongation factor Tu conformation control GTP hydrolysis. Proceedings of the National Academy of Sciences of the United States of America *106*, 1063-1068.

Voet, D., and Voet, J.G. (2004). Metabolism. In Biochemistry, D. Harris, and P. Fitzgerald, eds. (Hoboken, John Wiley and Sons Inc.).

Vogeley, L., Palm, G.J., Mesters, J.R., and Hilgenfeld, R. (2001). Conformational change of elongation factor Tu (EF-Tu) induced by antibiotic binding. The Journal of Biological Chemistry *276*, 17149-17155.

Voorhees, R.M., Schmeing, M.T., Kelley, A.C., and Ramakrishnan, V. (2010). The mechanism for activation of GTP hydrolysis on the ribosome. Science *330*, 835-838.

Vorstenbosch, E., Pape, T., Rodnina, M.V., Kraal, B., and Wintermeyer, W. (1996). The G222D mutation in elongation factor Tu inhibits the condon-induced conformational changes leading to GTPase activation on the ribosome. The EMBO Journal *15*, 6766-6774.

Wagner, A., Simon, I., Sprinzl, M., and Goody, R.S. (1995). Interaction of guanosine nucleotides and their analogs with elongation factor Tu from *Thermus thermophilus*. Biochemistry *34*, 12535-12542.

Walker, J.E., Saraste, M., Runswick, M.J., and Gay, N.J. (1982). Distantly related sequences in the α- and β-subunits of ATP synthase myosin, kinases and other ATP-requiring enzymes and a common nucleotide binding fold. The EMBO Journal *1*, 945-951.

Weijland, A., Parlato, G., and Parmeggiani, A. (1994). Elongation factor Tu D138N, a mutant with modified substrate specificity, as a tool to study energy consumption in protein biosynthesis. Biochemistry *33*, 10711-10717.

Weissbach, H., Miller, D.L., and Hachmann, J. (1970). Studies on the role of factor Ts in polypeptide synthesis. Archives of Biochemistry and Biophysics *137*, 262-269.

Whitford, P.C., Ahmed, A., Yu, Y., Hennelly, S.P., Tama, F., Spahn, C.M.T., Onuchic, J.N., and Sanbonmatsu, K.Y. (2011). Excited states of ribosome translocation revealed through integrative molecular modeling. Proceedings of the National Academy of Sciences of the United States of America *108*, 18943-18948.

Whitford, P.C., Geggier, P., Altman, R.B., Blanchard, S.C., Onuchic, J.N., and Sanbonmatsu, K.Y. (2010). Accommodation of amionoacyl-tRNA into the ribosome involves reversible excursions along multiple pathways. RNA *16*, 1196-1204.

Wieden, H.-J., Gromadski, K., Rodnin, D., and Rodnina, M.V. (2002). Mechanism of elongation factor (EF)-Ts-catalyzed nucleotide exchange in EF-Tu. Contribution of contacts at the guanine base. The Journal of Biochemistry *277*, 6032-6036.

Wieden, H.-J., Mercier, E., Gray, J., Steed, B., and Yawney, D. (2010). A combined molecular dynamics and rapid kinetics approach to identify conserved three-dimensional communication networks in elongation factor Tu. Biophysical Journal *99*, 3735-3743.

Wilden, B., Savelsbergh, A., Rodnina, M.V., and Wintermeyer, W. (2006). Role and timing of GTP binding and hydrolysis during EF-G-dependent tRNA translocation on the ribosome. Proceedings of the National Academy of Sciences of the United States of America *103*, 13670-13675.

Wilson, D., Madera, M., Vogel, C., Chothia, C., and Gough, J. (2007). The SUPERFAMILY database in 2007: families and functions. Nucleic Acids Research *35*, D308-D313.

Wittinghofer, A., and Vetter, I.R. (2011). Structure-function relationship of the G domain, a canonical switch motif. Annual Reviews of Biochemistry *80*, 943-971.

Wolf, H., Chinali, G., and Parmeggiani, A. (1974). Kirromycin, an inhibitor of protein biosynthesis that acts on elongation factor Tu. Proceedings of the National Academy of Sciences of the United States of America *71*, 4910-4914.

Wolf-Watz, M., Thai, V., Henzler-Wildman, K., Hadjipavlou, G., Eisenmesser, E.Z., and Kern, D. (2004). Linkage between dynamics and catalysis in a thermophilic-mesophilic enzyme pair. Nature Structural and Molecular Biology *11*, 945-949.

Yokosawa, H., Kawakita, M., Arai, K.-i., Inoue-Yokosawa, N., and Kaziro, Y. (1975). Binding of aminoacyl-tRNA to ribosomes promoted by Elongation Factor Tu. The Journal of Biochemistry *77*, 719-728.

Young, D.C. (2001a). Molecular dynamics and monte carlo simulations. In Computational Chemistry: A practical guide for applying techniques to real world problems (New York, John Wiley & Sons), pp. 60-66.

Young, D.C. (2001b). Molecular Mechanics. In Computational Chemistry: a practical guide for applying techniques to real world problems (New York, John Wiley & Sons), pp. 49-59.

Zavialov, A.V., Hauryliuk, V.V., and Ehrenberg, M. (2005). Guanine-nucleotide exchange on ribosome-bound elongation factor G initiates the translocation of tRNAs. Journal of Biology *4*.

Zeef, L.A.H., Bosch, L., Anborgh, P.H., Cetin, R., Parmeggiani, A., and Hilgenfeld, R. (1994). Pulvomycin-resistant mutants of *E. coli* elongation factor Tu. The EMBO Journal *13*, 5113-5120.

Zhang, X., Schaffitzel, C., Ban, N., and Shan, S.-o. (2009). Multiple conformational switches in a GTPase complex control co-translational protein targeting. Proceedings of the National Academy of Sciences of the United States of America *106*, 1754-1759.

Zhang, Y., Li, X., and Spremulli, L.L. (1996). Role of the conserved aspartate and phenylalanine residues in prokaryotic and mitochondrial elongation factor Ts in guanine nucleotide exchange. FEBS Letters *391*, 330-332.

Zhang, Y., Yu, N.-J., and Spremulli, L.L. (1998). Mutational analysis of the roles of residues in *Escherichia coli* elongation factor Ts in the interaction with elongation factor Tu. The Journal of Biological Chemistry *273*, 4556-4562.

Zuurmond, A.-M., Olsthoorn-Tieleman, L.N., Graaf, J.M.d., Parmeggiani, A., and Kraal, B. (1999). Mutant EF-Tu species reveal novel features of the enacyloxin IIa inhibition mechanism on the ribosome. Journal of Molecular Biology *294*, 627-637.

Appendix 1

Supplemental Material to Chapter 2

A.1.1. Supplemental Figures

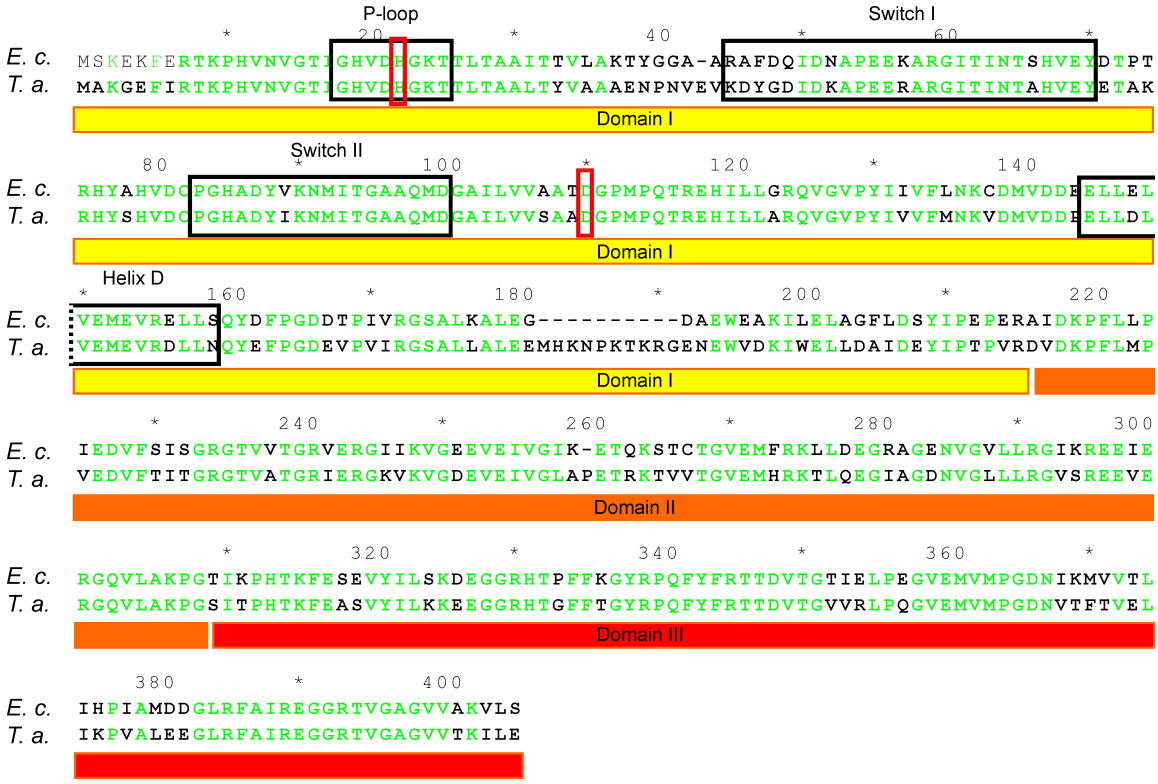

Figure A.1.1: Sequence alignment between *E. coli* and *T. aquaticus* EF-Tu used to construct the *E. coli* homology model of the GTP complex. Identical amino acids are shown in green and N-terminal amino acids missing in the EF-Tu•GDP structure (1EFC) from *E. coli* are shaded. Conserved structural features in the sequence of the G-domain involved in nucleotide binding or important for nucleotide exchange are labeled and boxed (black) as well as the conserved $Asp109_{Tu}$ and $His22_{Tu}$ (red box).

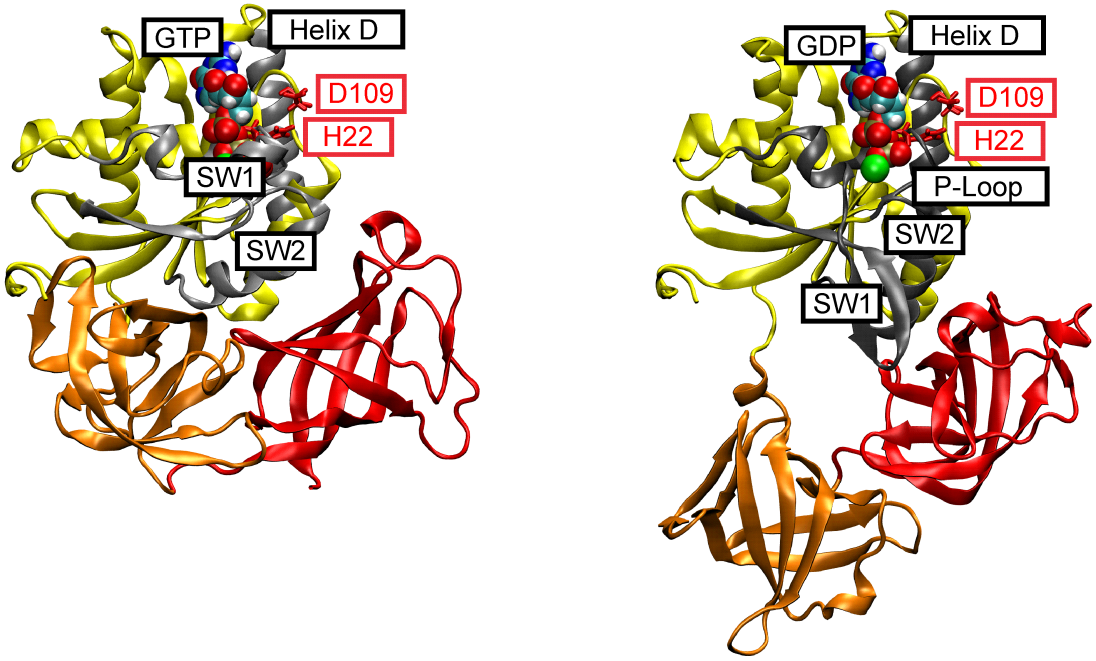

Figure A.1.2. Structures of EF-Tu•GTP and EF-Tu•GDP from *E. coli*. Comparison of the generated full-length models for EF-Tu•GTP (left) and EF-Tu•GDP (right) from *E. coli*. Conserved structural features, as indicated in **Figure A.1.1**, are labeled respectively (SW1 for Switch 1 and SW2 for Switch 2) and shaded in grey. The two conserved residues $Asp109_{Tu}$ and $His22_{Tu}$ are labeled (red) and their position within the G-domain is shown in wireframe, the nucleotide in space fill and the magnesium ion in green.

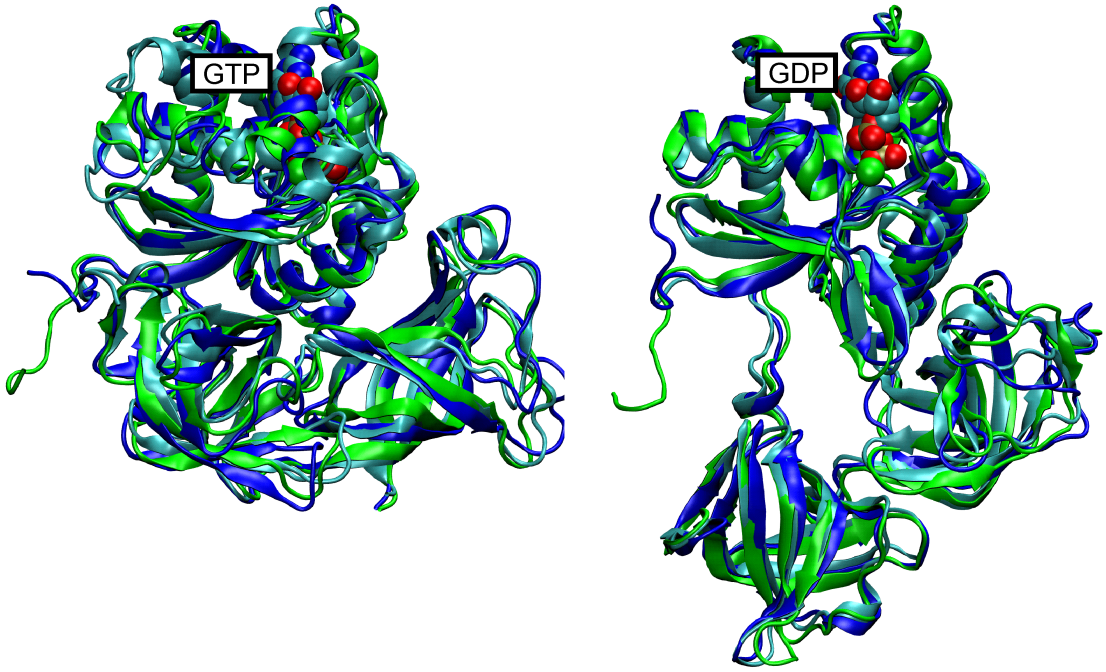

Figure A.1.3. Superimposition of structure snapshots at the end of the 10 ns long trajectories, for the respective GTP and GDP forms of EF-Tu_{wt} (green) and EF-Tu_{D109A} (blue) with the respective X-ray structures of the wild type complexes (cyan).

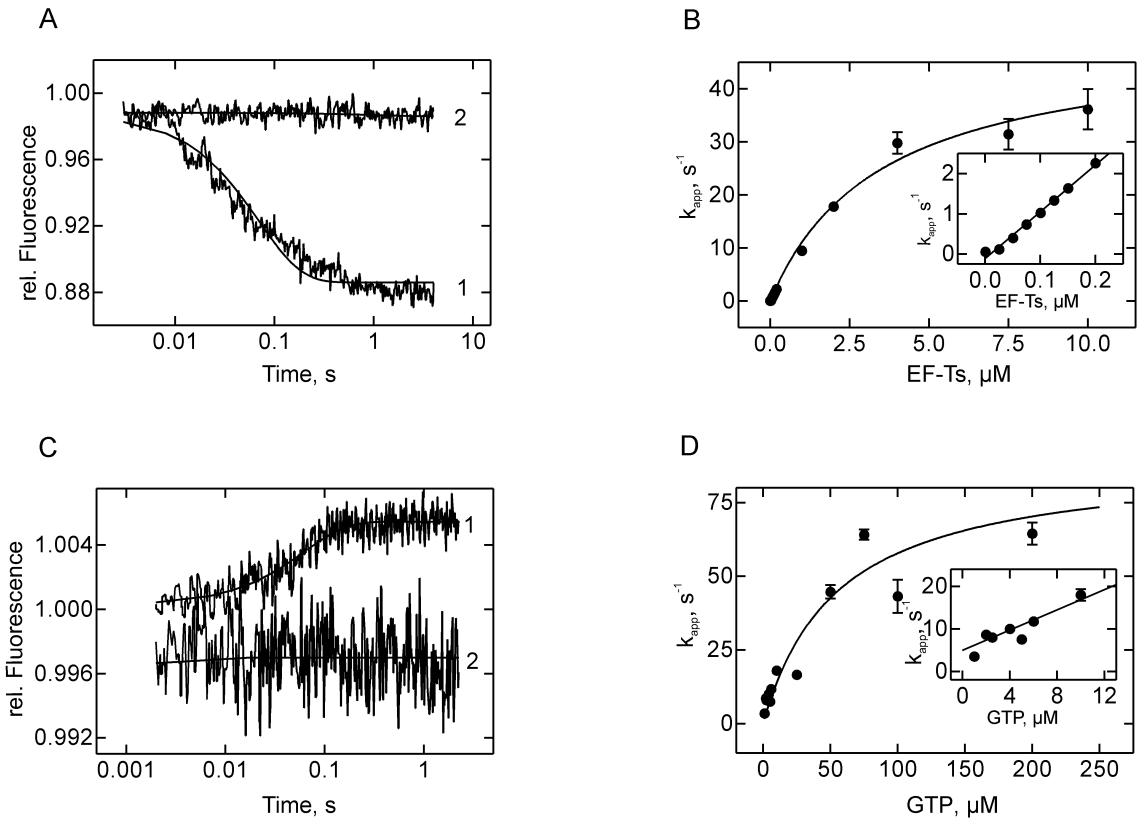

Figure A.1.4. Interaction of EF-Tu$_{D109A}$ with EF-Ts and GTP. (A) Time courses for dissociation of EF-Tu•mant-GTP (0.15 μM) in the presence of EF-Ts (4 μM) and excess unlabelled GTP (25 μM) (1) or in the absence of EF-Ts (2). The fluorescence of the mant group was monitored. GTP and mant-GTP solutions were preincubated with phosphoenolpyruvate and pyruvate kinase to minimize contamination with GDP. (B) Concentration dependence of k_{app} for EF-Tu•mant-GTP dissociation. The values of k_{app} were calculated by single-exponential fitting of the time courses in (A). (C) Time courses for the dissociation of EF-Tu•EF-Ts (0.5 μM) in the presence of GTP (50 μM) (1) or in the absence of GTP (2), as monitored by the fluorescence of Trp 184 in EF-Tu. (D) Concentration dependence of k_{app} for EF-Tu•EF-Ts dissociation in the presence of GTP. The values of k_{app} were calculated by single-exponential fitting of the time courses in (C).

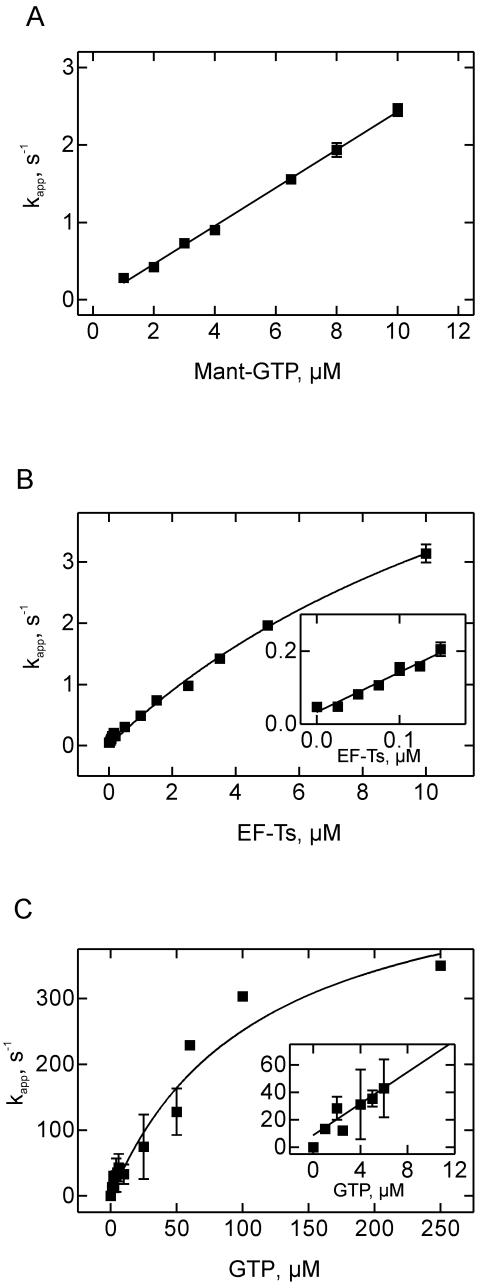

Figure A.1.5. Interaction of EF-Tu_{E152A} with EF-Ts and GTP. (A) Concentration dependence of k_{app} for mant-GTP binding to nucleotide-free EF-Tu_{E152A} (0.25μM). The values of k_{app} were calculated by single-exponential fitting from several time courses monitoring the fluorescence of the mant group at varying concentrations of mant-GTP (data not shown). (B) Concentration dependence of k_{app} for the dissociation of EF-Tu•EF-Ts (0.5μM) in the presence of varying concentrations of GTP. The values of k_{app} were calculated by single exponential fitting of the average of several time courses monitoring the fluorescence of Trp184 (data not shown). (C) Concentration dependence of k_{app} for EF-Ts catalyzed mant-GTP dissociation from EF-Tu. The values of k_{app} were calculated by single exponential fitting of several time courses monitoring the dissociation of EF-Tu•mant-GTP (0.15 μM) in the presence of varying concentrations of EF-Ts (data not shown).

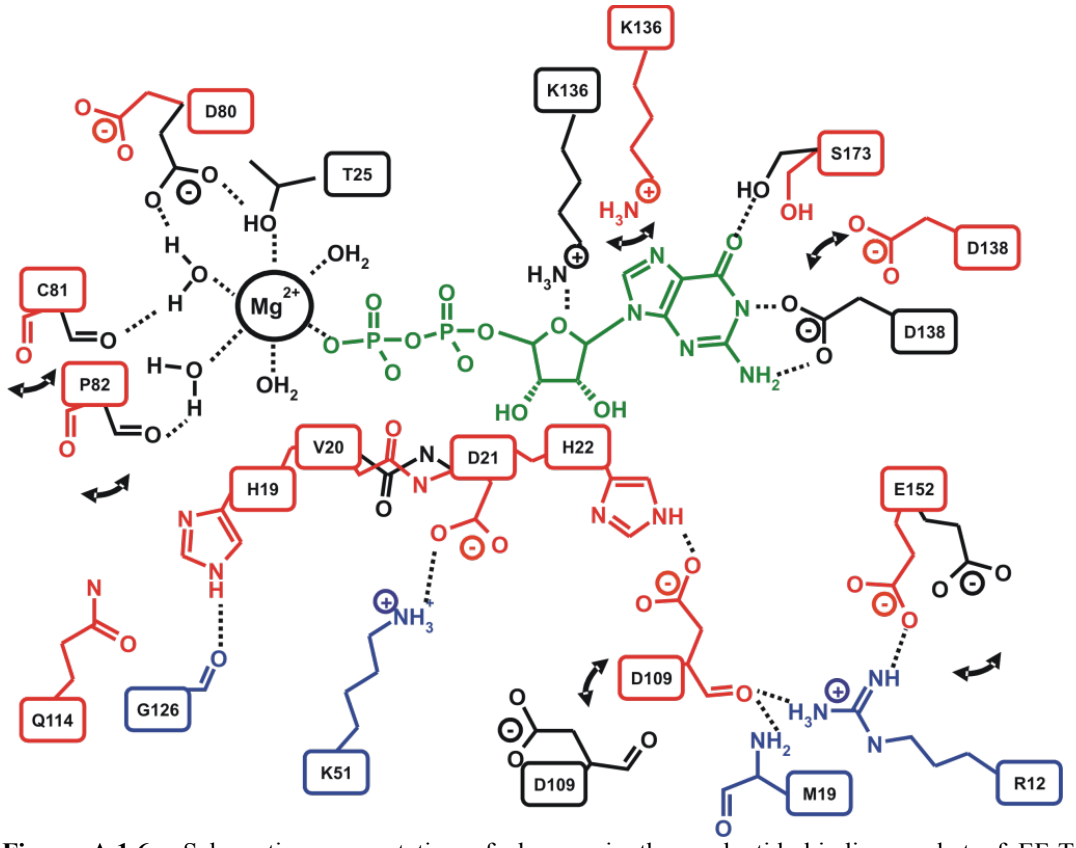

Figure A.1.6: Schematic representation of changes in the nucleotide-binding pocket of EF-Tu upon interaction with EF-Ts: EF-Tu residues are given for the EF-Tu•GDP complex in black and for the EF-Tu•EF-Ts complex in red. EF-Ts residues protruding into EF-Tu are depicted in blue. Movements induced by interaction with EF-Ts are indicated by the black arrows. The nucleotide (green) is positioned relative to EF-Tu residues based on the coordinates of 1EFC.

A.1.2 Materials and Methods

Protein preparation and complex purification

Wild-type and mutant EF-Tus containing a C-terminal oligohistidine tag were purified by Ni^{2+}-nitrilotriacetic acid affinity chromatography under nondenaturing conditions. Proteins were overexpressed in *E. coli* BL21 DE3 cells by addition of IPTG to a final concentration of 1mM. Cells were opened by sonication in buffer B (50 mM Tris-HCl pH 8.0 @4 °C, 60 mM NH_4Cl, 300 mM KCl, 7 mM $MgCl_2$, 7 mM 2-mercaptoethanol, 1mM phenylmethylsulfonyl fluoride, 50 μM GDP, 10 mM imidazole, 15% glycerol) and purified to homogeneity as described elsewhere (Daviter et al., 2003). The concentration of EF-Tu was determined photometrically at 280 nm using a molar extinction coefficient of 32900 M^{-1} cm^{-1} (Block and Pingoud, 1981). To avoid contamination with EF-Ts, which can co-purify with EF-Tu, GDP was present during all purification steps.

The plasmid for the expression of EF-Ts as a fusion protein containing a self-splicing intein element and a chitin binding domain in the IMPACT I system (NE Biolabs) was provided by Charlotte Knudsen (Åarhus, Denmark). EF-Ts was purified to homogeneity as described elsewhere (Gromadski et al., 2002; Wieden et al., 2002). EF-Ts concentrations were determined by absorbance at 210 nm (Tombs et al., 1959) and 205 nm (Scopes, 1974).

To prepare nucleotide free EF-Tu, EF-Tu was incubated for 10 minutes at 37 °C in buffer C (25 mM Tris-HCl, pH 7.5, 50 mM NH_4Cl, 10mM EDTA). Under these conditions, Mg^{2+} is chelated and nucleotide binding to EF-Tu is disrupted. The protein was separated from the free nucleotide by gel filtration on Superdex 75 (GE Healthcare) in buffer D (25 mM Tris-HCl, pH 7.5, and 50 mM NH_4Cl) in the absence of Mg^{2+}.

Fractions containing nucleotide-free EF-Tu were pooled and their concentration was determined photometrically at 280 nm (Block and Pingoud, 1981).

To prepare nucleotide-free EF-Tu•EF-Ts complex, equimolar amounts of EF-Tu and EF-Ts were incubated at 37 °C for 30 minutes in buffer C and the binary EF-Tu•EF-Ts complex was separated from the free factors by gel filtration on Superdex 75 (GE Healthcare) in buffer D. Fractions containing the binary complex were pooled and their concentration was determined spectroscopically at 210nm (Tombs et al., 1959).

Preparation of EF-Tu•mant-GDP/GTP

EF-Tu•GDP was incubated with a 10-fold excess of mant-GDP or mant-GTP for 15 minutes at 37 °C in buffer A. To convert all GDP contaminations to GTP, stock solutions of GTP were preincubated with phosphoenolpyruvate and pyruvate kinase and then diluted such that their final concentrations did not exceed 0.02 mM and 0.7 μg/mL, respectively.

A.1.3 Kinetic Analysis

GDP/GTP Interaction with EF-Tu$_{D109A}$ and EF-Tu$_{wt}$ (k_1, k_{-1}, k_5, k_{-5})

The rate constants of GDP and GTP interaction with EF-Tu, k_1 / k_{-1} and k_5 / k_{-5}, respectively (**Scheme 2.1**), were determined by Fluorescence Resonance Energy Transfer (FRET) between tryptophan (Trp) 184 in EF-Tu and mant-GDP (or mant-GTP), resulting in an increase of mant fluorescence upon binding (**Figure 2.3.A**) of the nucleotide to the factor (Gromadski et al., 2002; Wagner et al., 1995; Wieden et al., 2002). Time courses of binding were measured at a constant concentration of nucleotide-free EF-Tu and a varying concentration of either mant-GDP or mant-GTP. As only single-exponential time courses were observed, the data were treated on the basis of a one-step binding model, EF-Tu + mant-nucleotide ↔ EF-Tu•mant-nucleotide, and analyzed by exponential fitting to determine the value of k_{app} for each titration point. The bimolecular association rate constant, k_1/k_5, was determined from the slope of the linear concentration dependence of k_{app} on the mant-GDP/mant-GTP concentration (**Figure 2.3**). No difference in the nucleotide association rates was observed between the wild type or the mutant proteins.

The values obtained were D109A: $k_1/10^6$ $M^{-1}s^{-1}$ = 3.3 ± 0.1; $k_5/10^5$ $M^{-1}s^{-1}$ = 3.9 ± 0.1 and WT: $k_1/10^6$ $M^{-1}s^{-1}$ = 2.8 ± 0.1; k_5 10^5 $M^{-1}s^{-1}$ = 4.3 ± 0.1. In order to determine the elementary rate constants for nucleotide dissociation from EF-Tu•GDP (k_{-1}) and EF-Tu•GTP (k_{-5}) we performed FRET based nucleotide dissociation experiments in the presence of excess mant-GDP/mant-GTP (data not shown), similarly to previous studies (Dahl et al., 2006; Gromadski et al., 2002; Wieden et al., 2002). Under these conditions fast binding of the mant-nucleotide is limited by the rate of dissociation of the unlabeled nucleotide, and rebinding of the GDP/GTP is negligible. The rate of fluorescence

increase, due to binding of the mant-nucleotides, equals the dissociation rate constant of the unlabeled nucleotide. Again, only single exponential time courses were observed. The values obtained from single-exponential fitting of the obtained dissociation time courses were D109A: $k_{-1}/s^{-1} = 0.004 \pm 0.001$; k_{-5}/s^{-1} 0.05 ± 0.01 and WT: $k_{-1}/s^{-1} = 0.002 \pm 0.001$; k_{-5}/s^{-1} 0.02 ± 0.01 and did not reveal any significant difference between the mutant protein and the wild type. Similar values of k_{-1} were obtained for the reverse experiments following the dissociation of EF-Tu•mant-GDP in the presence of a large excess of unlabeled GDP. Values of association and dissociation rate constants obtained this way for the wild type are consistent with those previously obtained for EF-Tu from *E. coli* and are summarized in **Table 2.1** (Gromadski et al., 2002; Schümmer et al., 2007; Wieden et al., 2002).

Interaction of EF-Tu$_{D109A}$ and EF-Tu$_{wt}$ with EF-Ts in the presence of GDP (k_3, k_{-3}, k_4, k_{-4})

Effects on the EF-Ts-catalyzed dissociation of GDP were studied using the EF-Tu•mant-GDP complex. The fluorescence of mant was again excited via FRET from Trp184. Upon mixing of EF-Tu•mant-GDP with EF-Ts, single exponential fluorescence decays were observed due to the dissociation of the nucleotide and a corresponding drop of FRET efficiency as the distance increased between the two fluorophores localized on the protein and the nucleotide (**Figure 2.4.A**). The concentration of EF-Tu•mant-GDP was kept constant and titrated with increasing concentrations of EF-Ts. A large excess of GDP was added to the EF-Ts solution to prevent rebinding of the dissociated mant-GDP. The concentration dependence of the mant-GDP dissociation rate revealed two characteristic regions (**Figure 2.4.B**). First, at low concentrations of EF-Ts, the apparent rate (k_{app}) increased linearly as the observed rate is limited by EF-Ts binding to the

EF-Tu•GDP complex. Later, the observed rates saturated at higher EF-Ts concentrations. Under these conditions, since mant-GDP rebinding is negligible, the observed rate at saturation equals the dissociation rate constant from the ternary complex EF-Tu•GDP•EF-Ts (k_{-4}). Fitting a hyperbolic curve to the apparent rates revealed a 13 times slower dissociation rate constant for the D109A mutant than for the wild type enzyme (k_{-4}/s^{-1}= 16 ± 1 for D109A and k_{-4} /s^{-1} = 219 ± 25 for WT).

When k_{-4} and k_{-3} are known the value for k_3 can be calculated from the initial slope of the titration curve (inset in Figure 4B) and is equal to k_3 / (1 + k_{-3}/k_{-4}) (Fersht, 1999). In order to determine k_{-3} and ultimately k_3, we performed titrations using purified EF-Tu•EF-Ts complexes at fixed concentrations, initiating dissociation of the binary complex with increasing concentrations of GDP and monitoring the change of tryptophan fluorescence. In this system the observed fluorescence signal is independent of nucleotide binding and proportional to the amount of EF-Tu bound to EF-Ts (**Figure 2.4.C**). The rates of EF-Ts dissociation were determined from the time courses exemplified in **Figure 2.4.C** by single-exponential fitting. Plotting the obtained k_{app} as a function of GDP concentration (**Figure 2.4.D**) allowed us to determine values for k_{-3} by fitting the apparent rates to a hyperbolic function. At high GDP concentrations, GDP binding is no longer limiting and the saturation level therefore represents k_{-3}, the dissociation rate constant for EF-Ts from the ternary EF-Tu•GDP•EF-Ts complex. The values obtained, both for the wild type and D109A EF-Tu, were comparable. (D109A: k_{-3}/s^{-1}= 408 ± 64 and WT: k_{-3}/s^{-1}= 438 ± 50)

Since the contribution of the reverse reaction (i.e. re-binding of EF-Ts to EF-Tu•GDP) is determined by k_3[EF-Ts], it is insignificant at higher concentrations of GDP as the

concentration of free EF-Ts cannot exceed the initial concentration of the EF-Tu•EF-Ts complex (0.5 μM). The initial slope of the curve (inset in **Figure 2.4.D**) is $k_4 /(1+k_{-4}/k_{-3})$. Based on the initial slopes and the determined values of k_{-3} and k_{-4} the following rate constants were calculated, D109A: $k_3/10^6\ M^{-1}\ s^{-1}$= 40 ± 10, $k_4/10^6\ M^{-1}\ s^{-1}$= 7 ± 1; and WT: $k_3/10^6\ M^{-1}\ s^{-1}$= 30 ± 10, $k_4/10^6\ M^{-1}\ s^{-1}$= 7 ± 1. Therefore replacing aspartate with alanine neither affects EF-Ts dissociation from the EF-Tu•GDP•EF-Ts complex nor the association of EF-Ts with EF-Tu•GDP and GDP binding to the EF-Tu•EF-Ts complex.

Interaction of EF-Tu$_{D109A}$ and EF-Tu$_{wt}$ with EF-Ts in the presence of GTP (k_6, k_{-6}, k_7, k_{-7})

The above described approach to determine the rate constants governing the interaction between EF-Ts, EF-Tu and GDP has also been used to study the respective interactions with GTP. However, besides using GTP as the nucleotide, we also incubated all solutions with phosphoenolpyruvate and pyruvate kinase to convert any GDP present in the reactions to GTP. EF-Ts stimulated GTP dissociation from wild type EF-Tu and the D109A mutant was monitored using mant-fluorescence (**Figure A.1.4.A**). Increasing concentrations of EF-Ts were rapidly mixed with a constant concentration of EF-Tu•mant-GTP in the presence of excess unlabeled nucleotide (**Figure A.1.4.B**).

The rate constants for GTP dissociation in the presence of EF-Ts - k_{-7}/s^{-1}= 50 ± 5 (D109A) and k_{-7}/s^{-1}= 95 ± 10 (WT) - were determined at saturation by fitting the concentration dependence of k_{app} to a hyperbolic function and showed less than 2-fold slower GTP dissociation rate constant for EF-Tu$_{D109A}$ when compared to the EF-Tu$_{wt}$. Hence, the mutation of Asp109 significantly decreases the dissociation rate of GDP from

the EF-Tu•GDP•EF-Ts complex, but not the dissociation of GTP from the respective ternary complex, EF-Tu•GTP•EF-Ts.

GTP-induced dissociation of WT and mutant EF-Tu•EF-Ts complexes was monitored through changes in tryptophan fluorescence and revealed similar trends (**Figure A.1.4.D**). The values for k_{-6}/s^{-1}= 90 ± 10 (D109A) and k_{-6}/s^{-1} = 60 ± 10 (WT) were estimated at saturation with GTP and rate constants D109A: $k_6/10^6$ M^{-1} s^{-1}= 33 ± 2, $k_7/10^6$ M^{-1} s^{-1}= 1.8 ± 0.2; WT: $k_6/10^6$ M^{-1} s^{-1}= 124 ± 3, $k_7/10^6$ M^{-1} s^{-1}= 3.9 ± 0.7 were calculated, as described for GDP, from the initial slopes (**Figure A.1.4.D**). Again, these rate constants are similar for $EF\text{-}Tu_{wt}$ and $EF\text{-}Tu_{D109A}$.

Binding of $EF\text{-}Tu_{D109A}$ and $EF\text{-}Tu_{wt}$ to EF-Ts (k_2)

Changes in tryptophan fluorescence were also used to determine the elementary rate constants for EF-Tu•EF-Ts complex formation. Consistent with the experiments using binary complexes (e.g. EF-Tu•GDP), binding of EF-Ts to nucleotide-free EF-Tu resulted in a fluorescence decrease. Similarly to our previous studies (Gromadski et al., 2002; Wieden et al., 2002), we were able to use the linear dependence of k_{app} on the concentration of EF-Ts to determine k_2. The values of the association rate constants for EF-Tu with EF-Ts were $k_2/10^7$ M^{-1} s^{-1}= 0.3 ± 0.1 for the D109A mutant and $k_2/10^7$ M^{-1} s^{-1}= 1.3 ± 0.1 for the wild type, thus only showing a small effect for the D109A mutant. The intercept with the Y-axis was close to zero, and thus k_{-2} could not be determined from these plots with precision.

Interaction of $EF\text{-}Tu_{D109A}$ and $EF\text{-}Tu_{wt}$ with EF-Ts in the absence of nucleotides (k_{-2})

Values for k_{-2} could not be determined directly but were calculated from the GDP and the GTP branch of the kinetic scheme (**Scheme 2.1**) as described in **Section 2.3**. The calculated rate constants were D109A: 0.026 s^{-1} / 0.05 s^{-1} and WT: 0.009 s^{-1} / 0.01 s^{-1} for GDP and GTP, respectively. Given the standard deviations of the rate constants used for the calculation, the differences between corresponding values of k_{-2} are statistically insignificant and consistent with previous studies (Gromadski et al., 2002; Wieden et al., 2002). The equilibrium dissociation constants (K_D) for EF-Tu/EF-Ts interactions calculated from the above values and the respective k_2 are D109A: 7.6 x 10^{-9} M / 13.6 x 10^{-9} M and WT: 0.7 x 10^{-9} M / 0.9 x 10^{-9} M. The rate constant of EF-Tu•EF-Ts dissociation listed in **Table 2.1** were obtained by averaging k_{-2} values from the GDP and GTP branches of the kinetic mechanism, yielding the following values; k_{-2} = 0.04 s^{-1} and 0.01 s^{-1} for D109A and WT respectively. These constants compare well with constants determined independently under similar conditions (WT) (Gromadski et al., 2002; Wieden et al., 2002).

Interactions of GTP with EF-Tu$_{E152A}$ and EF-Ts (k_5, k_{-5}, k_6, k_{-6}, k_7, k_{-7})

By using the above reported approach we have determined the rate constants for previously unreported GTP dependent reactions (k_5, k_{-5}, k_6, k_{-6}, k_7, k_{-7}). Experimental results are summarized in **Figure A.1.5**. The obtained values for k_5= 2.5 ± 0.1 10^5 M^{-1} s^{-1}, k_{-5}= 0.05 ± 0.01 s^{-1}, k_6= 53 ± 16 10^6 M^{-1} s^{-1}, k_{-6} = 390 ± 90 s^{-1}, k_7 = 5.9 ± 2.7 10^6 M^{-1} s^{-1}, k_{-7} = 8.5 ± 1 s^{-1} indicate that disrupting the salt bridge between $Glu152_{Tu}$ and $Arg12_{Ts}$ is not specific for the dissociation of GDP from the respective ternary complex, it also affects the association of the proteins and the dissociation of GTP from the complex.

Thus, this interaction is not specific for the GDP branch of the kinetic scheme in contrast to the observed effects of the D109A mutation.

Appendix 2

Supplemental Figures to Chapter 3

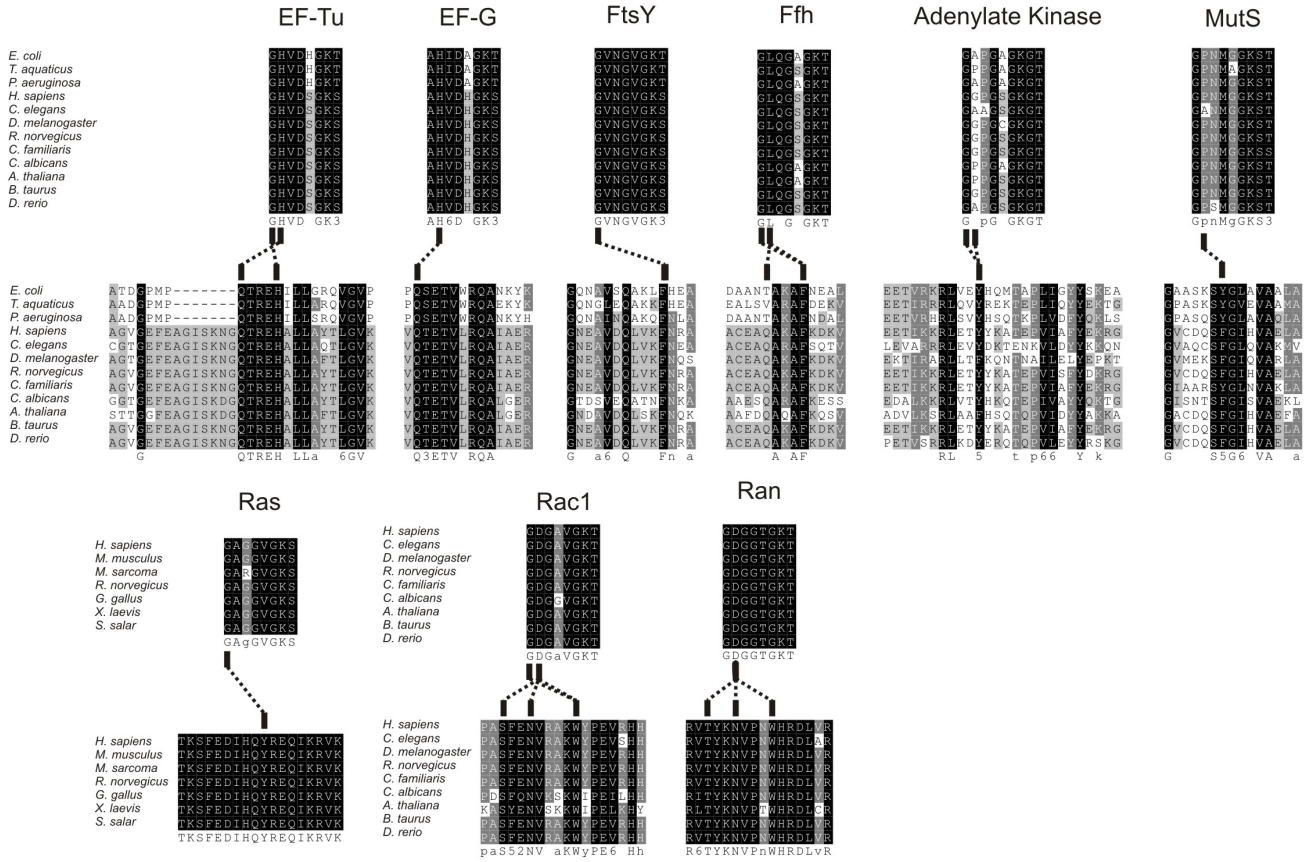

Figure A.2.1. Interactions between the two N-terminal P-loop amino acids and helix C are conserved in P-loop NTPases. Multiple sequence alignments of the G-proteins EF-Tu, EF-G, FtsY, Ffh, Ras, Rac1, and Ran as well as the ATPases adenylate kinase and MutS were performed in ClustalW (Larkin et al., 2007; Thompson et al., 1994). The P-loop (top) and helix C (bottom) alignments are shown for each protein with amino acids coloured according to conservation (black: 100%, grey: >80%, light grey: >60%). Interactions between amino acids of the P-loop and helix C, shown as dashed lines, were identified in crystal structures of each G-protein bound to a non-hydrolyzable GTP analogue. The PDBIDs for the structures investigated were as follows: EF-Tu:1EFT, EF-G: 2BV3, FtsY: 2Q9B, Ffh: 2CO4, Adenylate Kinase: 1AKE, MutS: 1E3M, Ras: 3L8Z, Rac1: 1MH1, Ran: 1IBR. Interacting amino acids were defined by close approach (<3.5Å; <3.8Å for FtsY and MutS) of heavy atoms.

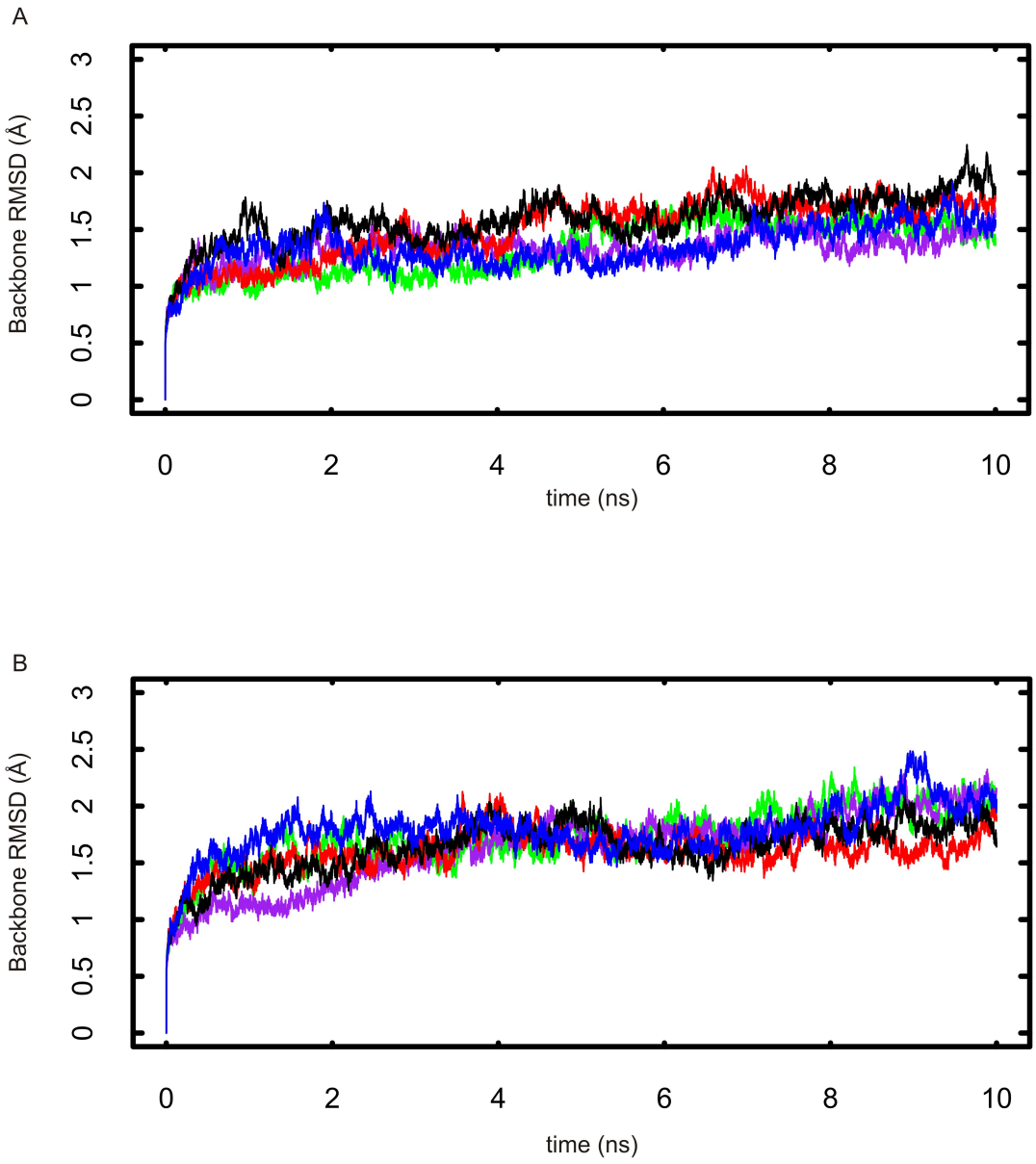

Figure A.2.2. Root mean-squared deviation (RMSD) of backbone atoms in EF-Tu during 10 ns molecular dynamics simulations. Simulations were performed with (A) and without (B) GTP•Mg^{2+} bound in the nucleotide-binding pocket. Each simulation was carried out with a 0.5 fs time step at 300K in an NPT ensemble; conformations were sampled every 0.5ps for RMSD analysis. The traces shown are wild type (blue), H22G (black), M112L (red), M112G (green), and M112A (purple) EF-Tu.

Appendix 3

Network Analysis

3.1 Network analysis

Molecular dynamics is used to simulate vibrations of atoms within biomolecular systems and thus, provides information about how amino acids influence each other's motions. This interplay between amino acids is interesting in the context of allosteric regulation where binding of a ligand to an allosteric site influences the activity of a distinct active site (Changeux, 2011). Network analyses of proteins and protein/RNA complexes have recently been developed using data from MD simulations to aid in identifying the contribution of structural dynamics to transmission of long-range signals (Dhulesia et al., 2008; Ma et al., 2012; Sethi et al., 2009). In the present work, MD simulations were used to construct communication networks of EF-Tu•GTP and EF-Tu•EF-Ts complexes to understand how the structural dynamics of EF-Tu contribute to GTPase activation on the ribosome and EF-Ts-stimulated nucleotide exchange, respectively. The networks presented in chapters four and five were constructed using different data sets from MD simulations. Networks in chapter five were constructed prior to development of the methods used in chapter four. The purpose of this appendix is to compare the two different methods of network construction.

Constructing networks based on data from MD simulations, like those presented in **Figures 4.8** and **5.3**, makes it possible to simultaneously visualize the dynamic interactions of hundreds of amino acids. This makes network analysis a useful first approach for comparing MD simulations of different macromolecular systems such as a protein and corresponding variants when the differences are not known *a priori*. Network analysis is particularly useful for studying allosteric regulation wherein binding of a small molecule to one site of a target protein alters the activity at a distant active site

(Changeux, 2011). In the context of allosteric regulation, a useful protein network should contain the path or paths that connect the signal input site to the active site (signal output). Several examples of network analysis of MD simulations exist in the recent literature (Dhulesia et al., 2008; Ma et al., 2012; Shi et al., 2012).

Inspired by the work of Luthey-Schulten's research group (Sethi et al., 2009), networks of EF-Tu were constructed in which each amino acid is represented by a node. Nodes were connected if they 1) were in contact and 2) demonstrated significant correlated motion during the simulation. In all of the networks presented in this work, a contact between two amino acids was identified if their heavy atoms were within 4.5 Å for 75% or more of the frames analyzed. The same criteria were employed in the work of Luthey-Schulten. However, unlike the networks constructed by Luthey-Schulten (Sethi et al., 2009) consecutive amino acids were included as contacts. This ensured that all amino acids were connected to the network, which might be critical in an enzyme that has evolved to perform a large number of independent functions within a relatively limited sequence space (e.g. EF-Tu).

Dynamic information has also been incorporated into networks presented here and elsewhere (Ma et al., 2012; Pyrkosz et al., 2010; Sethi et al., 2009). In general, amino acid pairs that are found to 'communicate' during MD simulations are connected in the network. The dynamic information employed by the Luthey-Schulten group was a normalized covariance matrix, computed from MD simulations using the software Carma (Glykos, 2006). The normalized covariance between amino acids *i* and *j* (C_{ij}) is a time-averaged value calculated according to **A.3.1**.

$$C_{ij} = \frac{\left\langle \left(v_i(t) - \bar{v}_i\right) \bullet \left(v_j(t) - \bar{v}_j\right) \right\rangle}{\left(\left\langle \left(v_i(t) - \bar{v}_i\right) \right\rangle^2 \left\langle \left(v_j(t) - \bar{v}_j\right) \right\rangle^2 \right)^{1/2}} \qquad \text{(A.3.1)}$$

In the above equation, $v_{i,t}$ are the Cartesian coordinates for the Cα of amino acid *i* at frame *t*, $\bar{v}_i$ are the time-averaged Cartesian coordinates for the Cα of amino acid *i*, • indicates a dot product, and $\langle\ \rangle$ indicates time-averaging of the quantities within the brackets. The normalized covariance matrix is thus normalized with respect to the diagonal such that C_{ij}=1 when *i*=*j*. The normalized covariance describes the tendency of each Cα pair to move in the same direction at the same time, relative to their respective average positions. The normalized covariance has been said to "define the probability of information transfer across each edge", although no strict rationale for this statement is evident (Pyrkosz et al., 2010). In general, one can envision amino acids moving in the same direction at the same time, which will have a positive covariance, are potentially transferring momentum and thus "communicating". In Sethi *et al.* (2009) and Pyrkosz *et al.* (2010), the edge between contacting connecting amino acids *i* and *j* in each network was given a weight equal to -log|C_{ij}|. The resulting networks are difficult to visualize since they are extremely dense (all contacting amino acids are connected by edges).

In the present work, all edges in each network were given equal weights, but statistical tests were used to identify which Cα pairs demonstrate *significantly* correlated motion during MD simulations. The inclusion of significance criteria results in the removal of edges from the network if the contacting amino acids do not demonstrate significantly correlated motion. The final network is less complicated than the contact network and therefore easier to visualize. For the networks presented in chapter five, a covariance analysis was performed using the software Carma (Glykos, 2006), as described in Sethi *et*

al. (2009). In order to identify significant covariances, each row of the normalized covariance matrix was used to plot a separate histogram. For simulations of EF-Tu•GTP (i.e. those studied in **Chapter 5**), each histogram resembles a normal distribution about zero. One example is shown in **Figure A.3.1**. A Gaussian curve was fit to each histogram, and the fitted parameters for mean covariance and standard deviation were obtained. Significant covariances were defined as those that were more than three standard deviations away from the mean. The significant covariances in **Figure A.3.1** are those lying outside the blue dashed lines.

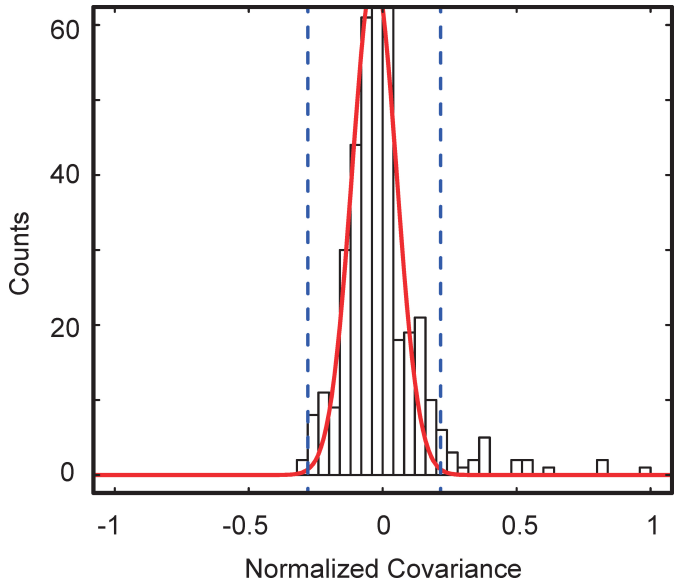

Figure A.3.1. Histogram of normalized covariances for each Cα with the Cα of $Asp207_{Tu}$ in EF-Tu•GTP. Covariance analysis was performed in Carma using snapshots saved every 10 ps from simulation of EF-Tu•GTP from 10-20 ns. The red curve is a Gaussian function fitted to the histogram and the blue vertical lines are drawn at ±3σ.

When simulations of EF-Tu•EF-Ts were analyzed, the histograms of normalized covariances differed significantly from those of EF-Tu•GTP complexes. As shown in **Figure A.3.2** below, for one amino acid the distribution of normalized covariances appears bimodal with a local minimum at zero. Visual inspection revealed that the

bimodal distribution was rooted in two different conformations being sampled during simulation of the EF-Tu•EF-Ts complex (not shown). For these simulations, the average structure did not represent a highly populated structure (a mode), but rather a midpoint between two populations. Since the statistical method employed on the EF-Tu•GTP data set would not be a reasonable analysis for EF-Tu•EF-Ts, another measure for correlated motion of amino acids was developed.

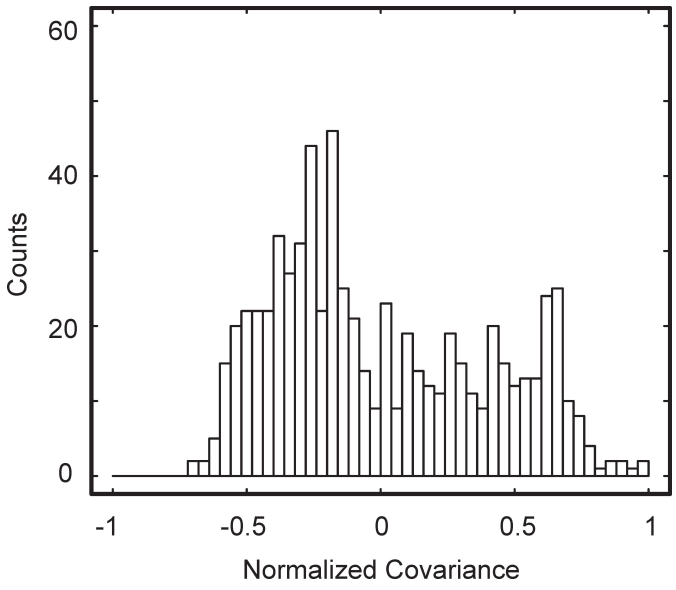

Figure A.3.2. Histogram of normalized covariances for each Cα with the Cα of $Asp207_{Tu}$ in EF-Tu•EF-Ts. Covariance analysis was performed in Carma using snapshots saved every 20 ps from simulation of EF-Tu•GTP from 10-20 ns.

In the spirit of the covariance analysis, MD simulations were analyzed to identify pairs of alpha-carbons that move in the same direction at the same time. This analysis was intended to be free of average atomic positions. In order to accomplish this, each Cα pair (i,j) in the MD simulation was used to compute the relative angle of displacement, $\theta_{ij}(t)$, over the time step dt as described in **Equation A.3.2**.

$$\theta_{ij}(t) = \arccos\left(\frac{v_i(t) \bullet v_j(t)}{|v_i(t)||v_j(t)|}\right) \qquad (A.3.2)$$

In **Equation A.3.2**, • indicates a dot product, || indicates a magnitude, and $v_i(t)$ represents the displacement vector for amino acid *i* computed over the time step d*t* as shown in **Equation A.3.3**.

$$v_i(t) = r_i(t) - r_i(t - dt) \qquad (A.3.3)$$

In **A.3.3**, $r_i(t)$ are the Cartesian coordinates at time *t*. Rather than computing a time-averaged relative angle of displacement, the values of $\theta_{ij}(t)$ were used to plot a histogram for each pair *ij* where $i \neq j$. Each histogram was analyzed to identify which Cα pairs moved in random directions relative to one another, and which ones deviated significantly from this random behaviour. A random distribution of $\theta(t)$, which should be observed if the motions of amino acids *i* and *j* are not correlated, was determined by integration in spherical coordinates as follows.

$$P(\theta) = \frac{\text{volume}(\delta < \theta < \delta + d\theta)}{\text{volume}(0 < \theta < \pi)} \qquad (A.3.4)$$

$$P(\theta) = \frac{\int_r \int_\phi r \sin\theta \, d\theta d\phi \, dr}{\int_r \int_\phi \int_\theta r \sin\theta \, d\theta d\phi \, dr} \qquad (A.3.5)$$

$$P(\theta) = \frac{1}{2}\sin\theta \, d\theta \qquad (A.3.6)$$

The expected number of counts for each bin in the histogram was computed by multiplying the probability $P(\theta)$ in **Equation A.3.6** by the total number of counts (i.e. the number of frames analyzed).

$$E(\theta) = C_{\text{total}} \frac{1}{2}\sin(\theta) d\theta \qquad (A.3.7)$$

The expected number of counts, $E(\theta)$, is a function of the total counts, C_{total}, the relative angle of displacement vectors (θ, the midpoint of each bin in the histogram), and the width of each bin ($d\theta = \pi/100$).

The relative angles of displacement for each Cα pair in the simulation of *E. coli* EF-Tu•EF-Ts was measured and plotted in histograms. Two examples of histograms are shown in **Figure A.3.3**. In order to identify significant deviations from the random distribution, a chi-squared analysis was performed on each histogram (Brase and Brase, 2003a). The directions of Cα motion were determined to be significantly correlated for $His84_{Tu}$ and $Leu121_{Tu}$ (**Figure A.3.3.A**) but not for $His84_{Tu}$ and $Ser253_{Tu}$ (**Figure A.3.3.B**). If the motion of Cα atoms for amino acids *i* and *j* were found to be correlated significantly, an edge was drawn between nodes *i* and *j* in the communication network provided these two amino acids were in contact during the MD simulation (*vide supra*).

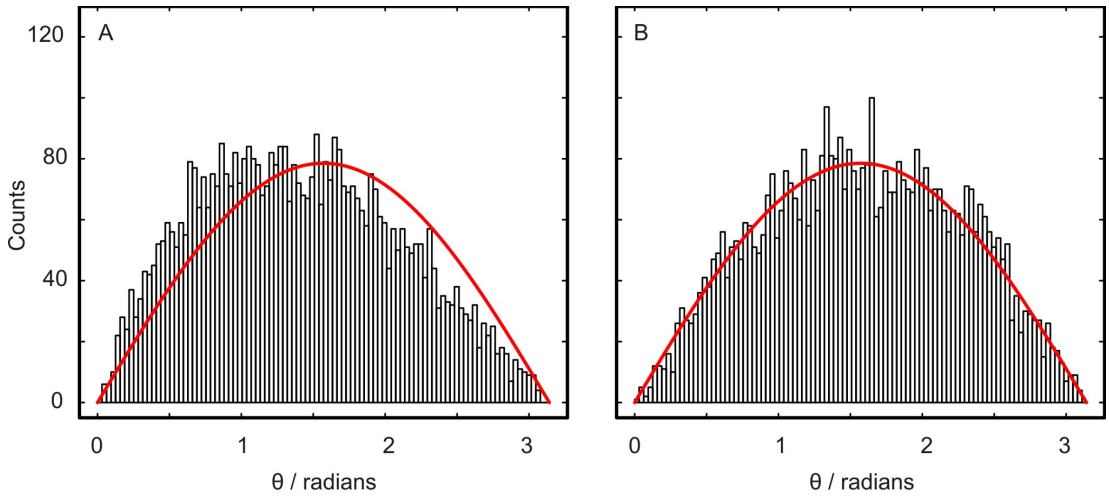

Figure A.3.3. Distribution for angles between Cα displacement vectors of $His84_{Tu}$ and $Leu121_{Tu}$ (A) or $Ser253_{Tu}$ (B). The red line indicates the distribution expected for amino acids moving randomly relative to one another. χ-squared analysis identified significant deviation from the random distribution in A, but not in B.

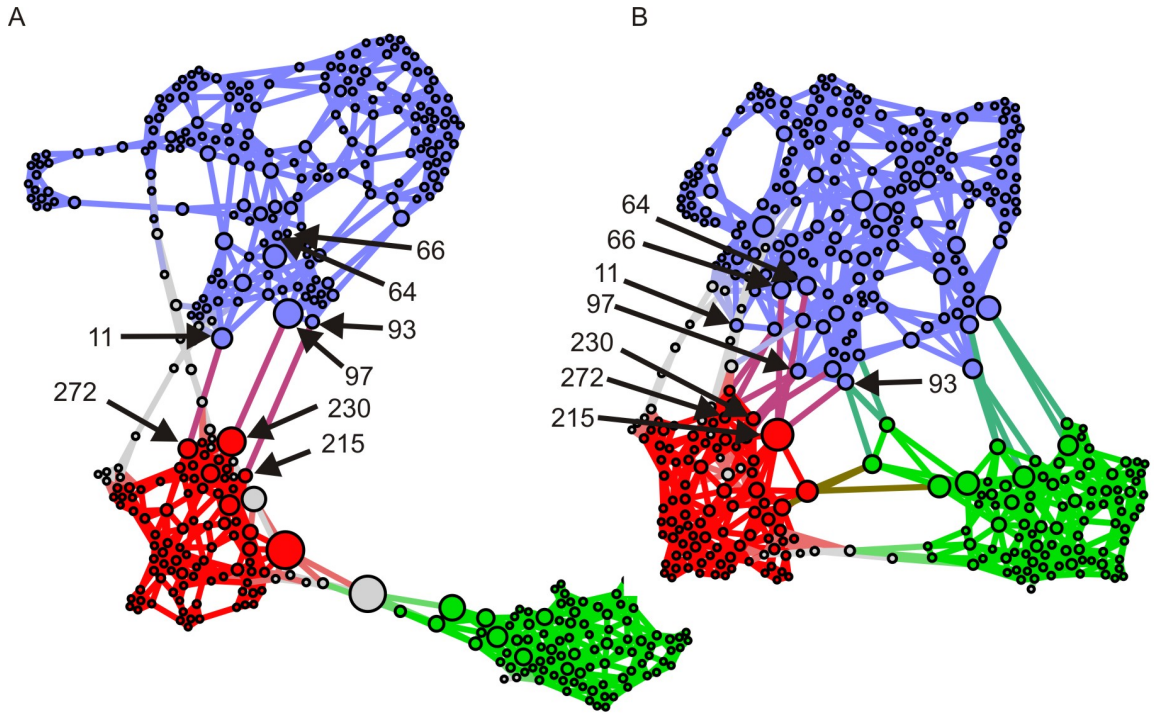

Figure A.3.4. Communication networks of EF-Tu•GTP constructed using contact information and normalized covariance (A) or correlated relative angle of displacement (B). Each amino acid is represented by a node (circle) in each network, coloured based on the domain in EF-Tu: domain I (blue), domain II (red), domain III (green). Edges are drawn between amino acids that were in contact during the MD simulation and showed significantly correlated motion between the respective Cα atoms. Specific amino acids are indicated.

For comparison, communication networks of EF-Tu•GTP constructed using normalized covariance from Carma (Glykos, 2006) and relative angle of displacement are presented in **Figure A.3.4**. Both of these networks are based on the same simulation trajectories and incorporate identical contact information. Construction of these two networks differed in the criteria for 'communication' for contacting amino acids. In **Figure A.3.4.A**, statistically significant covariances were used to define communication, while in **Figure A.3.4.B**, statistically significant correlation between relative angles of displacement was used. Overall, there is a larger number of significantly correlated relative displacement angles than significant normalized covariances in the MD simulation of EF-Tu•GTP (**Table A.3.1**). This results in a larger number of edges in the network presented in

Figure A.3.4.B compared to **Figure A.3.4.A**. The number of edges in each network is comparable and seems reasonable; important communication links between the domains are identifiable in both networks. There are two major advantages to using correlated relative displacement angles over normalized covariances in network construction. First, correlation via displacement angles can be based on clear statistical criteria relative to a random distribution. Assessing the statistical significance of a normalized covariance value, however, is complicated by the lack of a clearly defined uncorrelated, or random, behaviour. Second, correlated relative displacement angles are easily understood in a physical context; correlated Cα atoms move in the same direction over the same time interval in an MD simulation. The physical interpretation of a covariance is more abstract; correlated Cα atoms move in the same direction relative to their respective time-averaged positions during the same time interval in an MD simulation.

Table A.3.1. Comparison of global network metrics for EF-Tu•GTP.

	Number of Contacts	Non-trivial Contacts	Significant Correlations	Number of Edges	Non-trivial Edges
Normalized Covariance	1666	1274	2934	1337	947
Correlated displacement angle	1666	1274	3075	1503	1111

The networks in **Figure A.3.4** reveal that the same domain II/domain I bridges identified using the covariance approach (Glu272/His11, Glu215/Thr93, and Arg230/Gln97) are also identified using correlated displacement angles. Seven additional interdomain bridges were also present in the network constructed using correlated displacement angles (see **Table A.3.2**). In addition, there is significant correlation in the angles of displacement between Cα's of domain III and domain I while no such communication is identified by the covariance analysis. This likely results from the

greater number of significantly correlated displacement angles, compared to significant covariance values. It is possible that the bridges identified in the covariance network are detected by both analyses because they are the strongest communicators. Conversely, identifying significantly correlated displacement angles may report on more 'types of communication'. Addressing these hypotheses requires further study that will focus on two major questions: 1) what type of signals are transmitted through these intramolecular communication networks and 2) what are the most important and most frequently used signal pathways?

Table A.3.2. Bridges connecting domain II and domain I in EF-Tu•GTP networks.

Covariance		Correlated Displacement Angles	
domain I amino acid	domain II amino acid	domain I amino acid	domain II amino acid
93	215	93	215
97	230	97	230
11	272	11	272
		64	215
		66	215
		96	230
		97	229
		11	271
		13	271
		13	273

Table A.3.3 Interactions between EF-Tu and EF-Ts in each EF-Tu•EF-Ts communication network.

EF-Ts region ••• EF-Tu region	Wild Type		M112L		M112G		M112A	
	Tu a.a.	Ts a.a.	Tu a.a.	Ts a.a.	Tu a.a.	Ts a.a.	Tu a.a.	Ts a.a.
Helix C ••• N-terminal Domain	108	19	108	19	108	19	108	19
	108	20	108	20	108	20	108	20
	109	18	109	18	109	18	109	18
	109	19	109	19	109	19	109	19
	109	21	109	21	109	21	109	21
	117	81	112	125	110	19	113	124
			114	81	113	85	113	125
			114	125	113	125	114	125
			117	81	114	81	117	81
			118	81	114	82	117	84
					116	85		
					117	81		
					117	84		
					118	81		
Helix D ••• N-terminal Domain	144	5	144	5	140	20	144	5
	145	5	148	5	141	23	145	8
	145	8	148	9	145	19		
			152	12	145	23		
Loop E ••• C-terminal Motif	178	278	178	278			178	278
	178	280						
Domain III ••• C-terminal Domain	354	150	321	234	320	234	320	234
			349	170	321	234	347	147
					349	170	349	147
					351	174	353	150
					354	150	354	150

(continued on next page)

EF-Ts region ••• EF-Tu region	Wild Type		M112L		M112G		M112A	
	Tu a.a.	Ts a.a.	Tu a.a.	Ts a.a.	Tu a.a.	Ts a.a.	Tu a.a.	Ts a.a.
Domain I ••• C-terminal motif	25	271	25	270	25	271	25	271
	25	274	25	274	25	274	25	274
	25	275	25	275	25	275	25	275
	25	278	25	278	25	278	25	278
	26	278	26	278	26	278	26	278
	28	271	28	275	28	275	28	271
	28	275	29	275	29	275	28	275
	29	275	29	278	29	278	29	275
	29	278	29	279	29	279	29	278
	29	279	32	279	33	279	29	279
	32	275	33	279	65	271	32	279
	32	279	33	280	65	272	33	279
	33	279	62	268	67	271	65	272
	33	280	62	269	67	272	67	271
	33	281	63	271			67	272
	36	281	80	271			67	275
	37	281					79	271
	37	282					80	271
	62	269						
	65	272						
	67	271						
	67	272						
	67	275						
	80	271						
Switch II ••• N-Terminal Domain					83	80	83	80
					83	81	83	81
					84	80	84	80
					86	80	84	81
							86	80
P-loop ••• N-terminal Domain					20	79	21	51

Appendix 4

Supplemental Tables to Chapter 5

Table A.4.1. Betweenness and conservation of each amino acid in the *E. coli* EF-Tu•GTP communication network.

Rank	Amino Acid	Betweenness	Conservation
1	293	26779	0.72
2	298	25508	0.76
3	97	18910	0.99
4	230	18625	0.97
5	367	16180	0.98
6	210	15222	0.93
7	79	13677	0.89
8	368	11514	0.58
9	11	11513	1
10	212	11135	0.26
11	272	10446	0.26
12	231	9393	0.58
13	366	9053	0.73
14	304	8521	1
15	67	8150	0.84
16	77	8004	0.97
17	337	7933	0.95
18	300	7536	0.93
19	125	6999	0.97
20	292	6777	0.78
21	32	6604	0.78
22	24	6517	1
23	291	5748	0.96
24	93	5624	0.99
25	215	5505	1
26	80	5305	1
27	301	4776	0.97
28	81	4636	0.88
29	16	4593	1
30	100	4574	0.97
31	61	4532	1
32	274	4409	0.61
33	358	4297	0.46
34	242	4218	0.7
35	60	4154	0.99
36	22	3993	1
37	214	3964	0.52
38	59	3797	0.99
39	299	3736	0.38
40	95	3681	1
41	96	3561	0.99
42	106	3308	0.39
43	34	3244	0.72
44	36	3209	0.65
45	306	3194	0.17
46	13	3178	1
47	308	3131	0.79
48	127	3089	0.95
49	278	2939	0.97
50	201	2923	0.27
51	297	2688	0.19
52	228	2667	0.93
53	123	2597	0.82
54	199	2500	0.94
55	205	2492	0.3
56	162	2451	0.91
57	273	2430	1
58	362	2425	1
59	204	2220	0.99
60	203	2206	0.57
61	42	2204	0.16
62	131	2201	0.27
63	229	2198	0.99
64	28	2165	0.97
65	326	2114	1
66	129	2107	0.53
67	330	2100	0.99
68	372	2079	0.62
69	339	2002	1
70	135	1991	1
71	174	1989	0.95
72	26	1928	0.89
73	329	1914	1
74	119	1901	0.83
75	376	1900	0.97
76	243	1854	0.89
77	260	1830	0.99
78	196	1828	1
79	310	1780	0.34
80	9	1764	0.97
81	188	1741	0.8
82	255	1726	0.29
83	258	1696	0.74
84	107	1643	0.9
85	102	1620	1
86	121	1556	1
87	25	1523	0.98
88	103	1521	0.99
89	234	1500	1

Rank	Amino Acid	Betweenness	Conservation
90	156	1497	0.97
91	356	1496	0.28
92	44	1490	0.26
93	213	1454	0.88
94	365	1435	0.91
95	64	1435	0.8
96	30	1432	1
97	218	1364	0.94
98	343	1340	0.95
99	303	1337	0.59
100	184	1331	0.52
101	288	1319	1
102	177	1316	0.99
103	276	1311	0.28
104	56	1295	0.66
105	322	1292	0.97
106	157	1279	0.98
107	132	1268	0.99
108	122	1243	0.15
109	74	1223	0.99
110	138	1200	1
111	269	1180	0.22
112	377	1147	1
113	185	1101	0.54
114	311	1097	1
115	146	1096	0.78
116	78	1081	1
117	192	1080	0.17
118	75	1066	1
119	240	1035	0.43
120	19	1034	0.99
121	375	1032	0.69
122	76	1030	0.99
123	294	1028	0.83
124	233	1014	0.86
125	140	1005	0.84
126	225	1001	1
127	173	997	0.99
128	12	994	0.78
129	290	982	0.84
130	227	978	0.62
131	208	963	0.73
132	264	958	0.61
133	17	957	0.97
134	167	953	0.32
135	114	950	1
136	363	930	0.96
137	216	909	0.98
138	287	904	0.79
139	27	893	0.98
140	149	874	0.99
141	312	851	0.61
142	270	851	0.95
143	98	840	0.99
144	55	829	0.99
145	89	824	1
146	331	820	0.96
147	99	819	1
148	14	810	0.37
149	251	809	0.19
150	332	804	0.86
151	160	800	0.89
152	94	798	1
153	153	796	0.8
154	359	786	0.12
155	154	783	0.95
156	90	781	1
157	83	778	1
158	20	769	0.91
159	134	766	0.74
160	244	743	0.91
161	110	737	0.99
162	50	733	0.99
163	193	731	0.05
164	224	728	0.99
165	391	728	0.15
166	295	721	0.95
167	178	711	0.95
168	226	709	1
169	387	706	0.61
170	152	701	0.98
171	105	701	0.88
172	202	699	1
173	350	683	0.95
174	374	682	0.99
175	35	682	0.83
176	275	668	0.98
177	259	661	1
178	7	651	0.99
179	271	646	1
180	384	644	0.98
181	84	639	1
182	281	632	0.28
183	235	631	0.39
184	327	631	0.95
185	360	623	0.93

Rank	Amino Acid	Betweenness	Conservation
186	383	612	0.92
187	87	596	0.99
188	206	566	0.29
189	116	566	0.85
190	335	553	0.95
191	328	541	0.99
192	136	535	1
193	48	524	0.45
194	296	515	0.92
195	309	513	0.99
196	150	512	0.98
197	118	511	1
198	354	508	0.96
199	137	506	0.34
200	289	502	1
201	108	490	0.43
202	6	487	0.53
203	117	473	1
204	200	465	0.95
205	307	450	0.71
206	29	450	0.96
207	246	445	0.99
208	341	440	0.55
209	197	437	0.34
210	241	429	0.78
211	267	427	0.6
212	302	422	0.66
213	161	412	0.5
214	321	409	0.93
215	219	407	0.74
216	133	405	0.88
217	248	403	0.45
218	392	398	0.23
219	82	398	1
220	10	389	0.84
221	176	387	0.58
222	285	387	0.41
223	342	386	0.27
224	237	378	0.74
225	257	369	0.96
226	220	365	1
227	175	359	0.89
228	5	357	0.88
229	373	350	0.62
230	112	349	0.99
231	158	346	0.7
232	245	341	0.7
233	211	341	0.9
234	164	332	0.99
235	115	327	1
236	279	326	1
237	369	318	0.2
238	277	316	1
239	388	294	0.95
240	45	290	0.44
241	170	290	0.38
242	169	289	0.55
243	232	278	0.94
244	148	278	0.97
245	190	268	0.64
246	320	265	0.91
247	88	257	0.78
248	163	253	0.79
249	3	250	0.55
250	282	249	0.49
251	31	238	0.9
252	283	236	0.77
253	344	236	0.8
254	4	232	0.82
255	33	232	0.45
256	92	225	0.96
257	63	225	0.64
258	151	217	0.76
259	254	214	0.65
260	265	214	0.96
261	189	212	0.28
262	69	207	1
263	57	205	0.47
264	336	205	1
265	139	201	0.72
266	111	200	0.91
267	253	200	0.1
268	120	193	1
269	268	189	0.71
270	62	187	1
271	217	186	0.97
272	390	185	0.56
273	347	182	0.46
274	381	180	0.94
275	266	178	0.88
276	191	176	1
277	23	175	1
278	155	174	0.62
279	323	174	0.81
280	91	166	1
281	250	164	0.6

Rank	Amino Acid	Betweenness	Conservation
282	71	160	0.92
283	238	157	0.86
284	21	156	0.99
285	357	152	0.23
286	263	151	1
287	172	146	0.89
288	198	146	0.8
289	51	144	0.39
290	352	144	1
291	361	142	0.16
292	2	142	0.91
293	382	140	1
294	378	136	1
295	252	135	0.74
296	187	132	0.48
297	101	131	0.88
298	168	123	0.99
299	145	110	0.86
300	305	105	0.52
301	194	103	0.05
302	380	90	0.99
303	147	89	0.87
304	186	88	0.21
305	58	88	0.99
306	386	86	1
307	349	86	0.96
308	124	82	0.91
309	340	77	0.22
310	68	73	0.99
311	130	72	0.68
312	180	66	0.73
313	325	63	0.48
314	351	61	0.91
315	49	58	0.98
316	313	58	0.97
317	70	57	0.15
318	348	57	0.88
319	195	56	0.27
320	18	54	1
321	286	48	0.33
322	239	46	0.72
323	86	45	1
324	318	44	0.99
325	38	43	0.17
326	15	42	1
327	171	41	0.35
328	280	41	0.99
329	249	40	0.29
330	338	34	0.99
331	159	31	0.14
332	319	31	0.97
333	37	29	0.52
334	256	28	0.99
335	52	27	0.95
336	142	26	0.92
337	385	26	0.77
338	317	26	1
339	345	25	0.63
340	166	24	0.64
341	126	21	0.94
342	143	20	0.52
343	353	20	1
344	371	18	0.89
345	113	18	0.98
346	141	17	0.88
347	222	16	1
348	223	16	1
349	364	14	0.18
350	316	14	0.99
351	261	12	0.96
352	41	12	0.59
353	324	11	0.2
354	236	11	0.38
355	165	11	0.91
356	181	11	0.48
357	128	10	0.87
358	389	9	0.25
359	40	9	0.54
360	221	7	0.41
361	8	7	0.5
362	284	7	0.54
363	144	5	0.77
364	46	4	0.35
365	47	4	0.73
366	209	4	0.89
367	53	2	0.98
368	183	2	0.29
369	355	2	0.87
370	346	1	0.83
371	247	1	0.53
372	54	1	0.99
373	73	1	0.2
374	182	1	0.32
375	179	0	0.78
376	39	0	0.18
377	1	0	0.19

Rank	Amino Acid	Betweenness	Conservation
378	43	0	0.58
379	65	0	0.37
380	66	0	1
381	72	0	0.16
382	85	0	0.99
383	104	0	0.99
384	109	0	0.99
385	207	0	0.91
386	262	0	0.86
387	314	0	0.37
388	315	0	1
389	333	0	0.99
390	334	0	1
391	370	0	0.22
392	379	0	1
393	393	0	0.02

Table A.4.2. Conservation of amino acids that potentially communicate GTPase activating signals from helix 5 through domain II to the G-domain in various ribosome-associated G-proteins. Conservation was determined by multiple sequence alignment of 5-11 amino acid sequences in ClustalW (Larkin et al., 2007; Thompson et al., 1994).

	Domain II/helix 5		Domain II bridge		Domain I bridge	
EF-Tu[a] (125 seq.)	**Arg232**	**100% Arg**	**Glu215**	**100% Glu**	**Thr93**	**>99%**
	Arg279	**100% Arg**	**Arg230**	**100% Arg/Lys**	**Gln97**	**100% Gln/Glu**
	Arg283	**100% Arg/Lys**	**Glu272**	**>99% Glu/Asp**	**His11**	**100% His**
EF-G (10 seq.)	**Arg357**	**100% Arg/Lys**	**Phe322**	**100% Phe**	**Arg101**	**100% Arg**
	Arg359	**100% Arg**	**Arg337**	**100% Arg**	**Val105**	**100% Val**
	Arg362	**100% Arg**	Asp381	100% Asp/Glu	Tyr12	20% Tyr
RF3 (5 seq.)	**His310**	**100% His**	**Phe301**	**100% Phe**	**Arg101**	**100% Arg**
	Arg311	**100% Arg**	**Arg319**	**100% Arg**	**Ala105**	**100% Ala**
	Arg313	**100% Arg**	**Asp363**	**100% Asp**	**Arg13**	**100% Arg**
	Lys326	**100% Arg/Lys**	-	-	-	-
LepA (9 seq.)	**Lys263**	**100% Arg/Lys**	Ile196	>80% Ile/Phe	Arg90	100% Arg
	-	-	**Arg211**	**100% Arg**	**Ala94**	**100% Ala**
	-	-	Glu254	100% Asp/Glu	Ile4	>75% Ile
IF-2 (11 seq.)	**Arg607**	**100% Arg**	Leu568	100% Leu/Ile	Thr451	>70% Thr/Ser
	Arg605	**100% Arg/Lys**	Val584	>70% Val/Ile	Ala461	<30% Ala
	-	-	Ala645	<30% Ala	Val393	100% Ile/Val
TetM (7 seq.)	**Arg278**	**100% Arg**	**Arg269**	**100% Arg/His**	**Val91**	**100% Val/Leu**
	Lys288	>85% Lys	**Val253**	**100% Ile/Val**	**Arg87**	**100% Arg**
	Lys278	>70% Lys	Ser310	>85% Ser	Ile4	100% Ile/Leu

a From De Laurentiis *et al.* (2011).